REPORT DOCUMENTATION PAGE

Form Approved
OMB No. 0704-0188

1. AGENCY USE ONLY *(Leave blank)*	2. REPORT DATE	3. REPORT TYPE AND DATES COVERED
	21.Jul.05	THESIS

4. TITLE AND SUBTITLE
ELECTRON CONFORMAL RADIOTHERAPY FOR POST-MASTECTOMY IRRADIATION: A BOLUS-FREE, MULTI-ENERGY, MULTI-SEGMENTED FIELD ALGORITHM

5. FUNDING NUMBERS

6. AUTHOR(S)
MAJ RODGERS ROBERT A

7. PERFORMING ORGANIZATION NAME(S) AND ADDRESS(ES)
UNIVERSITY OF TEXAS HSC AT HOUSTON

8. PERFORMING ORGANIZATION REPORT NUMBER
CI04-1145

9. SPONSORING/MONITORING AGENCY NAME(S) AND ADDRESS(ES)
THE DEPARTMENT OF THE AIR FORCE
AFIT/CIA, BLDG 125
2950 P STREET
WPAFB OH 45433

10. SPONSORING/MONITORING AGENCY REPORT NUMBER

11. SUPPLEMENTARY NOTES

12a. DISTRIBUTION AVAILABILITY STATEMENT
Unlimited distribution
In Accordance With AFI 35-205/AFIT Sup 1

12b. DISTRIBUTION CODE

13. ABSTRACT *(Maximum 200 words)*

14. SUBJECT TERMS

15. NUMBER OF PAGES
204

16. PRICE CODE

17. SECURITY CLASSIFICATION OF REPORT	18. SECURITY CLASSIFICATION OF THIS PAGE	19. SECURITY CLASSIFICATION OF ABSTRACT	20. LIMITATION OF ABSTRACT

ELECTRON CONFORMAL RADIOTHERAPY FOR POST-MASTECTOMY IRRADIATION: A BOLUS-FREE, MULTI-ENERGY, MULTI-SEGMENTED FIELD ALGORITHM

A

THESIS

Presented to the Faculty of
The University of Texas Health Science Center at Houston
Graduate School of Biomedical Sciences

In Partial Fulfillment

of the Requirements

for the Degree of

MASTER OF SCIENCE

by

Robert Aubrey Rodgers, M.S.

Houston, Texas
August 2005

Electron conformal radiotherapy for post-mastectomy irradiation: A bolus-free, multi-energy, multi-segmented field algorithm

Robert Aubrey Rodgers, M.S.

Supervisory Professor: John A. Antolak, Ph.D.

Post-mastectomy irradiation is used to eliminate residual viable tumor remaining after mastectomy. It is a technically complex treatment requiring consideration of the primary tumor location, possible risk of internal mammary node involvement, varying chest wall thickness due to surgical defects or body habitus, and risk of damaging normal underlying structures (Perkins 2001). Electron conformal therapy (ECT) is a tool that can be used for treating these patients. Bolus ECT modulates the electron energy incident on the patient by varying the thickness of a bolus placed on the patient surface. Its clinical efficacy has been shown for chest wall treatments (Perkins 2001). As an alternative, segmented-field ECT uses multiple abutted electron fields to attempt to achieve a similar effect.

The purpose of this research was to evaluate the feasibility of producing conformal electron dose distributions for post-mastectomy irradiation without customized bolus by using multi-energy, multi-segmented electron fields. **The hypothesis was that compared to customized electron bolus radiotherapy for post-mastectomy irradiation, ECT with multi-energy, multi-segmented treatment fields has equivalent target coverage and equivalent (or better) normal tissue sparing and planning target volume (PTV) dose uniformity.** The specific aims of the research were to 1) develop an algorithm to generate multi-energy, multi-segmented conformal electron treatment plans, 2) verify that the algorithm can create optimized treatment plans for simple targets, and 3) verify that the algorithm can create optimized treatment plans for previously irradiated post-mastectomy patient cases.

For specific aim 1, an algorithm was developed that 1) segments an electron field based on PTV depth, and 2) modifies the segmentation to improve PTV coverage and/or critical structure sparing. The major goals of the algorithm were to ensure good PTV coverage (conformality and homogeneity), and to avoid delivering too much dose to critical structures. The Pinnacle^3 treatment planning system was used to create the segmented electron fields and dose was computed using the COPPERPlan 3D implementation (Starkschall 1991) of the M. D. Anderson pencil-beam algorithm (Hogstrom 1981). The algorithm was used to create computer treatment plans for six simple targets in a water phantom (specific aim 2). For each simple target case, the PTV dose coverage and homogeneity, and critical structure dose were examined. For a more clinically relevant evaluation of the algorithm (specific aim 3), five post-mastectomy clinical cases, previously treated with bolus ECT, were selected. The algorithm was used to create a treatment plan for each of the five clinical cases. PTV dose coverage and homogeneity, and critical structure sparing for each treatment plan were compared to the corresponding bolus ECT plan.

For the simple targets, the algorithm produced very conformal treatment plans; the PTV dose homogeneity was quite good. Use of the treatment plan modification techniques improved dose sparing for the non-target portion of the phantom. For the patient treatment plans, the algorithm provided acceptable results for PTV conformality and dose homogeneity, in comparison to the bolus ECT plans. In most cases, critical structure sparing was not as good as the bolus plan; however, for three of the five cases, the results were reasonable. Two of the patients used for the clinical evaluations had a very thin chest wall. The algorithm was limited in achieving better plans for these cases due to the limited selection of electron energies on the linear accelerator.

It was concluded that (1) a segmented-field ECT algorithm can be created to develop a treatment plan having acceptable PTV coverage (conformality and homogeneity within 5% of the bolus plan) and reasonable non-target sparing (dose to 20% of the non-target volume within 10% of bolus plan), (2) there are many technical issues that must be resolved prior to using this technique on a routine

basis, (3) linear accelerator energy steps are too wide for some clinical cases; and 4) electron energies below 5 MeV would have been useful for two of the clinical cases.

Electron conformal radiotherapy for post-mastectomy irradiation: A bolus-free, multi-energy, multi-segmented field algorithm

Robert Aubrey Rodgers, M.S.

Supervisory Professor: John A. Antolak, Ph.D.

Post-mastectomy irradiation is used to eliminate residual viable tumor remaining after mastectomy. It is a technically complex treatment requiring consideration of the primary tumor location, possible risk of internal mammary node involvement, varying chest wall thickness due to surgical defects or body habitus, and risk of damaging normal underlying structures (Perkins 2001). Electron conformal therapy (ECT) is a tool that can be used for treating these patients. Bolus ECT modulates the electron energy incident on the patient by varying the thickness of a bolus placed on the patient surface. Its clinical efficacy has been shown for chest wall treatments (Perkins 2001). As an alternative, segmented-field ECT uses multiple abutted electron fields to attempt to achieve a similar effect.

The purpose of this research was to evaluate the feasibility of producing conformal electron dose distributions for post-mastectomy irradiation without customized bolus by using multi-energy, multi-segmented electron fields. **The hypothesis was that compared to customized electron bolus radiotherapy for post-mastectomy irradiation, ECT with multi-energy, multi-segmented treatment fields has equivalent target coverage and equivalent (or better) normal tissue sparing and planning target volume (PTV) dose uniformity.** The specific aims of the research were to 1) develop an algorithm to generate multi-energy, multi-segmented conformal electron treatment plans, 2) verify that the algorithm can create optimized treatment plans for simple targets, and 3) verify that the algorithm can create optimized treatment plans for previously irradiated post-mastectomy patient cases.

For specific aim 1, an algorithm was developed that 1) segments an electron field based on PTV depth, and 2) modifies the segmentation to improve PTV coverage and/or critical structure sparing. The major goals of the algorithm were to ensure good PTV coverage (conformality and homogeneity), and to avoid delivering too much dose to critical structures. The Pinnacle^3 treatment planning system was used to create the segmented electron fields and dose was computed using the COPPERPlan 3D implementation (Starkschall 1991) of the M. D. Anderson pencil-beam algorithm (Hogstrom 1981). The algorithm was used to create computer treatment plans for six simple targets in a water phantom (specific aim 2). For each simple target case, the PTV dose coverage and homogeneity, and critical structure dose were examined. For a more clinically relevant evaluation of the algorithm (specific aim 3), five post-mastectomy clinical cases, previously treated with bolus ECT, were selected. The algorithm was used to create a treatment plan for each of the five clinical cases. PTV dose coverage and homogeneity, and critical structure sparing for each treatment plan were compared to the corresponding bolus ECT plan.

For the simple targets, the algorithm produced very conformal treatment plans; the PTV dose homogeneity was quite good. Use of the treatment plan modification techniques improved dose sparing for the non-target portion of the phantom. For the patient treatment plans, the algorithm provided acceptable results for PTV conformality and dose homogeneity, in comparison to the bolus ECT plans. In most cases, critical structure sparing was not as good as the bolus plan; however, for three of the five cases, the results were reasonable. Two of the patients used for the clinical evaluations had a very thin chest wall. The algorithm was limited in achieving better plans for these cases due to the limited selection of electron energies on the linear accelerator.

It was concluded that (1) a segmented-field ECT algorithm can be created to develop a treatment plan having acceptable PTV coverage (conformality and homogeneity within 5% of the bolus plan) and reasonable non-target sparing (dose to 20% of the non-target volume within 10% of bolus plan), (2) there are many technical issues that must be resolved prior to using this technique on a routine

basis, (3) linear accelerator energy steps are too wide for some clinical cases; and 4) electron energies below 5 MeV would have been useful for two of the clinical cases.

ELECTRON CONFORMAL RADIOTHERAPY FOR POST-MASTECTOMY IRRADIATION: A BOLUS-FREE, MULTI-ENERGY, MULTI-SEGMENTED FIELD ALGORITHM

by

Robert Aubrey Rodgers, M.S.

APPROVED:

_____
John Antolak, Ph.D. – Advisor

_____
Kenneth Hogstrom, Ph.D.

_____
George Starkschall, Ph.D.

_____
Mohammad Salehpour, Ph.D.

_____
Thomas Buchholz, M.D.

APPROVED:

_____
Dean, The University of Texas
Health Science Center at Houston
Graduate School of Biomedical Sciences

ELECTRON CONFORMAL RADIOTHERAPY FOR POST-MASTECTOMY IRRADIATION: A BOLUS-FREE, MULTI-ENERGY, MULTI-SEGMENTED FIELD ALGORITHM

A

THESIS

Presented to the Faculty of
The University of Texas Health Science Center at Houston
Graduate School of Biomedical Sciences

In Partial Fulfillment

of the Requirements

for the Degree of

MASTER OF SCIENCE

by

Robert Aubrey Rodgers, M.S.

Houston, Texas
August 2005

Dedication

I dedicate my work on this thesis to my maternal grandfather and to my paternal uncle. Both men bravely battled cancer during their lifetime.

To my parents (my best friends), for their lifelong love, guidance, support and encouragement they have given to me; also, for sharing their Faith with me and their dedication and sacrifices toward my education. In addition, I dedicate my efforts to my parents for their courageous fight against my father's cancer (diagnosed while I was working toward this degree at M. D. Anderson). I am so proud of you, both for your determination and inspiration, during this challenging time.

To my wife (also my best friend), who has been a pillar of strength to me since we met. Your un-wavering Faith, support of my academic and career pursuits, and dedication to our future provides wonderful encouragement and it instills a strong determination within me to face the new challenges that occur each day.

Acknowledgements

First, I would like to thank the United States Air Force for selecting me for an Air Force Institute of Technology tour (Civilian Institution Graduate Education Program), and for allowing me to study radiation therapy physics at the prestigious M. D. Anderson Cancer Center. *The views expressed in this thesis are those of the author and do not reflect the official policy or position of the United States Air Force, Department of Defense, or the U.S. Government.*

Second, I would like to thank the Medical Physics Academic Committee and the Graduate School of Biomedical Sciences Admissions Committee for selecting me to study medical physics, and their support to me during my allowed time of study in residence (August 2001 – August 2003).

I sincerely thank Dr. John Antolak for his guidance, support, and time that he provided to me during this research project. Dr. Antolak exemplified the highest standards of a medical physicist (both academically and clinically). I thank Dr. Antolak for the many challenging discussions regarding radiation therapy physics as he prepared me to respond to clinical issues with confidence.

In addition, I would like to thank the distinguished members of my thesis Supervisory Committee: Dr. Kenneth Hogstrom, Dr. George Starkschall, Dr. Mohammad Salehpour, and Dr. Thomas Buchholz. The expertise of this Committee and the opportunity to perform research under their guidance was a valuable experience as I develop into a clinical radiation therapy physicist.

I also would like to express my gratitude to the Department of Radiation Physics staff at The University of Texas M. D. Anderson Cancer Center who helped me during my time of study. I want to especially acknowledge and thank the following individuals: Mrs. Georgeanne Moore, Mrs. Hope Beach, Mr. Stan Bujnowski, Mr. Roy Steadham, Mr. Tzouh-Liang Sun, and Mr. Mitch Price.

Electron conformal radiotherapy for post-mastectomy irradiation: A bolus-free, multi-energy, multi-segmented field algorithm

Robert Aubrey Rodgers, M.S.

Supervisory Professor: John A. Antolak, Ph.D.

Post-mastectomy irradiation is used to eliminate residual viable tumor remaining after mastectomy. It is a technically complex treatment requiring consideration of the primary tumor location, possible risk of internal mammary node involvement, varying chest wall thickness due to surgical defects or body habitus, and risk of damaging normal underlying structures (Perkins 2001). Electron conformal therapy (ECT) is a tool that can be used for treating these patients. Bolus ECT modulates the electron energy incident on the patient by varying the thickness of a bolus placed on the patient surface. Its clinical efficacy has been shown for chest wall treatments (Perkins 2001). As an alternative, segmented-field ECT uses multiple abutted electron fields to attempt to achieve a similar effect.

The purpose of this research was to evaluate the feasibility of producing conformal electron dose distributions for post-mastectomy irradiation without customized bolus by using multi-energy, multi-segmented electron fields. **The hypothesis was that compared to customized electron bolus radiotherapy for post-mastectomy irradiation, ECT with multi-energy, multi-segmented treatment fields has equivalent target coverage and equivalent (or better) normal tissue sparing and planning target volume (PTV) dose uniformity.** The specific aims of the research were to 1) develop an algorithm to generate multi-energy, multi-segmented conformal electron treatment plans, 2) verify that the algorithm can create optimized treatment plans for simple targets, and 3) verify that the algorithm can create optimized treatment plans for previously irradiated post-mastectomy patient cases.

For specific aim 1, an algorithm was developed that 1) segments an electron field based on PTV depth, and 2) modifies the segmentation to improve PTV coverage and/or critical structure sparing. The major goals of the algorithm were to ensure good PTV coverage (conformality and homogeneity), and to avoid delivering too much dose to critical structures. The Pinnacle^3 treatment planning system was used to create the segmented electron fields and dose was computed using the COPPERPlan 3D implementation (Starkschall 1991) of the M. D. Anderson pencil-beam algorithm (Hogstrom 1981). The algorithm was used to create computer treatment plans for six simple targets in a water phantom (specific aim 2). For each simple target case, the PTV dose coverage and homogeneity, and critical structure dose were examined. For a more clinically relevant evaluation of the algorithm (specific aim 3), five post-mastectomy clinical cases, previously treated with bolus ECT, were selected. The algorithm was used to create a treatment plan for each of the five clinical cases. PTV dose coverage and homogeneity, and critical structure sparing for each treatment plan were compared to the corresponding bolus ECT plan.

For the simple targets, the algorithm produced very conformal treatment plans; the PTV dose homogeneity was quite good. Use of the treatment plan modification techniques improved dose sparing for the non-target portion of the phantom. For the patient treatment plans, the algorithm provided acceptable results for PTV conformality and dose homogeneity, in comparison to the bolus ECT plans. In most cases, critical structure sparing was not as good as the bolus plan; however, for three of the five cases, the results were reasonable. Two of the patients used for the clinical evaluations had a very thin chest wall. The algorithm was limited in achieving better plans for these cases due to the limited selection of electron energies on the linear accelerator.

It was concluded that (1) a segmented-field ECT algorithm can be created to develop a treatment plan having acceptable PTV coverage (conformality and homogeneity within 5% of the bolus plan) and reasonable non-target sparing (dose to 20% of the non-target volume within 10% of bolus plan), (2) there are many technical issues that must be resolved prior to using this technique on a routine

basis, (3) linear accelerator energy steps are too wide for some clinical cases; and 4) electron energies below 5 MeV would have been useful for two of the clinical cases.

Table of Contents

List of Figures

List of Tables

Chapter 1

Introduction and Background

1.1 Statement of problem

Breast cancer is the most frequently diagnosed non-skin cancer in women; an estimated 211,240 new cases of invasive breast cancer and 58,490 new cases of in situ breast cancer are expected to occur among women in the United States during 2005 (American Cancer Society 2005). Treatment options include lumpectomy, mastectomy, radiation therapy, chemotherapy, and hormone therapy; patient therapy often utilizes a combination of two or more treatment options. This study focuses on post-mastectomy radiation therapy.

Radiation therapy can eliminate residual viable cancer cells in tissue remaining after mastectomy. It is a technically complex treatment requiring consideration of the primary tumor location, possible risk of internal mammary node involvement, varying chest wall thickness due to surgical defects or body habitus, and risk of damaging normal underlying structures (Perkins 2001). The current standard of practice, at The University of Texas M. D. Anderson Cancer Center, is that regional node and chest wall irradiation is indicated after mastectomy for: 1) all Stage III patients; 2) all Stage II patients with four or more axillary nodes involved with metastatic tumor or those with any positive nodes with gross (>2 mm) extranodal disease in the axilla; 3) all patients with positive margins; and 4) all patients with locoregional recurrence (Strom 1999).

For patients with a thick or irregularly sloping chest wall, chest wall irradiation is typically given using a tangential photon technique with a separate matched electron internal mammary chain (IMC) field as described in Appendix A. The IMC field treats the IMC lymph nodes and the medial chest wall. The use of the IMC field decreases the treated lung volume compared to using only tangential fields to treat the IMC and chest wall together (Perkins 2001). For patients with a thin chest wall, an electron-only technique may be used (Tapley 1976). Another group of patients include those

who have a chest wall defect where standard tangential fields would incorporate a substantial amount of lung (>3 cm or 30% of the volume) in the treatment fields and those who are at high risk for recurrent disease in areas of typical field junctions. This group is not optimally treated with the above-mentioned techniques; however, modulated electron therapy (MET) has proven to be an effective option, in particular bolus electron conformal therapy (ECT) which has been used successfully in post-mastectomy radiation therapy (Perkins 2001, Hogstrom 2003). MET is ECT achieved through energy modulation and/or intensity modulation in the plane perpendicular to the central axis of the incident electron beam(s) (Hogstrom 2003). Presently, there is no technology that allows the incident electron beam to have its energy spatially modulated in real time; therefore, electron energy is modulated by one of two methods: bolus ECT or segmented-field ECT. This study will focus on developing an electron energy modulation therapy technique using segmented-field ECT for these latter types of patients, because they present the greatest challenge; however, the results should be more generally applicable for any patient treated with customized electron bolus or using multiple electron fields. Electron beam intensity modulation is beyond the scope of this study.

1.2 Electron conformal therapy

Electrons have a finite range in tissue that depends on the energy of the electrons. Electron beams with energies ranging from 6 to 25 MeV are limited to treating target volumes within approximately 7.5 cm of the patient surface. The finite range of electrons in tissue results in a rapid dose fall-off, particularly at depths beyond R_{90} (the depth of the descending 90% of maximum dose). This characteristic of electrons can be utilized to protect critical structures and normal tissues distal to the planning target volume (PTV) by choosing the appropriate energy.

Conformal radiation therapy is based on delivering a high dose of radiation to a three-dimensional (3D) target volume while minimizing the dose to surrounding healthy tissue. In ECT, the goals are to 1) conform the prescribed dose contour to the distal border of the target volume, 2) maintain a uniform dose within the PTV, and 3) minimize dose to nearby critical organs and normal tissues

(Hogstrom 1991, Low 1992, Kudchadker 2002). Internal heterogeneities, irregular patient surfaces, variable depth of the distal surface of the target volume, and radiation-sensitive organs distal to the target can make ECT planning very complex (Hogstrom 1991).

1.3 Bolus ECT

Hogstrom defines electron bolus as "a specifically shaped material, usually tissue equivalent, that is normally placed either in direct contact with the patient's skin surface, close to the patient's skin surface, or inside a body cavity; it is used to shape the dose distribution to conform the PTV and/or to provide a more uniform dose inside the target volume by providing extra scattering or energy degradation of the electron beam while improving sparing to nearby critical organs and normal tissue" (Hogstrom 1991). Bolus has proved to be useful when tumor underdose, normal tissue overdose, or non-uniform dose in the PTV occur due to internal heterogeneities, an irregular patient surface, or a highly variable depth of the distal surface of the target volume (Hogstrom 1991, Perkins 2001, Kudchadker 2002). ECT can be delivered using shaped bolus, which varies the penetration of the electrons across the incident beam so that the desired isodose surface conforms to the distal surface of the planning target; bolus thickness can be manufactured with 1 mm accuracy or better resulting in energy modulation in steps of 0.2 MeV or less (Hogstrom 2003).

Many methods have been used to design and fabricate bolus. Early efforts to design and fabricate customized electron bolus (bolus ECT) were reported by Archambeau et al. (1981) and Beach et al. (1981). The former used computed tomography (CT) data while the latter used an ultrasound technique to design the bolus. Both bolus fabrication techniques were very labor-intensive; more importantly, both ignored the effect of multiple Coulomb scattering of electrons on the bolus design and resultant dose distribution. The influence of multiple Coulomb scattering is two-fold: 1) Electrons experience range straggling (i.e., the penetration of electrons with depth below the surface varies), and 2) Electron trajectories become angulated with depth. For more convenient fabrication of electron bolus, Andrew and McParland (1987), and Smith et al. (1989) described the use of computers to control

milling processes to produce bolus. At M. D. Anderson, Low et al. (1992) and Starkschall et al. (1993) introduced a bolus design method that utilized CT data and the pencil-beam algorithm (Hogstrom 1981, Starkschall 1991) so that bolus design accounted for internal tissue heterogeneity and multiple Coulomb scattering. Their method allowed alteration of the dose distribution using operators to design the shape of the bolus. Three general classes of bolus operators were used: a creation operator that defined the thickness of the bolus based on target volume depth; modification operators that refined the bolus shape to account for electron scattering; and an extension operator that extended the bolus outside of the field to account for beam penumbra. The bolus operators were incorporated into M.D. Anderson's COPPERPlan treatment planning system (Starkschall 1994).

The American Association of Physicists in Medicine (AAPM) Radiation Therapy Committee Task Group 25 (TG-25) recommends that electron beam parameters, such as energy, field size, and bolus be selected so that the target volume is encompassed within 90% (or any other appropriate minimum dose) of the prescribed dose (Khan 1991). At M. D. Anderson, the usual goal is to encompass the PTV within the isodose surface corresponding to 90% of the given dose. Given dose is the maximum central axis dose delivered in a water phantom at the same source-to-surface distance (SSD) and with the smallest rectangular field that circumscribes the irregular field used on the patient (Hogstrom 2003).

At least five disadvantages are associated with bolus ECT: 1) specialized fabrication method, 2) bolus quality control, 3) very limited availability of bolus design software, 4) increased skin dose, and 5) suboptimal dose fall-off (R_{90-10}, the distance between R_{90} and R_{10}) (Hogstrom 2003).

Initially, the creation of the customized bolus was a very labor-intensive and time-consuming process; many hours were needed for manufacturing and verification of the bolus. However, this is no longer the case; M. D. Anderson uses a third-party vendor (.decimal, Sanford, FL) to manufacture the electron bolus. A text-file description of the bolus is sent to the company via email, and a computerized milling system creates the bolus. The bolus is shipped back to M. D. Anderson, usually within one

working day. The bolus verification process (quality control) requires a CT scan of the patient with the bolus in place and a dose calculation to verify its design.

Presently, the major limitation to the proliferation of this technology is that the software used to design the electron bolus is not currently available on any commercial treatment planning system. The code to design electron bolus was incorporated into an in-house treatment planning system over ten years ago; however, to date, no commercial treatment planning system vendor has incorporated this algorithm into their system.*

Bolus ECT produces higher skin dose. The use of bolus shifts the dose distribution closer to the skin surface thereby sparing distal normal tissue; however, the skin surface receives higher dose than when employing non-bolus electron techniques. This can be an advantage if a high skin dose is prescribed, but usually is a disadvantage leading to an undesirably high skin dose.

Bolus ECT also has suboptimal dose-fall off, $R_{90\text{-}10}$ (the minimum difference between the therapeutic depth and the organ-at-risk sparing depth), for portions of the PTV at shallower depths. This is because the shallower depth regions are treated with the same energy required to treat the deepest depth regions with overlying bolus. Treating with a lower energy and no bolus would decrease $R_{90\text{-}10}$, as $R_{90\text{-}10}$ increases proportionately with energy.

Advantages of bolus ECT include the following: 1) No modification to the electron treatment machine, 2) The quality control process is straight forward and well documented, and 3) The dose calculation uses the pencil-beam algorithm presently available in most 3-D treatment planning systems. Bolus ECT has been used clinically at M. D. Anderson for the past ten years, mainly for breast and head and neck therapy.

---

* M.D. Anderson has a contract with Philips for the bolus design software to be implemented on the Pinnacle[3] treatment planning system; Work is in progress.

1.4 Bolus ECT for post-mastectomy radiation therapy

Bolus ECT is a reasonable option for patients with altered chest wall geometry (congenital pectus excavatum) or recurrent disease in the medial chest wall and IMC area. Using electron beams without bolus can significantly over-irradiate lung in cases where there is a considerable variation in the depth of the PTV (or chest wall thickness) within a single treatment field (Perkins 2001). For every 1-cm difference in chest wall thickness, the electron beam (and hence the isodose lines) can penetrate 4-cm deeper in lung (assuming a lung density of 0.25). Similarly, a 2-MeV excess in energy (e.g. using 16 MeV when only 14 MeV is needed) results in an excess penetration of 4 cm. Bolus ECT potentially mitigates both of these effects (Perkins 2001).

The location of the disease is another factor in selection of the treatment plan. Because of the risk of recurrence, it is preferable that no field junctions are placed where there was gross disease (Perkins 2001). One main advantage of bolus ECT is that there are no field junctions, which gives less dose uncertainty across the area at risk (Perkins 2001). This method provides conformal dose distributions, may reduce dose heterogeneity, and minimizes normal tissue exposure. However, compared to non-bolus ECT, bolus ECT has two disadvantages for post-mastectomy radiation therapy: 1) Skin dose is higher, which may lead to undesirable skin changes (telangiectasias and skin fibrosis) that could interfere with breast reconstruction at a later date and 2) $R_{90\text{-}10}$ (dose fall-off) is increased which can result in excess normal tissue and/or critical organ dose distally (Perkins 2001).

Perkins (2001) showed that the bolus ECT method produces highly conformal electron therapy plans for post-mastectomy radiation therapy patients (Figure 1.1). It is not always possible to maintain dose uniformity (i.e., 90%-100%) inside the PTV using customized bolus, because of multiple Coulomb scattering and variable source-to-surface distance. Kudchaker (2002) showed that using intensity modulated electron beams with bolus ECT improved PTV dose homogeneity. However, intensity modulation is beyond the scope of this study; only energy modulation will be investigated.

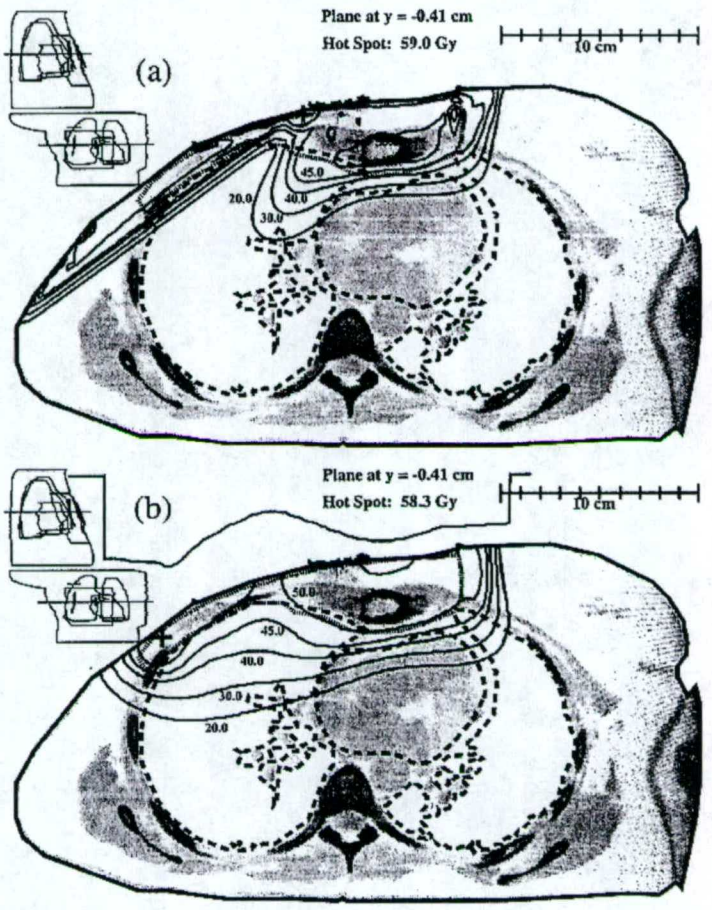

Figure 1.1. (a) Isodose curves (Gy) using standard tangent-IMC technique for a patient with a lesion in the right IMC area, with extension into the chest wall soft tissues. A dose of 50 Gy was prescribed to 100% of the given dose, using 12 MeV electrons for the IMC field, and the electron-field edge was matched to the medial tangent field edge on the patient's skin surface. The 45 Gy isodose line covers the target volume, except for the cold triangle directly beneath the junction line, an area of known disease. (b) Isodose curves (Gy) using the bolus ECT technique for the same patient. A dose of 50 Gy was prescribed to 100% of the given dose, using 16 MeV electrons, and the bolus was designed to deliver 90% of the given dose to the target volume (from Perkins 2001).

1.5 Segmented-field ECT

Segmented-field ECT provides an alternative to bolus ECT. This modality utilizes multiple abutted electron fields, each having a common virtual source position but each having its own energy and weight, so as to conform the therapeutic dose surface (e.g. 90% of given dose) to the PTV

(Hogstrom 2003). Figure 1.2 shows a comparison of bolus ECT to segmented-field ECT from Zackrisson and Karlson (1996).

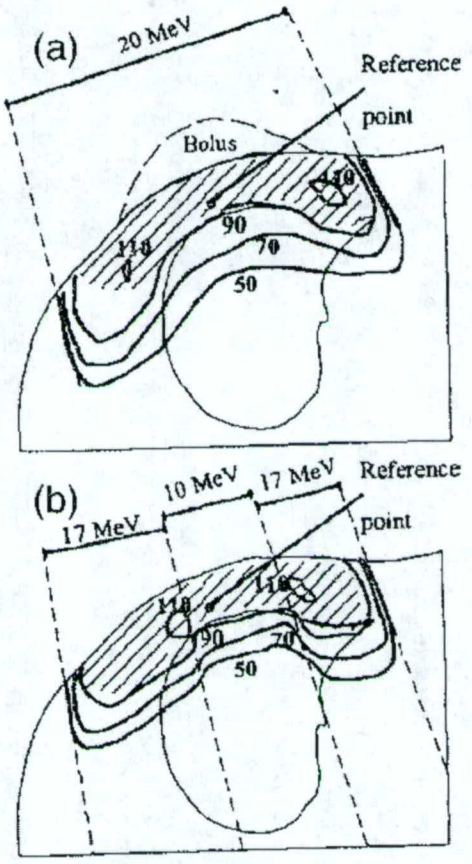

Figure 1.2. Comparison of bolus ECT to segmented-field ECT treatment plan for irradiation of the thoracic wall and the IMC after radical mastectomy. Dose distribution is shown in a transverse section for (a) the bolus ECT plan using 20 MeV electrons from a single portal and (b) the segmented-field ECT plan, which has three segments with a common isocenter. The segmented-field ECT plan uses 10 MeV electrons for the central segment and 17 MeV electrons for the medial and lateral segments. The reference point was used for dose normalization (from Zackrisson 1996).

Several advantages are associated with segmented-field ECT: 1) Treatment plans can be developed using existing technology; this requires an appropriate 3D treatment planning system that utilizes an accurate dose calculation algorithm (e.g. pencil-beam algorithm) and the ability to model beam edges accurately, 2) Dose-fall off (R_{90-10}) beyond the 90% isodose surface is sharper than with bolus ECT; and 3) This modality does not require fabrication of bolus (Hogstrom 2004).

Several disadvantages are associated with segmented-field ECT: 1) Commercial treatment planning systems do not provide a beam's eye view of PTV depth tool that could be used to help segmenting the field into smaller fields of different energies; this process, however, could be automated by incorporating some basic rules for abutting electron fields into treatment planning system algorithms, 2) Abutted electron fields not having matched penumbrae lead to increased/ decreased dose (hot/cold spots) in the abutment regions, 3) The ability to conform the 90% isodose surface may be limited by the coarse energy resolution of existing radiotherapy accelerators; 4) The use of many field segments can lead to increased beam-on time (monitor units), which results in more bremsstrahlung dose to the patient, and 5) Delivery of segmented-field ECT using current applicator-insert technology is impractical (Hogstrom 2004).

1.6 Electron multi-leaf collimation

Currently, the only way to deliver segmented-field ECT for most common linear accelerators is to fabricate lead-alloy insert(s) for each beam energy, with each insert possibly having multiple apertures. However, this method is suboptimal, in some cases impractical, because of the time required to accurately fabricate the inserts and to change the inserts during treatment.

Electron multi-leaf collimation (eMLC) can be used to produce segmented-field ECT dose distributions, and such a device could be used to produce highly conformal treatment plans. Numerous studies have been conducted on x-ray conformal therapy using multi-leaf collimation (MLC) (Brahme 1987, Powliss 1993, Webb 2001, Spirou 2003). Some preliminary studies have used an x-ray MLC for electron conformal therapy (Klein 1996, Zackrisson 1996, Klein 1998, Karlsson 1998). The potential for this technique has been illustrated by Klein (1998). However, the results suffer from large energy spacing and lack of a practical delivery method.

Other studies have also investigated the potential of using a dedicated electron multi-leaf collimator (eMLC) for ECT. Ma (2000) investigated the feasibility of optimizing energy- and intensity-modulated electron beams using a dedicated eMLC. They developed a thin-leaf eMLC and showed that

intensity-modulated electron fields can improve the homogeneity of dose to the breast and reduce the volume of lung treated to high dose. The Electron Research Group at M. D. Anderson also developed a prototype eMLC (Figure 1.3), which was shown to produce dose distributions and dose output similar to that using the applicator-lead alloy insert system (Antolak 2002, Boyd 2002, Hogstrom 2004).

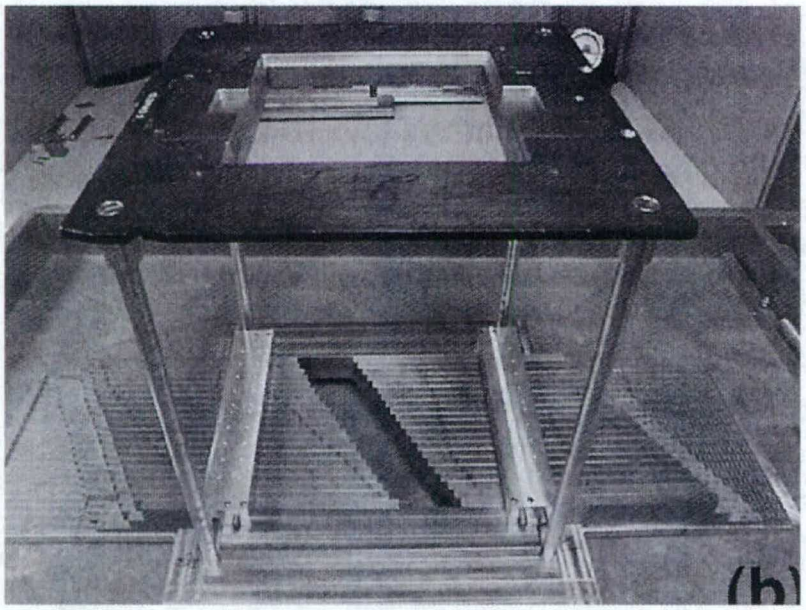

Figure 1.3. M.D. Anderson prototype eMLC designed for a Siemens Primus accelerator (Antolak 2002, Hogstrom 2004).

1.7 Hypothesis and specific aims

This work focuses on developing a method to produce conformal electron dose distributions for post-mastectomy radiation therapy by using multi-energy, multi-segmented electron fields rather than customized electron bolus. Compared to bolus ECT, this method should improve skin sparing and minimize $R_{90\text{-}10}$.

The hypothesis of this study is as follows: **Compared to bolus ECT for post-mastectomy irradiation, ECT with multi-energy, multi-segmented treatment fields has equivalent target coverage and equivalent (or better) normal tissue sparing and PTV dose uniformity**. The specific aims of the research are as follows: 1) Develop an algorithm to generate multi-energy, multi-segmented conformal electron treatment plans, 2) Verify that the algorithm can create optimized treatment plans for

simple targets, and 3) Verify that the algorithm can create optimized treatment plans for post-mastectomy patients that were previously treated with bolus ECT.

To achieve specific aim 1, an algorithm was developed that 1) segments an electron field based on PTV depth and 2) modifies the field segmentation to improve PTV coverage and/or critical structure sparing. The major goals of the algorithm are to ensure good PTV coverage (conformality and homogeneity) and to avoid delivering excessive dose to critical structures.

To achieve specific aim 2, the algorithm was used to create computer treatment plans for simple targets in a water phantom. For each simple target case, the PTV dose coverage and homogeneity, and critical structure sparing were examined.

To achieve specific aim 3, five post-mastectomy radiotherapy clinical cases, previously treated with bolus ECT, were selected. The algorithm was used to create a treatment plan for each of the five clinical cases. For each clinical case, the isodose distributions and dose volume histograms for each treatment plan were compared to the corresponding bolus ECT treatment plan. Specifically, PTV dose coverage and homogeneity, and critical structure sparing were compared.

Favorable results from this study should allow radiotherapy clinics that use an eMLC to provide electron conformal therapy for post-mastectomy radiation therapy without the added complexity of customized electron bolus manufacturing. Clinics without eMLC might be able to use lead-alloy inserts to achieve an equivalent result.

Chapter 2

Materials and Methods

2.1 Treatment planning and dose calculation

2.1.1 Electron beam treatment planning principles

The goal of treatment planning is to attempt to meet the prescription specifications of the radiation oncologist, which can include such things as target dose homogeneity and critical structure avoidance. At least five aspects must be considered when treatment planning: 1) properties of the electron beam, 2) effects of the patient's anatomy on the electron beam, 3) proper use of electron bolus, 4) proper use of collimation, 5) and methods of field abutment (Hogstrom 1991).

The most probable electron energy at the patient surface, $E_{p,0}$ is given by

$$E_{p,0} = C_1 + C_2 R_p + C_3 R_p^2 \qquad (2.1)$$

where $C_1 = 0.22$ MeV, $C_2 = 1.98$ MeV cm^{-1}, $C_3 = 0.0025$ MeV cm^{-2}, and R_p is the practical range of the electrons as determined from a broad beam depth-dose curve measured in water according to the recommendations of AAPM TG-25 (Khan 1991). At our institution, the 90% (of given dose) dose level is usually prescribed to cover the PTV. For maximum sparing of critical structures, the structure should be beyond the practical range of the electrons. A general rule of thumb is that the critical structure should be deeper than $E_{p,0}/2$ and the minimum energy for target volume coverage is $E_{p,0}$ (MeV) $\approx 3.3\ R_{90}$ (cm), where R_{90} is the depth of the distal 90% dose (Khan 1991). Normal tissues beyond R_p will be spared except for bremsstrahlung radiation, which is usually less than 5% of the maximum dose for energies below 20 MeV (Hogstrom 1991). There can be a strong field-size dependence of depth dose that must be considered in selecting beam energy, and it should be emphasized that the above "rules of thumb" hold for field sizes large enough to have side-scatter equilibrium on central axis.

The presence of irregular external surfaces and internal heterogeneities affects the dose distribution for an electron beam. A sharp gradient on the patient's external surface causes side-scatter equilibrium to be lost, resulting in a volume of decreased dose (cold spot) and a volume of increased dose (hot spot); this can occur as a result of bolus, surgical defects, or normal anatomy (Hogstrom 1991). The treatment planning system (TPS) is used to generate dose distributions corrected for heterogeneities. The treatment plan is optimized considering the dose distribution in the entire target volume. The planner tries to ensure that the prescribed dose covers the target and that critical and normal tissues are spared.

The planner should be aware that broadening of the penumbra with depth pulls in the 90% dose contour. The 90% isodose line falls inside the geometric field edge (projection of light field) at the depth of maximum dose by a margin of approximately 1 cm or less. A good standard practice is to leave a margin of at least 1 cm between the lateral edge of the target volume and the projected edge of the collimator (Hogstrom 1991). In addition, the lateral coverage of the 90% contour depends on air gap and depth for each beam energy. It is also important to ensure that adjacent treatment fields are abutted appropriately. Adjacent fields that overlap will produce a hot spot and fields that are separated will produce a cold spot in the treatment plan, resulting in dose inhomogeneity within the target.

2.1.2 Dose calculation

2.1.2.1 Hogstrom pencil-beam algorithm

A 3D implementation of the Hogstrom pencil-beam algorithm (PBA) was used for electron dose calculation. The Hogstrom PBA combines the Fermi-Eyges multiple Coulomb scattering theory with measured data to produce dose distributions (Hogstrom 1981). The algorithm models a broad electron beam as the sum of small pencil-beams, typically 2 mm x 2 mm, each beginning at the plane of final collimation. The pencil beams are propagated through air until they reach the patient surface, then through the patient CT data set. The fluence distribution of each pencil beam is a convolution of the

square pencil beam and a Gaussian function whose standard deviation, σ, is a function of the angular scattering power of the electrons at the calculation depth (Hogstrom 1981). The strength of the Hogstrom PBA has been its accurate dose calculation for irregular fields, varying air gaps, and irregular patient surfaces (Hogstrom 1981, 1983). The latter is unique to the Hogstrom PBA because it deconvolves the initial angular divergence, resulting in its being equivalent to redefining the pencil beams at the patient surface.

2.1.2.2 Pinnacle^3 script for COPPERPlan implementation of PBA

The Pinnacle^3 PBA is based on a 3D implementation (Starkschall 1991) of the Hogstrom PBA (Hogstrom 1981); however, it has many problems that prevent its use for segmented-field ECT (see Appendix C). Some of these problems were also found in the Starkschall (1991) implementation that was in COPPERPlan, our in-house TPS (Starkschall 1994). However, source code for this implementation was available. A new version, suitable for segmented-field ECT, was integrated with Pinnacle^3 through the use of a Pinnacle^3 script (jaa-compute_eTrial) and accessory scripts written in the Perl language. Together, the scripts extract beam and patient information from Pinnacle^3, convert that information into a format suitable for the COPPERPlan PBA, initiate the dose computation, and then send the dose information back into Pinnacle^3. The scripts are activated by pressing a button within the Pinnacle^3 Hot Scripts window.

2.1.3 Treatment plan evaluation

The TPS provides a variety of tools for evaluating and comparing treatment plans (see Appendix B). 2D and 3D isodose displays allow the planner to examine the isodose distribution with or without the patient CT data. In 2D displays, the isodose levels can be displayed as both a colorwash and as isodose lines. In 3D displays, the isodose levels can be displayed as solid or transparent surfaces. When evaluating plans, it is useful to set up a 3D isosurface display that shows the target volume and a

particular isodose surface. Transparent surface displays allow the planner to see through the isodose cloud to the target volume surface and evaluate the target coverage in three dimensions.

Dose statistics, including the minimum, maximum and mean dose, can be generated for any structure defined as a region of interest (ROI). The dose distribution to any ROI can also be summarized by a dose-volume histogram (DVH). The DVH provides plots of normalized or absolute volume versus normalized or absolute dose and displays the total volume that receives a given dose or greater. A DVH allows the planner to determine if the treatment plan has significant hot or cold spots. However, it does not provide any spatial information about the dose distribution.

Plans will be evaluated using several dose and dose-volume metrics for the PTV, critical structures, and non-target tissue. The mean dose to the target volume will be evaluated; dose homogeneity will be determined using the standard deviation of the target dose and the dose difference between the 90% and 10% volumes on the PTV DVH. For the non-target region, the volume receiving more than 4500 cGy will be evaluated; for the clinical cases, the absolute volume of the lung treated to more than 20 Gy will be used as the metric.

For a standard electron treatment plan, the dose is generally prescribed to 90% of given dose. However, segmented-field ECT involves several beams, so dose specification is slightly more complicated. As a starting point, each field will have the same given dose. However, individual field weights (or MU) may be adjusted up or down to give a better dose distribution (coverage or homogeneity).

2.2 Segmented-field ECT algorithm

2.2.1 General overview

An algorithm was developed to design a bolus-free, multi-energy, multi-segmented field treatment plan for post-mastectomy targets. The algorithm consists of two parts: a creation phase and a modification phase. The creation phase establishes a topographic energy map by utilizing electron beam R_{90} depth values to segment the PTV depth. Treatment fields are designed using three criteria: adequate

dose delivery to the target volume, dose homogeneity within the target volume, and avoidance of critical structures. Dose is then computed, and the resulting dose distribution is evaluated using the design criteria. The modification phase uses the existing plan (energy map and treatment fields) as the starting point for treatment planning, and outputs a new plan (field pattern) to better meet the design criteria. The treatment planning tools available in the Pinnacle[3] TPS were used as much as possible. Figure 2.1 shows a flow chart of the segmented-field ECT algorithm.

The planner begins designing the treatment plan by specifying a single orientation (gantry, couch and collimator angles) for an electron beam that is suitable to treat the PTV. In general, the PTV is approximately centered within the treatment field and perpendicular to the beam central axis. The electron beam is then divided up into a collection of sub-beams, each of which is assigned its own energy and weighting based on the PTV depth it covers and its contribution to the resulting dose distribution. The associated treatment fields are abutted to each other, i.e., the fields are neither gapped nor overlapped.

The creation phase can be broken down into six sub-tasks:

1) establish the planning target volume less margin (PTVLM),
2) create the topographic target depth map,
3) apply an extension margin to the PTV,
4) create the segmented target energy map,
5) quantize the segmented target energy map by placing the treatment fields using electron cutouts or eMLC,
6) compute dose.

The plan created using these tasks is the starting point for any subsequent field and/or energy changes in the modification phase. Once the initial plan is established and dose has been computed, the planner will examine the plan and determine if the treatment plan criteria have been meet. If the treatment plan criteria are satisfied, then the planner is finished. If the treatment plan criteria are not

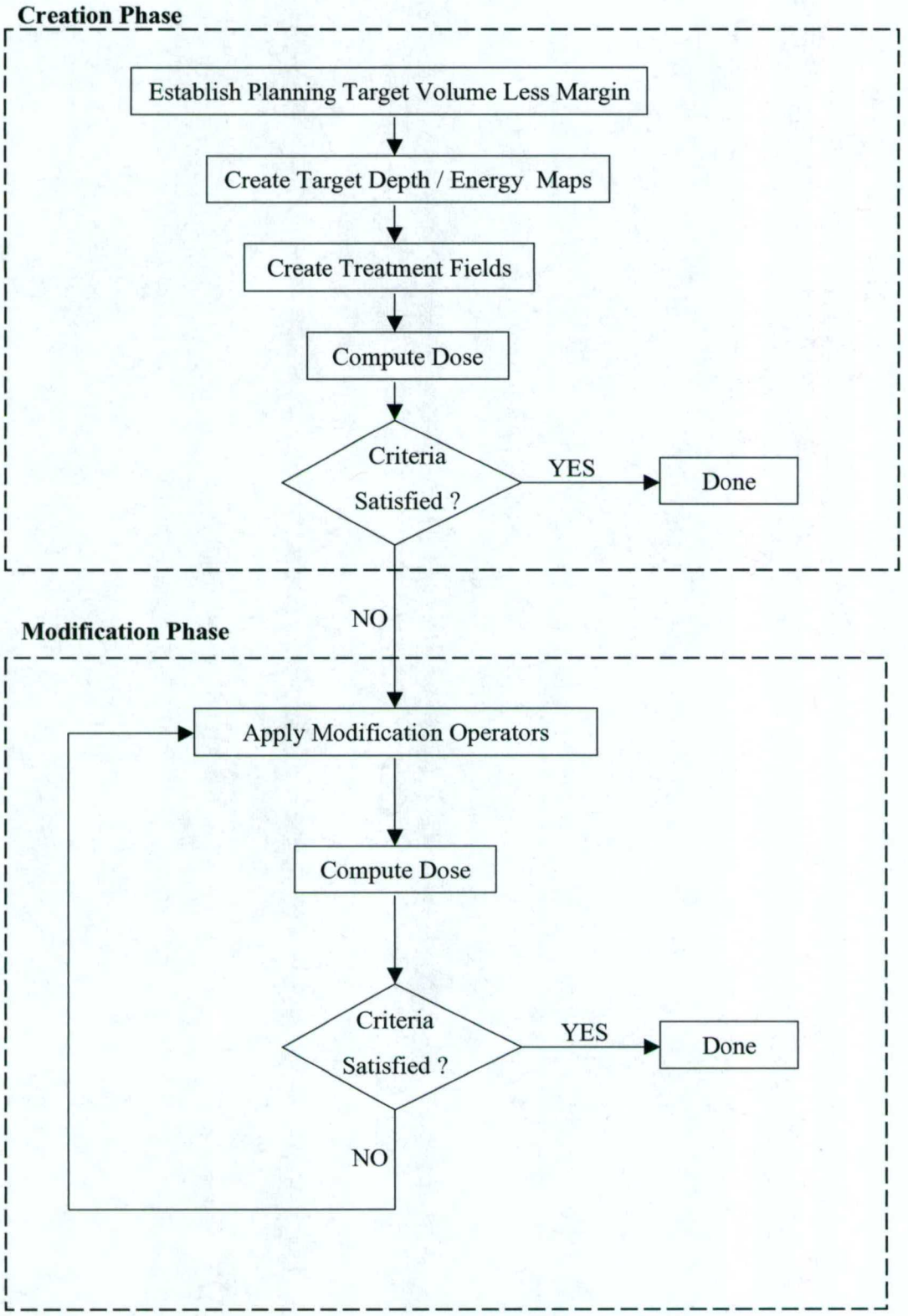

Figure 2.1. Flow chart showing the steps of the segmented-field ECT algorithm. The algorithm has two main phases: Creation and Modification phases.

satisfied, then the planner moves into the modification phase, where a variety of tools can be used to help meet the treatment plan criteria.

2.2.1.1 Establish the PTVLM

Several ROIs are usually defined in performing post-mastectomy radiation therapy: PTV, skin, lungs, and heart. The dose calculation algorithm requires that the skin surface contour be listed as the first ROI. All ROIs, except the PTV, were drawn by the treatment planner. The radiation oncologist outlines the PTV, which is the target area that will be treated with electrons. Figure 2.2 shows a clinical example of the skin surface, lungs, heart, and PTV ROIs.

The PTV less margin (PTVLM) is the PTV reduced (in the beam's eye view) by a PTV internal margin (Δ), usually between 0.5 and 1.5 cm. An internal margin is required because the edges of the PTV tend to slope towards the surface and the isodose contours for an electron beam naturally do the same at the field edge. Without this internal margin, the energy at the edge of the PTV would be needlessly reduced. This is similar to what Low et al. (1992) did when designing customized electron bolus.

A four-step process, shown in Figure 2.3, is used to obtain PTVLM. First, the PTV is expanded by a large margin (e.g. 5 cm) in the directions toward and away from the beam to obtain volume PTV′. Second, PTV′ is contracted (0.5, 1.0, or 1.5 cm) in all directions except towards and away from the beam to obtain PTV″. Third, the PTV is expanded by 0 cm using PTV″ as the limiting structure to obtain PTV‴. The volume PTV‴ is the volume that we wish to exclude from the energy map. Finally, the PTV is expanded by 0 cm using PTV‴ as the limiting structure to obtain the PTVLM.

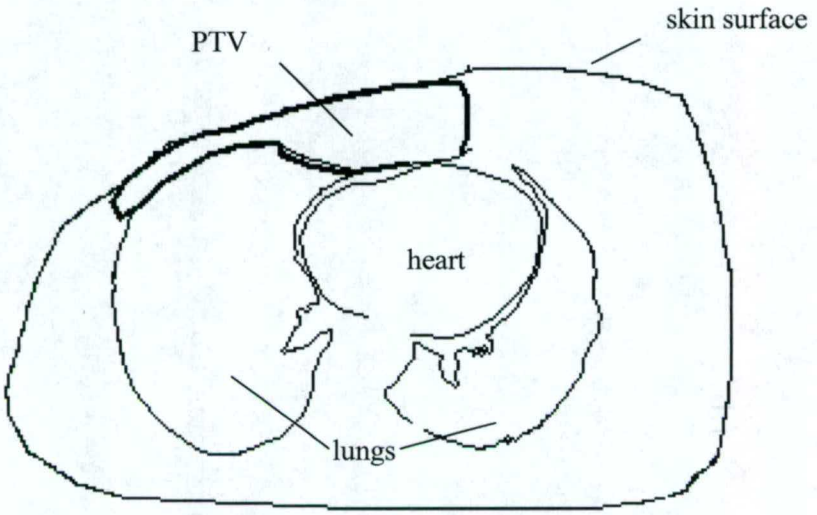

Figure 2.2. A transverse plane image showing the regions of interest (ROI) that are important in post-mastectomy radiation therapy. The PTV is the region to be treated.

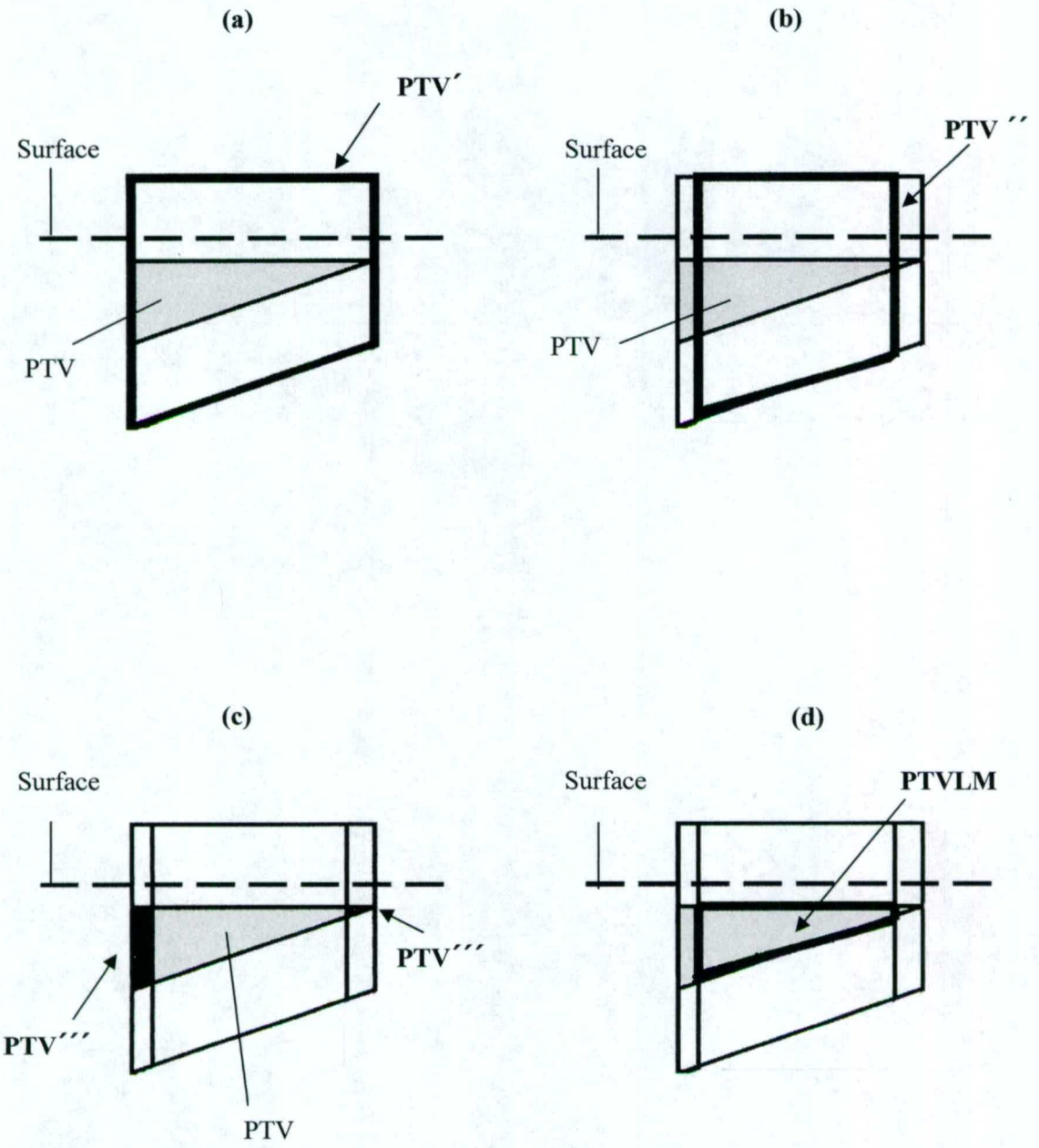

Figure 2.3. Planning target volume less margin (PTVLM) creation method. Each picture shows a transverse plane of a simple target (smooth wedge) in a water phantom. The horizontal (black dash) line represents the water phantom surface. The triangle (gray) represents the PTV. (a) PTV′ is created by expanding the PTV by 5 cm in the direction towards and away from the beam. (b) PTV″ is created by contracting PTV′ by 1 cm in all directions except toward and away from the beam. (c) PTV‴ is the volume of the PTV outside of PTV″ , and is obtained by expanding the PTV by 0 cm using PTV″ as the limiting structure. (d) PTVLM is created by expanding the PTV by 0 cm using PTV‴ as a limiting structure.

2.2.1.2 Target depth map

The topographic target depth mapping process begins by dividing the PTVLM into depth intervals based on the depth of the PTVLM distal surface from the skin surface. Each field is designed based on a specific target depth interval, and the electron energy is assigned according to the PTVLM depth using equilibrium field size (e.g. 10 cm x 10 cm) R_{90} values. Table 2.1 lists the most probable electron energy values ($E_{p,0}$) and equilibrium field size R_{90} values for all electron beam energies for two machines (Siemens Primus and Varian 2100C); the Varian 2100C machine offers higher electron energies than the Siemens Primus.

Table 2.1. The equilibrium field size (e.g. 10 cm x 10 cm) R_{90} values as a function of nominal beam energy for the Siemens Primus and Varian 2100 machines. These values were measured by the medical physics staff at M. D. Anderson during the commissioning process.

Primus	Nominal Energy (MeV)	5	7	8	10	12	15
	$E_{p,0}$ (MeV)	5.1	6. 8	8.1	9.5	11.9	14.2
	R_{90} (cm) distal	1.5	2.0	2.5	3.0	3.7	4.5
Varian	Nominal Energy (MeV)	6	9	12	16	20	NA
	$E_{p,0}$ (MeV)	6.5	9.3	12.3	15.5	20.5	NA
	R_{90} (cm) distal	2.0	3.0	4.0	5.0	6.1	NA

The process used to create the energy map is shown in Figure 2.4. First, the skin surface is contracted away from the beam by a distance equal to R_{90} to create a contracted skin volume (skin_[depth]). Second, the PTVLM is expanded by 0 cm using the contracted skin surface as a limiting structure to create a PTV depth region (PTV_[depth]), which is the portion of the PTV shallower than

the R_{90} depth. Finally, the PTV is expanded by 0 cm using the previous region as a limiting structure, which gives the portion of the PTV deeper than the R_{90} depth.

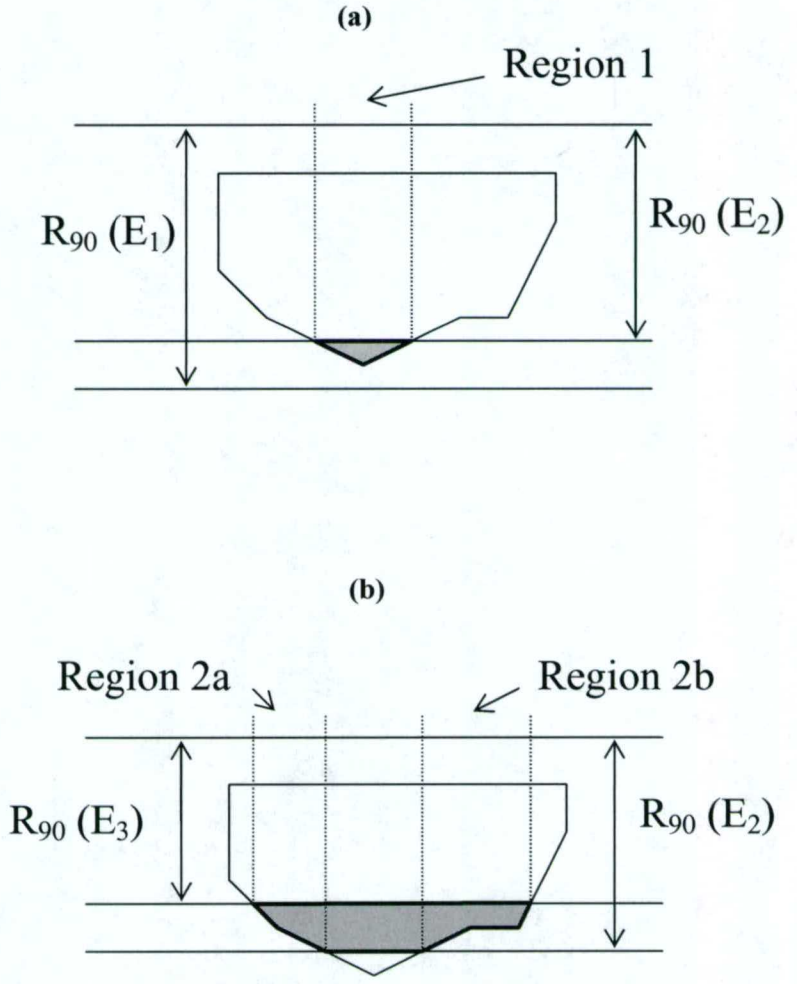

Figure 2.4. Illustration of depth region segmentation. (a) The energy E_1 is the lowest energy with an R_{90} greater than the PTV depth, and energy E_2 is the next lower energy. The skin surface is contracted by R_{90} (E_2) and the intersection between the PTVLM and the contracted skin surface is the first depth region. The outer boundary of this depth region is shown as "Region 1". This region requires an energy of E_1 to have adequate depth penetration of the electrons. (b) The intersection between the contracted skin surface for the next lower energy (E_3) and the PTVLM is the second depth region. By visualizing the first and second depth regions together, two regions of the PTVLM with depths between R_{90} (E_2) and R_{90} (E_3) can be identified. These regions require energy E_2 for adequate depth penetration of the electrons. This is repeated for all energies. For illustrative purposes, beam divergence is not shown.

2.2.1.3 Treatment field creation

The electron treatment field must be larger than the beam's eye view (BEV) projection of the PTV to allow for beam penumbra; therefore we need to extend the sub-beams outside the BEV projection of the PTV. For a given sub-beam at the edge of the PTVLM, the amount of extension depends on the depth at the edge of the PTV, the energy of the sub-beam, and the amount of normal tissue lateral to the PTV to spare. Initially, a 1-cm extension is applied uniformly to the PTV. A simple approach is to expand PTV in all directions perpendicular to the beam by 1 cm, which is referred to as the PTV plus margin (PTVPM).

Figure 2.5 illustrates how the initial treatment fields are created for this work. The auto-block tool is used to create the initial electron field cutouts for each depth interval. Starting with the deepest PTVLM depth interval, fields are created to expose the depth intervals while blocking the other depth intervals. After creating the fields, the block outline is converted to "manual" mode, which makes the block coordinates editable. Block coordinates can be edited using the tools available in Pinnacle[3], or by directly editing the text file describing the treatment plan (plan.Trial). The latter is particularly useful for ensuring that there are no field gaps or overlaps that will affect the dose distribution. Fields at the edge of the PTVLM are extended outside the PTV to ensure PTV coverage. In this work, fields with straight-line boundaries were used where possible, which made the field editing process easier. Once field(s) for the deepest regions of the PTVLM have been established, the next shallower depth interval is displayed in the BEV. Fields are then drawn to cover this depth interval while avoiding fields that cover deeper depth intervals. This process is repeated for the remaining PTVLM depths. The result is the creation of non-overlapping fields based on PTVLM depth to treat the PTV. To ensure that there are no gaps or overlaps, the field outline coordinates are also plotted using a spreadsheet program.

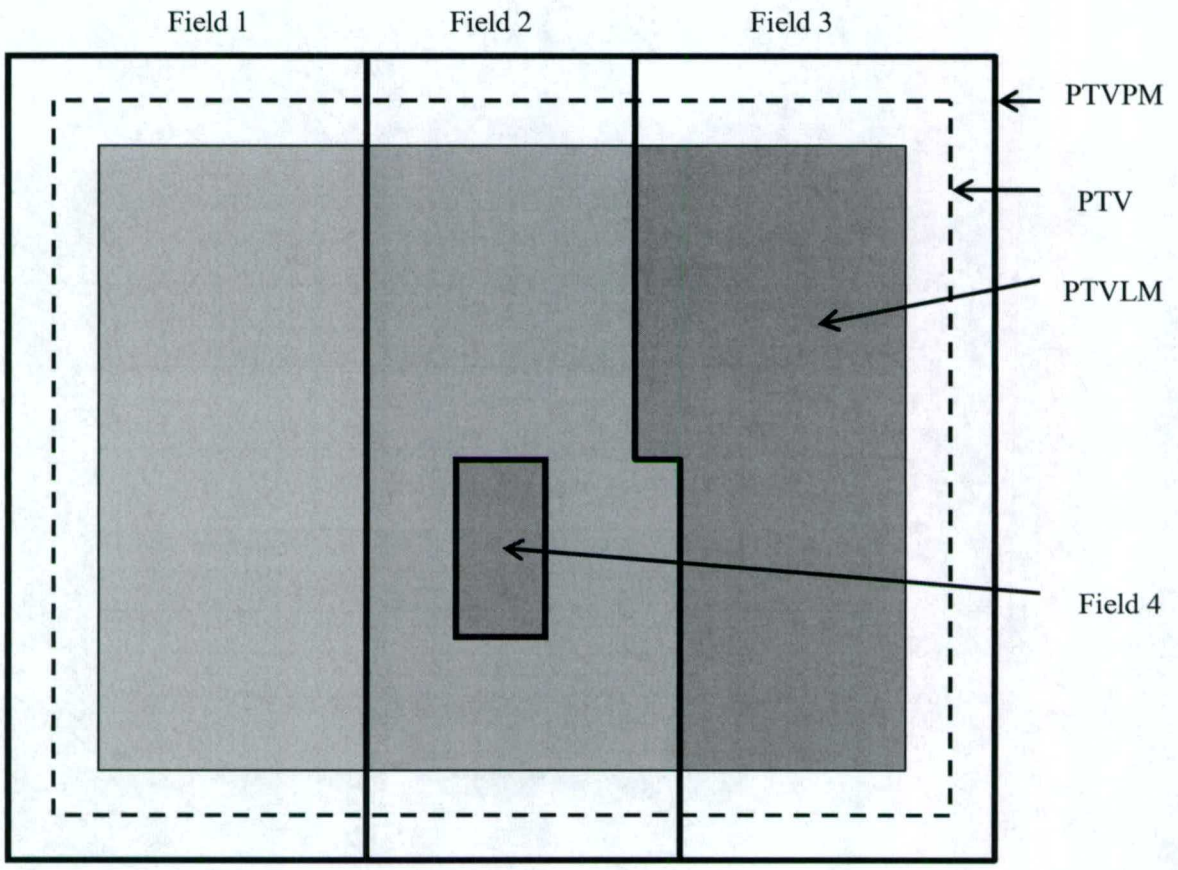

Figure 2.5. Schematic BEV of field segmentation. The gray-shaded regions are different depth regions of the PTVLM. The electron field (PTVPM, or PTV plus 1-cm margin) is divided into subfields based on the depth regions. Depth regions at the edge of the PTVLM are extended to fill the PTVPM as shown.

2.2.1.3.1 Dealing with small depth regions

The above example is a fairly simple case for creating an initial treatment plan. More realistic treatments plans present a greater challenge. The procedure used for creating electron fields can produce many small fields for realistic patient cases.

For each region less than 2 cm x 2 cm, some field adjustments are required. Dose for field sizes smaller than 2 cm x 2 cm can not be computed because the relative output factors for these field sizes were not measured during the machine commissioning process. Either margin expansions and/or "connector" regions are used to make the field size at least 2 cm x 2 cm. Unfortunately, the procedure

used for creating the electron fields (described earlier) can produce such small fields at different depth intervals. If so, then these fields are dealt with in the following manner:

(a) If a single target region exists that is less than 2 cm x 2 cm, then a field is placed about the region and the field is expanded by some margin to ensure the R_{90} value will cover the target depth region. If expanding the field does not result in the R_{90} covering the region, then the beam energy is increased. For fields smaller than the equilibrium field size (i.e., the field size after which there is little to no change in percentage depth dose), the R_{90} value for the smaller field is closer to the surface than for the equilibrium field size R_{90} value; therefore, a higher energy beam is required to cover the target depth. Table 2.2 show R_{90} values as a function of field size and beam energy for two linear accelerators used in this study. These tables are used to determine the minimum energy required for the desired isodose coverage at the PTV depth.

(b) If multiple target regions (i.e., smaller than 2 cm x 2 cm) exist and have similar size, then a treatment field is placed about each target region and a diagonal "connector" region of 0 cm width can be used to connect the fields. Due to the dose grid spacing (2 mm), the use of non-diagonal "connector" regions can possibly produce dose artifacts within the dose distribution if the "connector" region happens to be positioned along a dose grid line. The resulting "connected" field size must be at least 2 cm x 2 cm; otherwise, each target region is treated using a single field as described in (a) above.

Table 2.2 R_{90} values as a function of field size and beam energy for the (a) Siemens Primus machine and (b) Varian 2100 machine. This data was measured during the machine commissioning process by the M. D. Anderson medical physics staff.

(a)	R_{90} as a Function of Field Size and Energy					
Field Size (cm^2)	5 MeV	7 MeV	8 MeV	10 MeV	12 MeV	15 MeV
2 x 2	1.3	1.6	1.8	2.0	2.3	2.5
3 x 3	1.5	1.9	2.3	2.6	3.0	3.3
4 x 4	1.5	2.0	2.4	2.8	3.5	3.9
5 x 5	1.5	2.0	2.4	2.9	3.6	4.3
6 x 6	1.5	2.0	2.4	2.9	3.6	4.3
8 x 8	1.5	2.0	2.4	2.9	3.7	4.5
25 x 25	1.5	2.0	2.4	2.9	3.7	4.5

(b)	R_{90} as a Function of Field Size and Energy				
Field Size (cm^2)	6 MeV	9 MeV	12 MeV	16 MeV	20 MeV
2 x 2	1.6	2.0	2.4	2.8	3.2
3 x 3	1.9	2.7	3.1	3.6	4.1
4 x 4	2.0	2.9	3.6	4.1	4.7
5 x 5	2.0	3.0	3.8	4.5	5.2
6 x 6	2.0	3.0	4.0	4.8	5.5
8 x 8	2.0	3.0	4.0	5.0	5.9
25 x 25	2.0	3.0	4.0	5.0	6.1

2.2.1.4 Segmented target energy map quantization

After the treatment fields have been determined using the segmented target energy map, a decision on how to quantize the electron beams must be made: electron cutouts or eMLC. If electron cutouts are used, then the shape of the cutouts will coincide with the segmented target energy map treatment fields. If an eMLC is used, then the leaf resolution and leaf placement characteristics must be considered with respect to the segmented target energy map treatment fields.

2.2.1.5 Dose computation

The last step in the Creation Phase is to compute dose. For the initial plan, the default beam weight of unity (100% for each beam) is used with a prescribed dose of 4500 cGy (90% of 5000 cGy); this is equivalent to setting a given dose of 200 cGy for each beam. Dose is then computed and the plan is evaluated.

The next step is to optimize the weighting for each beam to obtain better PTV coverage. This can also reduce any hot and/or cold spots that exist within the PTV due to the multiple field junctions. The Pinnacle^3 TPS IMRT module provides a way to optimize beam weighting using dose-volume based objective functions and constraints. An objective function is a goal that the planner would like to meet and the Pinnacle^3 TPS penalizes solutions that do not meet the objective. A constraint is a limit that must be satisfied. The optimization algorithm uses a sequential method to minimize a quadratic objective function, which is constructed from a set of dose-based or dose-volume-based objectives for individual ROIs (ADAC, 2001). During optimization, the software attempts to meet each objective without violating the constraints. If the software cannot meet an objective, the objective value it assigns is directly related to the difference between the computed and specified dose, and proportional to the weight assigned to the objective. Objectives and constraints can be set to one of five types: 1) maximum dose to a region of interest (ROI), 2) maximum dose to a percentage of an ROI, 3) minimum dose to an ROI, 4) minimum dose to a percentage of an ROI, and 5) uniform dose to an ROI. After optimizing the plan, the planner must evaluate the dose results to ensure that the plan is clinically acceptable. If so, then

the planner is finished. If the plan is not clinically acceptable, then the planner continues the Modification Phase, described below. The optimization process can be used as often as needed during the modification phase.

2.2.2 Modification phase

The Modification Phase is used to adjust (1) the shape of the fields, (2) the beam energy, and/or (3) the beam weighting to better satisfy the design criteria, e.g. to improve PTV coverage and/or critical structure sparing. All of the modification techniques operate within the BEV projection of the PTV. The treatment planning tools available in Pinnacle^3 TPS are used as much as possible. One or more of the techniques described below are applied to the treatment plans. Then the dose is re-computed and beam weights optimized before re-evaluating the treatment plans.

2.2.2.1 Field edge expansion (contraction)

The purpose of field edge expansion (contraction) is to expand (contract) the field edge margin in 0.25 cm increments to improve dose coverage at the edge of the PTV. During the creation phase, a default PTV margin extension of 1.0 cm is used. After computation of the initial plan, the planner might discover that some portions of the PTV are not completely covered by the 90% isodose line. One technique that can be used to improve coverage is to expand (contract) the field edge margin from 1.0 cm to a higher (lower) value. To do this, the planner edits the plan.Trial field coordinates that need to be adjusted. Only those portions of the sub-fields that are located along the edge of the treatment field are adjusted. The interior treatment sub-fields are not adjusted. The extent of the field expansion can be limited by the presence of adjacent critical structures and the available field size (i.e., defined by the electron cone size or eMLC leaf translation range).

2.2.2.2 Energy-smoothing

The purpose of energy-smoothing is to adjust the beam energy of the field so that dose coverage of the PTV region is improved and sharp energy gradients at adjacent fields are reduced. During the creation phase, fields are placed beginning with the deepest portion of the PTV. In many cases, shallower PTV depth is adjacent to a deeper PTV depth. Based on the creation phase of placing fields and setting beam energies, a low-energy subfield might be adjacent to or contained within a high-energy subfield. If a small low-energy subfield is located inside a higher-energy subfield, then the two subfields will be merged and assigned to the higher energy. If a low-energy subfield is located adjacent to a high-energy subfield, the dose coverage might be improved by reducing the energy difference between the two subfields by increasing the energy in the lower energy region.

2.2.2.3 Dilation of internal field size

The purpose of dilation is to expand the field size (if it results in increasing R_{90}) which can result in better coverage of the PTV. This is used on interior fields only, not fields at the edge of the PTV (i.e., field expansion/contraction). In the creation phase, the PTV depth map was determined using equilibrium field size R_{90} values. The resulting subfield might be smaller than the equilibrium field size; this will cause the dose to not cover the PTV depth completely. By expanding the size of a field, the R_{90} value for that subfield increases, resulting in better PTV coverage. Table 2.2 shows the R_{90} values for the two linear accelerators used in this study. Note that as the field size decreases, the R_{90} value shifts closer to the water phantom surface for a given nominal energy.

For each local peak in the energy distribution, the maximum depth of the PTV is determined. The effective size of the local peak is calculated (ignoring the surrounding areas) and the percentage depth dose at the maximum PTV depth is compared to the desired isodose coverage. If the percentage depth dose is less than the local maximum of the PTV depth, which can happen due to loss of lateral scatter equilibrium, then the local peak in the energy distribution is expanded equally in all directions until the effective field size is sufficent to cover the PTV depth. The range of the field expansion value

is between the initial field size and a field size that ensures that the 90% isodose line covers the local PTV depth.

2.2.2.4 Increase (decrease)-coverage

Increase-coverage is used to move the 90% isodose line beyond the PTV by uniformly increasing all beam energies. This can be useful if the 90% isodose line is shallower than the PTV distal surface. Similarly, if the 90% isodose line is deeper than the PTV, decrease-coverage will decrease the beam energy. Beam-weight optimization will then be used to move the 90% dose coverage towards the PTV depth.

2.2.2.5 Region connectors

Region connectors are used to join regions located at the same PTV depth that are distantly separated or concentrically displaced. For the case of small (less than 2 cm x 2 cm) distantly separated regions that are of similar size, it would perhaps be useful to join the regions to form a larger treatment field.

2.2.2.6 Energy increase (decrease)

Energy increase (decrease) is used to increase (decrease) the energy of a single subfield. This technique is used when the treatment plan may be acceptable except for a single region (or a few regions) for which the 90% isodose line does not cover the PTV. The planner would increase (decrease) the beam energy of the field in an attempt to move the 90% isodose line away (toward) from the PTV region. This differs from the previously described "coverage" modifier that modifies the energy of all subfields.

2.2.2.7 Electron fluence increase (decrease)

Electron fluence increase (decrease) is used to increase (decrease) the MU for a beam used to treat a single field using the beam weight optimizer. This technique is used when the treatment plan may be acceptable except for a single region for which the 90% isodose line that dose not quite cover (extends beyond) the distal target edge or where cold spots appear at field junctions and within the PTV. If a considerable increase (decrease) in MU is needed, then the plan should be re-evaluated and the beam weight optimizer utilized again using different objectives and constraints.

2.2.2.8 Segmented-field ECT algorithm limitations

The tools available in the Pinnacle^3 TPS make it very difficult to create a depth map for gantry angles other than the ordinal angles (0°, 90°, 180°, 270°). However, for other gantry angles, it is possible to temporarily rotate the PTV and skin contours, create the depth map, then restore the original contours with the aid of scripts.

A limitation of the dose-computation algorithm is that it requires that all fields be at least 2 cm x 2 cm. If the depth map produces target regions smaller than 2 cm x 2 cm, then the planner must modify the subfields to be able to compute dose. Methods for doing this were described above.

2.3 Water phantom simple targets

2.3.1 General overview

Six simple targets placed in a 30 x 30 x 30 cm^3 water phantom were designed to test the algorithm without the additional complexities associated with clinical cases. The shapes of the targets were chosen to evaluate certain aspects of common clinical cases. Two key questions, related to algorithm development, were answered by developing treatment plans for the simple targets: (1) How to select the beam energy and (2) How to place the fields to conform the 90% isodose line to the distal target edge. As the simple targets were used, the capabilities and limitations of the algorithm and TPS became apparent, and the algorithm was modified as a result.

2.3.1.1 Smooth wedge-shaped target

The first simple target is a smooth wedge as shown in Figure 2.6. It is positioned 1 cm deep from the anterior surface of the water phantom. The target depth varies from 1 cm (target proximal surface) to 3.5 cm (most distal target depth); the dimensions of the smooth wedge are 12 cm x 11 cm. Although a simple-shaped target, it forces the planner to establish a method for selecting the appropriate electron energy based on target depth and it provides insight on where to place the initial fields and how to modify them. This target might also provide insight into the energy resolution needed to perform electron conformal therapy, margins required between the target and beam edge, and hot/cold spots resulting from numerous abutted electron fields.

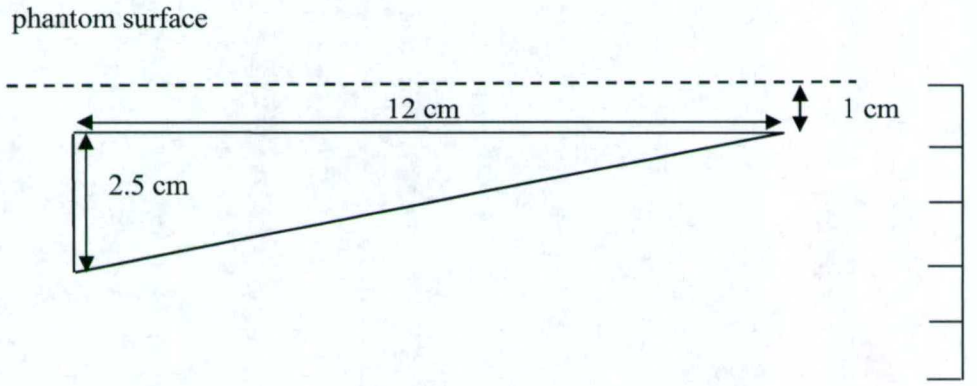

Figure 2.6. A transverse plane of a smooth wedge simple target in a water phantom. The target (black solid) is positioned 1 cm deep from the anterior surface (black dash) of the water phantom. The target depth varies from 1 cm (target proximal surface) to 3.5 cm (most distal target depth); the dimensions of the smooth wedge are 12 cm x 11 cm.

2.3.1.2 Step wedge-shaped target

The second simple target is a step wedge target having dimensions of 14 cm x 9 cm as shown in Figure 2.7. It is positioned 1 cm deep from the anterior surface of the water phantom, and the target depth varies from 1 cm (target proximal surface) to 3.5 (most distal target depth) and each step of the wedge is 0.5 cm. The defined steps along the target distal surface provide a challenge in determining which energy to choose at target boundaries that lie between two electron beam R_{90} values. Also, where the fields are placed will depend on the sharp target gradient.

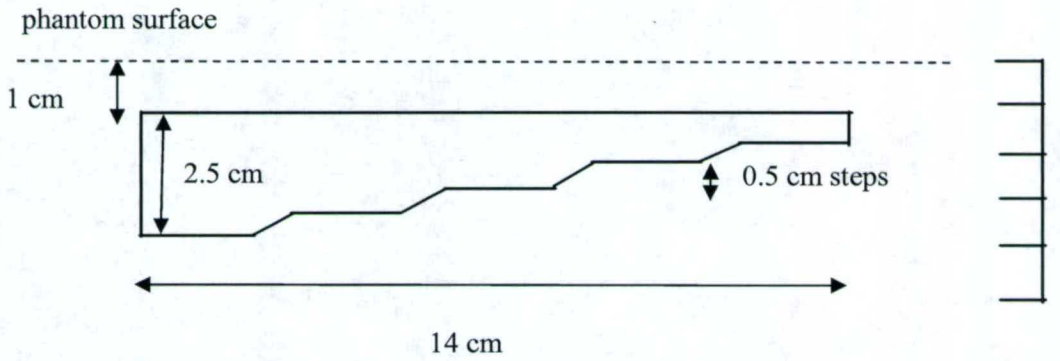

Figure 2.7. A transverse plane of a step wedge simple target in a water phantom. The target (black solid) is positioned 1 cm deep from the anterior surface (black dash) of the water phantom. The target depth varies from 1 cm (target proximal surface) to 3.5 (most distal target depth) and, each step of the wedge is 0.5 cm. The dimensions of the step wedge are 14 cm x 9 cm

2.3.1.3 Inverted well-shaped target

The third simple target is an inverted well target with dimensions of 8 cm x 9 cm, as shown in Figure 2.8. This target is positioned 1 cm deep from the anterior surface of the water phantom, and its depth varies from 1 cm (target proximal surface) to 3 cm (most distal target depth), and the step of the well is 1 cm. This particular shape is more clinically realistic than the first two simple targets. It represents, for example, a target that lies superior, yet adjacent to some critical structure. The challenge lies in selecting the appropriate beam energy so that a critical structure in the "well" is not over-dosed.

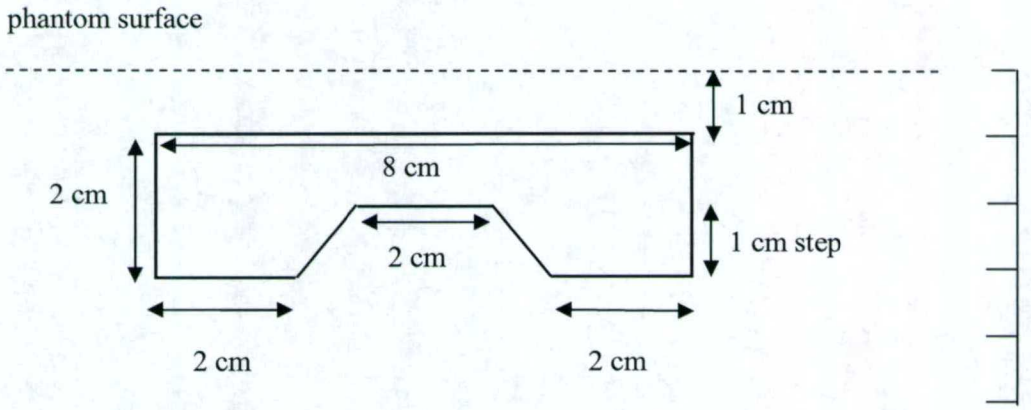

Figure 2.8. A transverse plane of an inverted well simple target in a water phantom. The target (black solid) is positioned 1 cm deep from the anterior surface (black dash) of the water phantom. The target depth varies from 1 cm (target proximal surface) to 3 cm (most distal target depth) and, the step of the well is 1 cm. The dimensions of the inverted well target are 8 cm x 9 cm.

2.3.1.4 Pentagon-shaped target

The fourth simple target is a pentagon shaped-target having dimensions of 12 cm x 9 cm, as shown in Figure 2.9. It is positioned 1 cm deep from the anterior surface of the water phantom. This target varies in depth from 1 cm (target proximal surface) to 3.5 cm (most distal target depth). The pentagon target is the inverse case of the well target, i.e., it is deepest in the middle.

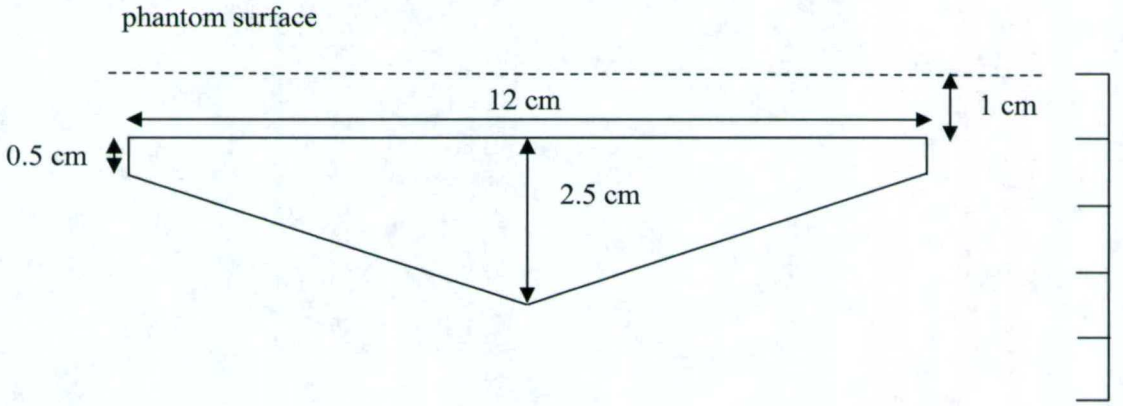

Figure 2.9. A transverse plane of a pentagon-shaped simple target in a water phantom. The target (black solid) is positioned 1 cm deep from the anterior surface (black dash) of the water phantom. The target depth varies from 1 cm (target proximal surface) to 3.5 cm (most distal target depth). The dimensions of the pentagon-shaped target are 12 cm x 9 cm.

2.3.1.5 Rectangular toroid-shaped target

The fifth simple target is a rectangular toroid target having dimensions of 12 cm x 9 cm, as shown in Figure 2.10. It is positioned 1 cm deep from the anterior surface of the water phantom. The target depth varies from 1 cm (target proximal surface) to 3.5 (most distal target depth). A central opening measures 4 cm x 3 cm. It represents a target that completely surrounds a critical structure. The challenge associated with this target is how the fields are chosen.

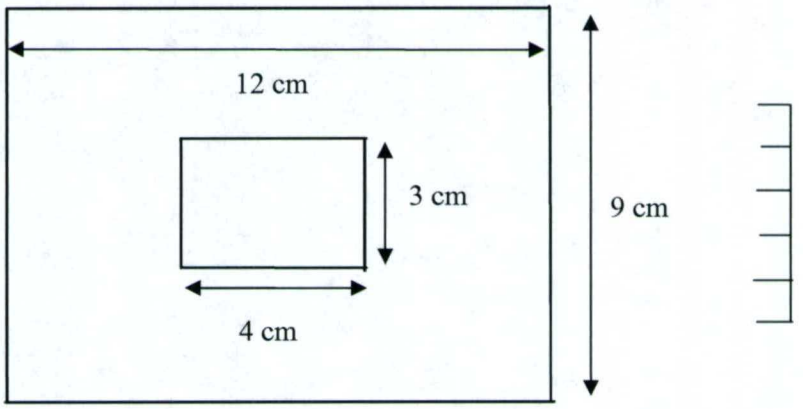

Figure 2.10. A coronal plane of a rectangular toroid simple target in a water phantom. The target (black solid) is positioned 1 cm deep from the anterior surface of the water phantom. The target depth varies from 1 cm (target proximal surface) to 3.5 (most distal target depth). The dimensions of the toroid target are 12 cm x 9 cm. A central opening measures 4 cm x 3 cm.

2.3.1.6 Three-dimensional shaped target

The first four simple targets have translational symmetry in the superior-inferior direction, and the fifth simple target has eight-fold mirror symmetry. Because of the high degree of symmetry, it is expected that it will be relatively easy to create treatment plans for these targets. The sixth target, a three-dimensional target, does not have any translational or mirror symmetry, and is a more realistic test for the algorithm. The target, shown in Figure 2.11 is 14 cm x 13 cm x 2.5 cm and it is located 1 cm from the anterior surface of the water phantom.

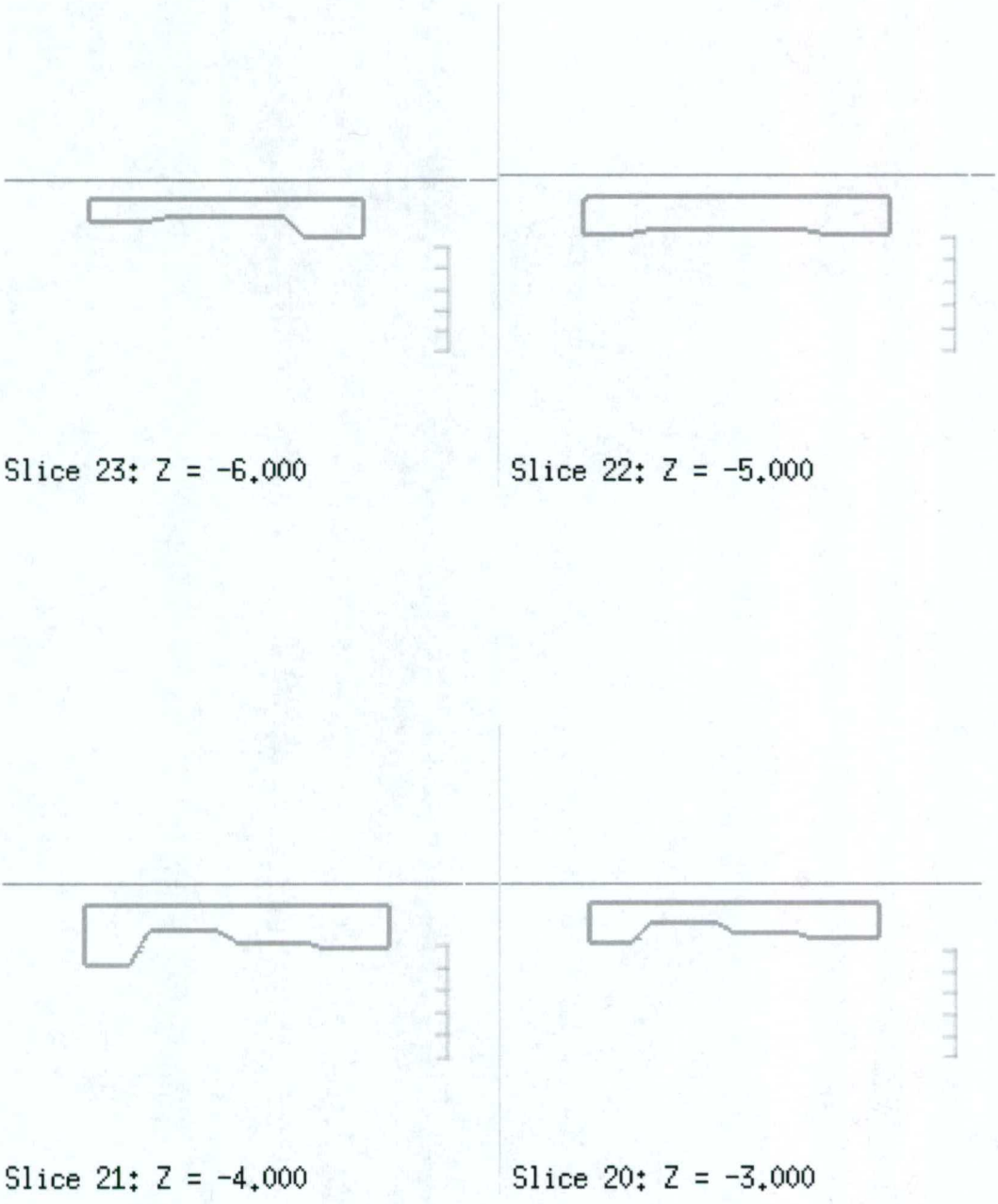

Figure 2.11. Series of transverse planes of the 3-D target in a water phantom. The proximal surface of the target is 1 cm below the water phantom surface; the target distal surface varies in depth (up to 3.5 cm) from the water phantom surface. Target dimensions are 14 cm (width, indicated) x 13 cm (length, series of images).

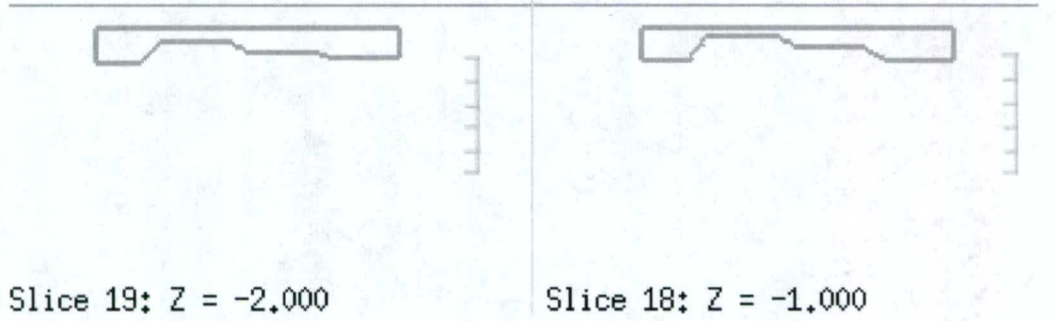

Slice 19: Z = -2.000

Slice 18: Z = -1.000

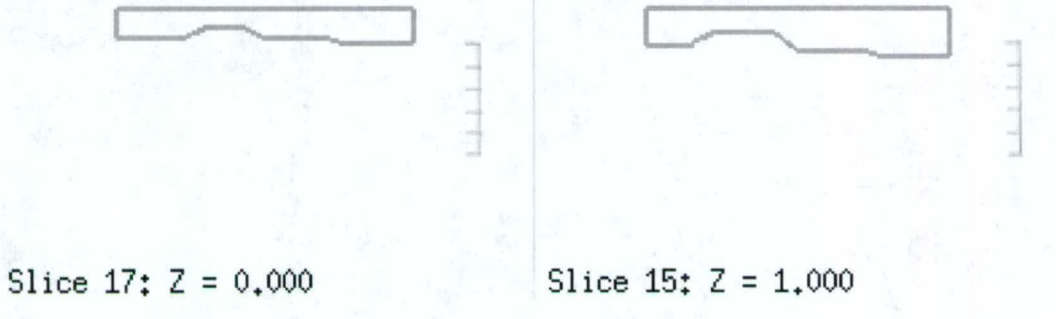

Slice 17: Z = 0.000

Slice 15: Z = 1.000

Figure 2.11. Continued.

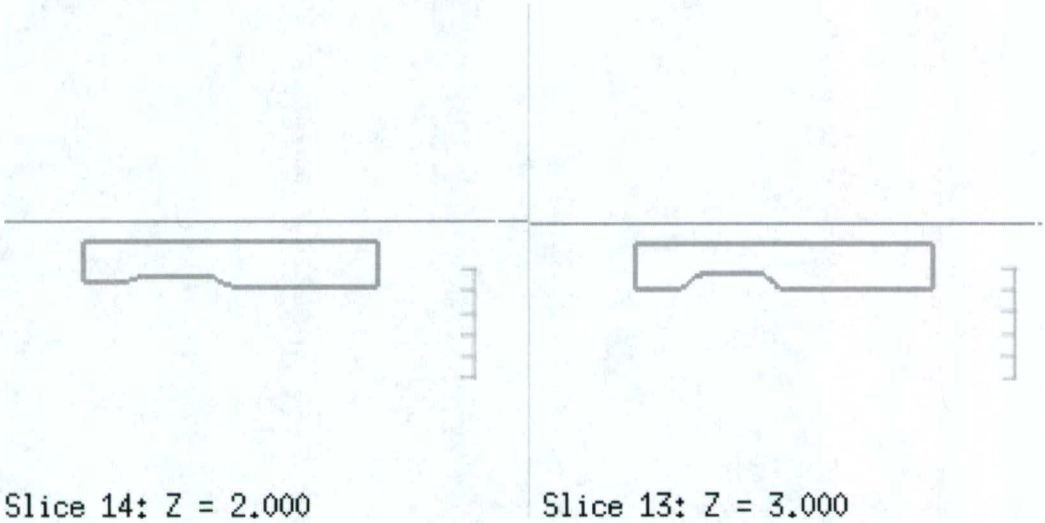

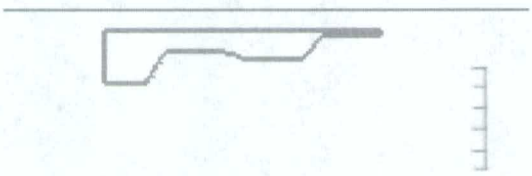

Figure 2.11. Continued.

2.4 Patient cases

2.4.1 General overview

Using simple targets to test and evaluate the algorithm is beneficial; however, to be useful in a clinical setting, more rigorous testing of the algorithm must be performed. One method to do this is to subject the algorithm to the challenge of planning actual clinical targets. With more complex 3-D target

shapes that are located near critical structures, additional limitations of the algorithm will be identified. Five patients who received post-mastectomy radiotherapy with bolus ECT will be utilized for this study. CT images of each patient were obtained in treatment position and the PTV was delineated by the patient's radiation oncologist.

For these patients, treatment plans were generated using M. D. Anderson's COPPERPlan treatment planning system (Starkschall 1994). Customized electron bolus was designed using Low et al.'s (1992) algorithms in COPPERPlan so that the distal surface of the wax bolus matched the skin surface, and the proximal surface was designed to conform to the 90% isodose surface to the distal surface of the PTV (Starkschall 1993, 1994). Dose was calculated using a PBA with heterogeneity corrections (Hogstrom 1981, Starkschall 1991). The resulting customized bolus was manufactured and then used for patient treatment. Perkins (2001) described the treatment plans for two of the patient cases studied here (patients #2 and #3).

For this study, all CT image data sets, along with PTV contours and bolus ECT dose distributions were transferred to the Pinnacle^3 TPS. This provided a way to compare the dose distributions for treatment plans developed in this study to those for the actual customized bolus plans, the current M. D. Anderson standard of treatment for ECT. Although the individualized patient prescriptions varied widely, for comparison purposes the electron bolus plans were normalized to deliver 50 Gy in 25 fractions (to 100% of given dose). All segmented-field ECT plans were also planned to deliver 50 Gy in 25 fractions.

2.4.2 Patient 1

Patient 1, a 62-year old female, was diagnosed with a T_2N_0 carcinoma of the left breast. The primary tumor was 3.0 cm x 1.5 cm x 1.5 cm in size and 0/8 lymph nodes were positive. She was treated with a left-modified radical mastectomy and axillary nodal dissection with no adjuvant therapy.

Several years later, the patient was found to have a 4.2-cm recurrence in the inferomedial third of the surgical scar. There was no palpable axillary or supraclavicular adenopathy. Radiographic examinations revealed adenocarcinoma consistent with a recurrence of the original primary breast disease. A fine needle aspirate was obtained that was consistent with metastatic adenocarcinoma. She was noted to have two separate nodules of primary disease, one being 2.0 cm x 1.8 cm x 1.8 cm and the second being 1.5 cm x 1.5 cm x 1.5 cm. The nodules were excised with a negative deep margin but a positive superior margin.

Without the use of bolus, the highly variable chest wall thickness would cause needless irradiation of portions of the lung, and this effect would be enhanced by variations in the skin surface that create dose heterogeneities in the underlying treatment volume. Because of the partial resection of the ribs, it was desired to fill the surgical scar with bolus to protect the left lung from excessive dose.

The skin surface and the general location of the distal surface of the PTV were at an angle of 35° with respect to a surface perpendicular to the anterior-posterior direction. A gantry angle of 35° was selected for the electron beam, placing the distal surface of the PTV approximately perpendicular to the beam's central axis. The maximum depth of the PTV was determined to be 2 cm from the skin surface (Figure 2.12).

The left chest wall was treated with medial and lateral tangential fields of Cobalt-60 photons to a dose of 50 Gy in 25 fractions over five weeks. The tumor bed was boosted an additional 16 Gy at 2 Gy per fraction using appositional electrons with the customized bolus. The left supraclavicular fossa was treated with 9 MeV electrons to 50 Gy in 25 fractions over five weeks. The left internal mammary chain and medial chest were treated with 12 MeV electrons to 50 Gy in 25 fractions over five weeks. For the purposes of this study, the 16 Gy bolus plan was delivered as 45 Gy (to 90% given dose) in 25 fractions.

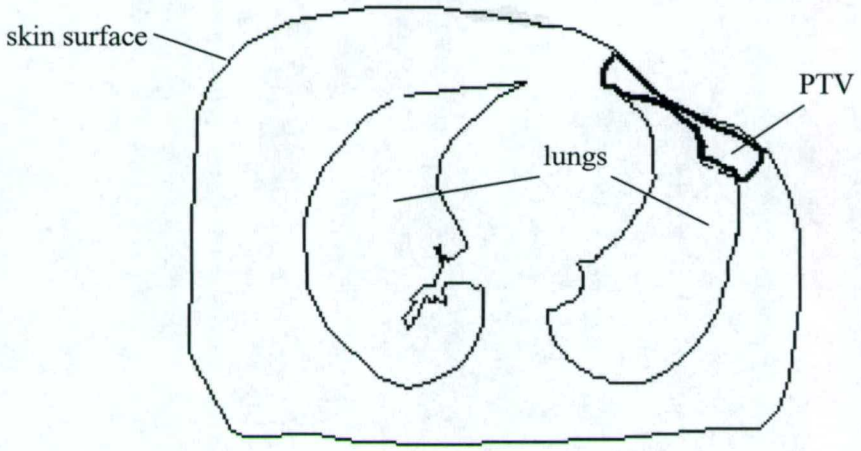

Figure 2.12. Transverse plane of Patient #1showing the skin, lung, and PTV contours.

2.4.3 Patient 2

Patient 2, a 37-year old female, was diagnosed with a 2.5-cm invasive ductal carcinoma of the right breast with extensive lymph-vascular space invasion and perineural invasion. She underwent a right modified radical mastectomy including removal of a portion of the underlying pectoralis muscle; 0/8 lymph nodes were positive.

One year after the surgery, she presented with a painful mass in the right chest wall. Fine needle aspirate was positive for recurrent carcinoma. A CT scan showed involvement of internal mammary chain lymph nodes and destruction of the sternum and ribs.

The skin surface and the general location of the distal surface of the PTV were at an angle of 20° with respect to a surface perpendicular to the anterior-posterior direction. However, a gantry angle of 0° was chosen for convenience; maximum depth of the PTV was about 4 cm from the skin surface (Figure 2.13).

The IMC area, sternum, and right chest wall and supraclavicular and axillary apical area were treated with a dose of 50 Gy in 25 fractions over 5 weeks. Bolus ECT was used to treat the IMC and

chest wall area; photons were used for the right supraclavicular and axilla volumes. This was followed by 16 Gy in 8 fractions using Bolus ECT for the medial portion of the chest wall and the sternum. Only the first 50 Gy treatment was compared for this case.

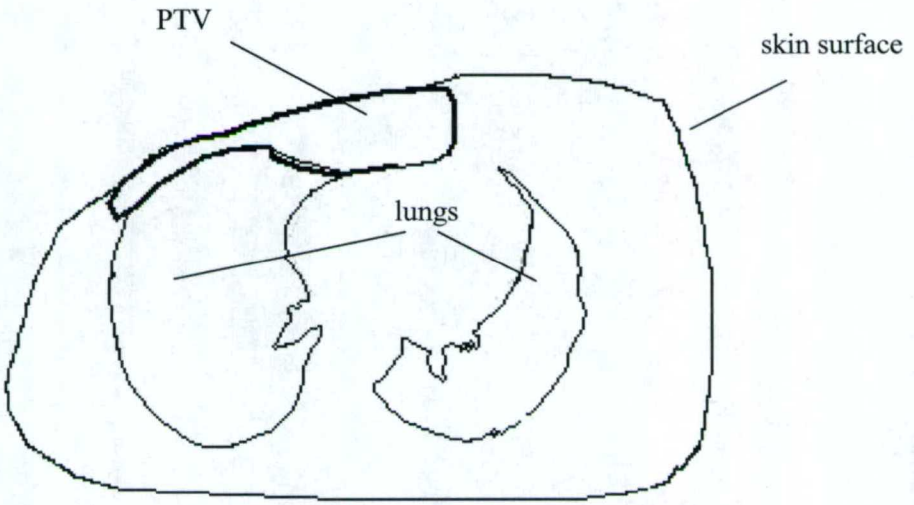

Figure 2.13. Transverse plane of Patient #2 showing the skin, lung and PTV contours.

2.4.4 Patient 3

Patient 3, a 55-year old female, was diagnosed with a $T_{4b}N_1M_0$ adenocarcinoma of the right breast. She underwent a right modified radical mastectomy; 1/22 lymph nodes were positive and all surgical margins were negative. Because of the irregular shape of the patient chest wall and target volume, bolus ECT was used to treat the chest wall. The skin surface and the general location of the distal surface of the PTV were at an angle of 0° with respect to a surface perpendicular to the anterior-posterior direction; the maximum depth of the PTV was approximately 3 cm from the skin surface (Figure 2.14).

The chest wall field was junctioned with the right supraclavicular and axillary apex 6 MV photon fields, and bolus was in place over the entire anterior chest wall. All fields were treated to 51 Gy

in 34 fractions of 1.5 Gy b.i.d. The junction between the supraclavicular and axillary apex fields and the bolus ECT field was moved three times during the course of therapy. The patient received a 9 Gy (1.5 b.i.d) boost to the chest wall using the same bolus.

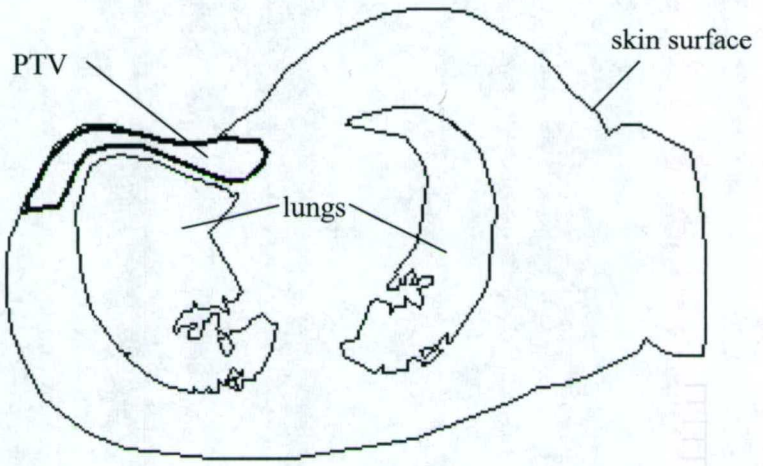

Figure 2.14. Transverse plane of Patient #3 showing the skin, lung, and PTV contours.

2.4.5 Patient 4

Patient 4, a 65-year old female, was diagnosed with a 3.5 cm invasive ductal carcinoma of the right breast. She was treated with a modified radical mastectomy and nodal dissection; 0/13 lymph nodes were positive for metastatic disease. Six years following the initial surgery, the patient palpated a nodule in the right chest wall, and a biopsy of this lesion was positive for infiltrating ductal carcinoma. The lesion was removed, and final pathology revealed a 2.0 cm x 1.1 cm infiltrating ductal carcinoma involving the subcutaneous tissue but not the skin. Surgical margins were negative.

The skin surface and the general location of the distal surface of the PTV were at an angle of 0° with respect to a surface perpendicular to the anterior-posterior direction. The maximum depth of the PTV was determined to be 2.3 cm from the skin surface (Figure 2.15).

The right chest wall, including the surgical bed, was treated using bolus ECT with 10 MeV electrons to a total dose of 50.4 Gy in 28 fractions. An additional 10 Gy in 5 fractions was delivered to the surgical bed using the same bolus.

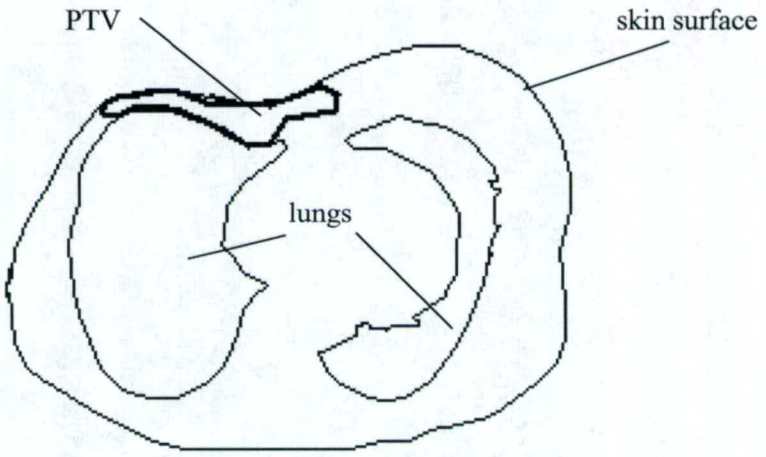

Figure 2.15. Transverse plane of Patient #4 showing the skin, lung, and PTV contours.

2.4.6 Patient 5

Patient 5, a 56-year old female, was diagnosed with a T_3N_1 Stage III invasive ductal carcinoma of the right breast. The patient underwent a needle localization and excisional biopsy of the primary lesion. Lymph node dissection revealed 20/27 positive lymph nodes with evidence of gross extracapsular extension.

This patient then underwent a complete mastectomy that revealed no residual tumor. Radiation was used for postoperative treatment to the right chest wall, internal mammary, and supraclavicular lymph nodes.

The skin surface and the general location of the distal surface of the PTV were at an angle of 50° with respect to a surface perpendicular to the anterior-posterior direction. The maximum depth of the PTV was approximately 1.9 cm from the skin surface (Figure 2.16).

The patient received a total of 50 Gy in 25 fractions to the internal mammary lymph node chain, medial and lateral chest wall, and the supraclavicular lymph node basins. The right chest wall and IMC was treated using bolus ECT with 12 MeV electrons. The supraclavicular fossa/axillary apex was treated using 6 MV photons with a 15-degree AP lateral tilt technique. The chest wall was boosted an additional 10 Gy in 5 fractions using bolus ECT with 12 MeV electrons.

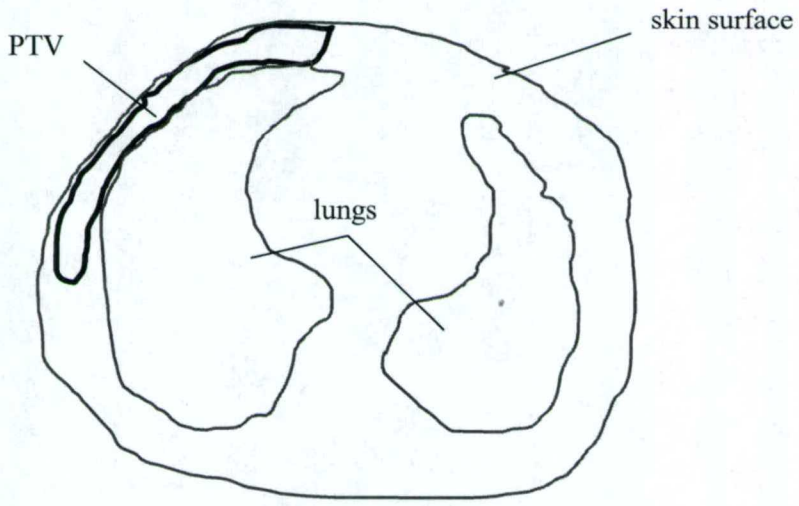

Figure 2.16. Transverse plane of Patient #5 showing the skin and PTV contours.

CHAPTER 3

Results and Discussion

3.1 Simple target 1

Simple target 1 was a smooth wedge (133 cm^3) with translational symmetry in the superior–inferior direction. The algorithm was used to divide the PTV into depth regions and five strip-fields were created using a 1-cm margin around the PTV. The energies of the strips were set according to the depth of the PTV and ranged from 12 MeV for the deepest portion of the PTV to 5 MeV for the shallowest portion of the PTV. Monitor units (MU) were set to deliver 200 cGy given dose per fraction for each field and dose was computed. The resulting dose distribution for 25 fractions is shown in Figure 3.1. The 4500 cGy (90%) dose line does not completely cover the deepest portion of the PTV. In addition, there was a significant portion of the PTV receiving 5250 cGy (105%). The mean dose to the PTV was 5121 ± 221 cGy and 122 cm^3 of non-target tissue received more than 4500 cGy. The quoted uncertainty in the mean PTV dose is one standard deviation, as reported by the TPS.

The Pinnacle^3 IMRT module was used to optimize the beam weighting. The objectives were set to deliver a minimum dose value of 4500 cGy and a maximum dose value of 5250 cGy to the PTV. These values represent 90% and 105% of the given dose respectively. Non-target tissue objectives were not needed because the energy selection gave distal conformality. The resulting dose distribution is shown in Figures 3.2 – 3.3. The 4500 cGy isodose line did not completely cover the deepest portion of the PTV; however, the dose homogeneity within the PTV was improved (volume of PTV receiving 5250 cGy decreased). The mean dose to the PTV was 4969 ± 154 cGy, and 96 cm^3 of the non-target tissue received more than 4500 cGy.

Three options are available to improve the dose coverage at the deepest portion of the PTV: 1) increase the beam weighting, which is the same as increasing the electron fluence; 2) increase the beam energy, which results in deeper electron penetration; or 3) increase the lateral field margins, which

results in lateral extension of the isodose lines. Option number one increased the PTV volume receiving more than 105% of the prescribed dose and the results are not shown. The other two options for this case are discussed below.

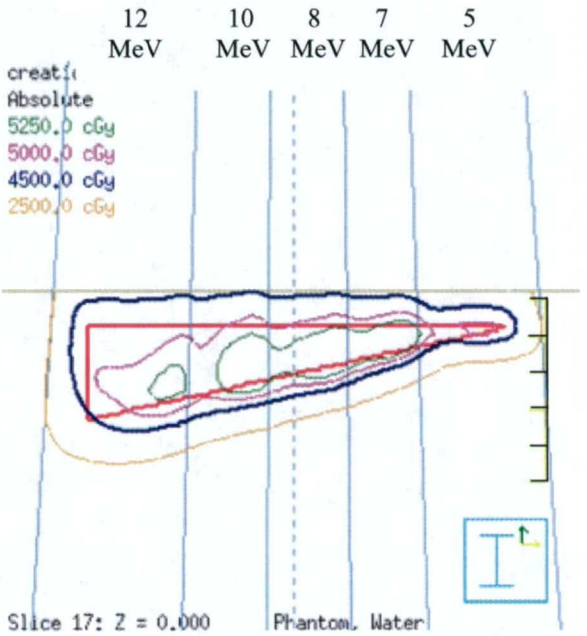

Figure 3.1. The central transverse plane of the smooth wedge simple target (PTV) with five strip fields used to treat the PTV. The field sizes (from left to right) are 4 x 11 cm^2, 2.25 x 11 cm^2, 2.25 x 11 cm^2, 2 x 11 cm^2, and 3.5 x 11 cm^2.

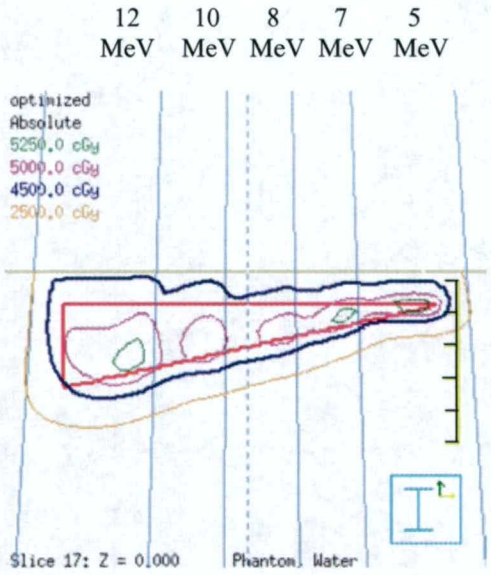

Figure 3.2. A central transverse plane of the smooth wedge simple target (PTV) for the same treatment plan shown in Figure 3.1, but after beam weight optimization.

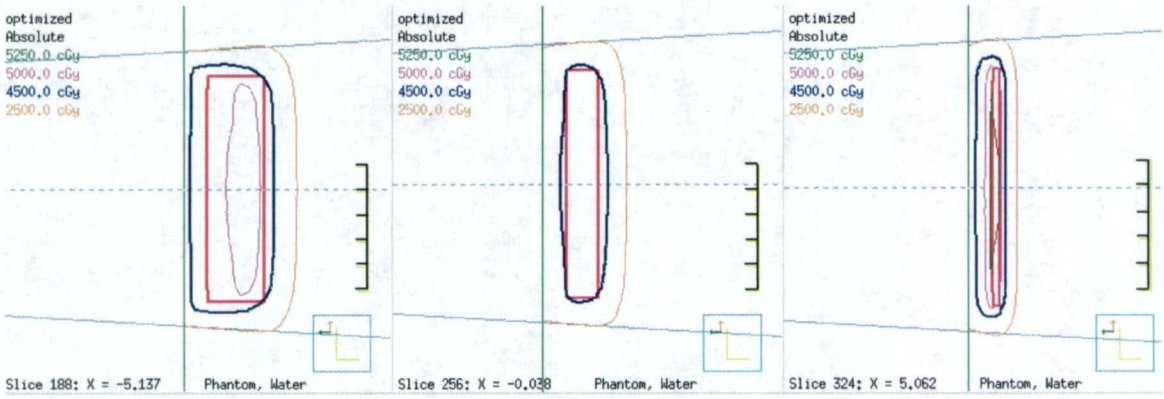

Figure 3.3. Central and lateral planes of the smooth wedge simple target dose distributions for the same treatment plan shown in Figure 3.2. Note that the 4500 cGy isodose line encompasses the distal target surface at the shallow depth but not at the deeper target regions.

3.1.1 Simple target 1: Energy increase, field edge expansion plan revision

The first plan revision was to increase the electron beam energy for the field covering the deepest region of the PTV [from 12 MeV to 15 MeV (Energy Increase)]. This resulted in a slight

improvement in the 4500 cGy dose coverage for that PTV region (not shown). However, it was apparent that the margin of the higher energy strip was also not adequate. The field edge margin was increased (Field Edge Expansion) by 0.25 cm (Figure 3.4). Dose was computed and beam weights were optimized using the same objectives as before. The dose distribution for this plan is shown in Figures 3.5 – 3.6.

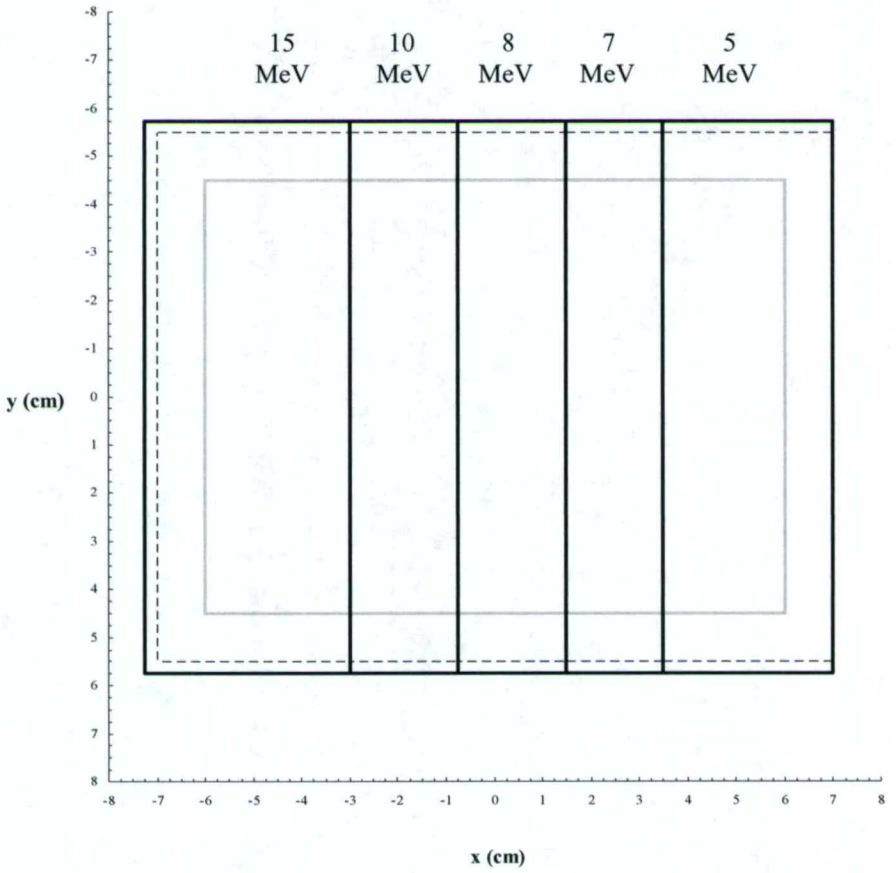

Figure 3.4. A BEV display of the smooth wedge simple target (gray) with applied field margins. In the creation phase, a uniform margin of 1 cm was applied and those fields are represented with the dashed line. For this plan revision, the fields were expanded by 0.25 cm in all directions, except for the lowest energy (far right field edge), where the 1-cm margin was already adequate. The modified fields are shown as solid black lines.

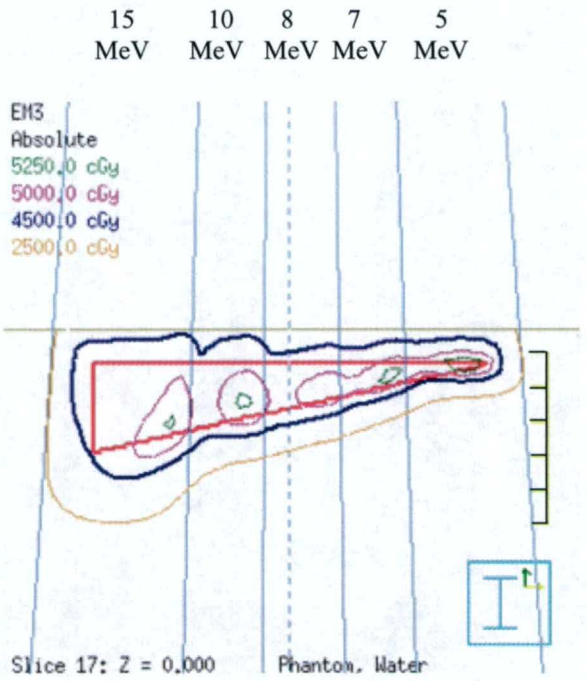

Figure 3.5. A central transverse plane of the smooth wedge simple target showing a 2D dose distribution for the modified treatment fields. The 12 MeV energy was increased to 15 MeV, and the margins were expanded by 0.25 cm as shown in Figure 3.4.

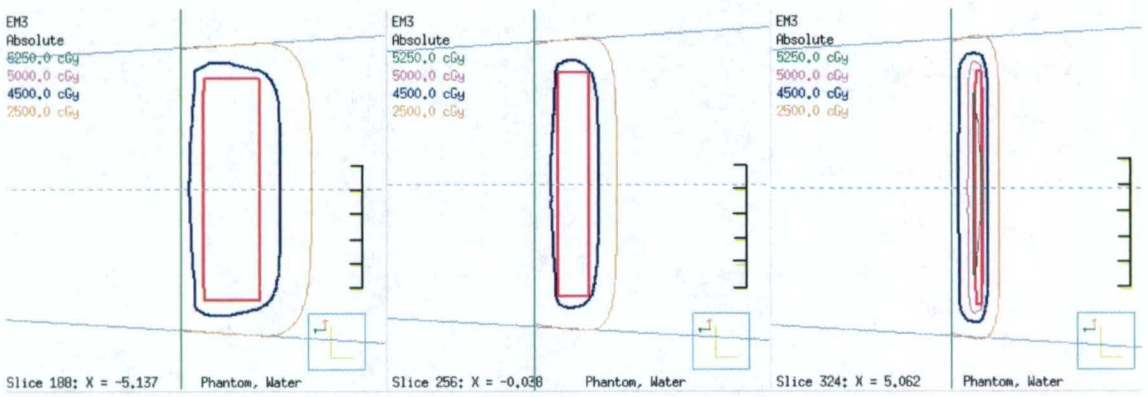

Figure 3.6. Central and lateral planes of the smooth wedge simple target for the same treatment plan shown in Figure 3.5.

In general, the 4500 cGy dose line conforms to the distal edge of the PTV except for the region containing the deepest portion of the target, which is where the energy was increased from 12 MeV to 15 MeV. The mean dose to the PTV was 4914 ± 169 cGy, and 129 cm^3 of the non-target tissue received more than 4500 cGy.

3.1.2 Simple target 1: Field edge expansion plan revision

Another option for modification of the original plan was to keep the original energies intact but expand the field margin so that the deepest target regions are contained by the 4500 cGy dose surface. Field Edge Expansion was used to increase the margin around the PTV. Figure 3.7 shows the field outlines for the treatment plan with margin expansion compared to the original field outlines. For the strip-field covering the deepest PTV region, the lateral edge was expanded by 0.75 cm, and the superior and inferior edges were expanded by 0.25 cm. For the other fields, only the superior and inferior edges were expanded by 0.25 cm. Dose was computed and beam weights optimized using the same objectives as before. This produced a treatment plan in which the 4500 cGy dose line closely tracked the PTV distal edge as shown in Figures 3.8 – 3.9. Because of the large margin around the deepest portion of the PTV, non-target tissue lateral to the 12-MeV field was irradiated more than desired. However, the non-target tissue distal to the deepest portion of the PTV is spared. The mean dose to the PTV was 4948 ± 148 cGy, and 138 cm^3 of the non-target tissue received more than 4500 cGy.

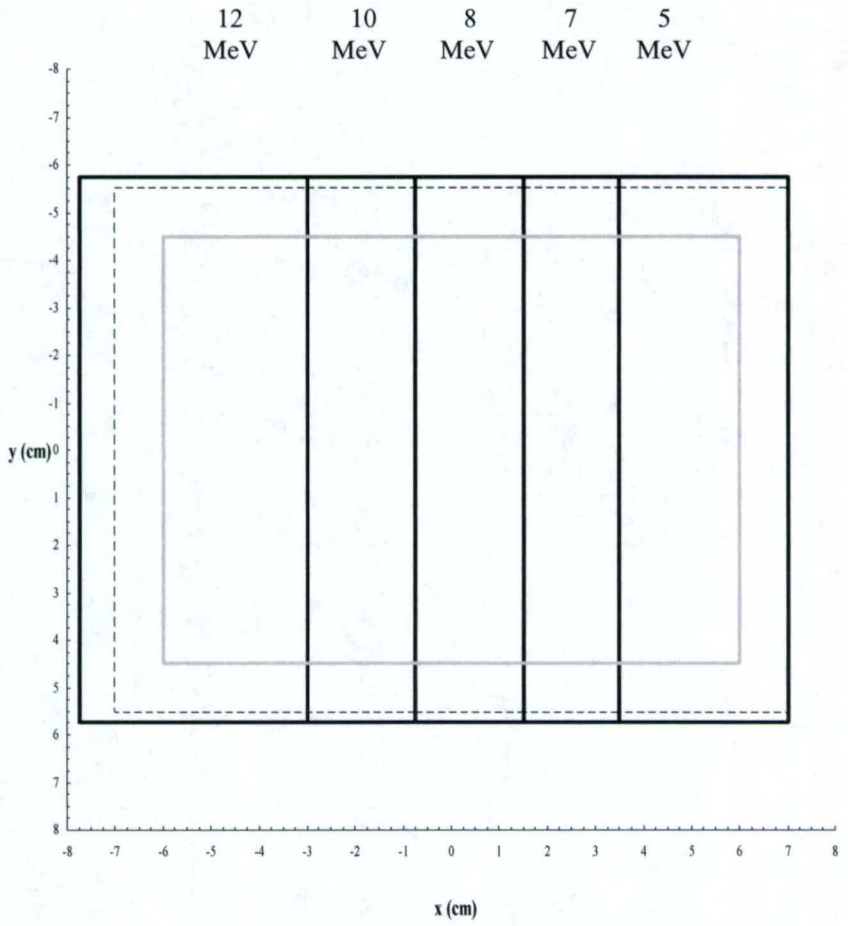

Figure 3.7. A BEV display of the smooth wedge simple target (gray) with applied field margins. In the creation phase, a uniform margin of 1 cm was applied and those fields are represented with the dashed line. For this plan, the far left field edge was expanded by 0.75 cm, the superior and inferior field edges were expanded by 0.25 cm, and no expansion was made for the right field edge because the 1-cm margin was already adequate. The modified fields are shown as solid black lines.

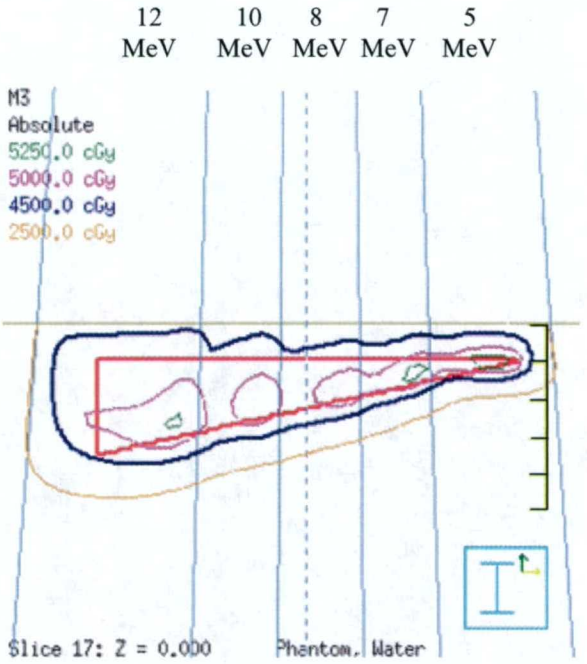

Figure 3.8. A central transverse plane of the smooth wedge simple target showing a 2D dose distribution for the modified treatment fields shown in Figure 3.7.

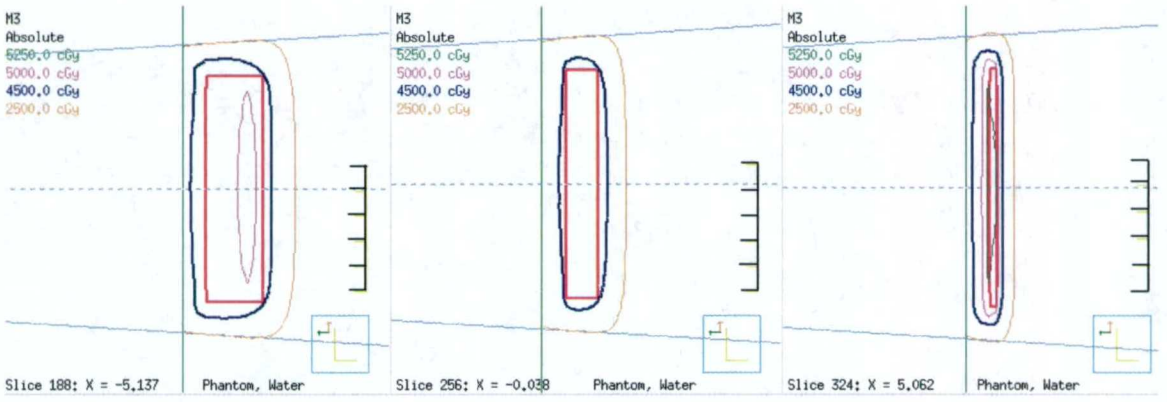

Figure 3.9. Central and lateral slices of the smooth wedge simple target for the same treatment plan shown in Figure 3.8.

3.1.3 Simple target 1: Summary

Figure 3.10 compares the DVH of the PTV and non-target tissue for these treatment plans, and Table 3.1 summarizes the PTV dose homogeneity and the dose to non-target tissue. Comparing the two modified plans, the first modified plan (energy and margin) irradiates more tissue distal to the PTV, but less tissue lateral to the PTV than the second modified plan (margin only). The margin only plan has slightly improved PTV dose homogeneity, and it delivers about the same amount of dose to non-target tissue. Choosing one plan over the other depends on the location of the critical structures and the clinician's preferences.

Table 3.1. Dose statistics for the smooth wedge simple target treatment plans.

	PTV (133 cm^3)			Non-target tissue	
Treatment Plans	Mean Dose (cGy)	Standard Deviation (cGy)	$D(V_{90}) - D(V_{10})$ (cGy)	Volume > 45 Gy (cm^3)	Maximum Dose (cGy)
Creation, Optimized	4969	154	402	96	5334
Modification, energy-margin	4914	169	454	129	5311
Modification, margin	4948	148	398	138	5313

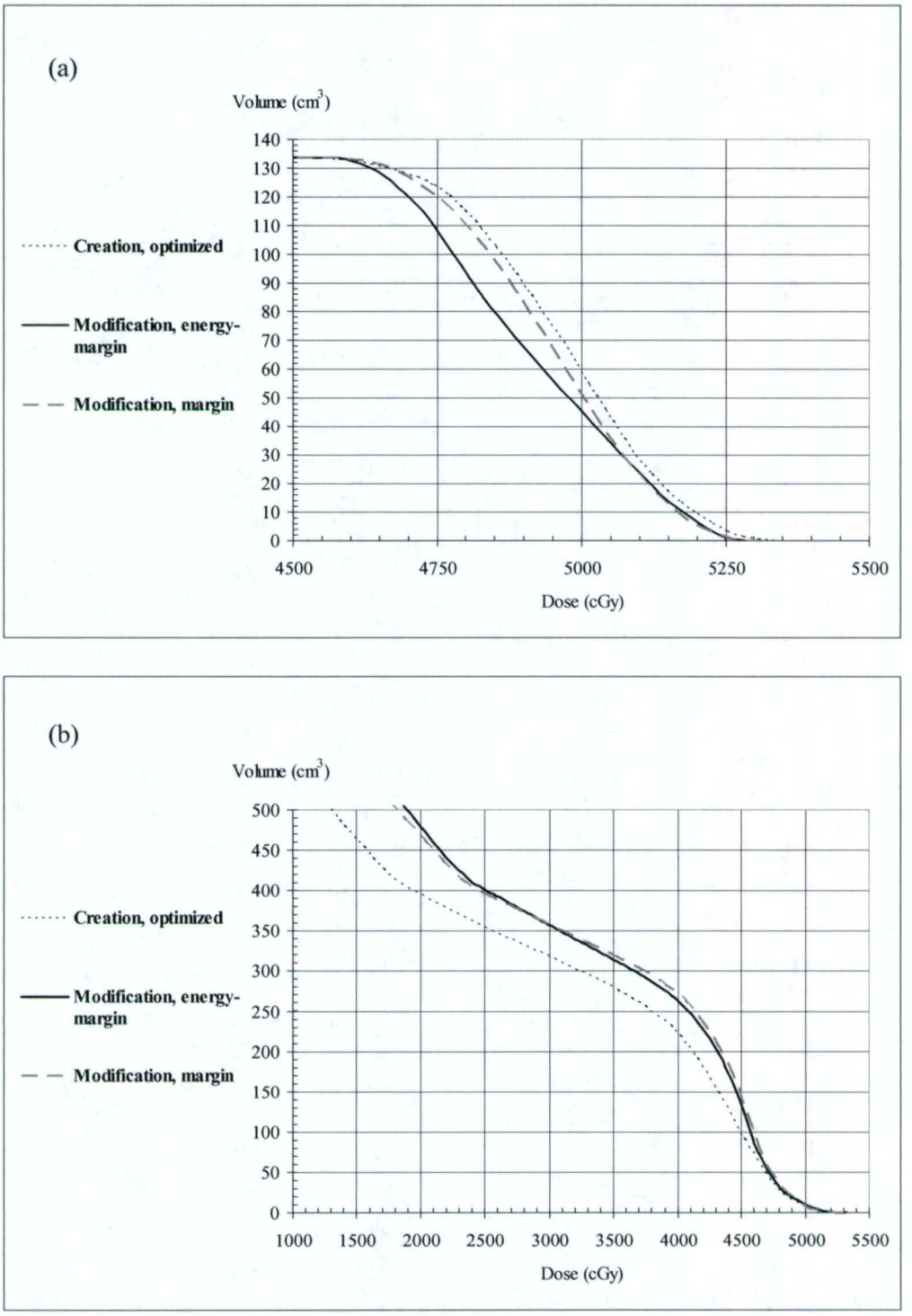

Figure 3.10. Dose volume histogram (DVH) for the smooth wedge simple target PTV (a) and non-target tissue (b).

3.2 Simple target 2

Simple target 2 was a step wedge (189 cm^3) with translational symmetry in the superior–inferior direction. The algorithm was used to divide the PTV into depth intervals and four strip-fields were created using a 1-cm margin about the PTV; the energies of the strips were set according to the depth of the PTV and ranged from 12 MeV for the deepest portion of the PTV to 7 MeV for the shallowest portion of the PTV. MU were set to deliver 200 cGy given dose for each field and dose was computed. The dose distribution (not shown) resulted in the 4500 cGy (90%) isodose line to not completely cover the deepest portion of the PTV. In addition, there were small regions of the PTV receiving 5250 cGy (105%). The mean dose to the PTV was 4947 ± 168 cGy.

The Pinnacle^3 IMRT Module was then used to optimize the beam weighting. The objectives were set to deliver a minimum dose value of 4500 cGy and a maximum dose value of 5250 cGy to the PTV. The resulting dose distribution is shown in Figures 3.11 – 3.12. The 4500 cGy isodose line did not completely cover the deepest portion of the PTV; however, the dose homogeneity within the PTV was improved (volume of PTV receiving 5250 cGy decreased). The mean dose to the PTV was 4972 ± 161 cGy, and 109 cm^3 of the non-target tissue received more than 4500 cGy.

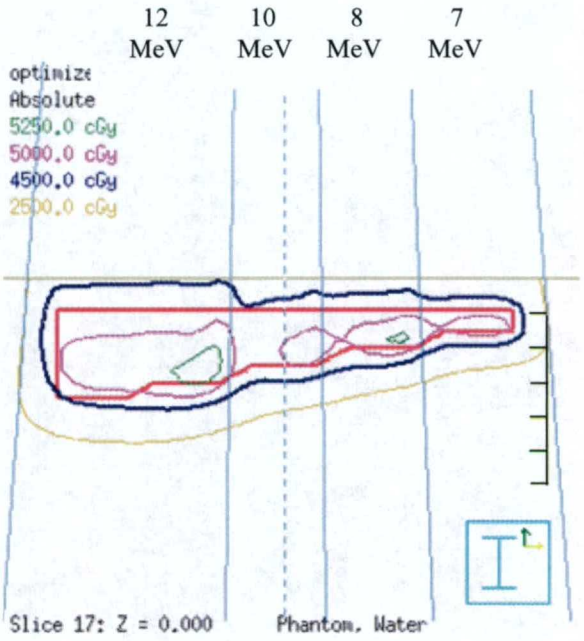

Figure 3.11. The central transverse plane of the step wedge simple target (PTV) showing the dose distribution following beam weight optimization. The field sizes (from left to right) are 6.3 x 11 cm², 2.8 x 11 cm², 3 x 11 cm², and 3.9 x 11 cm².

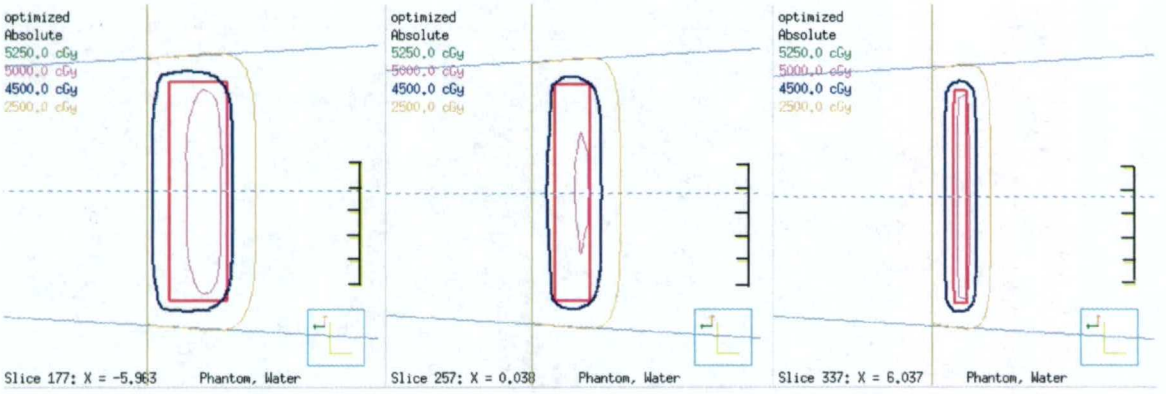

Figure 3.12. Central and lateral planes of the step wedge simple target dose distributions for the same treatment plan shown in Figure 3.11. The 4500 cGy isodose line coverage looks good except along the deepest region distal surface (picture on the left).

3.2.1 Simple target 2: Energy increase, field edge expansion plan revision

The first plan revision was to increase the electron beam energy for the field covering the deepest region of the PTV [from 12 MeV to 15 MeV (Energy Increase)]. This resulted in a slight improvement in the 4500 cGy dose coverage for that PTV region (not shown). It was apparent from the previous plan that the margin of the higher energy strip was not adequate; therefore, the field edge margin was also increased (Field Edge Expansion) by 0.25 cm (Figure 3.13). Dose was computed and beam weights were optimized using the same objectives as before. The dose distribution for this plan is shown in Figures 3.14 – 3.15. In general, the 4500 cGy dose line conforms to the distal edge of the PTV except for the region containing the deepest portion of the target, which is where the energy was increased from 12 MeV to 15 MeV. The mean dose to the PTV was 4879 ± 168 cGy, and 159 cm^3 of the non-target tissue receives more than 4500 cGy.

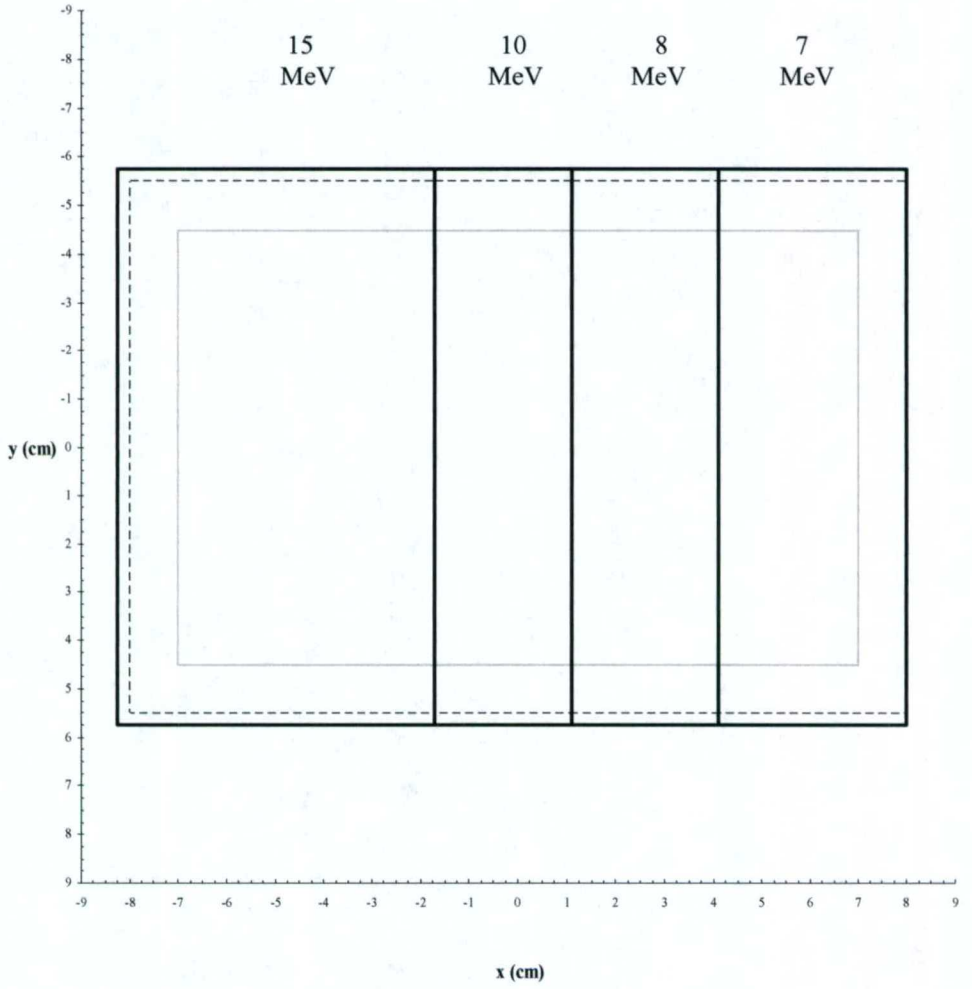

Figure 3.13. A BEV display of the step wedge simple target with applied field margins. The gray line shows the PTV and it's associated depth regions. The dash lines represent the fields after the creation phase, with a uniform 1 cm margin around the PTV. The solid black line shows the fields expanded in three directions by 0.25 to give better coverage at the PTV edges.

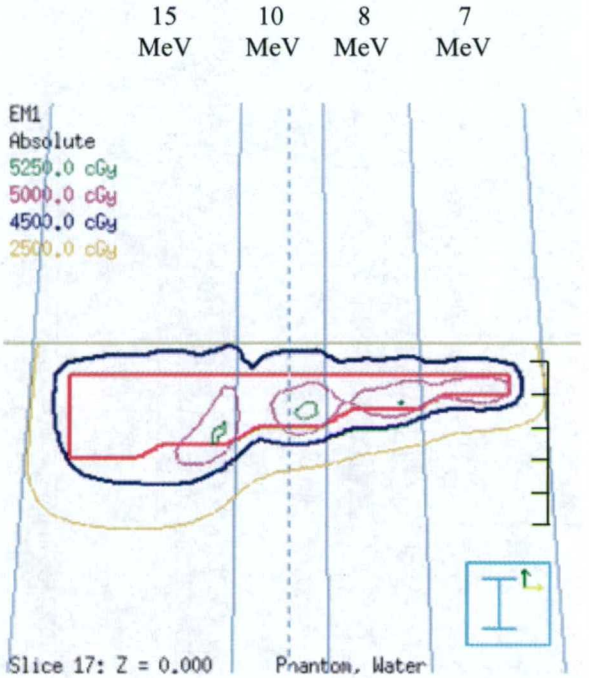

Figure 3.14. A central transverse plane of the step wedge simple target showing a 2D dose distribution for the modified treatment fields shown in Figure 3.13.

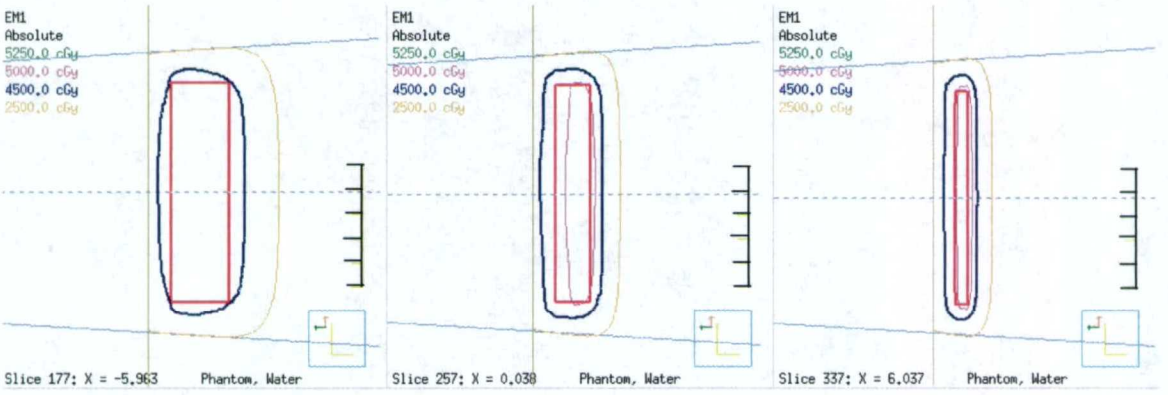

Figure 3.15. Central and lateral planes of the step wedge simple target for the same treatment plan shown in Figure 3.14. In comparison to Figure 3.12, the 10, 8, and 7 MeV fields probably did not need to be expanded.

3.2.2 Simple target 2: Field edge expansion plan revision

Another option for modification of the original plan was to keep the original energies intact but expand the field margin so that the deepest target regions are contained by the 4500 cGy dose surface. Field edge expansion was used to increase the margin around the PTV. Figure 3.16 shows the field outlines for the treatment plan with margin expansion compared to the original field outlines. For the strip-field covering the deepest PTV region, the lateral edge was expanded by 0.75 cm, and the superior and inferior edges were expanded by 0.25 cm. For the other fields, only the superior and inferior edges were expanded by 0.25 cm. Dose was computed and beam weights optimized using the same objectives as before. This produced a treatment plan in which the 4500 cGy dose line closely tracked the PTV distal edge as shown in Figures 3.17 – 3.18. Because of the large margin around the deepest portion of the PTV, non-target tissue lateral to the 12 MeV field was irradiated more than desired. However, the non-target tissue distal to the deepest portion of the PTV is spared. The mean dose to the PTV was 4941 ± 153 cGy, and 147 cm^3 of the non-target tissue receives more than 4500 cGy.

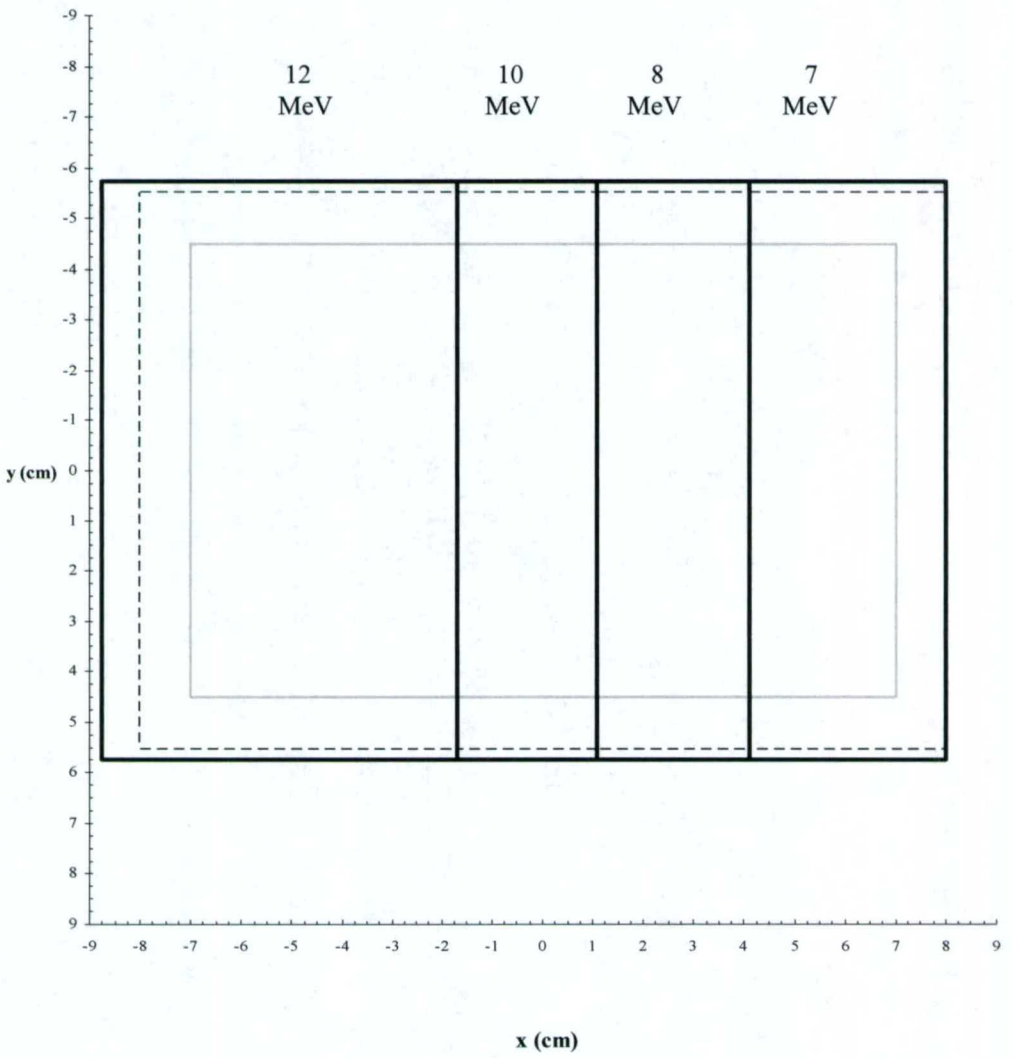

Figure 3.16. BEV display of the step wedge simple target (gray) with applied field margins. In the creation phase, a uniform margin of 1 cm was applied and those fields are represented with the dashed line. For this plan, the left field was expanded by 0.75 cm, the superior and inferior field margins were expanded by 0.25 cm, and no expansion was made for the right field because the 1-cm margin was already adequate. The modified fields are shown as solid black lines.

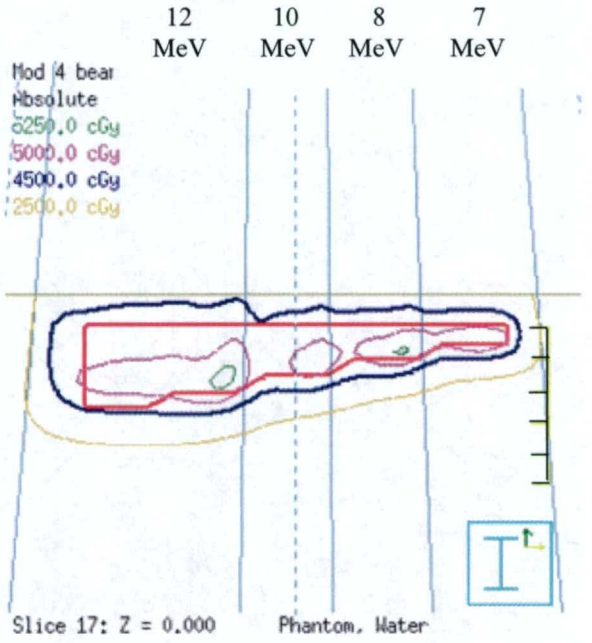

Figure 3.17. A central transverse plane of the step wedge simple target showing a 2D dose distribution for the modified treatment fields shown in Figure 3.16.

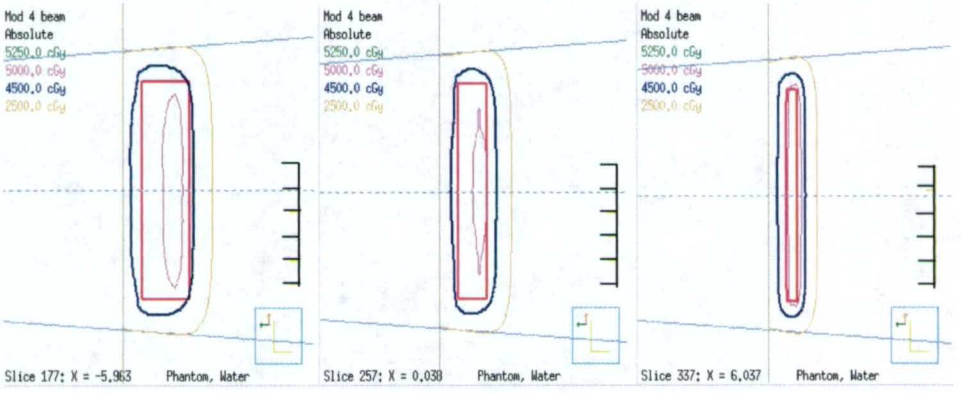

Figure 3.18. Central and lateral planes of the step wedge simple target for the same treatment plan shown in Figure 3.17.

3.2.3 Simple target 2: Summary

Figure 3.19 compares the DVH of the PTV and non-target tissue for these treatment plans. Table 3.2 summarizes the PTV dose homogeneity and the dose to non-target tissue. Comparing the two modified plans, the first modified plan (energy and margin) irradiates more tissue distal to the PTV, but less tissue lateral to the PTV than the second modified plan (margin only). The margin only plan has slightly improved PTV dose homogeneity, and it delivers about the same amount of dose to non-target tissue. Choosing one plan over the other depends on the location of the critical structures and the clinician's preferences.

Table 3.2. Dose statistics for the step wedge simple target treatment plans.

	PTV (189 cm^3)			Non-target tissue	
Treatment Plans	Mean Dose (cGy)	Standard Deviation (cGy)	$D(V_{90}) - D(V_{10})$ (cGy)	Volume > 45 Gy (cm^3)	Maximum Dose (cGy)
Creation, Optimized	4972	161	414	109	5374
Modification, energy-margin	4879	168	454	159	5299
Modification, margin	4941	153	401	147	5322

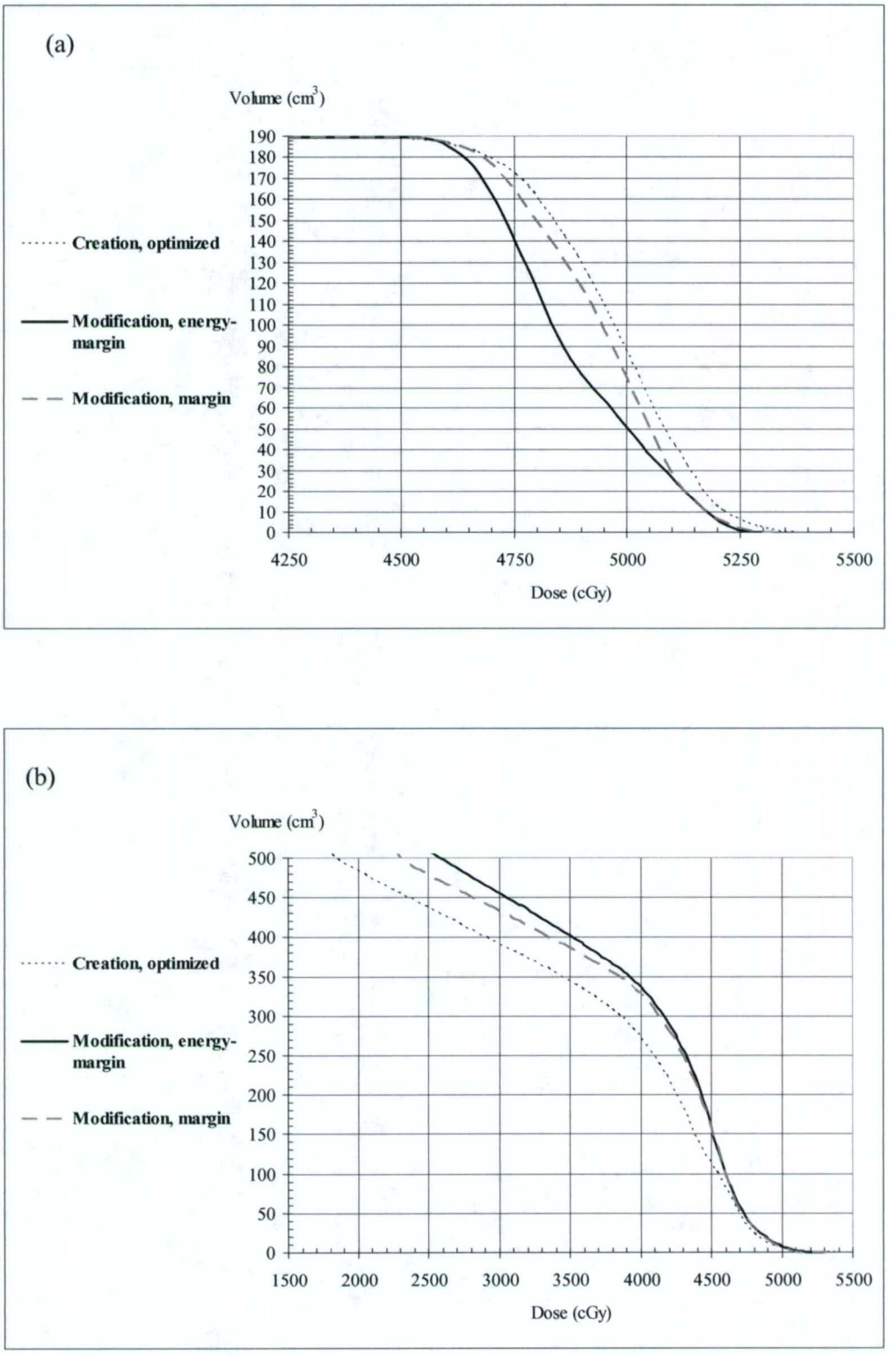

Figure 3.19. Dose volume histogram (DVH) for the step wedge simple target PTV (a) and non-target tissue (b).

3.3 Simple target 3

Simple target 3 was an inverted well (118 cm^3) with translational symmetry in the superior–inferior direction. The algorithm was used to divide the PTV into depth regions and three strip-fields were created using a 1-cm margin about the PTV. The energies of the strips were set according to the depth of the PTV and ranged from 12 MeV for the deepest portion of the PTV to 8 MeV for the shallowest portion of the PTV. The field-creation step did produce two narrow strips that could be treated using 10 MeV; however, the widths of the strips were less than 2 cm, so the regions were incorporated into the 12 MeV strip-fields. Dose was computed and MU were set to deliver 200 cGy given dose for each field. The dose distribution (not shown) resulted in the 4500 cGy (90%) isodose line encompassing the deepest portion of the PTV. However, there were several regions within the PTV receiving dose above 5250 cGy (105%). The mean dose to the PTV was 5010 ± 186 cGy.

The Pinnacle^3 IMRT Module was then used to optimize the beam weighting. The objectives were set to deliver a minimum dose value of 4500 cGy and a maximum dose value of 5250 cGy to the PTV. The resulting dose distribution is shown in Figures 3.20 – 3.21. The 4500 cGy isodose line tracks the deepest portion of the PTV; the dose homogeneity within the PTV improved relative to the non-optimized plan. The mean dose to the PTV was 4890 ± 183 cGy, and 52 cm^3 of the non-target issue received more than 4500 cGy.

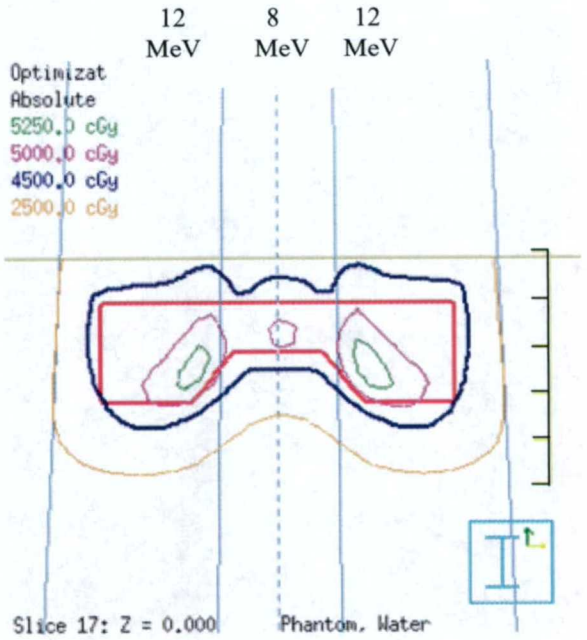

Figure 3.20. The central transverse plane of the inverted well simple target (PTV) showing the dose distribution following beam weight optimization. The field sizes (from left to right) are 3.7 x 11 cm², 2.6 x 11 cm², and 3.7 x 11 cm².

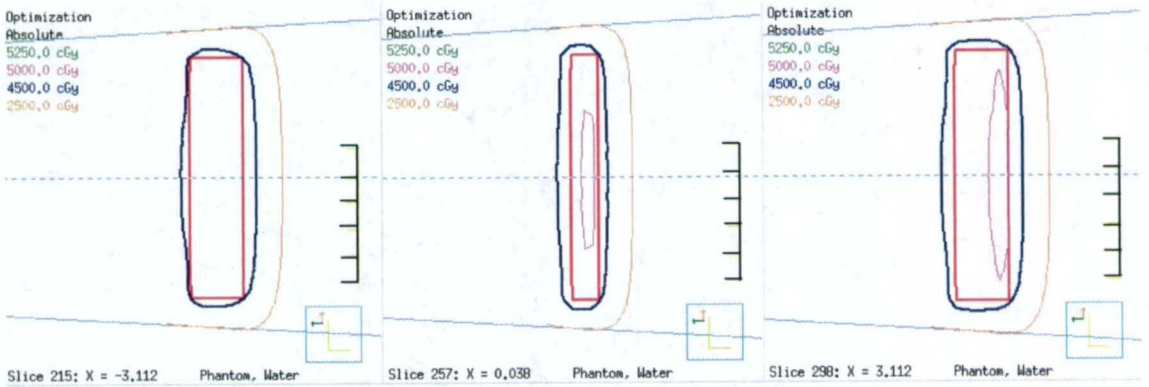

Figure 3.21. Central and lateral planes of the inverted well simple target showing the dose distribution for the same treatment plan shown in Figure 3.20.

3.3.1 Simple target 3: Energy increase/decrease, field edge expansion plan revision

The first plan revision was to increase the electron beam energy for the field covering the deepest region of the PTV [from 12 MeV to 15 MeV (Energy Increase)] and to decrease the energy for the field covering the shallowest region of the PTV [from 8 MeV to 7 MeV (Energy Decrease)]. The field edge margin was increased (Field Edge Expansion) by 0.25 cm (Figure 3.22). Dose was computed and beam weights were optimized using the same objective as before. The dose distribution for this plan is shown in Figures 3.23 – 3.24. In general, the 4500 cGy dose coverage is too deep for the deepest regions of the PTV. The mean dose to the PTV was 4875 ± 252 cGy, and 61 cm^3 of the non-target tissue receives more than 4500 cGy.

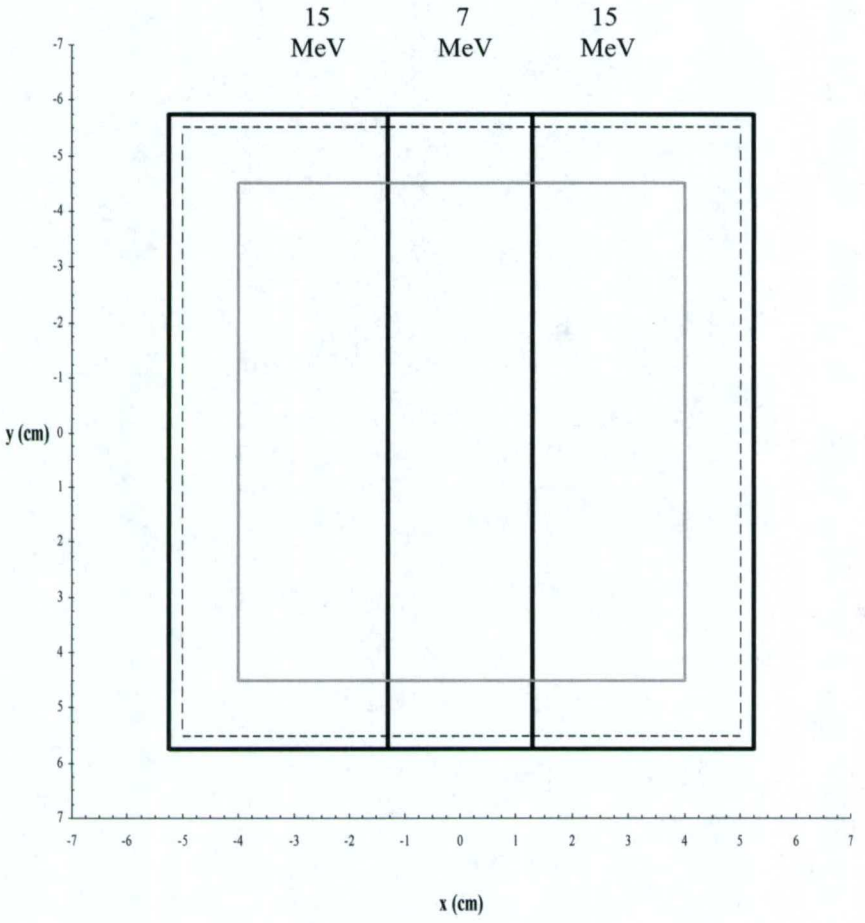

Figure 3.22. A BEV display of the inverted well simple target (gray) with applied field margins. In the creation phase, a uniform margin of 1 cm was applied and those fields are represented with the dashed line. For this plan, the fields were expanded by 0.25 cm in all directions. The modified fields are shown as solid black lines.

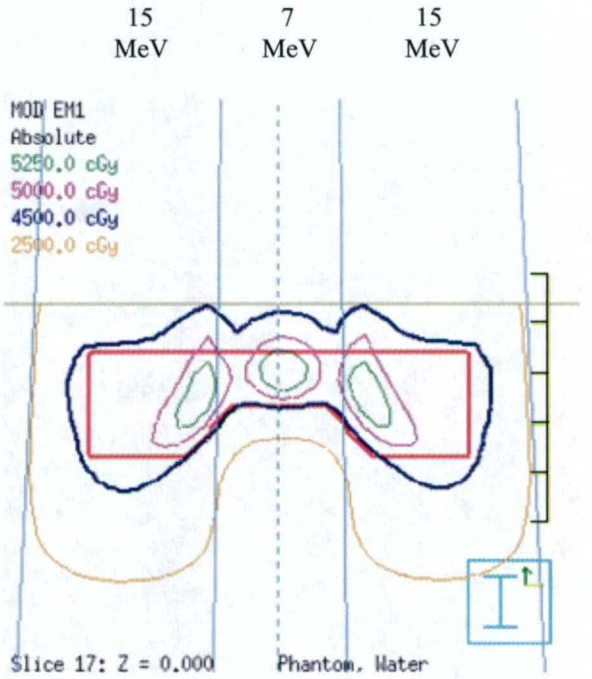

Figure 3.23. A central transverse plane of the inverted well simple target showing a 2D dose distribution for the modified treatment fields shown in Figure 3.22. The 12 MeV energy was increased to 15 MeV, the 8 MeV energy was decreased to 7 MeV, and the margins were expanded by 0.25 cm on all sides.

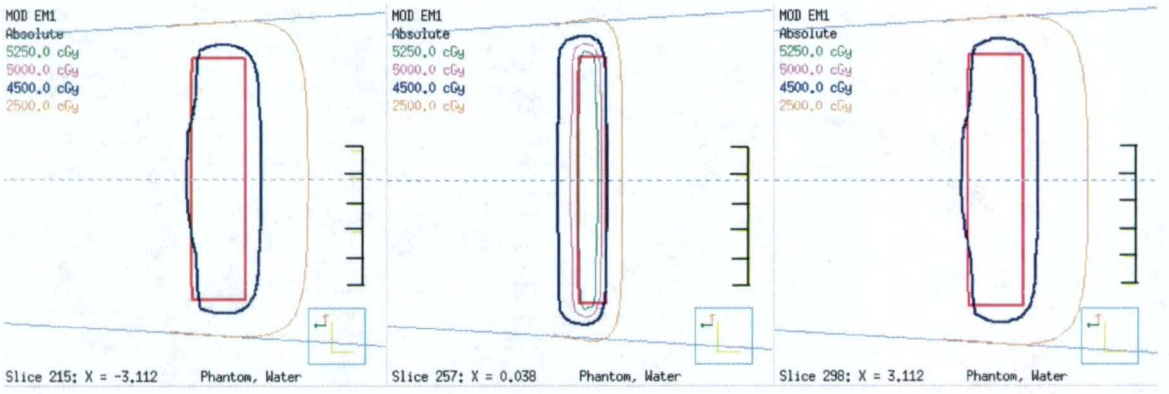

Figure 3.24. Central and lateral slices of the inverted well simple target for the same treatment plan shown in Figure 3.23.

3.3.2 Simple target 3: Field edge expansion plan revision

Another option for modification of the original plan was to keep the original energies intact but expand the field margin so that the deepest target regions (most lateral edges) are better contained by the 4500 cGy dose line. Field Edge Expansion was used to increase the margin 0.25 cm in all directions around the PTV (same as in Figure 3.22 except with no adjustments of the original beam energies). Dose was computed and beam weights were optimized using the same objectives as before. This plan modification resulted in the 4500 cGy isodose line tracking the distal edge of the target (Figures 3.25 – 3.26) better than the previous plan although still needlessly deep. However, the beam weight optimizer did not reduce the distance between the 4500 cGy isodose line and the distal edge of the target because the coverage was optimal and inferior slices would be compromised (cf., Figure 3.24). In addition, the 5250 cGy (105%) dose line appeared near the field junctions but was contained within the target. The mean dose to the PTV was 4926 ± 181 cGy, and 96 cm^3 of the non-target tissue received more than 4500 cGy.

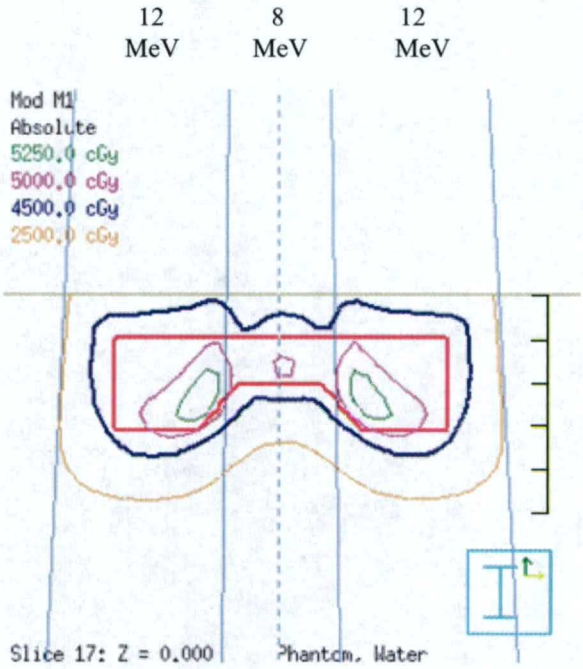

Figure 3.25. A central transverse slice of the inverted well simple target showing a 2D dose distribution for the modified treatment fields shown in Figure 3.22. The margins were expanded by 0.25 cm on all sides of the PTV.

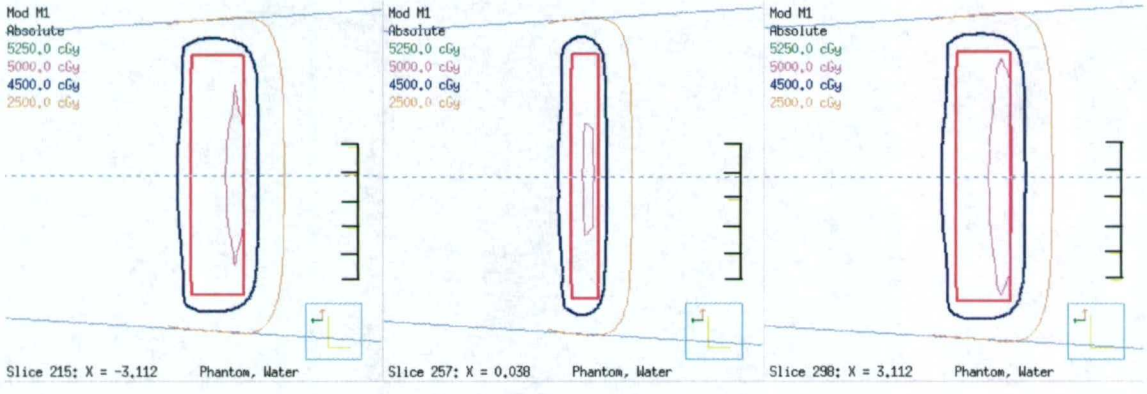

Figure 3.26. Central and lateral slices of the inverted well simple target for the same treatment plan shown in Figure 3.25.

3.3.3 Simple target 3: Field edge expansion, fluence decrease plan revision

The previous revised plan provided reasonable 4500 cGy isodose coverage of the target. In an attempt to reduce the volume of target receiving 5250 cGy near the field junctions and to improve (decrease) the 4500 cGy isodose coverage, the MU were slightly changed. The resulting dose distribution is shown in Figures 3.27 – 3.28. The mean dose to the PTV was 4825 ± 175 cGy, and 53 cm^3 of the non-target tissue receives more than 4500 cGy.

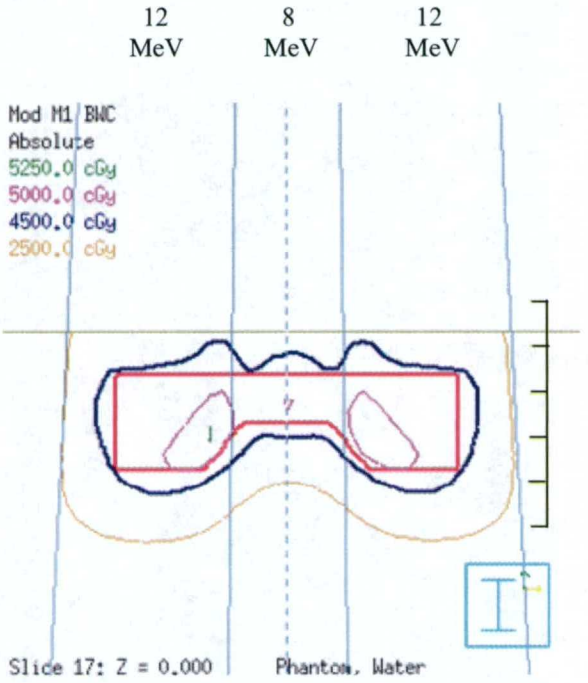

Figure 3.27. A central transverse slice of the inverted well simple target showing a 2D dose distribution for the modified treatment fields shown in Figure 3.22. The margins were expanded by 0.25 cm on all sides of the PTV. The MU were slightly decreased.

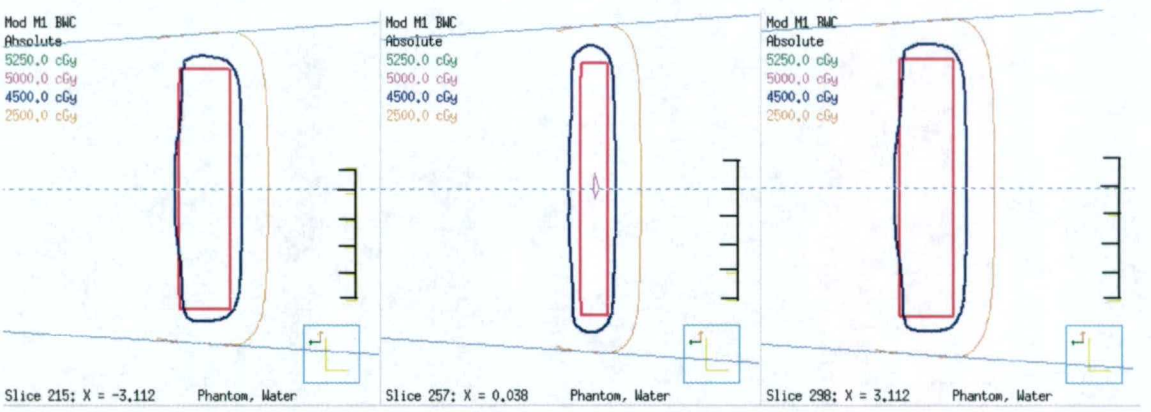

Figure 3.28. Central and lateral slices of the inverted well simple target for the same treatment plan shown in Figure 3.27.

3.3.4 Simple target 3: Summary

Figure 3.29 compares the DVH of the PTV and non-target tissue for these treatment plans, and Table 3.3 summarizes the PTV dose homogeneity and the dose to non-target tissue. Comparing the three modified plans, the first modified plan (energy and margin) irradiates more tissue distal to the PTV, than the second modified plan (margin only) and the third modified plan (margin and fluence). The last two plans (margin only, margin and fluence) have very similar results except for the volume of non-target tissue receiving 4500 cGy. The (margin, fluence) plan has slightly improved PTV dose homogenity and better non-target tissue sparing. A fluence reduction only revision to the original plan could have been another option for this simple target.

Table 3.3. Dose statistics for the inverted well simple target treatment plans.

	PTV (118 cm^3)			Non-target tissue	
Treatment Plans	Mean Dose (cGy)	Standard Deviation (cGy)	$D(V_{90}) - D(V_{10})$ (cGy)	Volume > 45 Gy (cm^3)	Maximum Dose (cGy)
Creation, Optimized	4890	183	498	52	5346
Modification, energy-margin	4875	252	682	61	5490
Modification, margin	4926	181	498	96	5366
Modification, fluence-margin	4825	175	484	53	5252

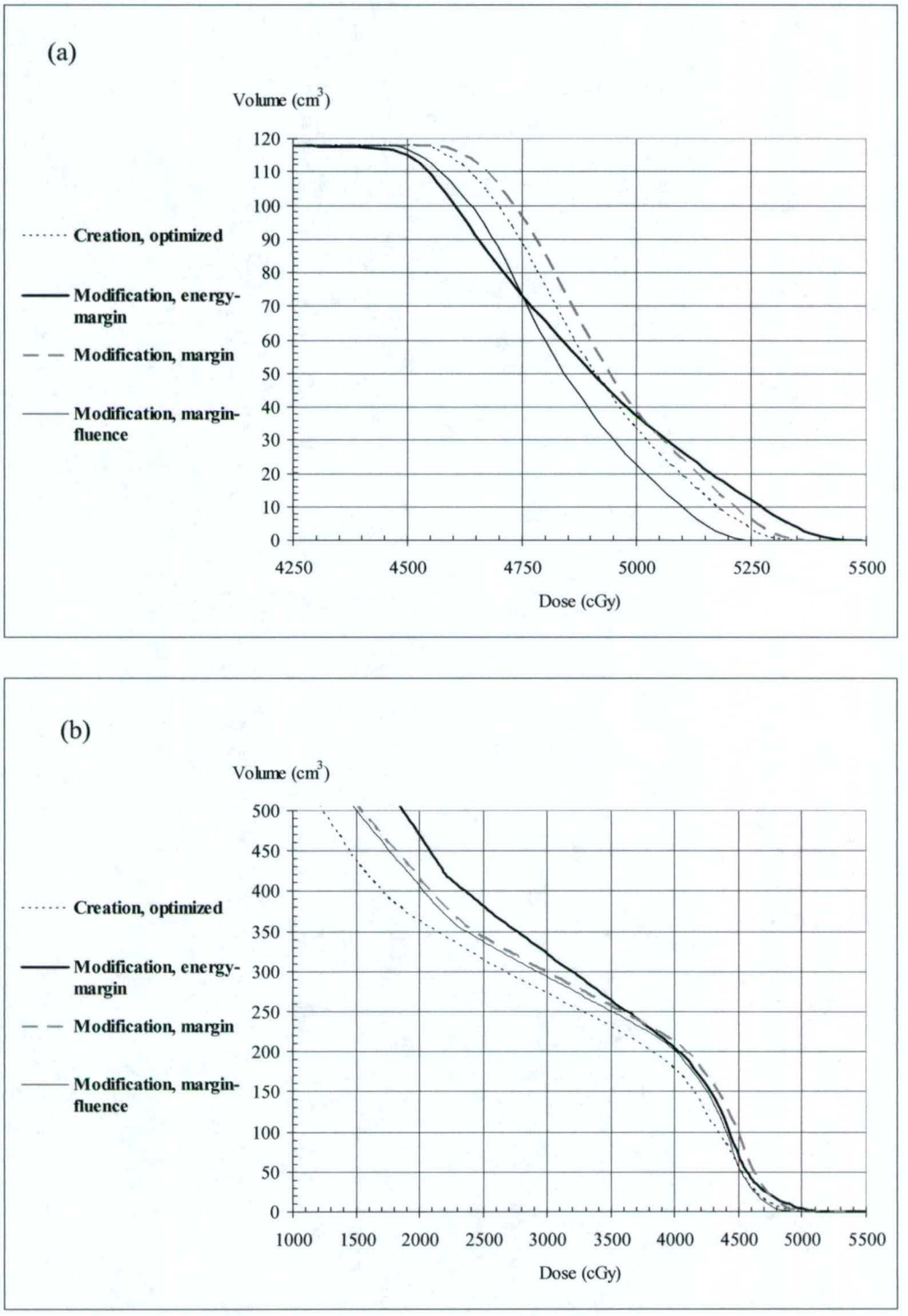

Figure 3.29. Dose volume histogram (DVH) for the inverted well simple target PTV (a) and non-target tissue (b).

3.4 Simple target 4

Simple target 4 was a pentagon-shaped target (162 cm^3) with translational symmetry in the superior–inferior direction. The algorithm was used to divide the PTV into depth regions and five strip-fields were created using a 1-cm margin about the PTV. The energies of the strips were set according to the depth of the PTV and ranged from 12 MeV for the deepest portion of the PTV to 7 MeV for the shallowest portion of the PTV. The field-creation step did produce two narrow strips that could be treated using 8 MeV; however, the widths of the strips were less than 2 cm, so the regions were incorporated into the 10 MeV strip-fields. Dose was computed and set to deliver 200 cGy given dose for each field. The dose distribution (not shown) resulted in the 4500 cGy (90%) isodose surface to completely cover the deepest portion of the PTV. In addition, there was a significant portion of the PTV receiving 5250 cGy (105%). The mean dose to the PTV was 5073 ± 162 cGy.

The Pinnacle^3 IMRT Module was used to optimize the beam weighting. The standard objectives were used in an attempt to improve the dose homogenity within the PTV,without considerably degrading the dose conformality. The resulting dose distribution is shown in Figures 3.30 - 3.31. The 4500 cGy isodose line covered the deepest portion of the PTV; the dose homogeneity within the PTV improved (volume of PTV receiving 5250 cGy decreased). The mean dose to the PTV was 4931 ± 163 cGy, and 102 cm^3 of the non-target tissue received more than 4500 cGy.

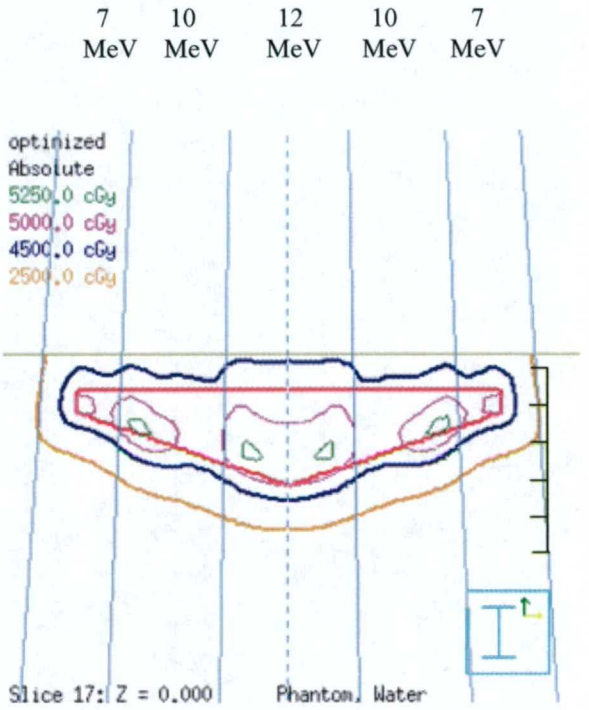

Figure 3.30. The central transverse plane of the pentagon-shaped target (PTV) showing the dose distribution following beam weight optimization. The field sizes (from left to right) are 2.25 x 11 cm², 2.95 x 11 cm², 3.6 x 11 cm², 2.95 x 11 cm², and 2.25 x 11 cm².

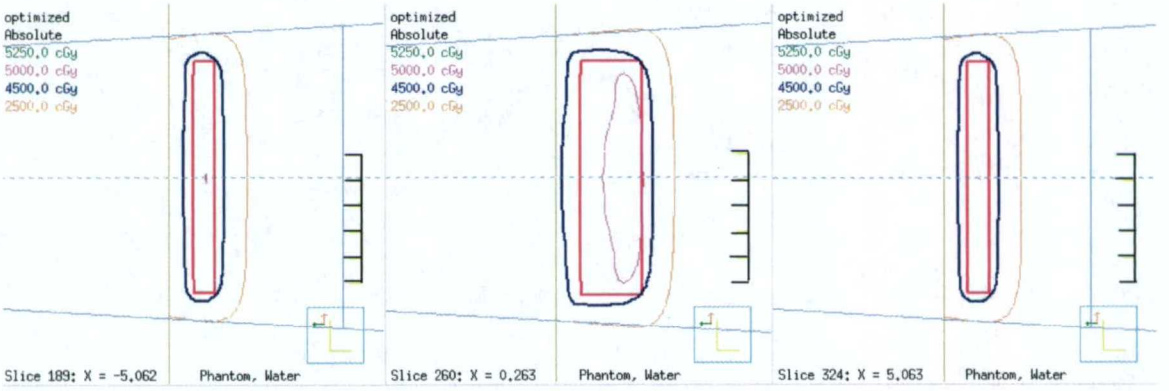

Figure 3.31. Central and lateral planes of the pentagon-shaped simple target for the same treatment plan shown in Figure 3.30.

3.4.1 Simple target 4: Fluence decrease plan revision

The creation plan provided reasonable 4500 cGy isodose coverage of the target. In an attempt to reduce the volume of target receiving 5250 cGy (105%), the MU were slightly adjusted. The resulting dose distribution is shown in Figures 3.32 – 3.33. The mean dose to the PTV was 4863 ± 156 cGy, and 71 cm^3 of the non-target tissue received more than 4500 cGy.

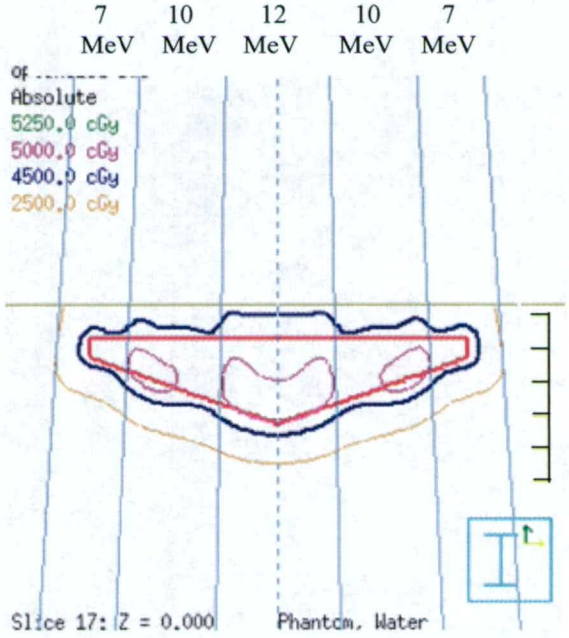

Figure 3.32. A central transverse plane of the pentagon-shaped simple target showing a 2D dose distribution as shown in Figure 3.30. The MU were slightly decreased.

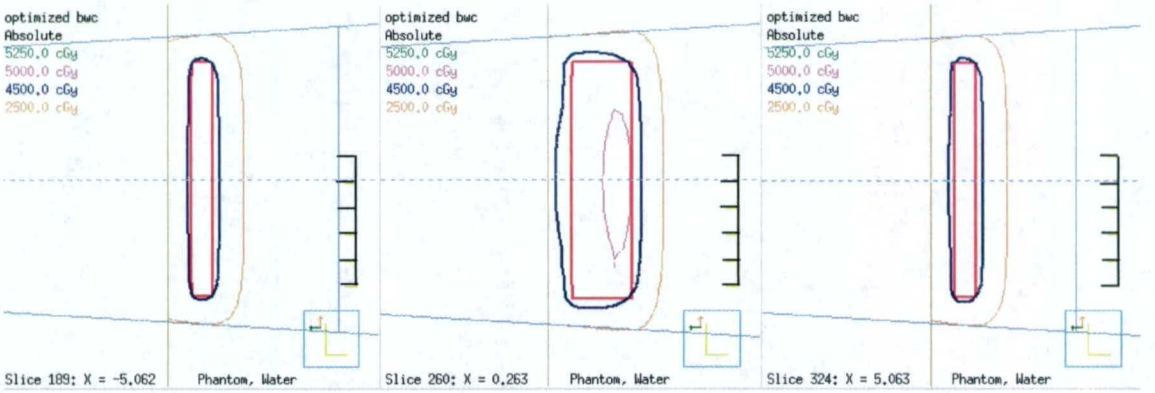

Figure 3.33. Central and lateral planes of the pentagon-shaped simple target for the same treatment plan shown in Figure 3.32. Slightly expanding the margins (superior-inferior direction) is a possibility, for this case.

3.4.2 Simple target 4: Summary

Figure 3.34 compares the DHV of the PTV and non-target tissue for these treatment plans, and Table 3.4 summarizes the PTV dose homogeneity and the dose to non-target tissue. The optimized-creation plan and the beam weight modification plan provided a high mean dose to the PTV with some inhomogeneity, and they also spared the non-target tissue well. The latter plan reduced the volume of non-target tissue receiving more than 4500 cGy.

Table 3.4. Dose statistics for the pentagon-shaped simple target treatment plans.

	PTV (162 cm^3)			Non-target tissue	
Treatment Plans	Mean Dose (cGy)	Standard Deviation (cGy)	$D(V_{90}) - D(V_{10})$ (cGy)	Volume > 45 Gy (cm^3)	Maximum Dose (cGy)
Creation, Optimized	4931	163	436	102	5285
Modification, fluence	4863	156	418	71	5231

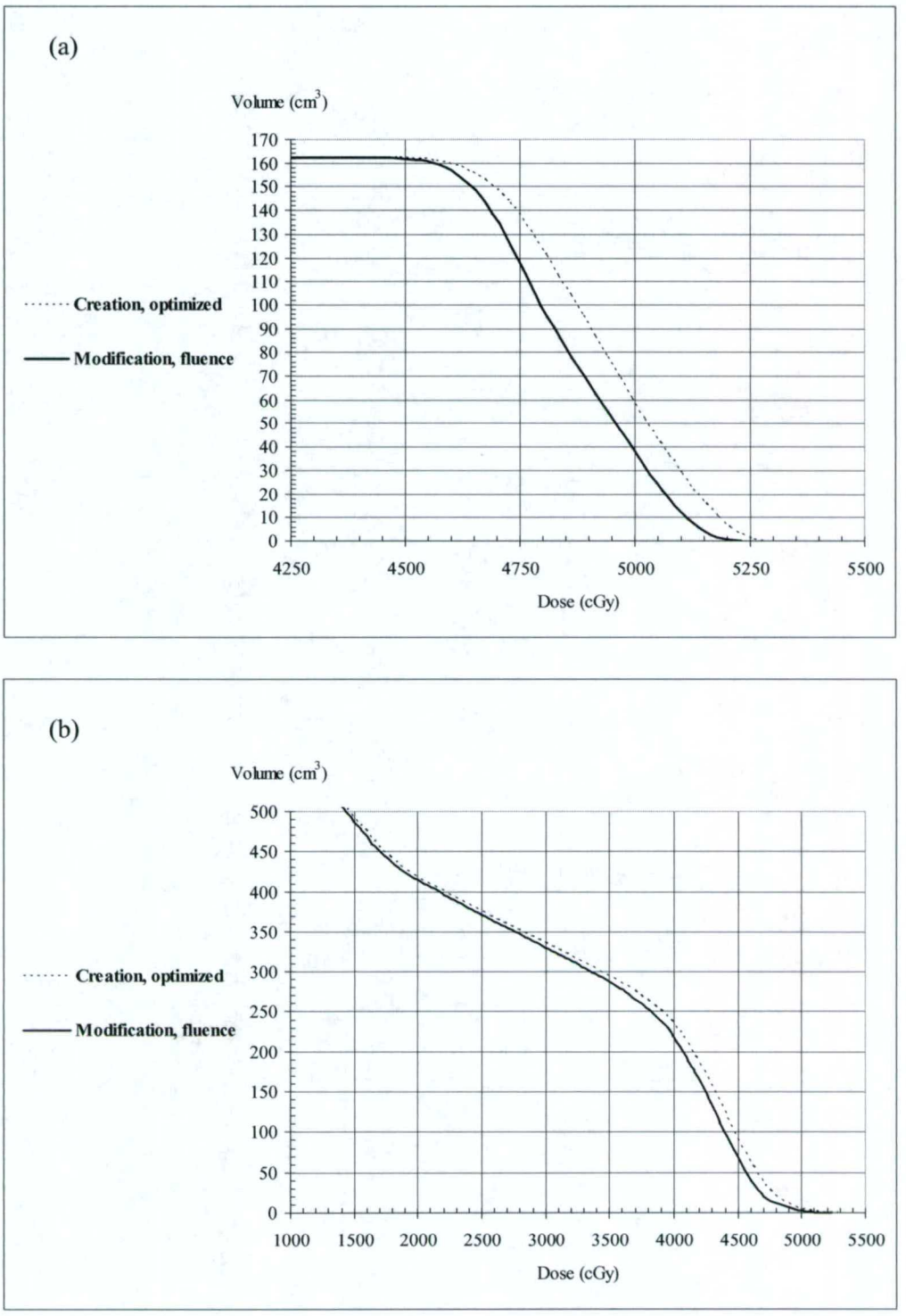

Figure 3.34. Dose volume histogram (DVH) for the pentagon-shaped simple target PTV (a) and non-target tissue (b).

3.5 Simple target 5

Simple target 5 was a rectangular toroid (233 cm^3) and it has eight-fold mirror symmetry. The algorithm was used to divide the PTV into depth regions and two fields were created using a 1-cm margin about the PTV: a C-shaped field and a strip field (Figure 3.35). These field shapes were chosen based on their ease to deliver with an eMLC, for example. The energies of the fields were set according to the depth of the PTV (12 MeV). Dose was computed and MU were set to deliver 200 cGy given for both fields. The resulting dose distribution (not shown) resulted in the 4500 cGy (90%) dose line encompassing the PTV with the exception of a small distal edge of the target. The mean dose to the PTV was 4803 ± 132 cGy.

The Pinnacle^3 IMRT Module was used to optimize the beam weighting, and the objectives were set to deliver a minimum dose value of 4500 cGy and a maximum dose value of 5250 cGy to the PTV. The resulting dose distribution is shown in Figures 3.36 – 3.37. The 4500 cGy isodose line did cover the deepest portion of the PTV; however, the dose homogeneity within the PTV decreased (volume of PTV receiving 5250 cGy increased). The mean dose to the PTV was 5037 ± 135 cGy, and 143 cm^3 of the non-target tissue receives more than 4500 cGy.

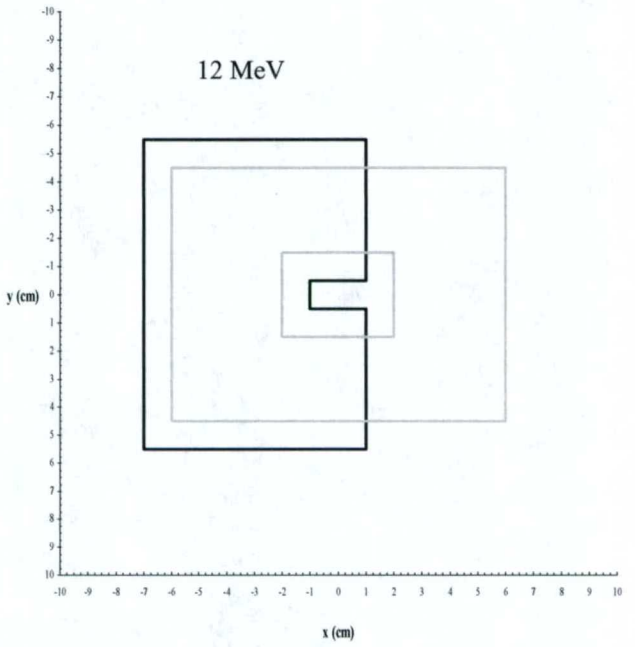

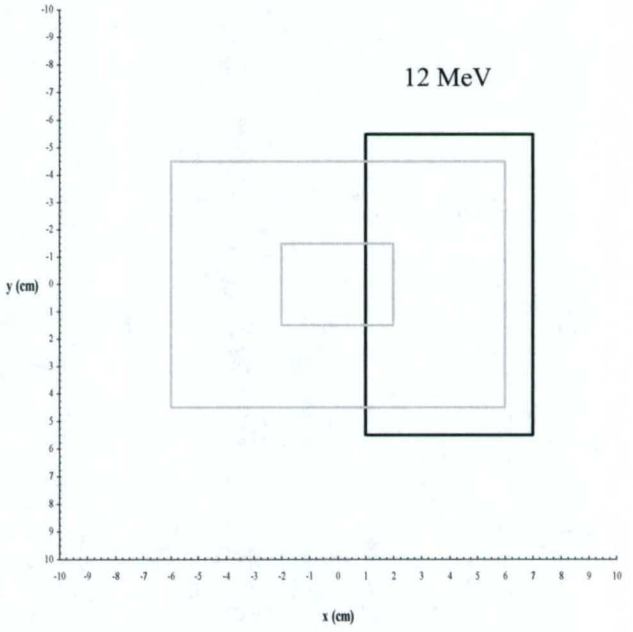

Figure 3.35. BEV of a C-shaped (A) and strip field (B) with a 1-cm margin (thin line) used to treat the rectangular toroid simple target (bold line).

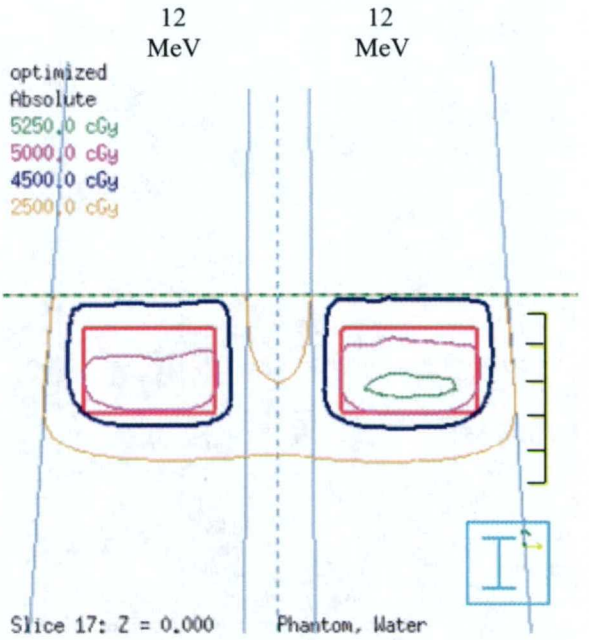

Figure 3.36. The central transverse plane of the rectangular toroid simple target (PTV) showing the dose distribution following beam weight optimization.

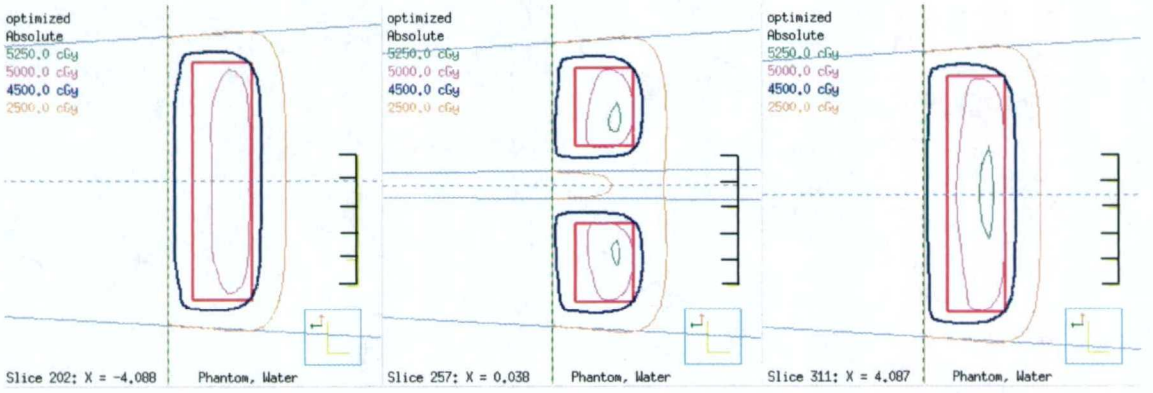

Figure 3.37. Central and lateral planes of the rectangular toroid simple target for the same treatment plan shown in Figure 3.36.

3.5.1 Simple target 5: Fluence decrease plan revision

The creation plan provided good 4500 cGy isodose coverage of the target. In an attempt to reduce the volume of target receiving 5250 cGy (105%) dose within the target, the MU were slightly adjusted. The resulting dose distribution is shown in Figures 3.38 – 3.39. The mean dose to the PTV was 4954 ± 132 cGy, and 120 cm^3 of the non-target tissue received more than 4500 cGy.

3.5.2 Simple target 5: Energy increase plan revision

Another plan revision option was to increase the electron beam energy [from 12 MeV to 15 MeV (Energy Increase)]. Dose was computed and beam weights were optimized using the same objective as before. The dose distribution for this plan is shown in Figures 3.40 – 3.41. This resulted in the 4500 cGy dose coverage extending further beyond the PTV. The mean dose to the PTV was 4959 ± 138 cGy, 316 cm^3 of the non-target tissue received more than 4500 cGy.

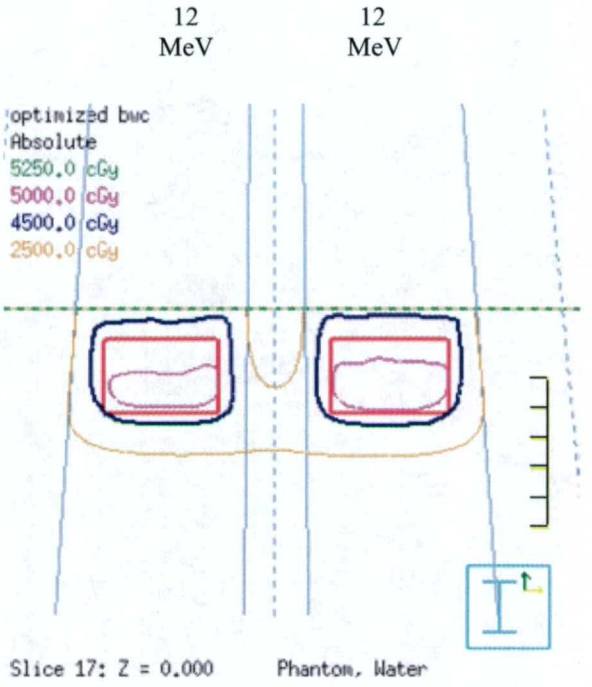

Figure 3.38. A central transverse plane of the rectangular toroid target showing a 2D dose distribution. The MU were slightly decreased in attempt to improve dose homogeneity (c.g. Figure 3.36).

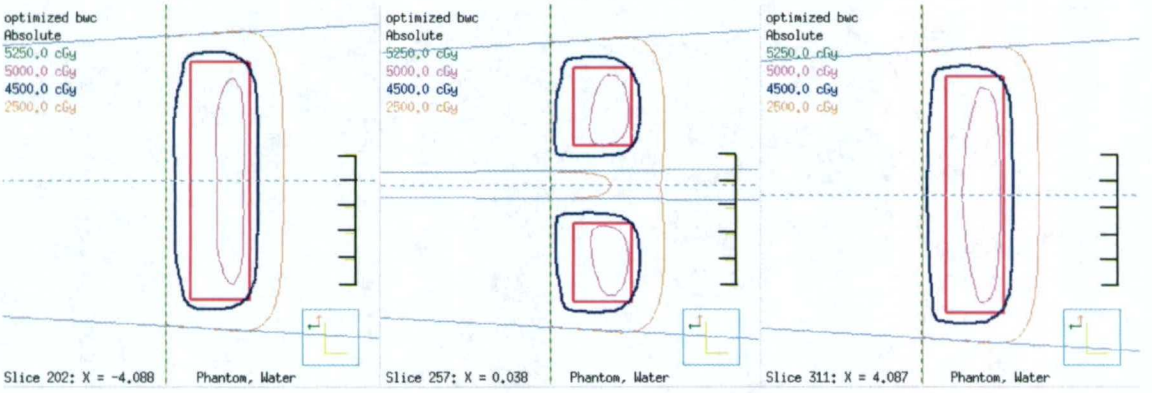

Figure 3.39. Central and lateral planes of the rectangular toroid simple target for the same treatment plan shown in Figure 3.38.

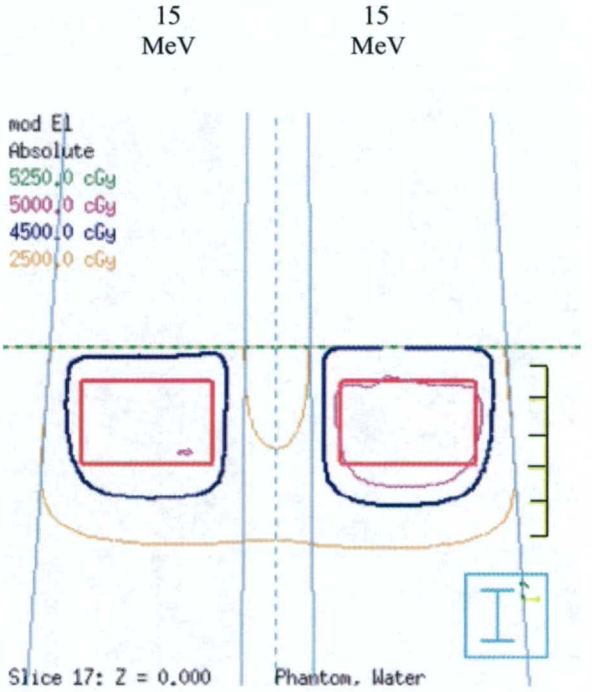

Figure 3.40. A central transverse plane of the rectangular toroid simple target showing a 2D dose distribution. The 12 MeV energy was increased to 15 MeV.

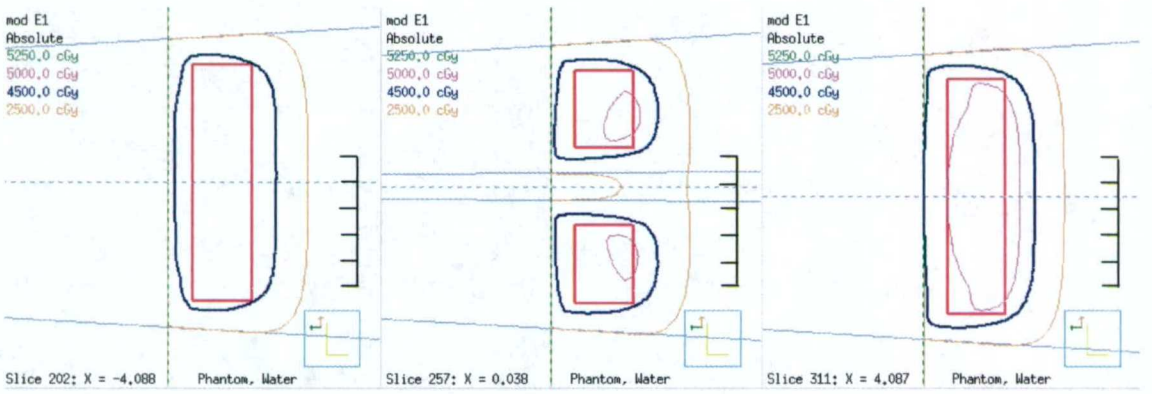

Figure 3.41. Central and lateral planes of the rectangular toroid simple target for the same treatment plan shown in Figure 3.40.

3.5.3 Simple target 5: Energy increase, field edge contraction plan revision

In an attempt to improve the 4500 cGy dose coverage of the previous revised plan, Field Edge Contraction was used to decrease the margin of the rectangular toroid at the central opening (Figure 3.42), and Electron Fluence Decrease was used to decrease the MU to shift the 4500 cGy isodose line closer to the target. Dose was computed and beam weights were optimized using a minimum dose value of 4500 cGy and a maximum dose value of 5150 cGy to the PTV. The resulting dose distribution is shown in Figures 3.43 – 3.44. The mean dose to the PTV was 4916 ± 109 cGy, and 255 cm^3 of the non-target tissue received more than 4500 cGy.

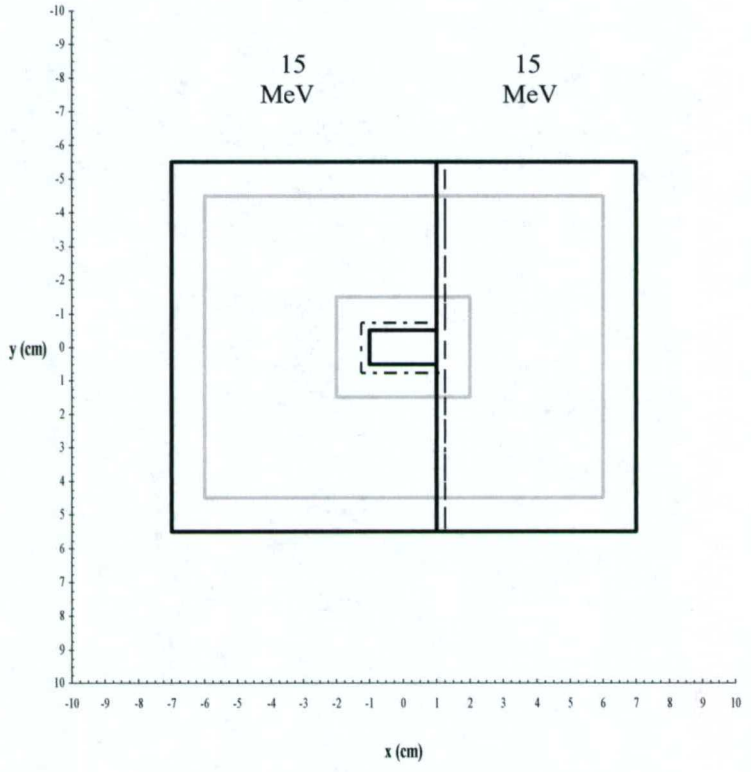

Figure 3.42. BEV display of the rectangular toroid simple target (gray) with applied field margins. In the creation phase, a uniform margin of 1 cm was applied and those fields are represented with the thin solid black line. For this plan, the field margins about the central opening were contracted by 0.25 cm. The modified fields are as dashed black lines.

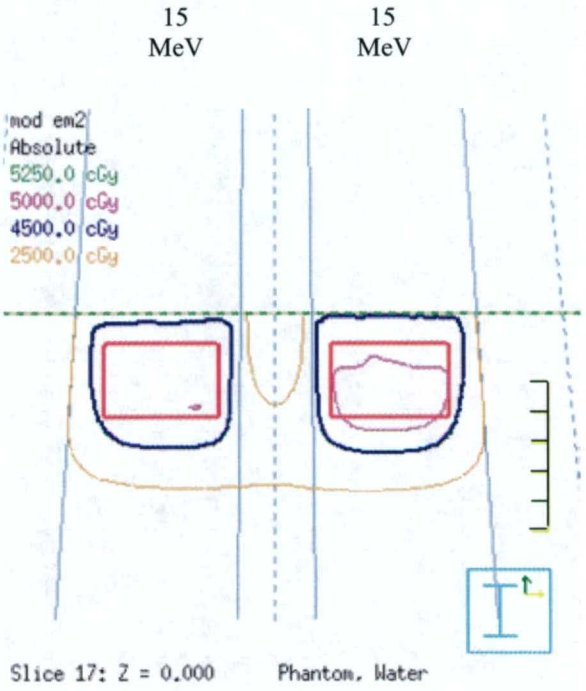

Figure 3.43. A central transverse plane of the rectangular toroid simple target showing a 2D dose distribution. The 12 MeV energy was increased to 15 MeV; the upper limit objective for beam weight optimization was decreased (from 5250 cGy to 5150 cGy), and the field margins about the center opening of the target was decreased by 0.25 cm.

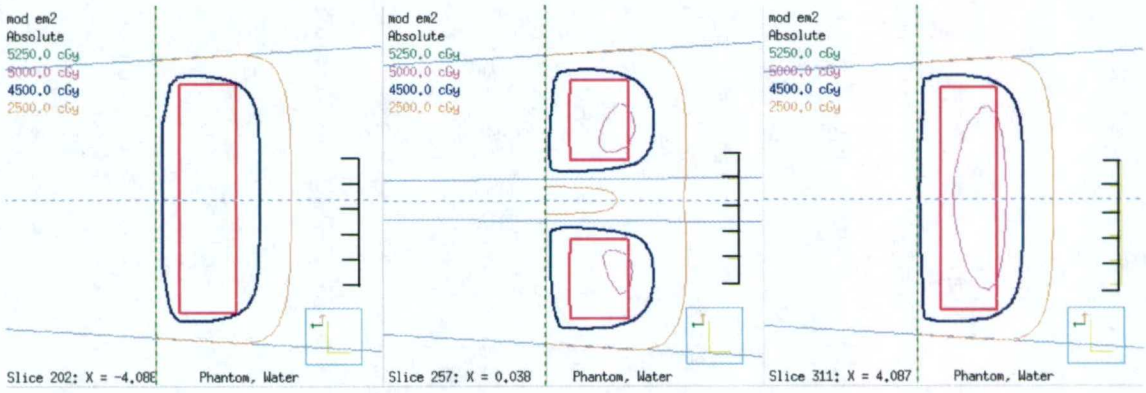

Figure 3.44. Central and lateral planes of the rectangular toroid simple target for the same treatment plan shown in Figure 3.43.

3.5.4 Simple target 5: Summary

Figure 3.45 compares the DVH of the PTV and non-target tissue for these treatment plans. Table 3.5 summarizes the PTV dose homogeneity and the dose to non-target tissue. The (energy increase, field edge expansion) plan had better PTV dose homogenity and lower $D(V_{90}) - D(V_{10})$ than the other plans. The 12 MeV (fluence decrease) plan spared the non-target tissue better than the other plans, i.e., less volume of tissue receiving more than 4500 cGy.

Table 3.5. Dose statistics for the rectangular toroid simple target treatment plans

	PTV (233 cm^3)			Non-target tissue	
Treatment Plans	Mean Dose (cGy)	Standard Deviation (cGy)	$D(V_{90}) - D(V_{10})$ (cGy)	Volume > 45 Gy (cm^3)	Maximum Dose (cGy)
Creation, Optimized	5037	135	361	143	5304
Modification, fluence	4954	132	353	120	5222
Modification, energy	4959	138	376	316	5250
Modification, energy-margin contraction	4916	109	293	255	5152

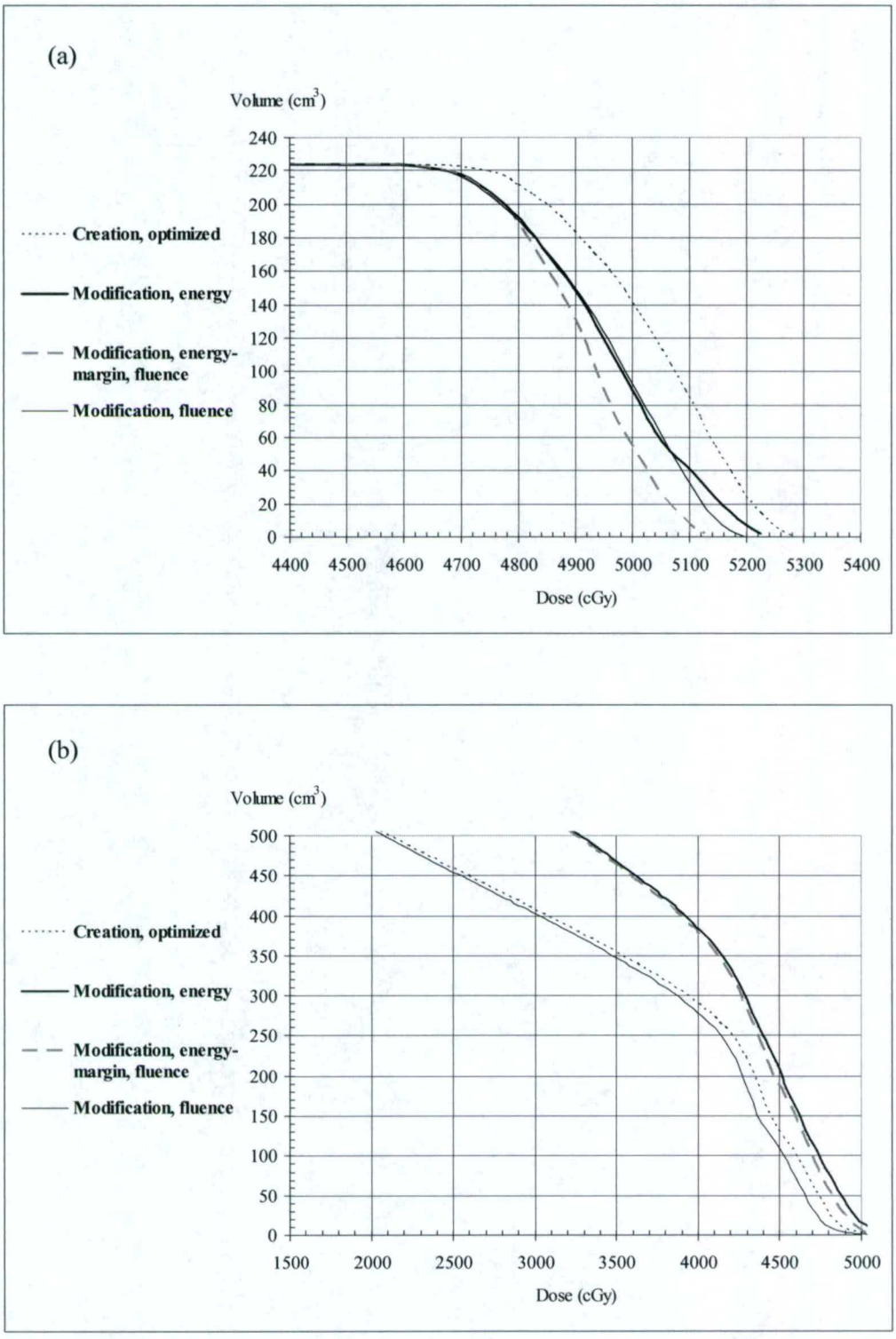

Figure 3.45. Dose volume histogram (DVH) for the rectangular toroid simple target PTV (a) and non-target tissue (b).

3.6 Simple target 6

Simple target 6 was a volume (238 cm^3) with greater variability than the previous simple targets. It does not have translational or mirror symmetry; therefore it is more clinically realistic. The algorithm was used to divide the PTV into depth regions and thirteen-fields were created (Figure 3.46). The energies of the fields were set according to the depth of the PTV and ranged from 12 MeV for the deepest portions of the PTV to 5 MeV for the shallowest portions of the PTV. Dose was computed and MU were set to deliver 200 cGy given dose for each field.

The Pinnacle^3 IMRT Module was then used to optimize the beam weighting. The objectives were set to deliver a minimum dose of 4500 cGy and a maximum dose of 5250 cGy to the PTV. The resulting dose distribution is shown in Figure 3.47. The mean dose to the PTV was 4995 ± 299 cGy, and 143 cm^3 of the non-target tissue received more than 4500 cGy. For most slices, coverage (4500 cGy isodose line) is good, except for a few slices (z = 6; z = -4).

3.6.1 Simple target 6: Energy smooth, region connector, energy increase plan revision

To move the 4500 cGy isodose line toward the distal surface of the PTV, several modification techniques were utilized: Energy-Smoothing, Region Connectors, and Energy Increase. The new fields are shown in Figure 3.48. These operations were performed on fields on the lower left side of the treatment plan. The resulting dose distributions are shown in Figure 3.49. The mean dose to the PTV was 4971 ± 199 cGy, and 176 cm^3 of the non-target tissue receives more than 4500 cGy. The same beam-weight optimization was used as above.

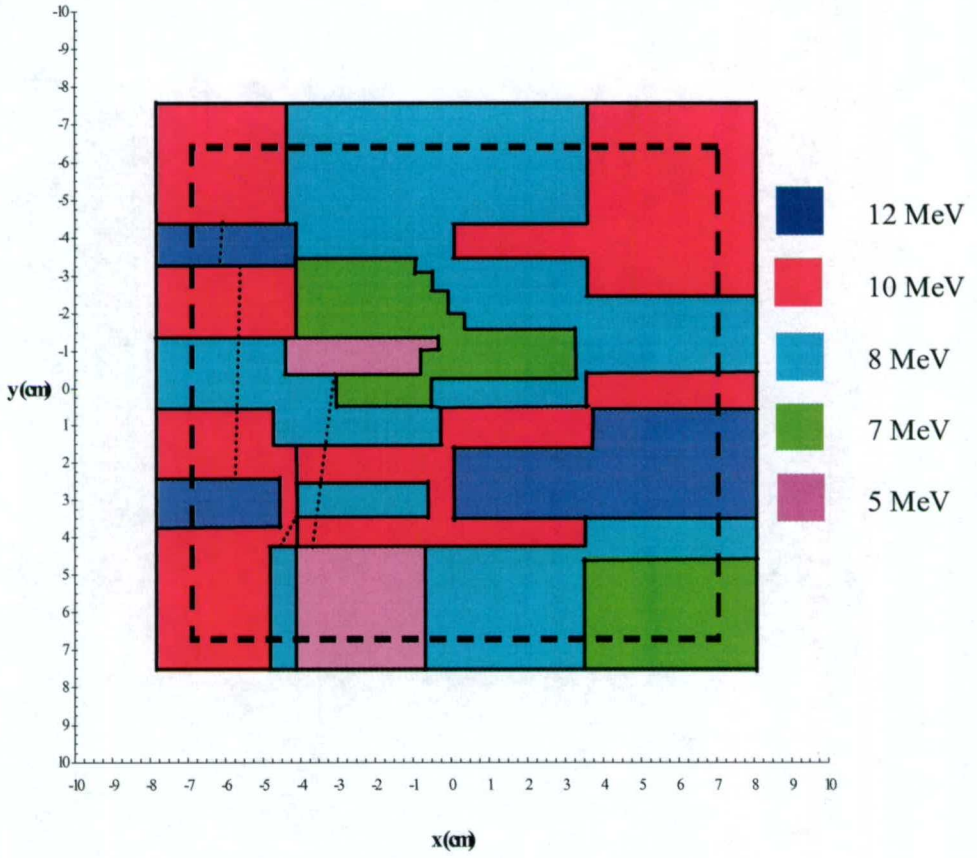

Figure 3.46. A BEV display of a simple target (thick dashed line) with applied field margins. This target has more variation along the distal surface then the previous simple targets. In the creation phase, a uniform margin of 1 cm was applied. Region Connectors (dotted lines) were used to combine smaller fields at the same target depth.

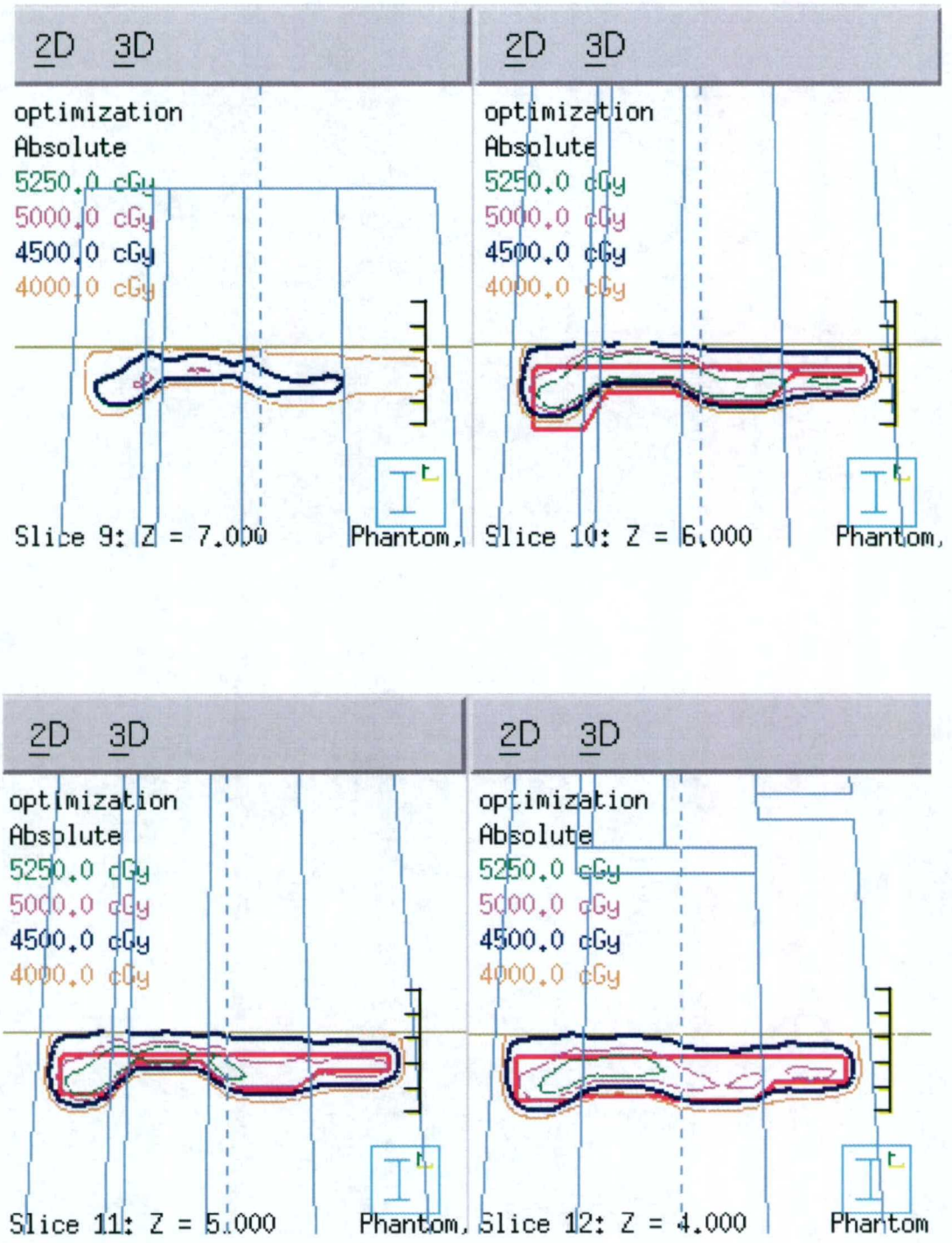

Figure 3.47. Transverse planes of the target (PTV) showing the dose distributions following beam weight optimization. The 5250 cGy (105% of given dose), 5000 cGy (given dose), 4500 cGy (90% of given dose), and 2500 cGy (50% of given dose) dose lines are shown.

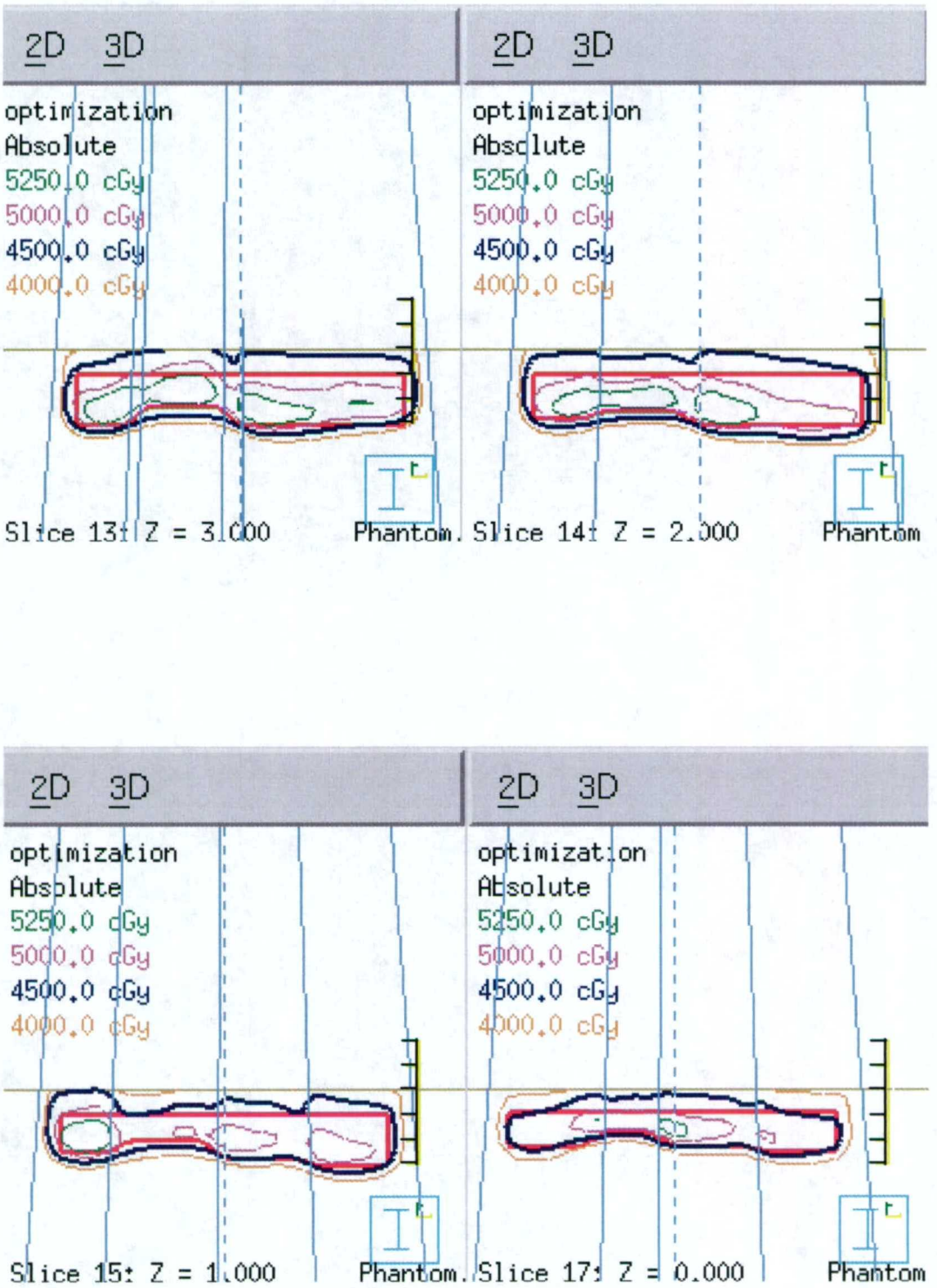

Figure 3.47. Continued.

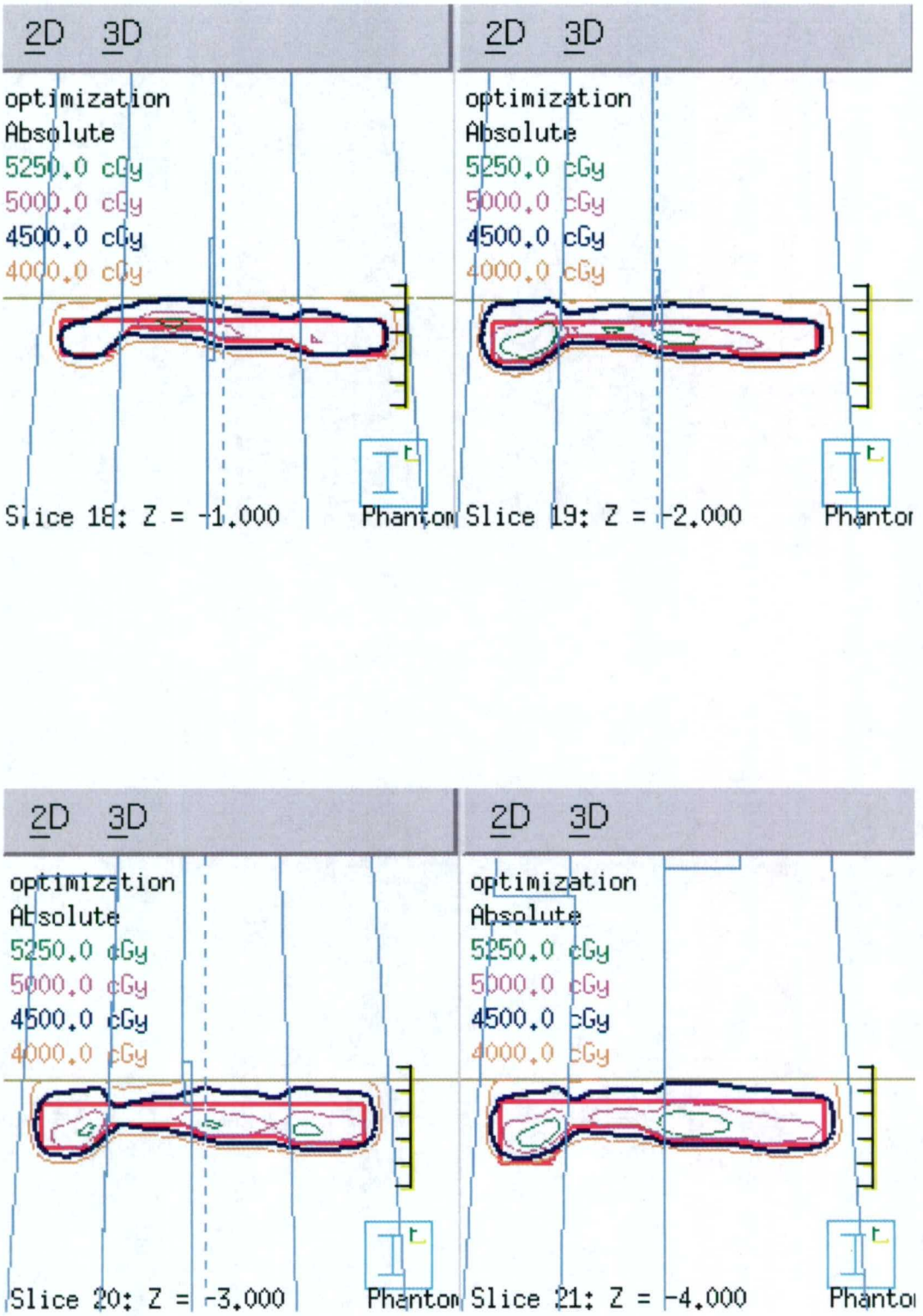

Figure 3.47. Continued.

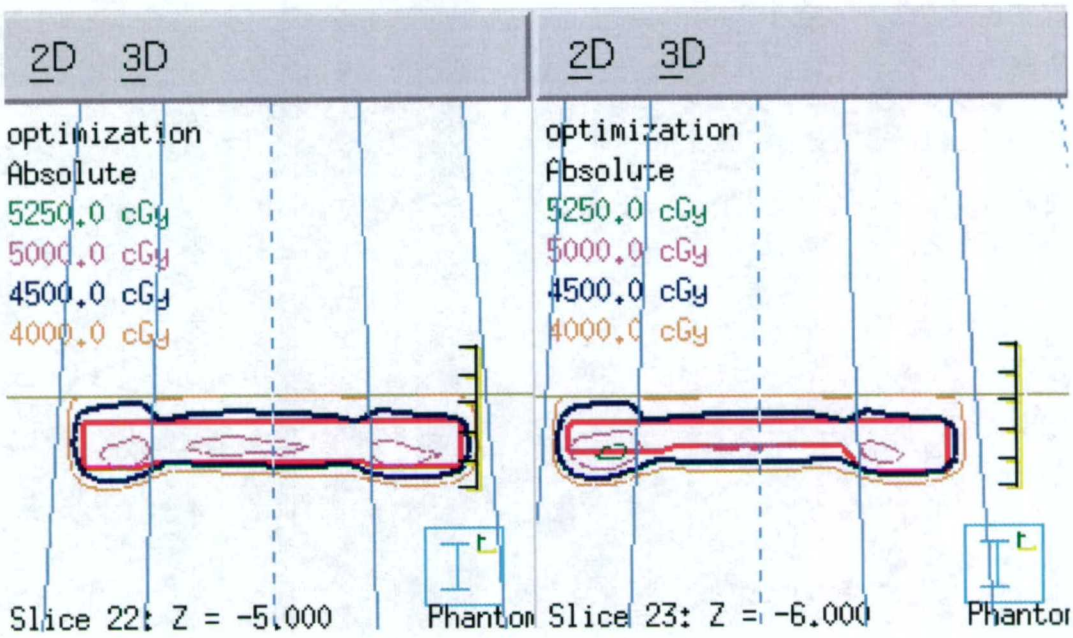

Figure 3.47. Continued.

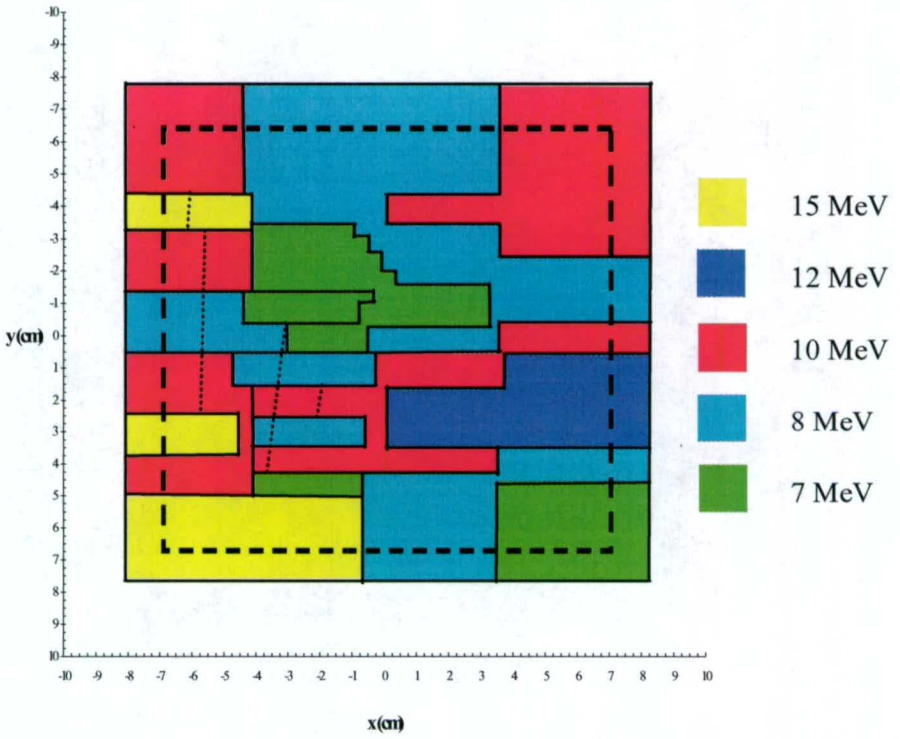

Figure 3.48. BEV display of the target (black bold dashed line) with applied field margins. In the creation phase, a uniform margin of 1 cm was applied and optimization of the beam weights were performed. Various modifications techniques (Energy Smooth, Region Connector, and Energy Decrease) were used to move the 4500 cGy isodose line closer the distal edge of the PTV. These techniques were applied primarily to the fields located in the lower left corner of the treatment plan.

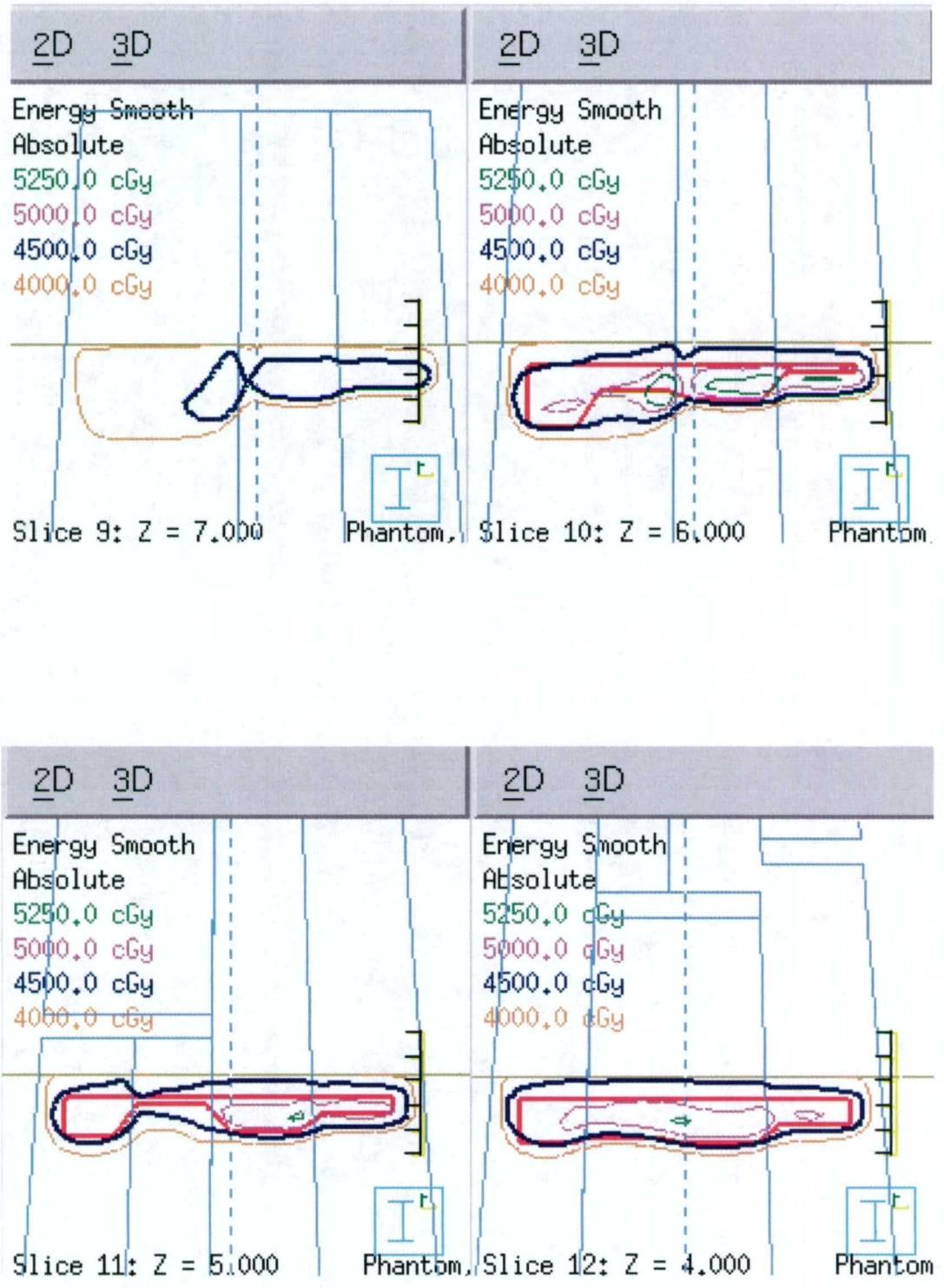

Figure 3.49. Transverse planes of the target (PTV) showing the dose distributions following beam weight optimization. The 5250 cGy (105% of given dose), 5000 cGy (given dose), 4500 cGy (90% of given dose), and 2500 cGy (50% of given dose) dose lines are shown.

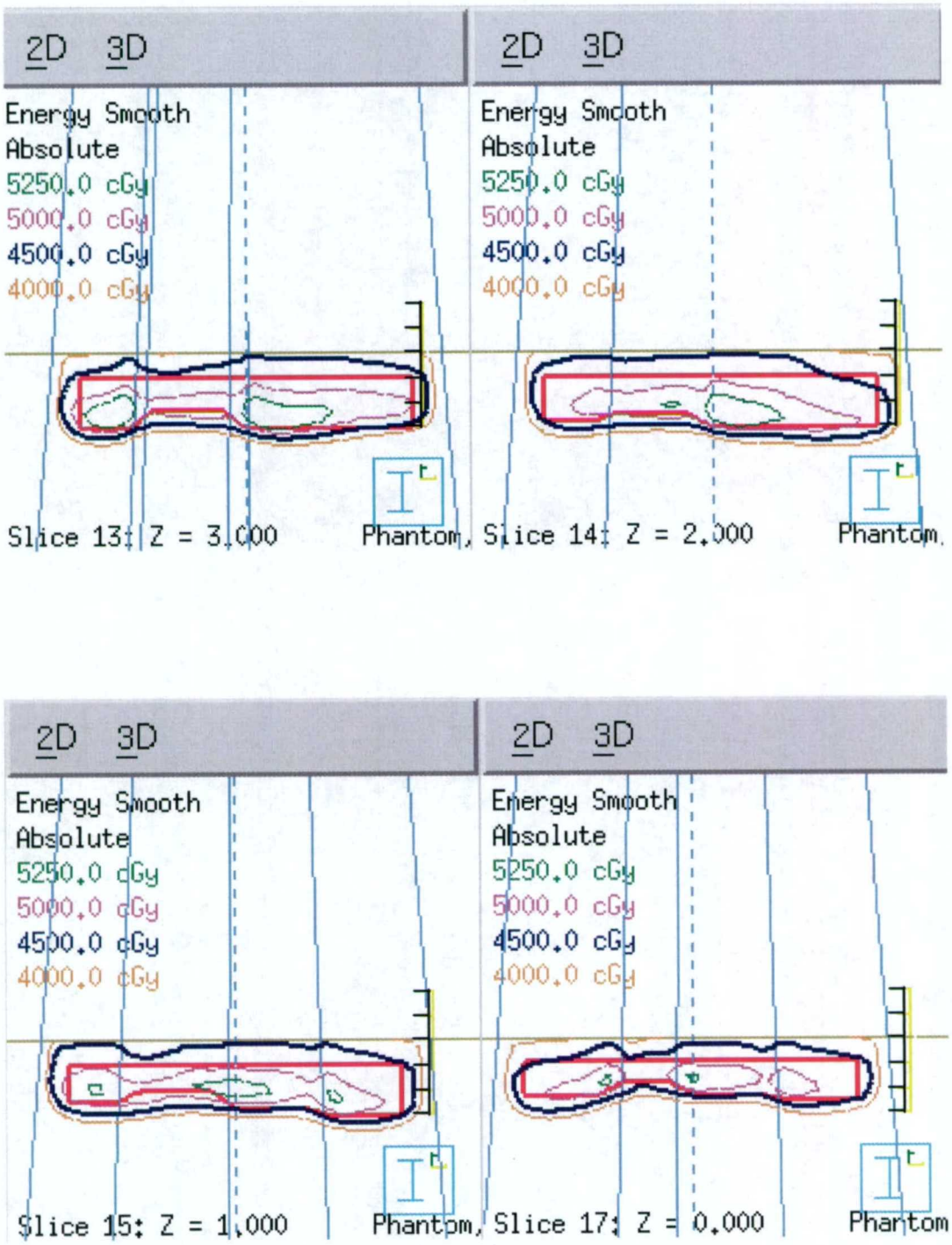

Figure 3.49. Continued.

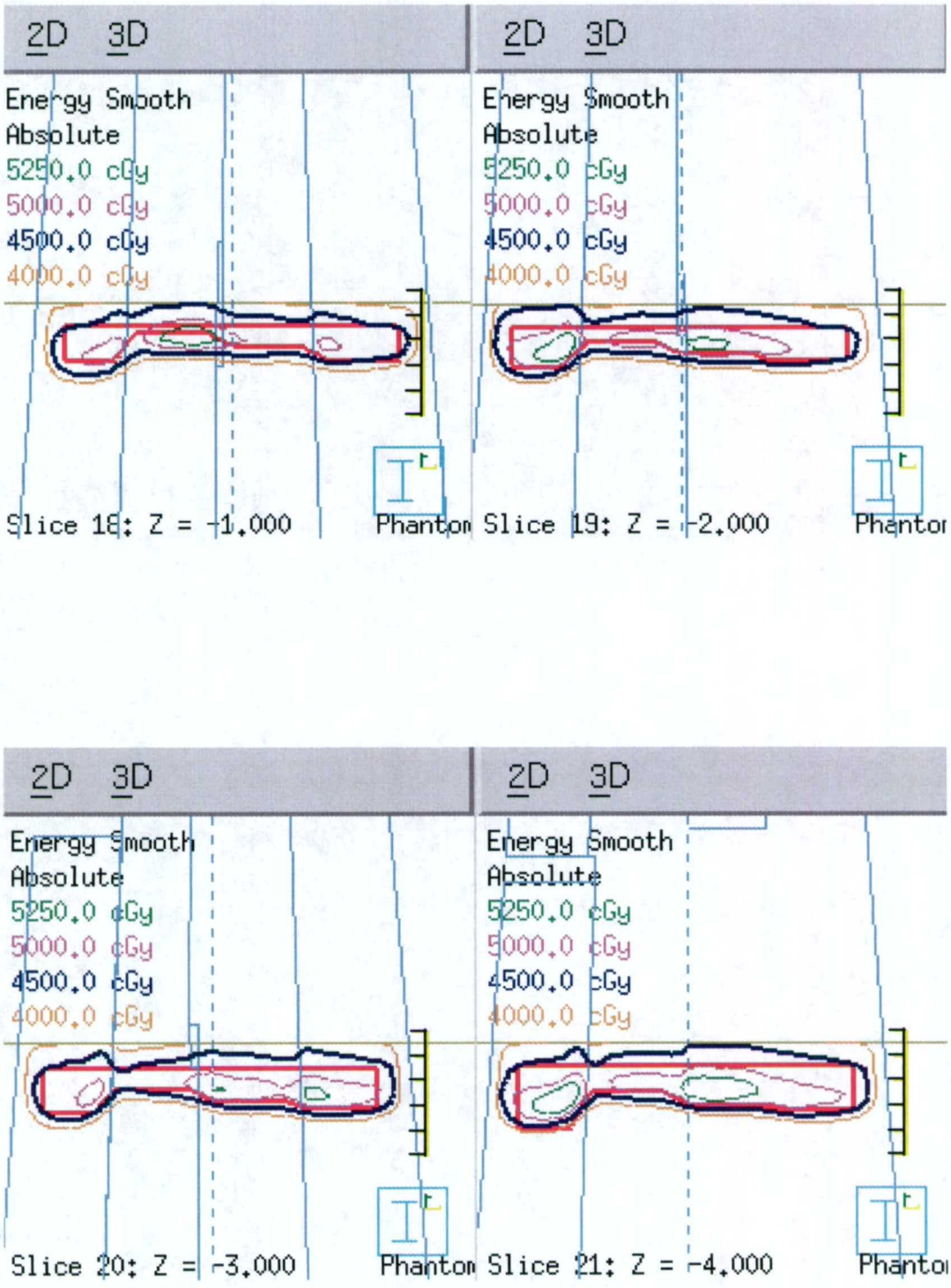

Figure 3.49. Continued.

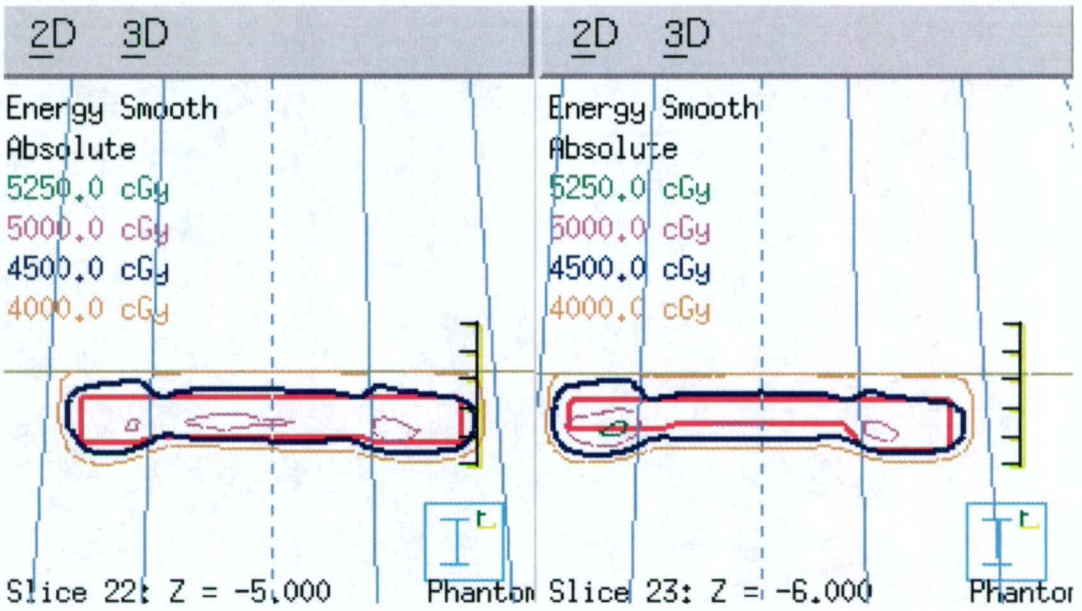

Figure 3.49. Continued.

3.6.2 Simple target 6: Summary

Figure 3.50 compares the DVH of the PTV and non-target tissue for these treatment plans. Table 3.6 summarizes the PTV dose homogeneity and the dose to non-target tissue. The optimized creation plan provided a good starting point for treating this target. The energy modified plan improved target coverage and homogeneity at the expense of normal tissue dose (volume of non-target tissue receiving more than 4500 cGy), although the maximum dose received by the non-target tissue was reduced (note: this does not appear to be significant on the DVH).

Table 3.6. Dose statistics for the 3D simple target treatment plans.

	PTV (238 cm^3)			Non-target tissue	
Treatment Plans	Mean Dose (cGy)	Standard Deviation (cGy)	$D(V_{90}) - D(V_{10})$ (cGy)	Volume > 45 Gy (cm^3)	Maximum Dose (cGy)
Creation, Optimized	4995	299	625	143	6006
Modification, energy-margin	4971	199	548	176	5562

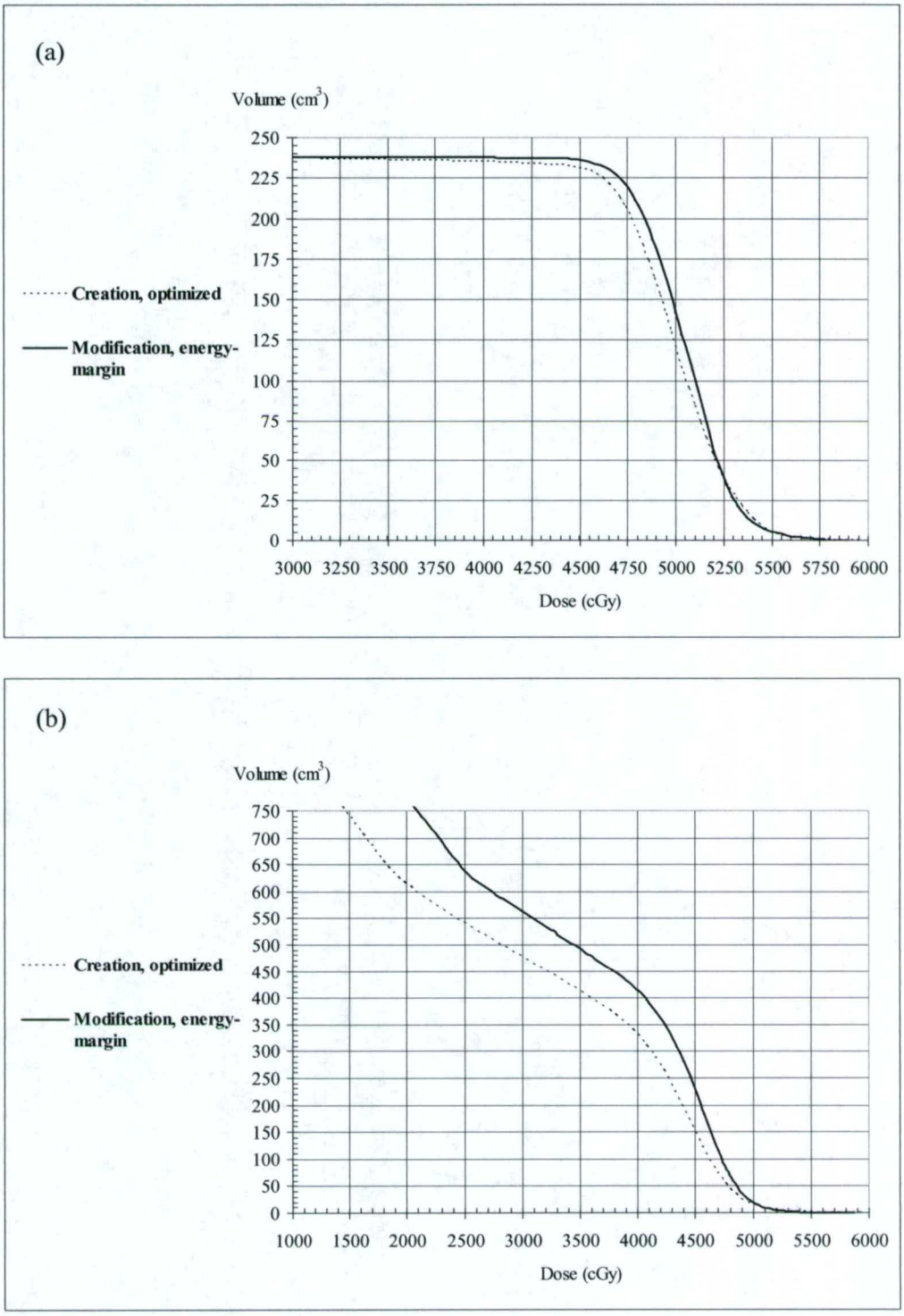

Figure 3.50. Dose volume histogram (DVH) for the 3-D simple target PTV (a) and non-target tissue (b).

3.7 Patient 1

3.7.1 Patient 1: Bolus plan

The patient was treated using customized bolus. Figure 3.51 shows the dose distribution; the MU were adjusted to deliver 200 cGy given dose per fraction in order to compare the bolus plan to the segmented-field ECT plans. The mean dose to the PTV was 4989 ± 336 cGy, and 11% of the left lung received more than 2000 cGy.

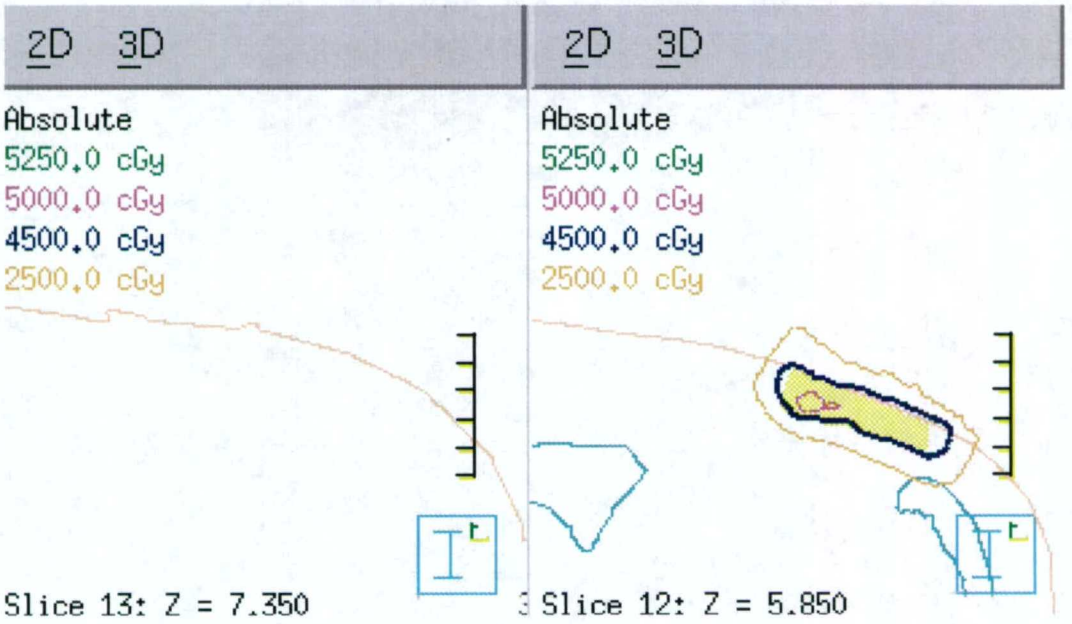

Figure 3.51. Transverse planes of patient 1 showing the dose distribution of the bolus treatment plan.

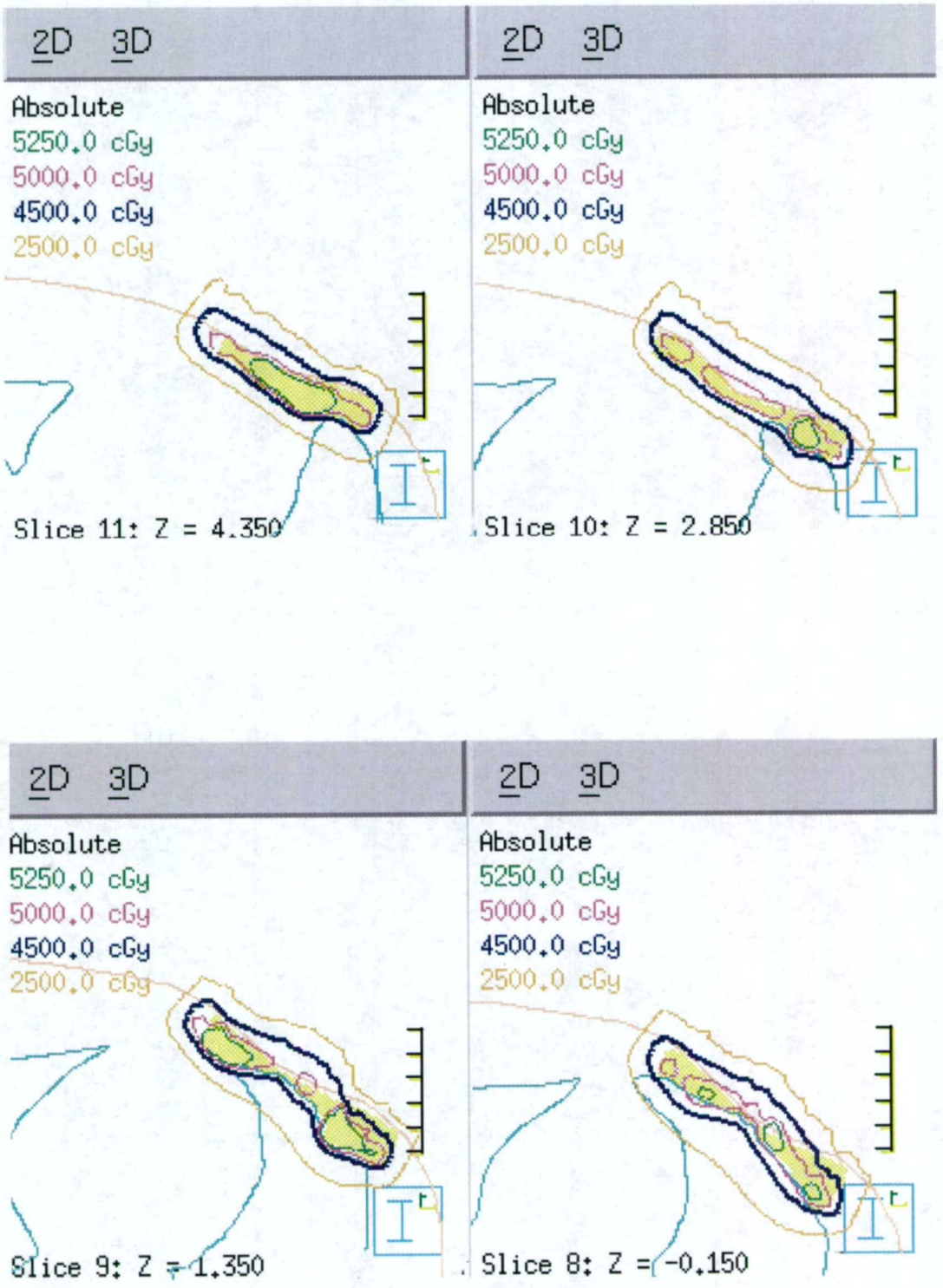

Figure 3.51. Continued.

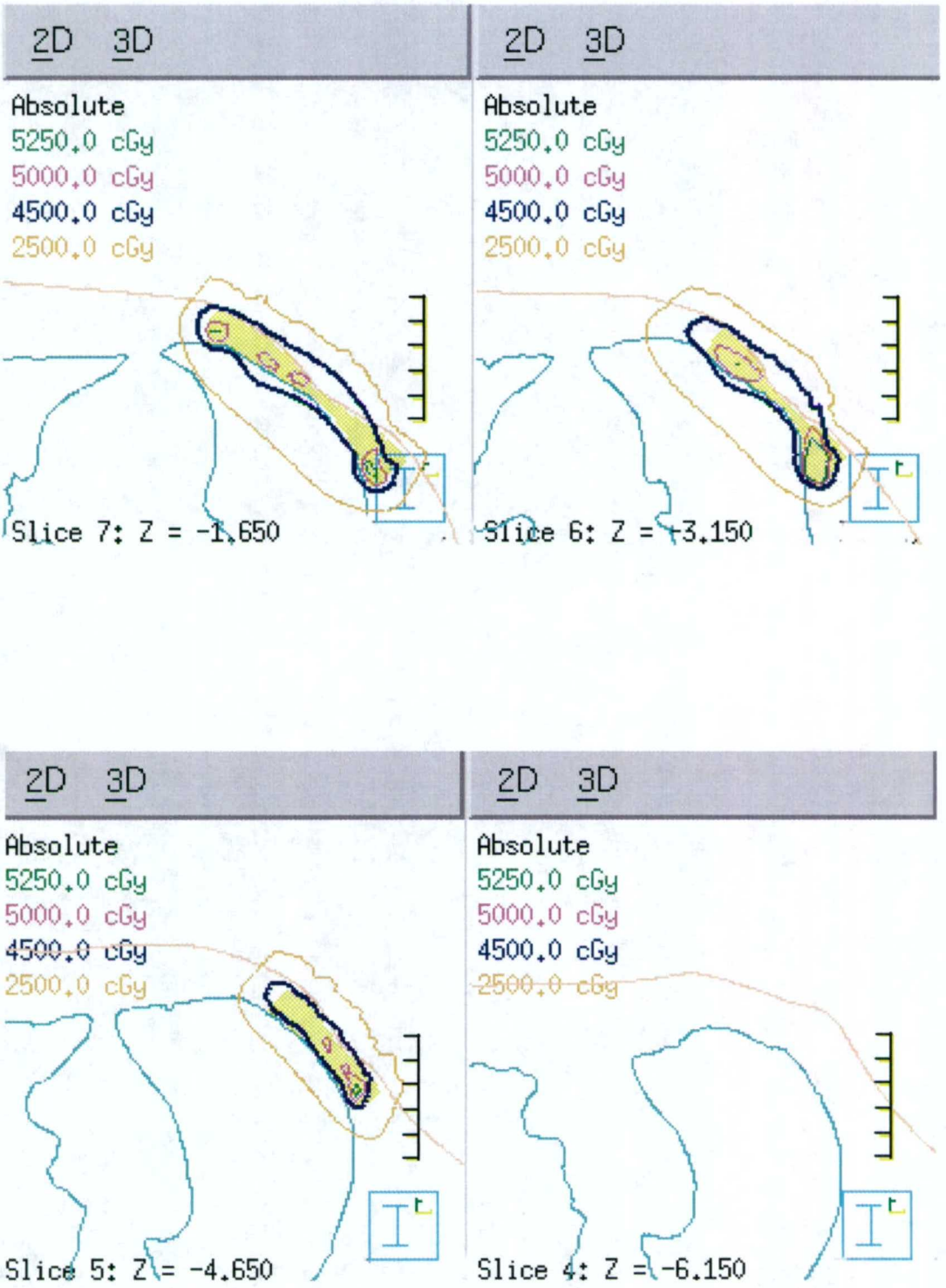

Figure 3.51. Continued.

3.7.2 Patient 1: Creation

The segmented-field ECT algorithm requires that the incident beam use a gantry angle of 0°. To accomplish this, the patient CT image set was rotated counter-clockwise 35° placing the distal surface of the PTV approximately perpendicular to the beam's central axis. An initial treatment plan was created based on PTV depth. Eight treatment fields comprising electron energies ranging from 5 MeV to 8 MeV were used with a 1-cm margin around the PTV. Figure 3.52 shows a BEV of the treatment fields in relation to the PTV. MU were set to deliver 200 cGy given dose for each field and dose was computed. The resulting dose distribution is shown in Figure 3.53. The 4500 cGy (90%) dose line does not completely cover the entire surface of the PTV. The mean dose to the PTV was 4625 ± 397 cGy, and 17% of the left lung receives more than 2000 cGy.

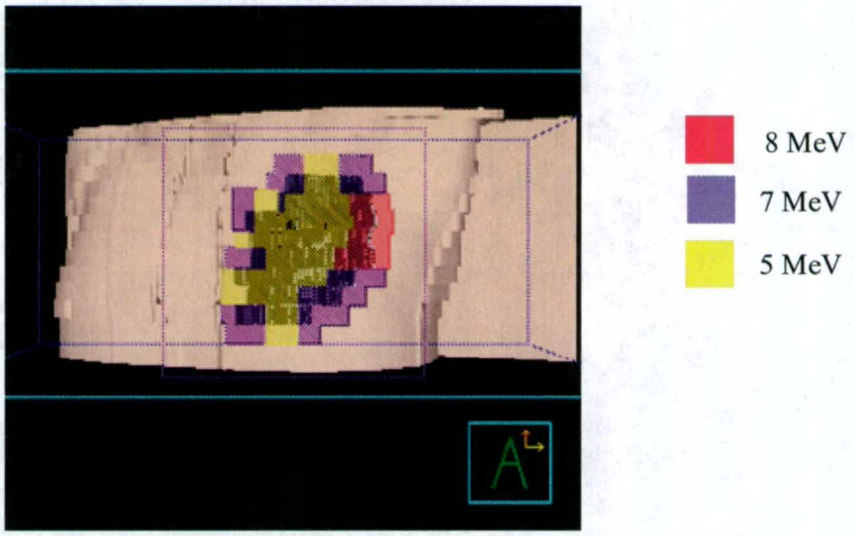

Figure 3.52. A BEV of the treatment fields superimposed on the PTV (dark gray).

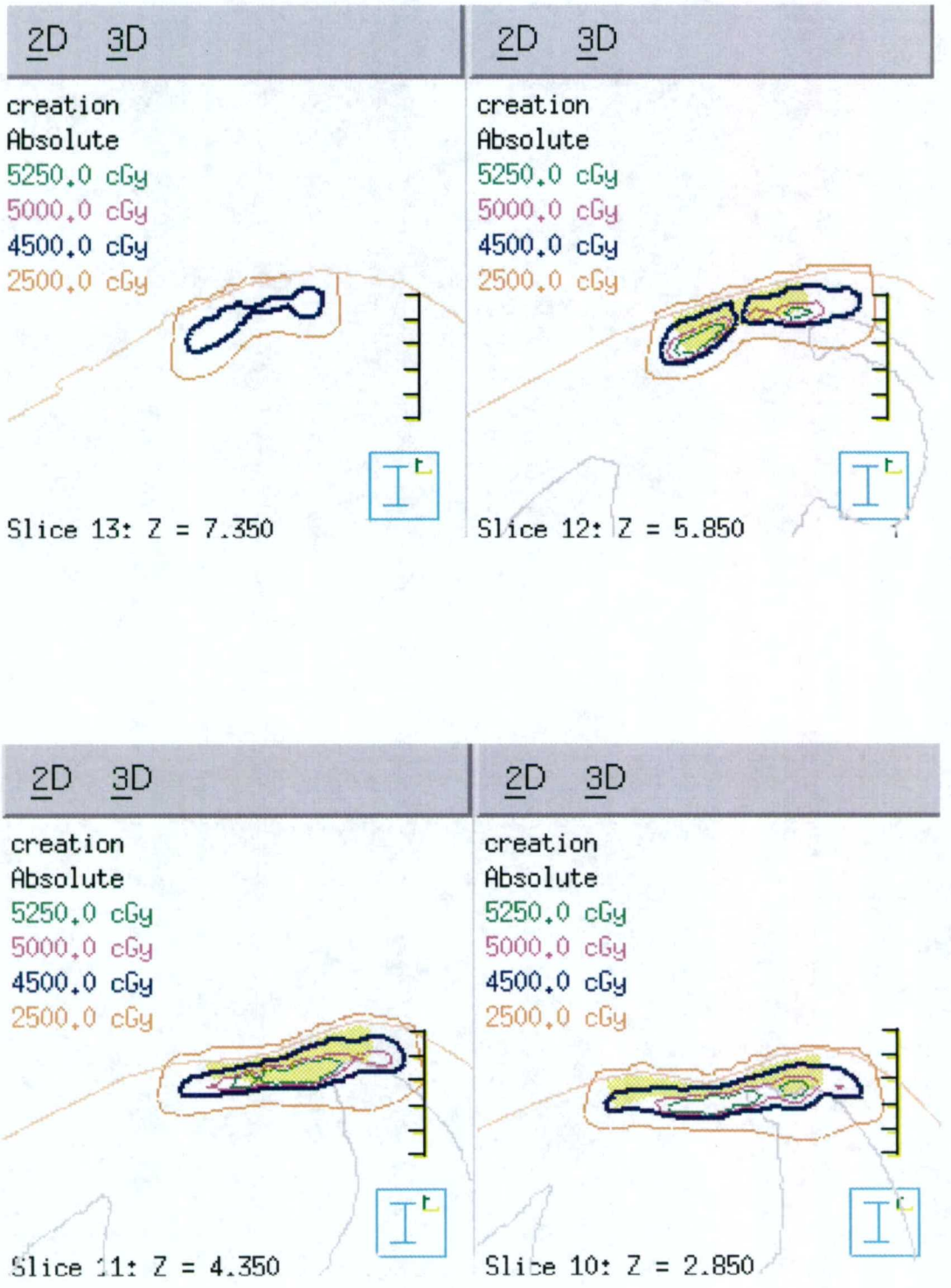

Figure 3.53. Transverse planes of patient 1 showing the dose distribution of the creation step treatment plan. The PTV is shown in solid yellow and the lungs are outlined in gray.

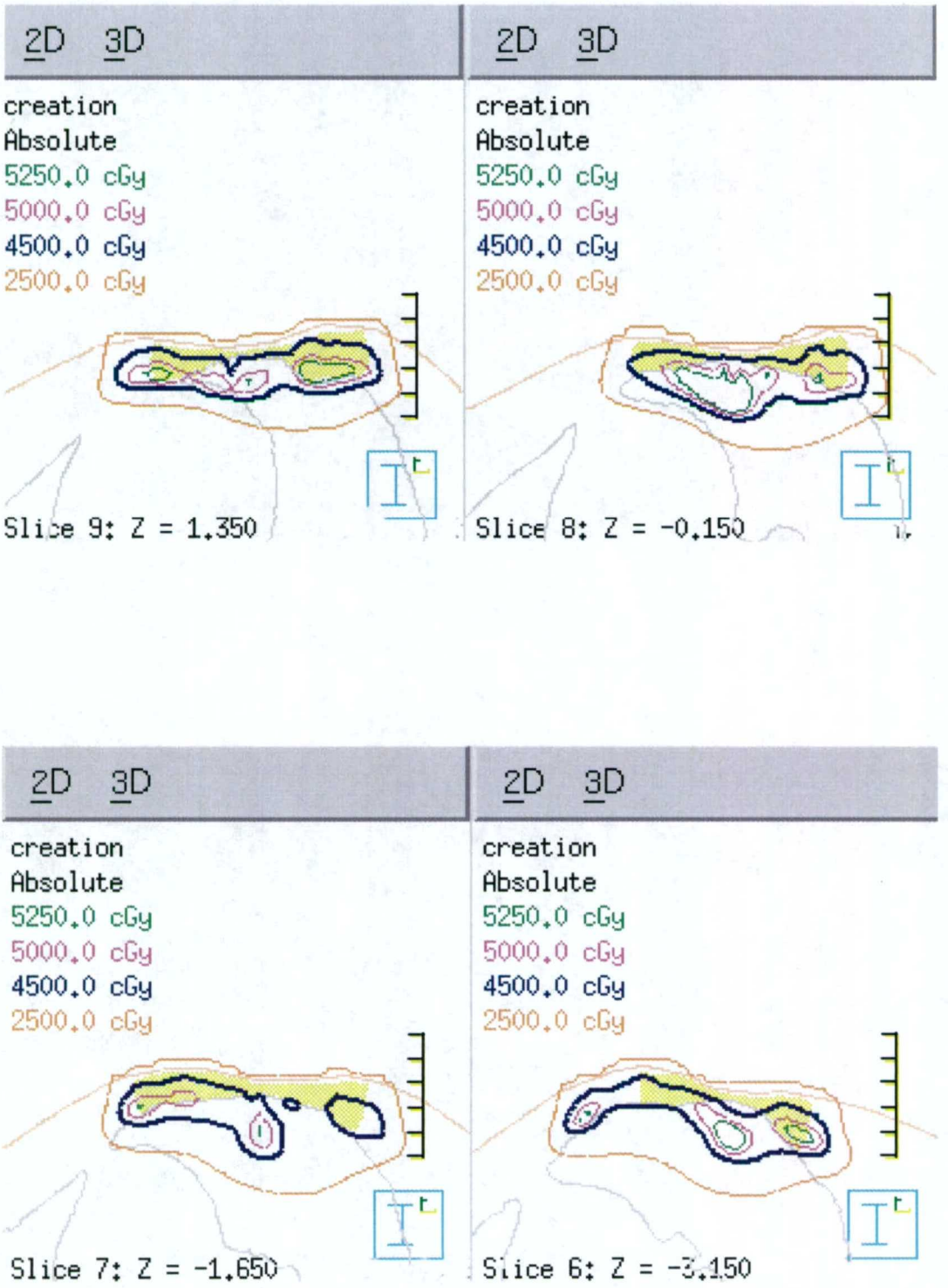

Figure 3.53. Continued.

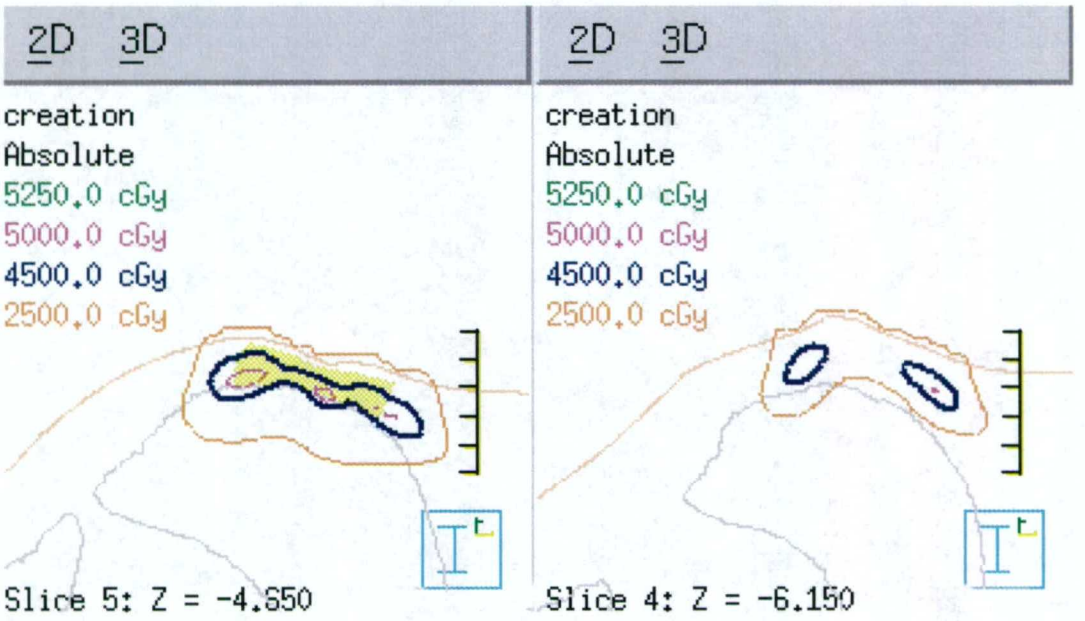

Figure 3.53. Continued.

3.7.3 Patient 1: Optimization

The Pinnacle^3 IMRT module was used to optimize the beam weighting, and the objectives were set to deliver a minimum dose of 4500 cGy and a maximum dose of 5250 cGy to the PTV. No lung tissue dose objectives were set. The resulting dose distribution is shown in Figure 3.54. The 4500 cGy isodose line coverage of the PTV improved (i.e., along the anterior surface of the PTV), and the dose homogeneity within the PTV improved in comparison to the creation step plan. The mean dose to the PTV was 5071 cGy, and 19% of the left lung received more than 2000 cGy.

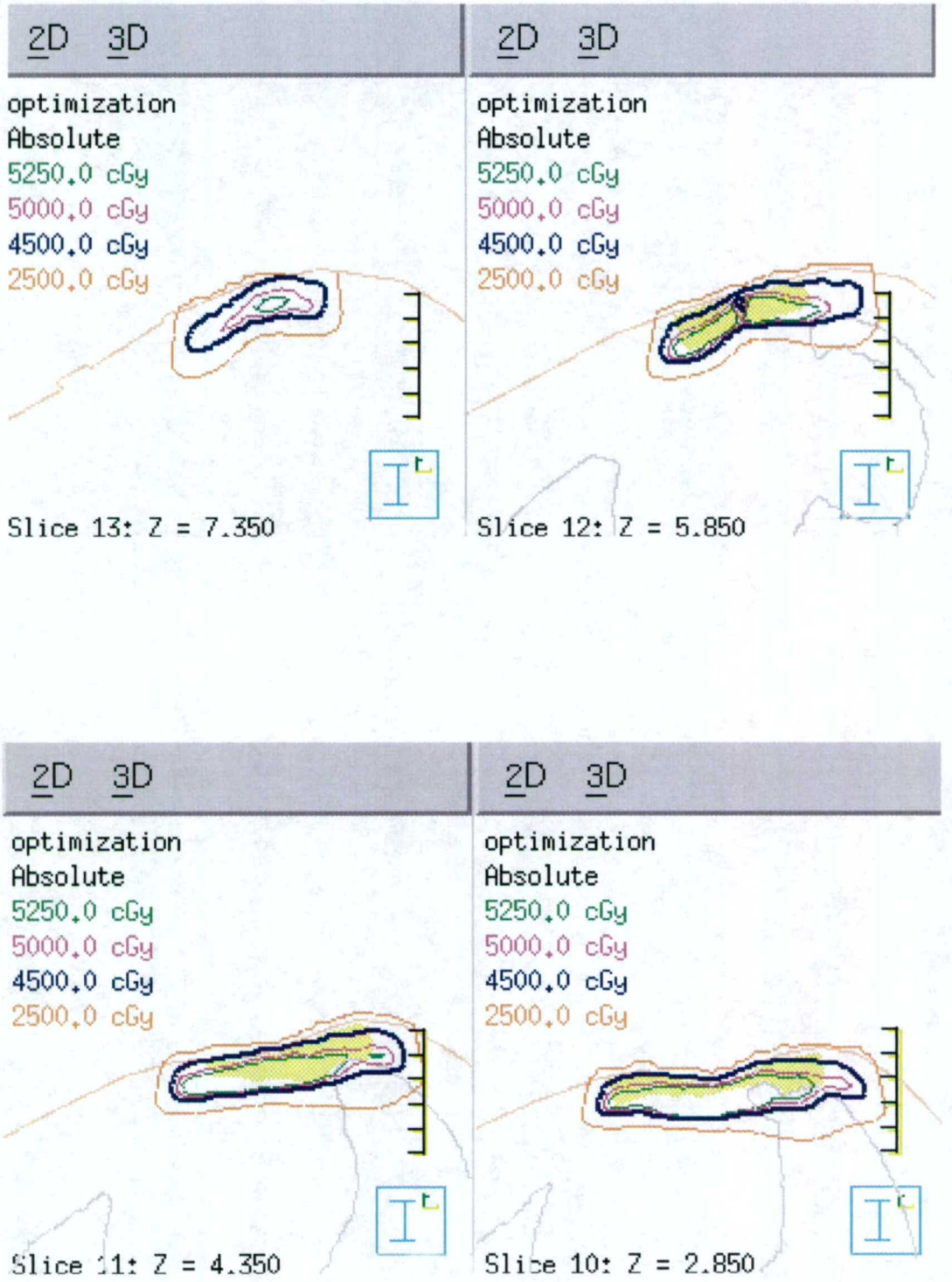

Figure 3.54. Transverse planes of patient 1 showing the creation phase treatment plan dose distribution after beam weight optimization. See text for dose objective information.

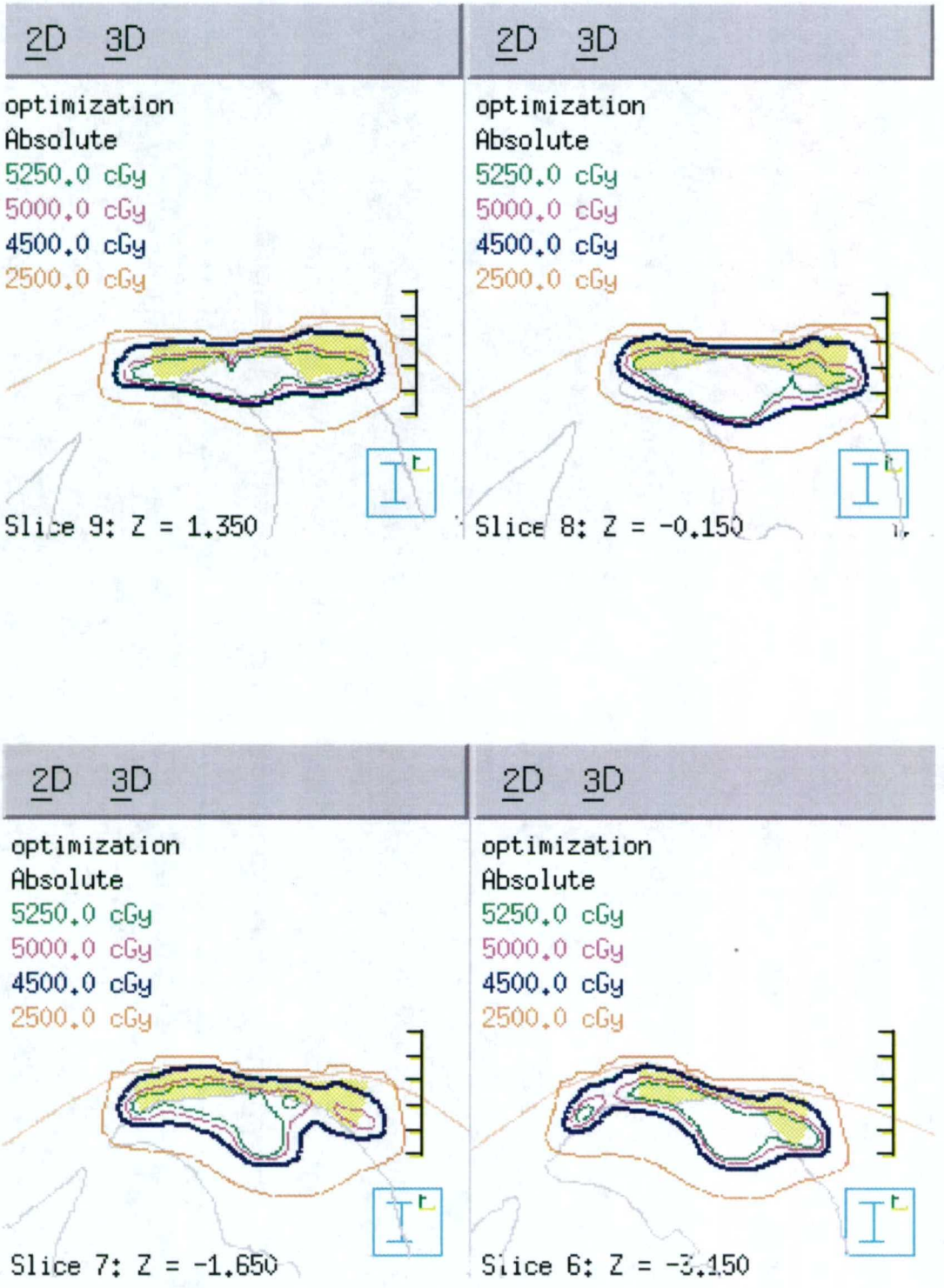

Figure 3.54. Continued.

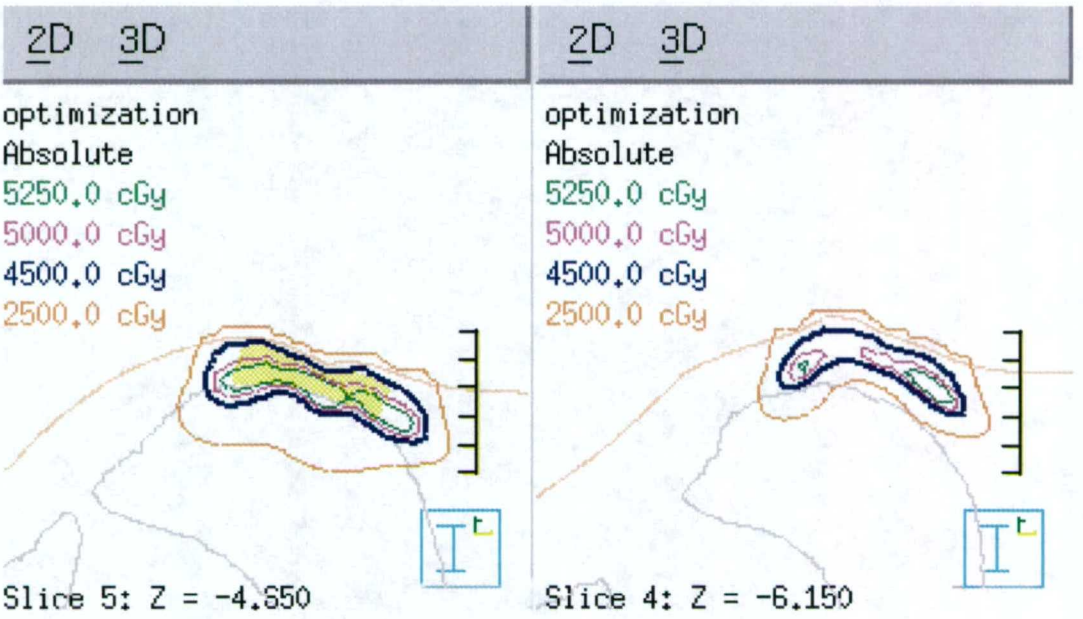

Figure 3.54. Continued.

3.7.4 Patient 1: Modification

For this patient, a large area (approximately 8 cm x 8 cm) of the treatment plan uses 5 MeV electrons because of the shallow chest wall. These fields are centrally located in the treatment plan, and can be identified in the resultant dose distribution as the region of the 4500 cGy isodose line that extends into the lung. One option available, via the modification phase, to improve the dose coverage in the central portion of the treatment plan is to use the energy decrease technique to move the 4500 cGy isodose line toward the distal edge of the PTV; however, the field already uses the lowest available energy beam.

Another revision option is to use the electron fluence decrease technique, where the MU for the 5 MeV fields are decreased in an attempt to move the 4500 cGy isodose line coverage toward the distal edge of the PTV. This option was attempted and the lung dose could be reduced; however, the 4500 cGy isodose line coverage along the anterior surface of the PTV degraded as did the target dose homogeneity. One should note that the skin dose for 5 MeV is quite low, which is why the optimization

increased the weight of the 5 MeV beams; the optimizer was attempting to achieve minimum PTV dose (as specified above), and the lung did not have a dose objective.

In an attempt to improve the plan further, different dose objectives were investigated. The objectives were set to deliver a minimum of 4000 cGy to 90% of the PTV, a maximum of 5500 cGy to 10% of the PTV, and a maximum dose of 2000 cGy to 18% of the lung volume. The resultant dose distribution is shown in Figure 3.55. The mean dose to the PTV was 4941 cGy, and 18% of the left lung received more than 2000 cGy. Decreasing the lung volume constraint to 15% improved the dose distribution only slightly, but the 4500 cGy isodose line coverage along the distal surface of the PTV degraded as did the target dose homogeneity.

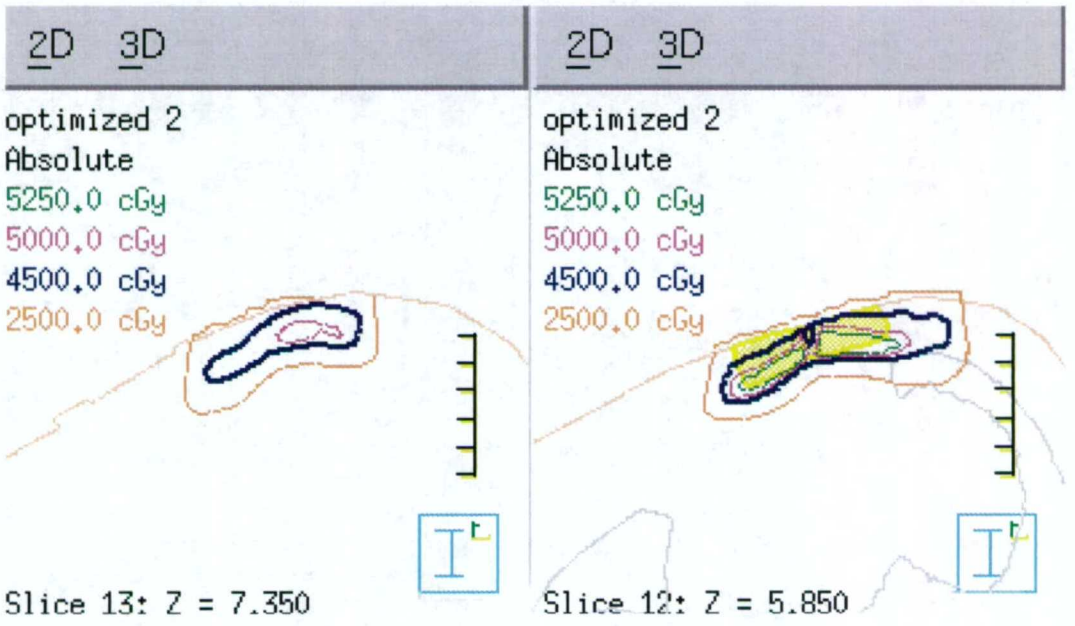

Figure 3.55. Transverse planes of patient 1 showing the dose distribution of the modified treatment plan. The beam weights were optimized using different dose objectives than the creation plan.

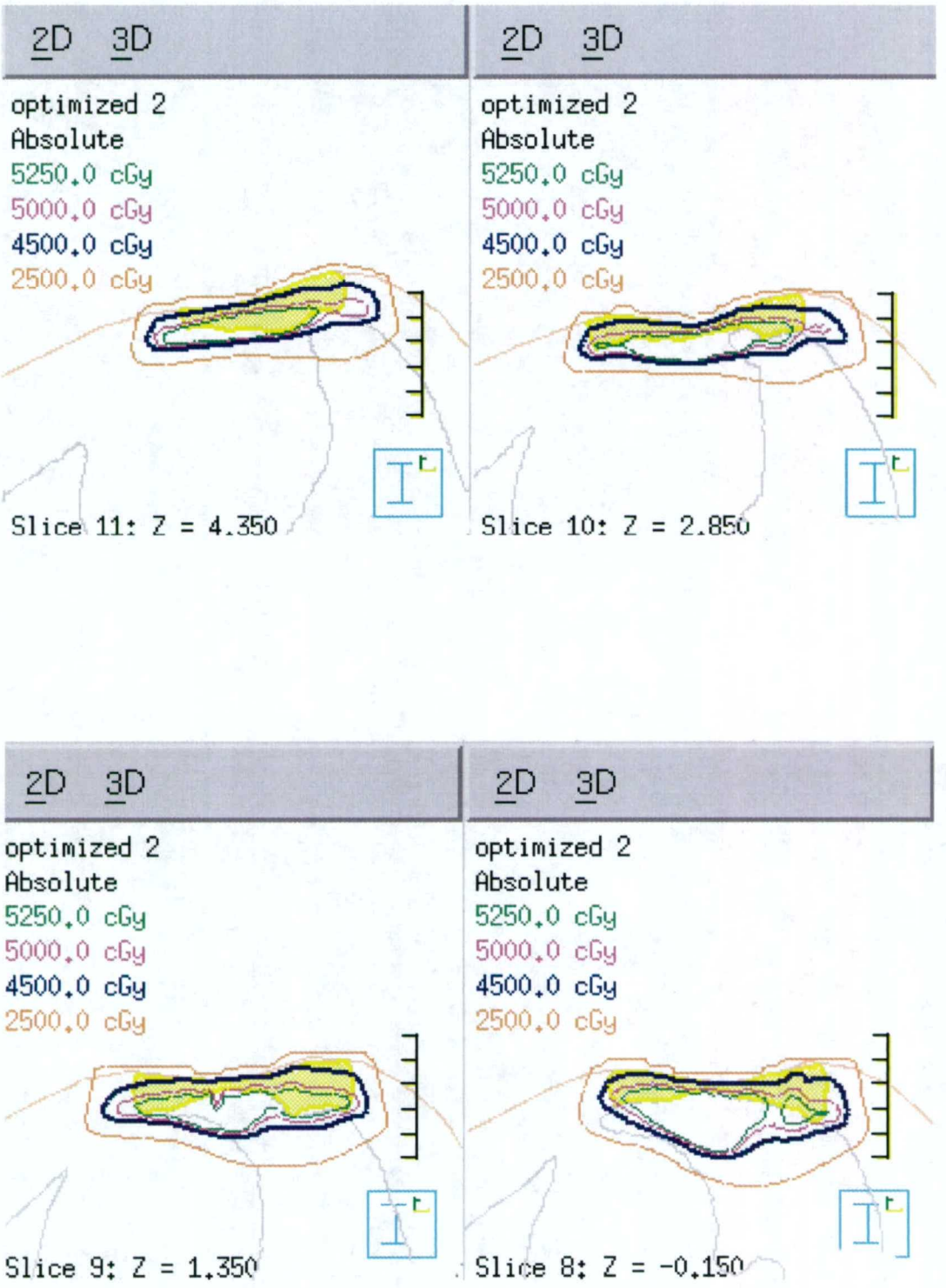

Figure 3.55. Continued.

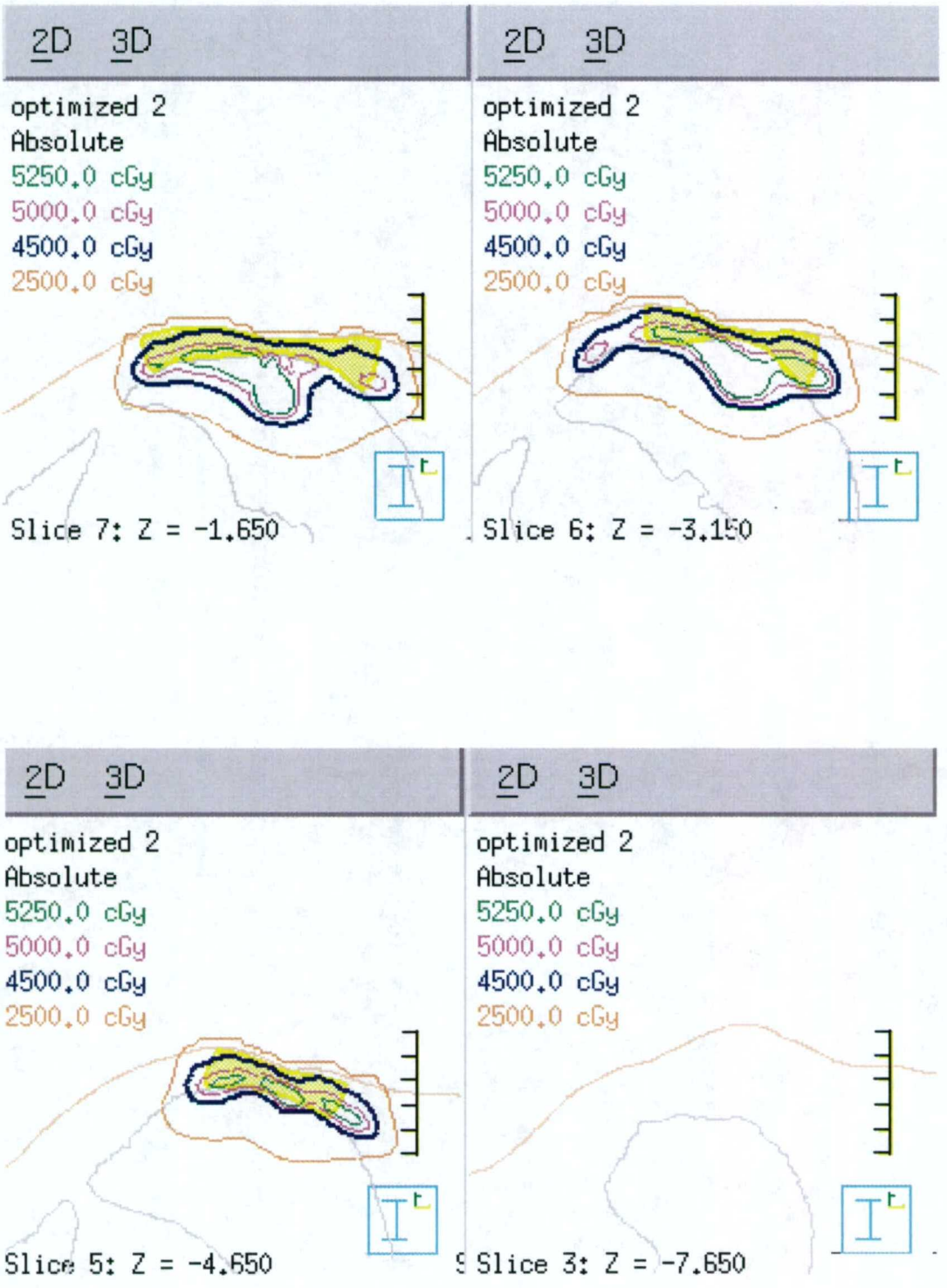

Figure 3.55. Continued.

3.7.5 Patient 1: Summary

Figure 3.56 compares the DVH of the PTV and left lung tissue for these treatment plans, and Table 3.7 summarizes the PTV dose homogeneity and the dose to the left lung. The creation step provided an adequate starting point for treating the PTV, i.e., the 90% isodose line encompassed a majority of the PTV. The optimized creation plan improved the 90% isodose line coverage of the PTV, especially along the anterior surface; however, the 4500 cGy isodose line penetrated too far into the lung. Although the central portion of the treatment plan already utilized the lowest available electron energy (5 MeV), attempts to decrease the lung dose were made. The fluence-modified plan slightly decreased the dose to the lung, but did not decrease the depth of 4500 cGy isodose line penetration. The target dose gradient for the modified plan was slightly better than the creation optimized plan.

The bolus plan was better for this patient than the segmented-field ECT plans. For low energy electron beams, the skin dose was low; therefore, beam weights were increased because of how close the target is to the skin surface. Use of a 0.5 – 1.0 cm thick bolus material with segmented-field ECT would probably improve the results, however, use of constant thickness bolus with the segmented-field ECT algorithm was not available.

Table 3.7. Dose statistics for patient 1.

	PTV (92 cm^3)			Left Lung (1188 cm^3)	
Treatment Plans	Mean Dose (cGy)	Standard Deviation (cGy)	$D(V_{90}) - D(V_{10})$ (cGy)	Volume > 20 Gy (%)	Mean Dose (cGy)
Creation	4625	397	751	17	916
Creation, optimized	5071	410	1045	19	1007
Modification, fluence	4941	393	1008	18	980
Bolus	4989	336	797	11	579

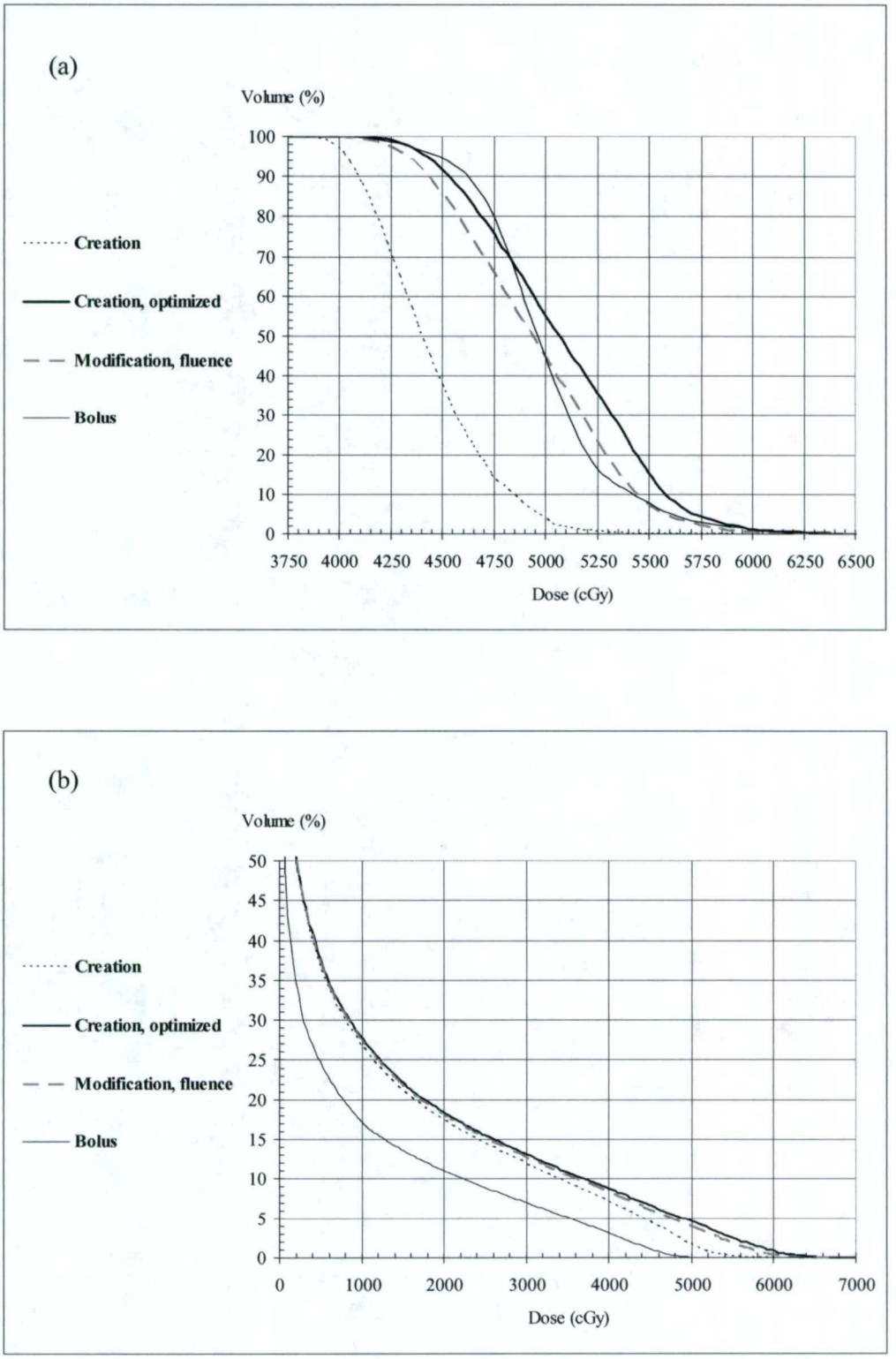

Figure 3.56. Dose volume histogram (DVH) of the PTV (a) and left lung (b) for patient 1.

3.8 Patient 2

3.8.1 Patient 2: Bolus plan

The patient was treated using customized bolus. Figure 3.57 shows the dose distribution; the MU were adjusted to deliver 200 cGy given dose in order to compare the bolus plan to the segmented-field ECT plans. The mean dose to the PTV was 5206 ± 283 cGy, and 33% of the right lung received more than 2000 cGy.

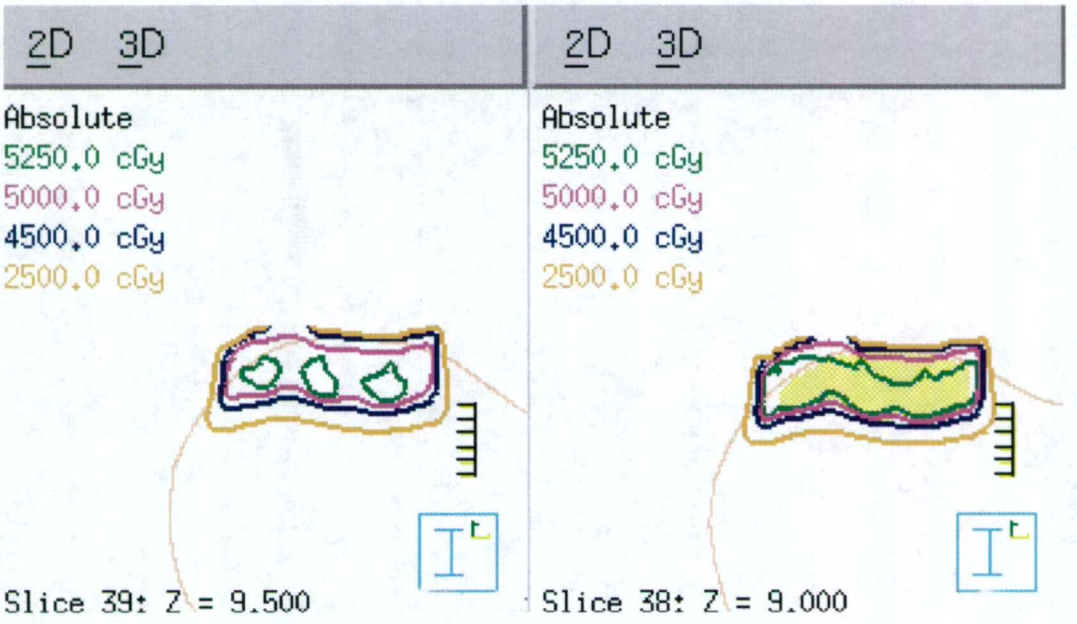

Figure 3.57. Transverse planes of patient 2 showing the dose distribution of the bolus treatment plan.

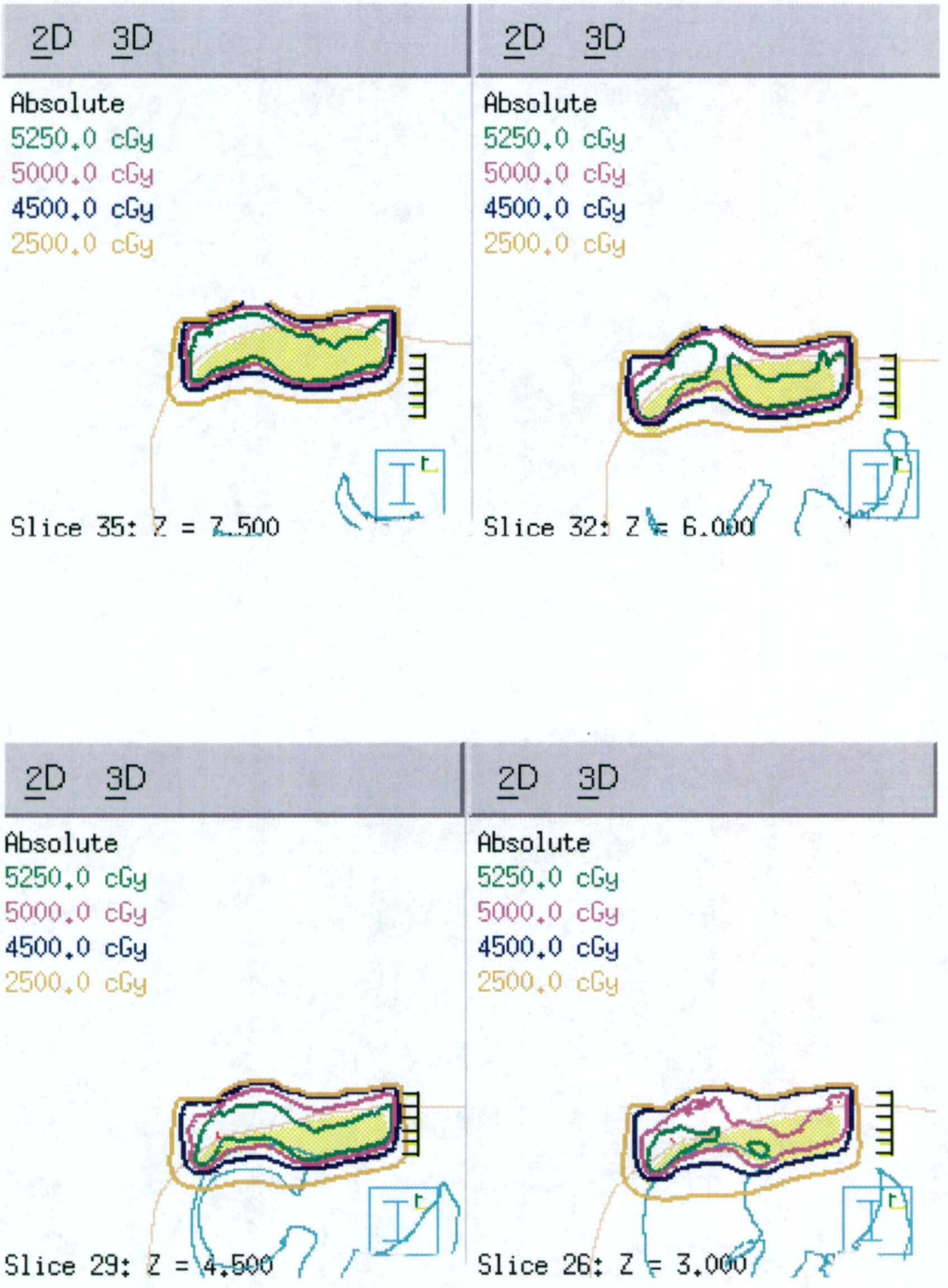

Figure 3.57. Continued.

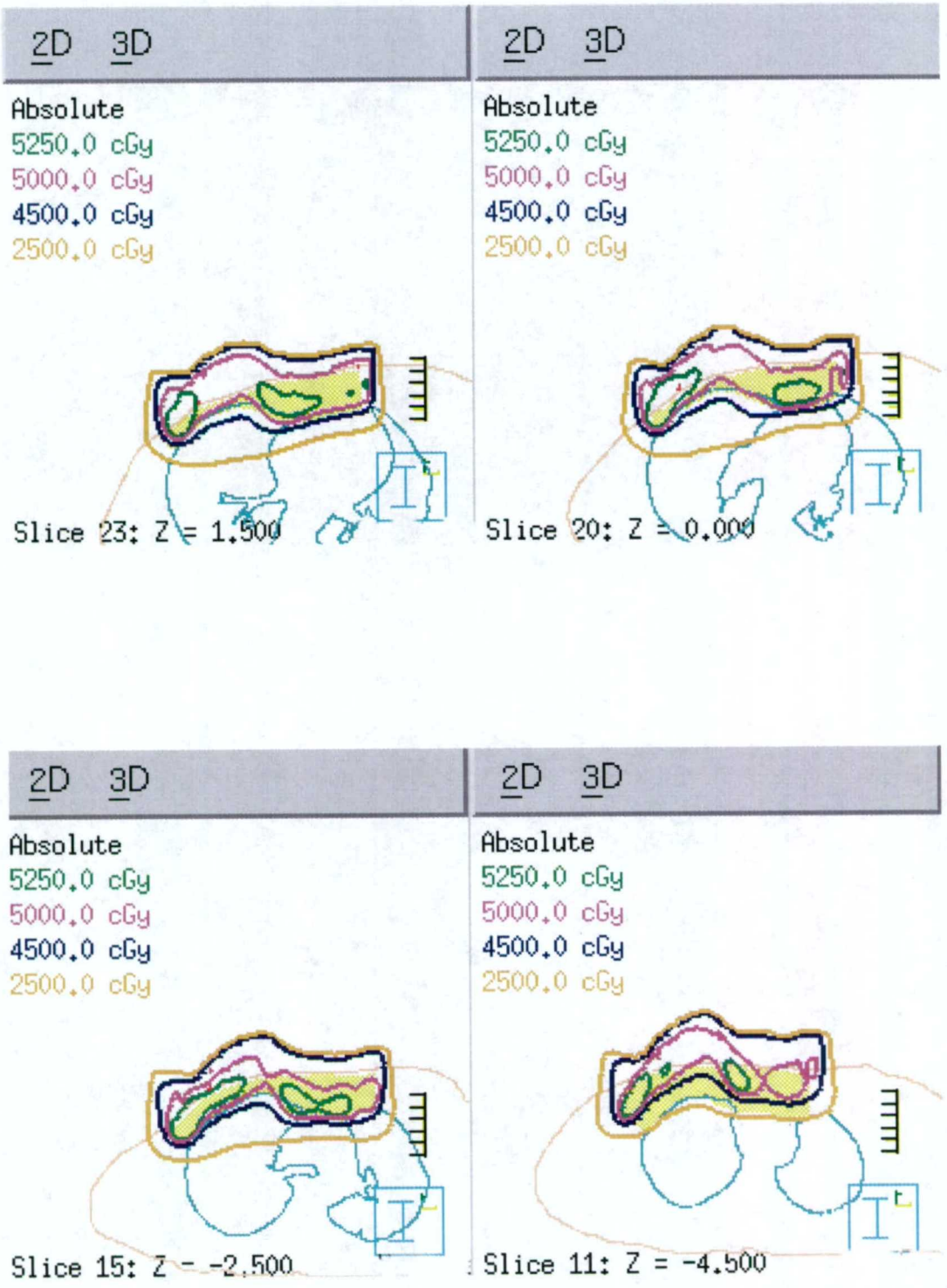

Figure 3.57. Continued.

3.8.2 Patient 2: Creation

The initial treatment plan used eleven fields with electron energies ranging from 6 MeV to 20 MeV, with a 1-cm margin around the PTV. Figure 3.58 shows a BEV of the treatment fields in relation to the PTV. MU were set to deliver 200 cGy given dose for each field and dose was computed. The resulting dose distribution is shown in Figure 3.59. The 4500 cGy (90%) dose line conforms to the PTV reasonably well. The mean dose to the PTV was 5117 ± 449 cGy, and 34% of the right lung received more than 2000 cGy.

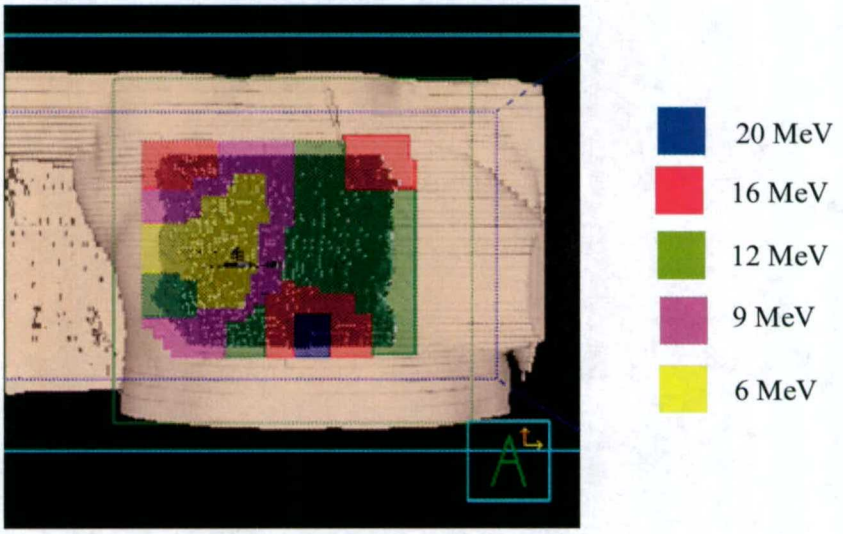

Figure 3.58. A BEV of treatment fields superimposed on the PTV (dark gray).

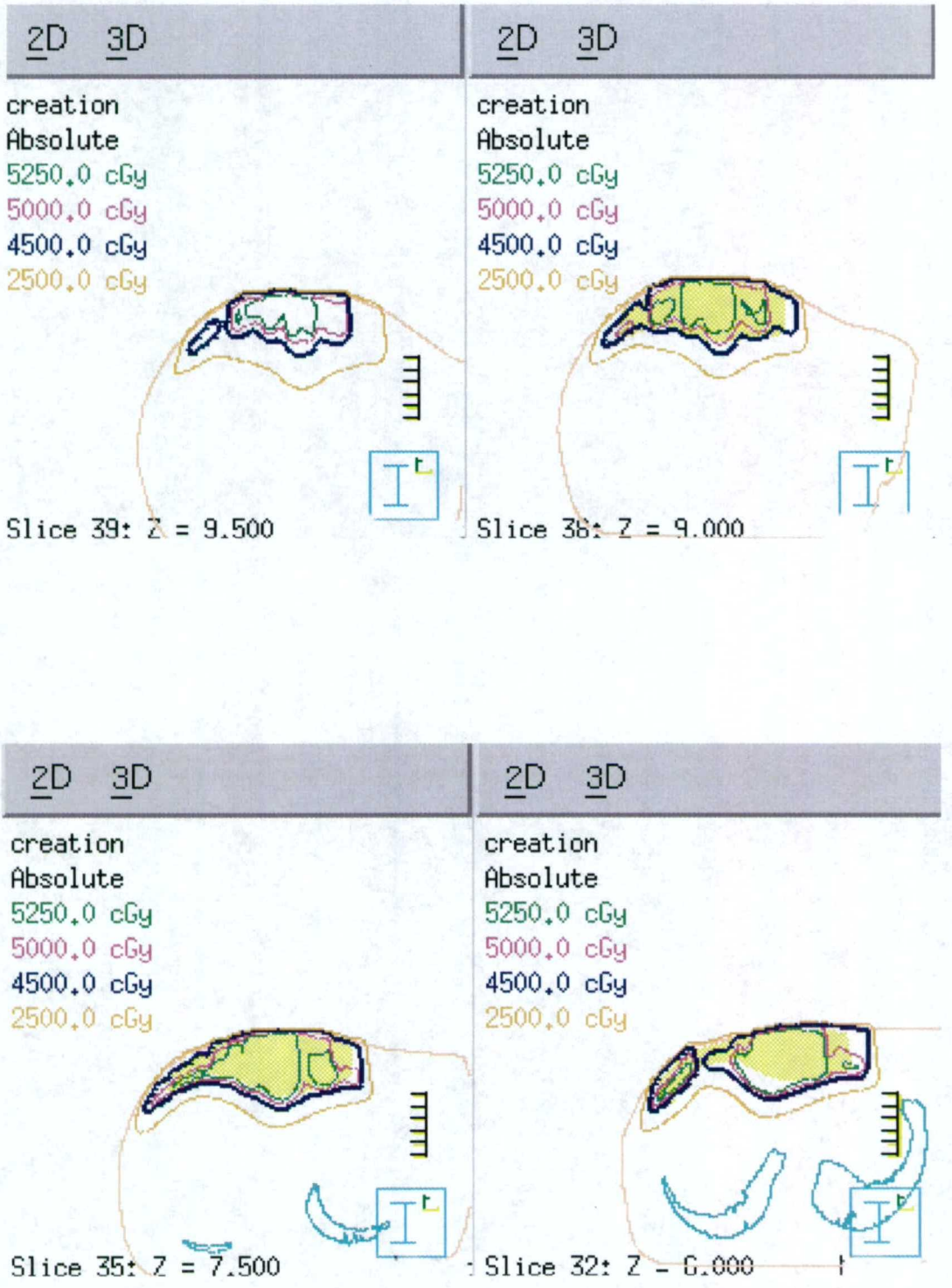

Figure 3.59. Transverse planes of patient 2 showing the dose distribution of the treatment plan using 11-electron fields determined in the creation step. The PTV is shown in solid yellow and the lungs are outlined in aqua.

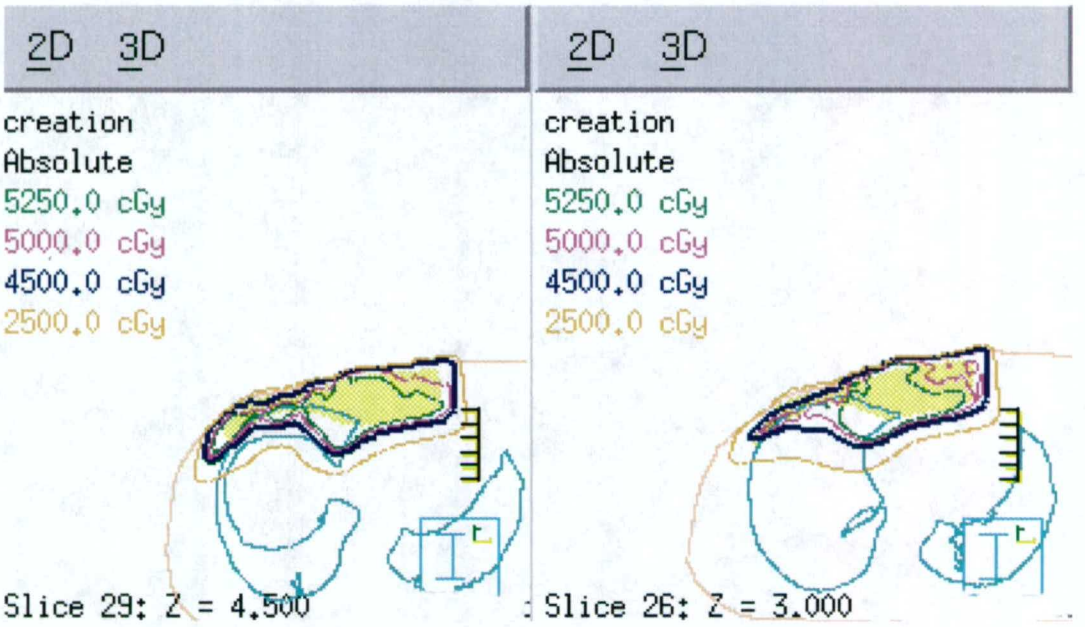

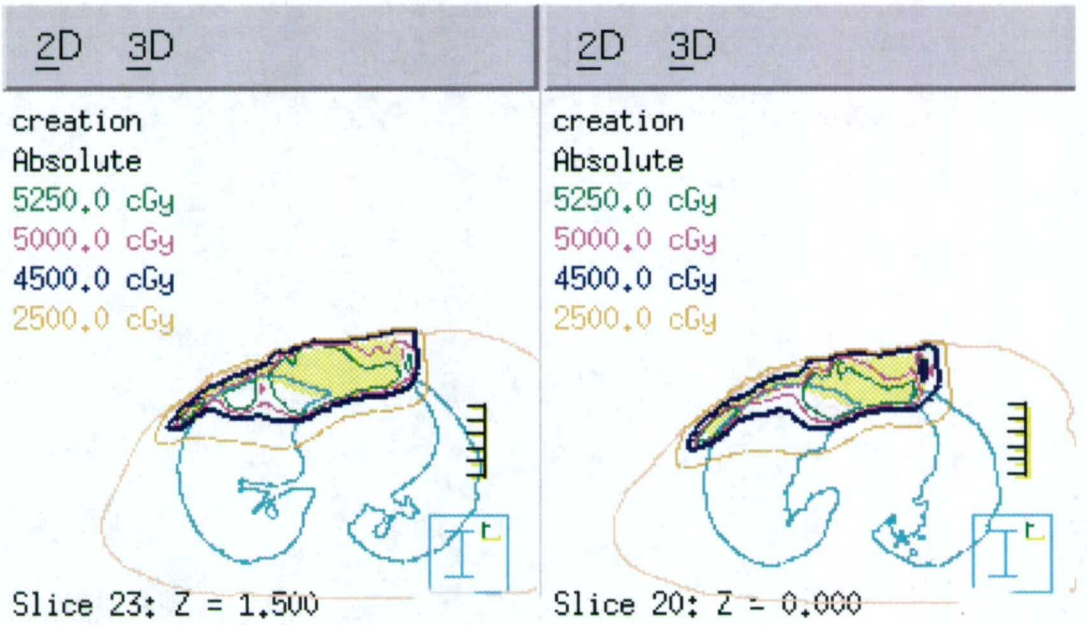

Figure 3.59. Continued.

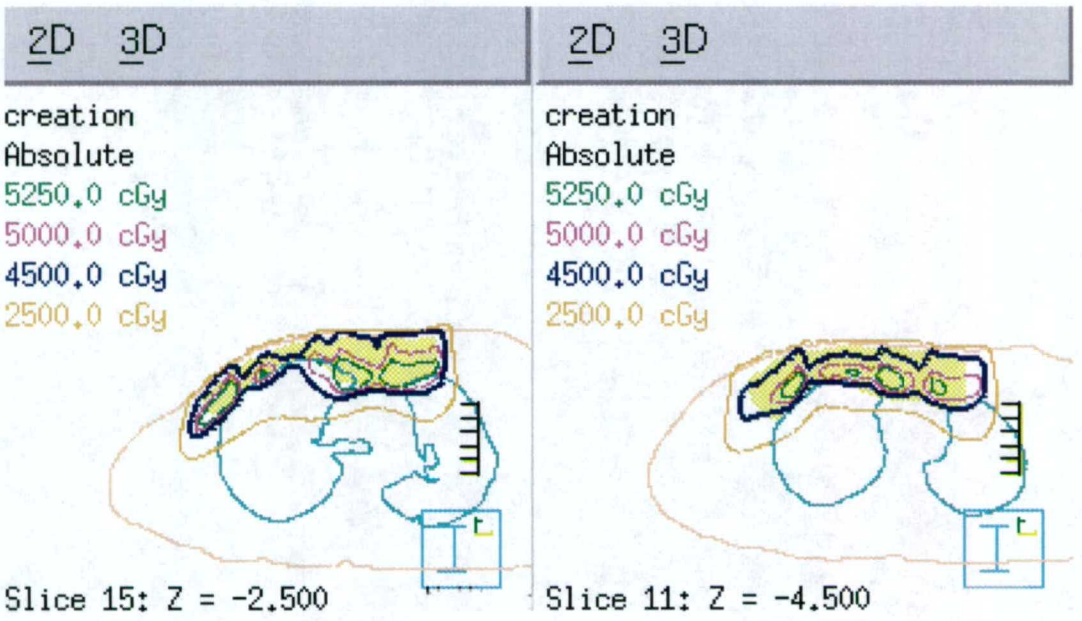

Figure 3.59. Continued.

3.8.3 Patient 2: Optimization

The Pinnacle[3] IMRT module was used to optimize the beam weighting, and the objectives were set to deliver a minimum dose of 4500 cGy and a maximum dose of 5250 cGy to the PTV. The resulting dose distribution is shown in Figure 3.60. The mean dose to the PTV was 4889 ± 362 cGy, and 35% of the lung received more than 2000 cGy. For the lung, this was slightly worse than the creation plan with no optimization, however, no dose constraint was placed on the lung.

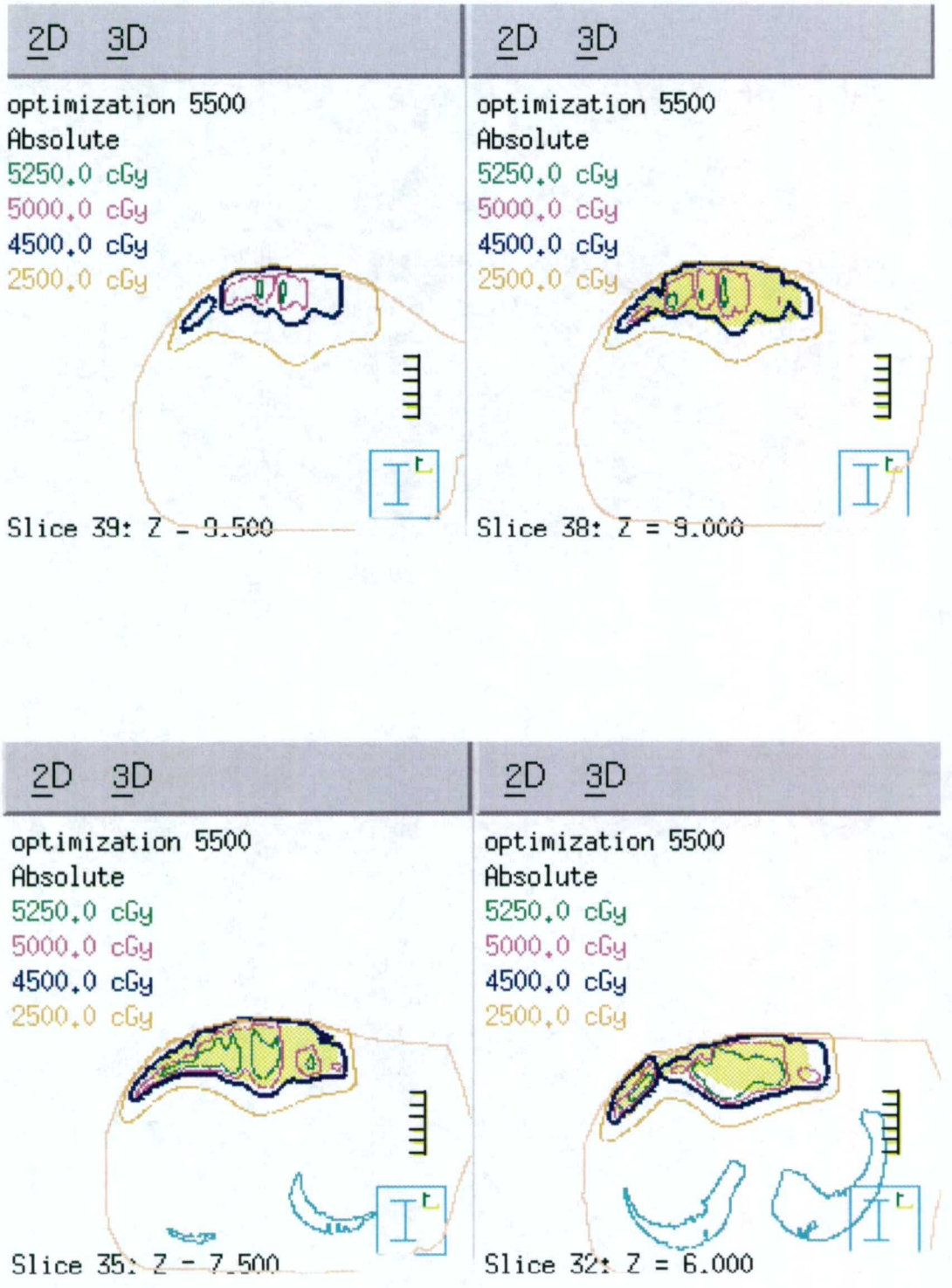

Figure 3.60. Transverse planes of patient 2 showing the creation step treatment plan dose distribution after beam weight optimization. See text for dose objective information.

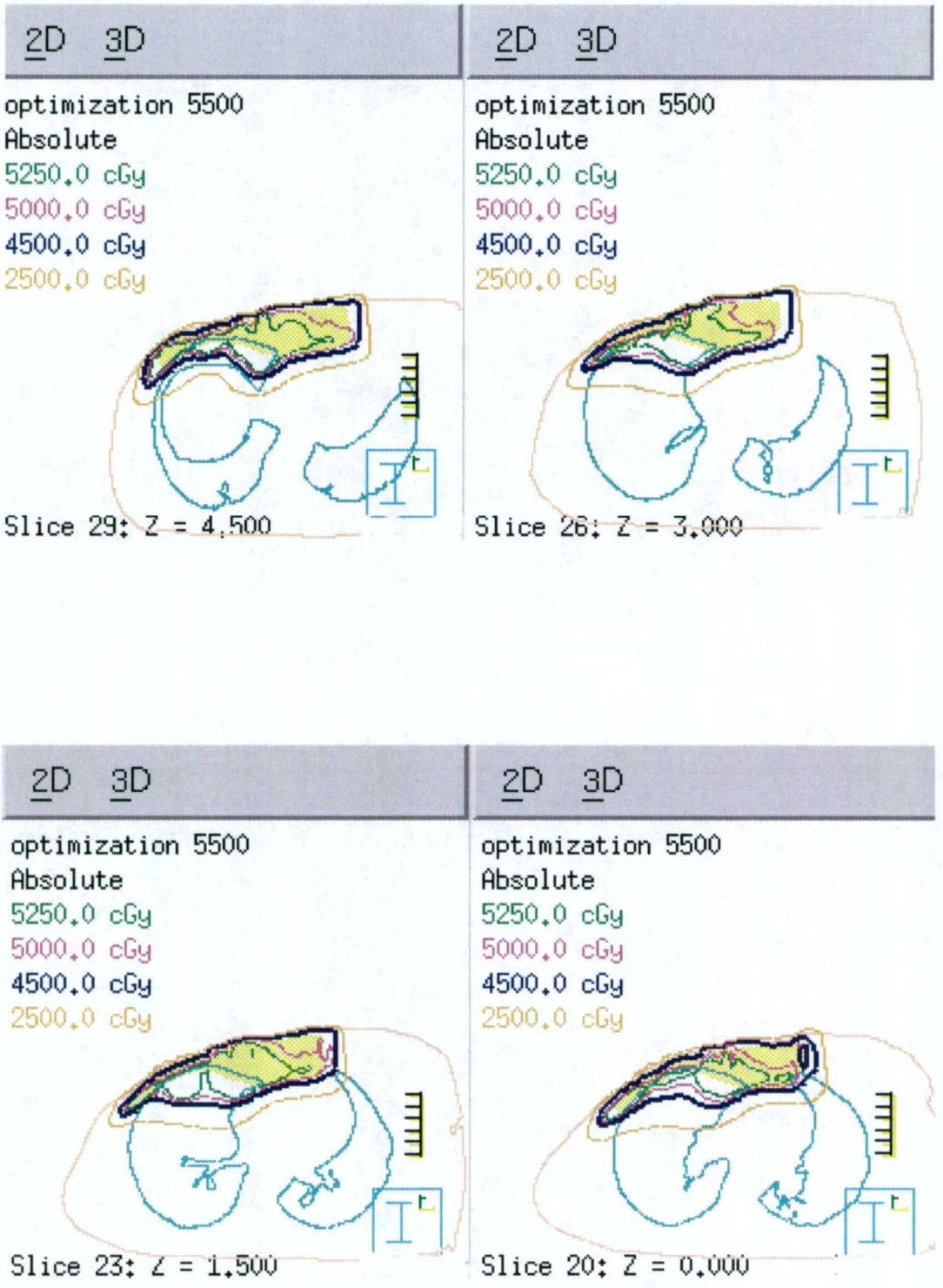

Figure 3.60. Continued.

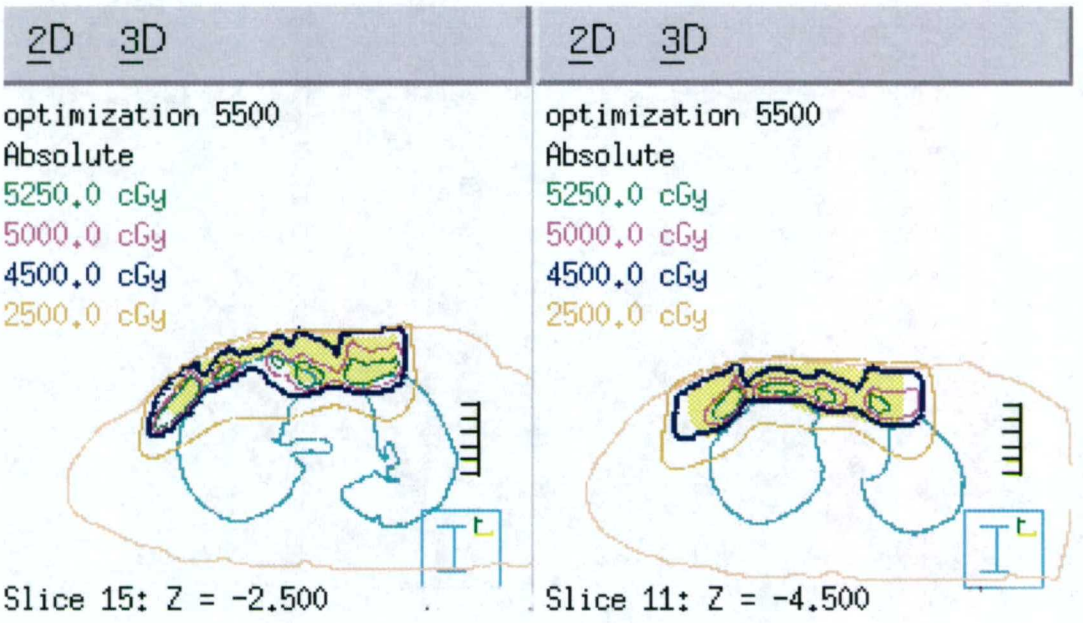

Figure 3.60. Continued.

3.8.4 Patient 2: Modification

Several modification techniques were used to move the 4500 cGy isodose line closer to the PTV surface and out of the lung. The energy of the right inferiomedial field was reduced from 9 MeV to 6 MeV. Also, the electron fluence decrease technique was used to decrease the MU for the 6 MeV fields. Figure 3.61 shows the resulting dose distribution after performing these operations. The mean dose to the PTV was 4824 ± 412 cGy, and 34% of the right lung received more than 2000 cGy.

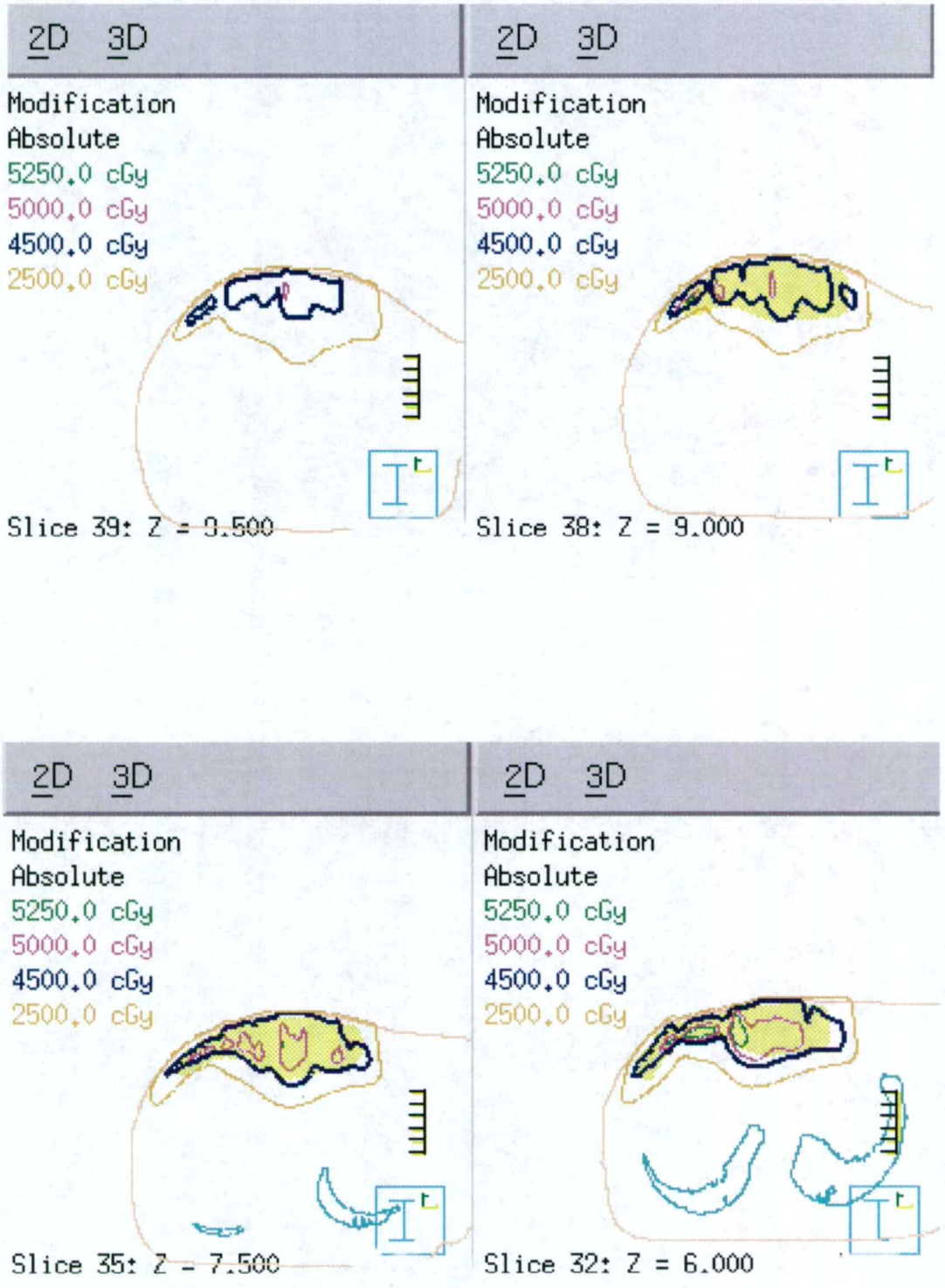

Figure 3.61. Transverse planes of patient 2 showing the dose distribution after modification of the initial treatment plan.

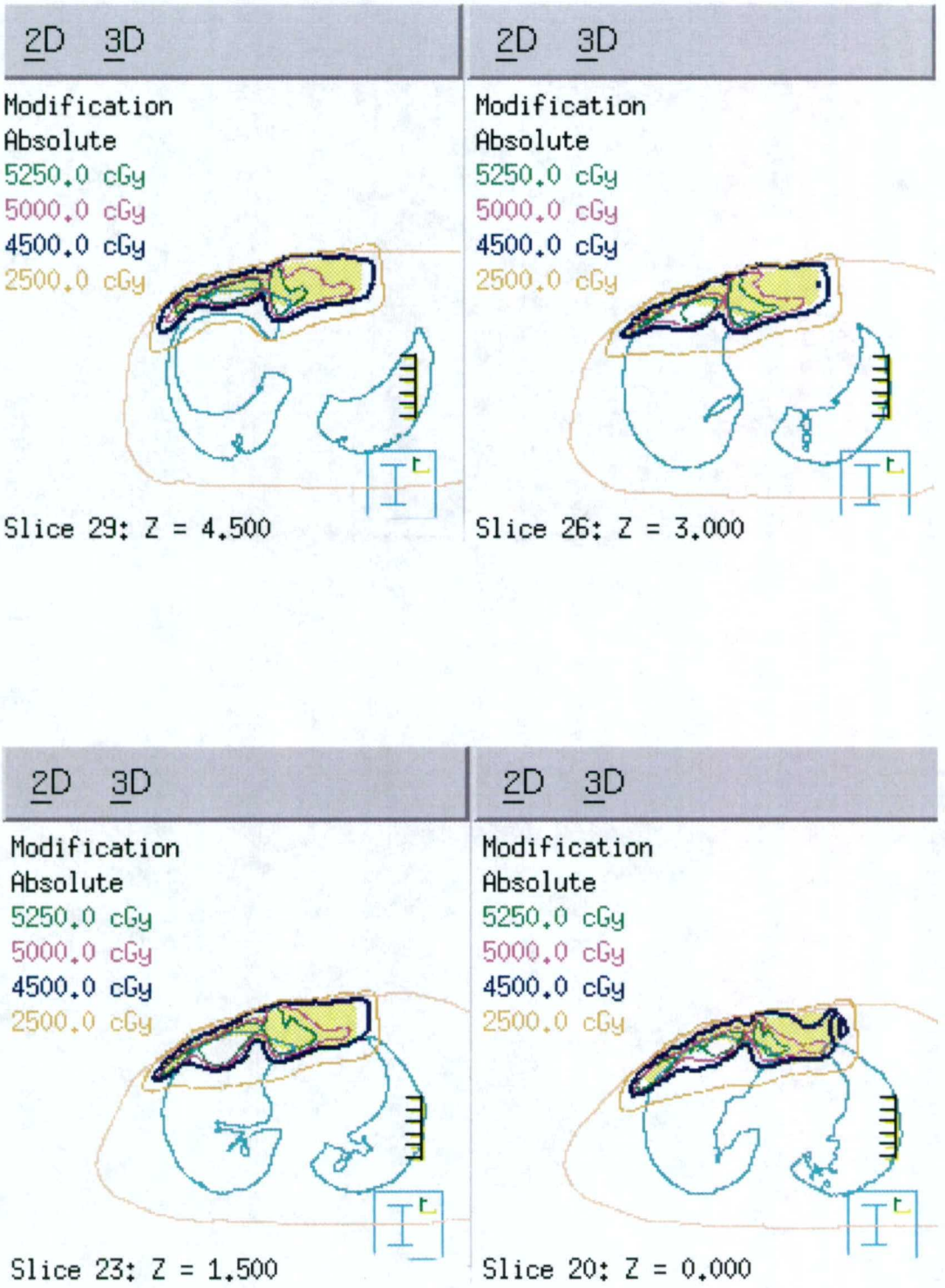

Figure 3.61. Continued.

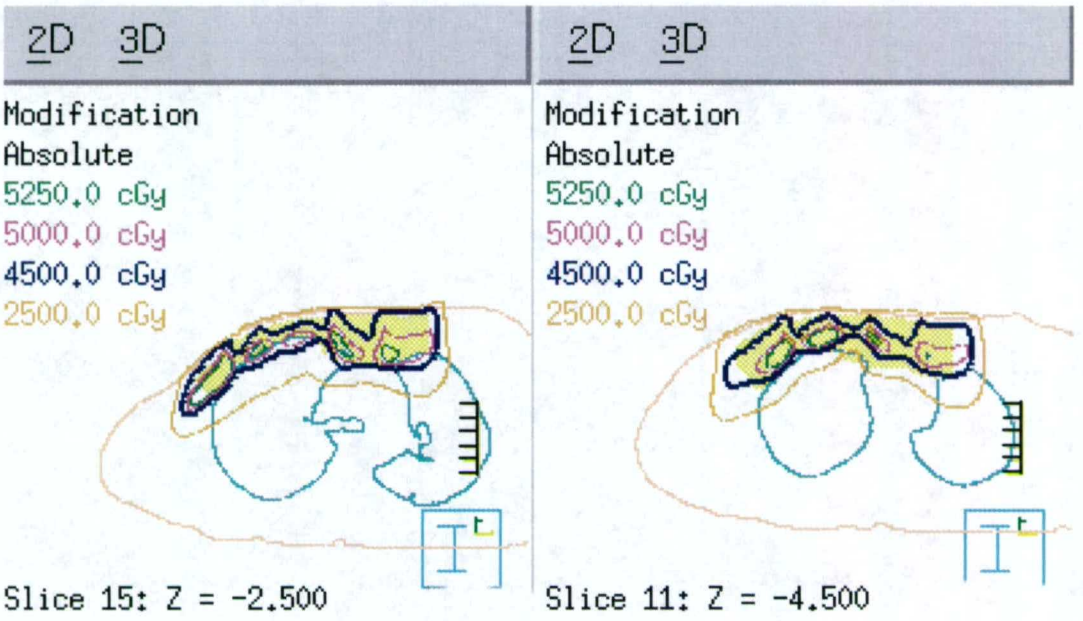

Figure 3.61. Continued.

3.8.5 Patient 2: Summary

Figure 3.62 shows the DVH of the PTV and right lung tissue for these treatment plans, and Table 3.8 summarizes the PTV dose homogeneity and the dose to the right lung. The segmented-field ECT algorithm provides a good initial treatment plan. The plan provides good 4500 cGy isodose line coverage around the PTV, especially along the distal surface of the target; however, there are some regions along the PTV anterior surface that are not enclosed by the 4500 cGy isodose line. This is because the PTV is very close to the skin surface in some locations, and the skin dose for lower energy beams is less than 90%. Optimizing the beam weights of the creation plan using the standard objectives produced a plan with lower mean dose to the PTV and more dose to the lung. However, dose homogeneity improved. Using several modification techniques, the volume of lung that received more than 2000 cGy was slightly reduced, and the mean lung dose was reduced without significantly reducing the 4500 cGy isodose line coverage of the PTV and the target dose homogeneity.

Compared to the bolus plan that was used clinically to treat the patient, the bolus plan has better PTV mean dose, dose homogeneity, and better anterior surface coverage (4500 isodose line). However, the modified plan has comparable dose to the lung. Use of a 0.5 – 1.0 cm thick bolus material with segmented-field ECT would probably improve the results for this patient, by decreasing the lung dose and improving the anterior PTV 4500 cGy isodose line coverage.

Table 3.8. Dose statistics for patient 2.

	PTV (585 cm^3)			Right Lung (995 cm^3)	
Treatment Plans	Mean Dose (cGy)	Standard Deviation (cGy)	$D(V_{90}) - D(V_{10})$ (cGy)	Volume > 20 Gy (%)	Mean Dose (cGy)
Creation	5117	449	1134	34	1885
Creation, Optimized	4889	362	967	35	1883
Modification, energy-fluence	4824	412	922	34	1697
Bolus	5206	283	505	33	1645

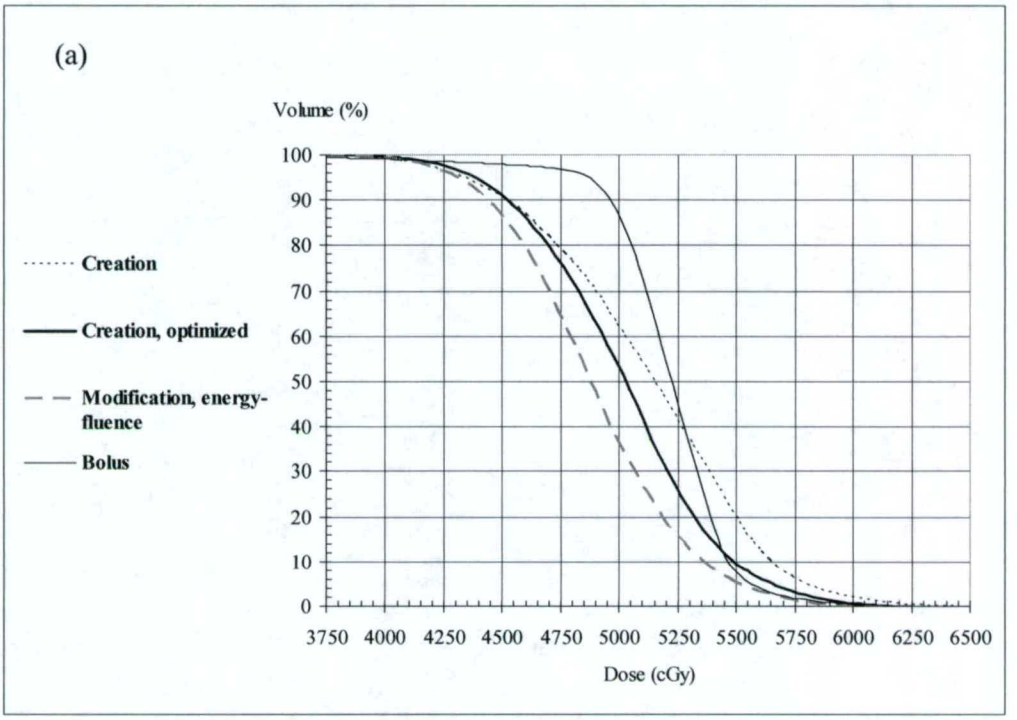

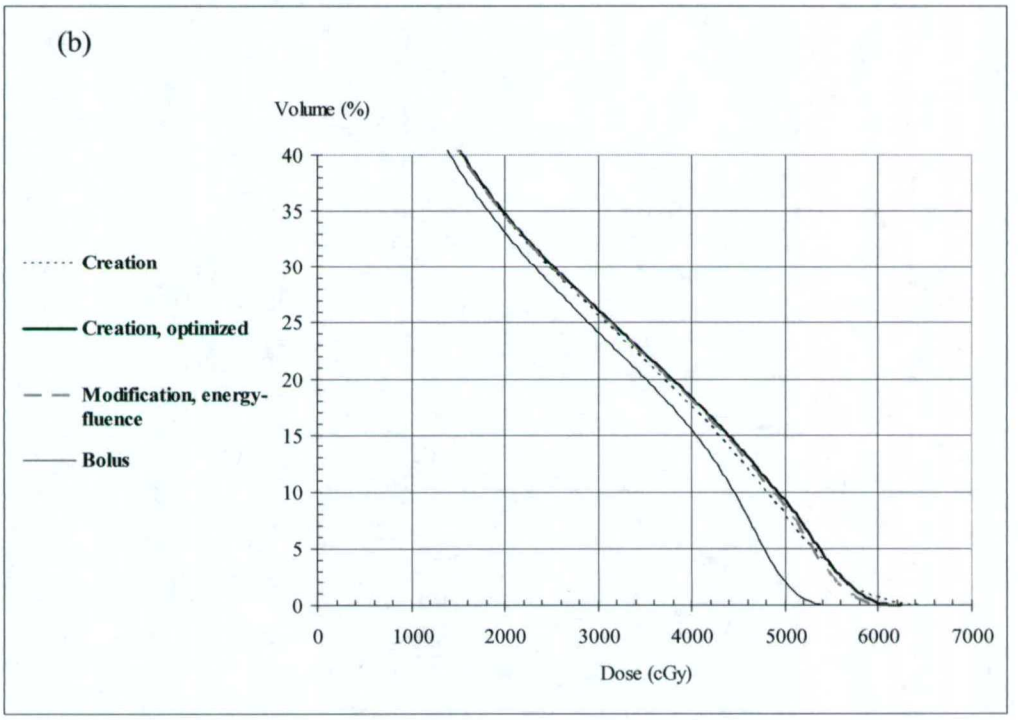

Figure 3.62. Dose volume histogram (DVH) for the PTV (a) and right lung (b) for patient 2.

3.9 Patient 3

3.9.1 Patient 3: Bolus plan

The patient was treated using customized bolus, and Figure 3.63 shows the dose distribution. The MU were adjusted to deliver 200 cGy given dose in order to compare the bolus plan to the segmented-field ECT plans. The mean dose to the PTV was 5163 ± 512 cGy, and 16% of the right lung received more than 2000 cGy.

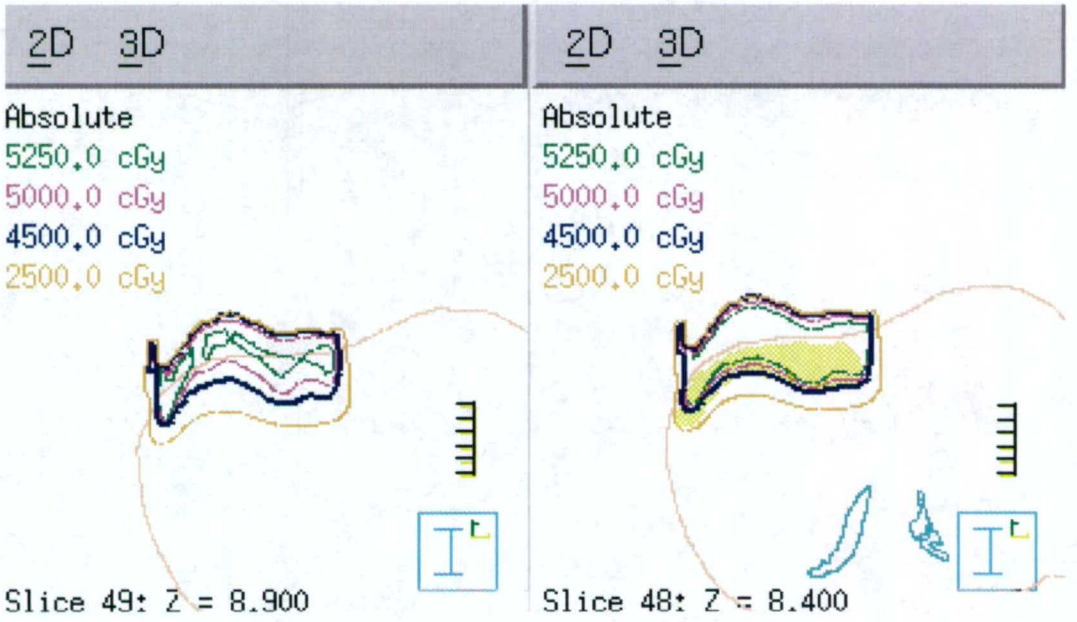

Figure 3.63. Transverse planes of patient 3 showing the dose distribution of the bolus treatment plan.

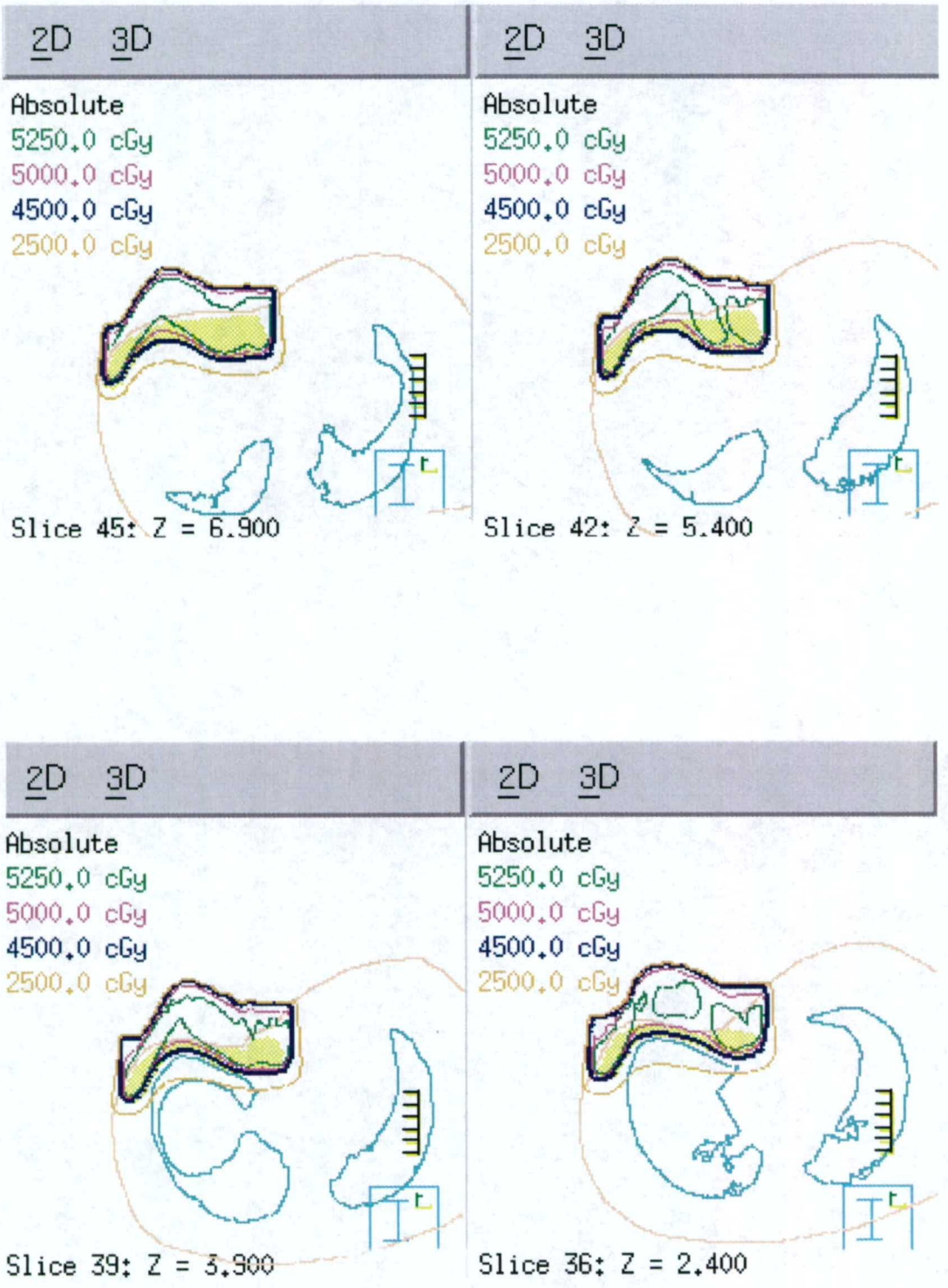

Figure 3.63. Continued.

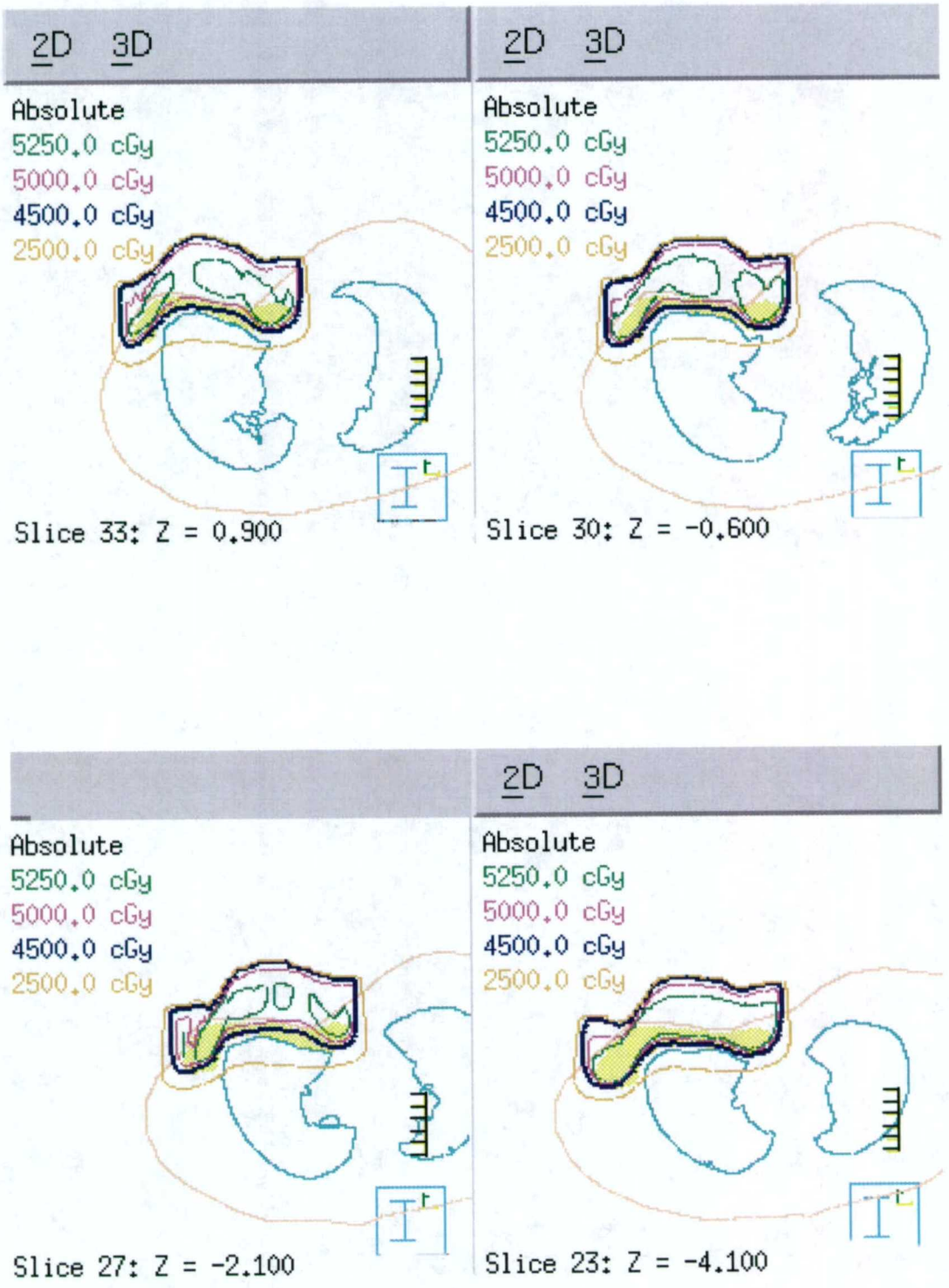

Figure 3.63. Continued.

3.9.2 Patient 3: Creation

The energies of the fields were set according to the PTV depth; eleven treatment fields comprising electron energies ranging from 6 MeV to 20 MeV were used with a 1-cm margin around the PTV. Figure 3.64 shows a BEV of the treatment fields in relation to the PTV. MU were set to deliver 200 cGy given dose for each field and dose was computed. The resulting dose distribution is shown in Figure 3.65. The 4500 cGy (90%) isodose line encompasses the PTV well. The mean dose to the PTV was 5066 ± 437 cGy, and 28% of the right lung receives more than 2000 cGy.

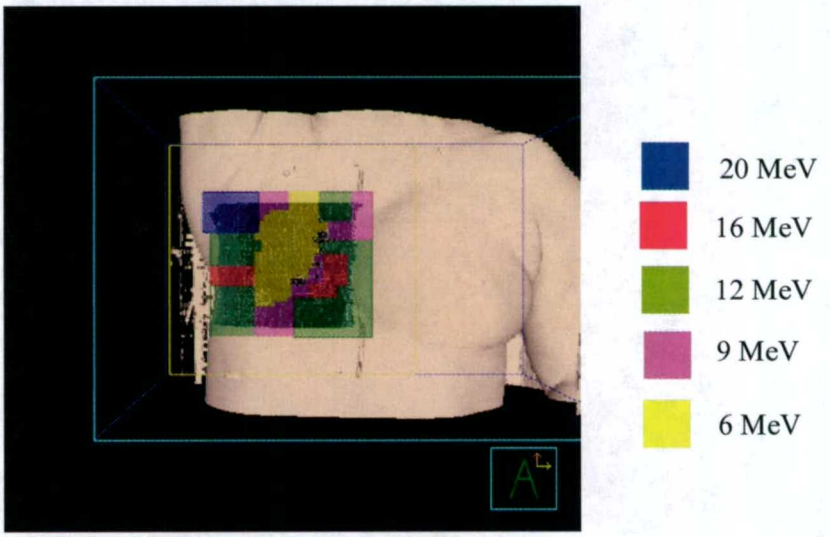

Figure 3.64. A BEV of the treatment fields superimposed on the PTV (dark gray).

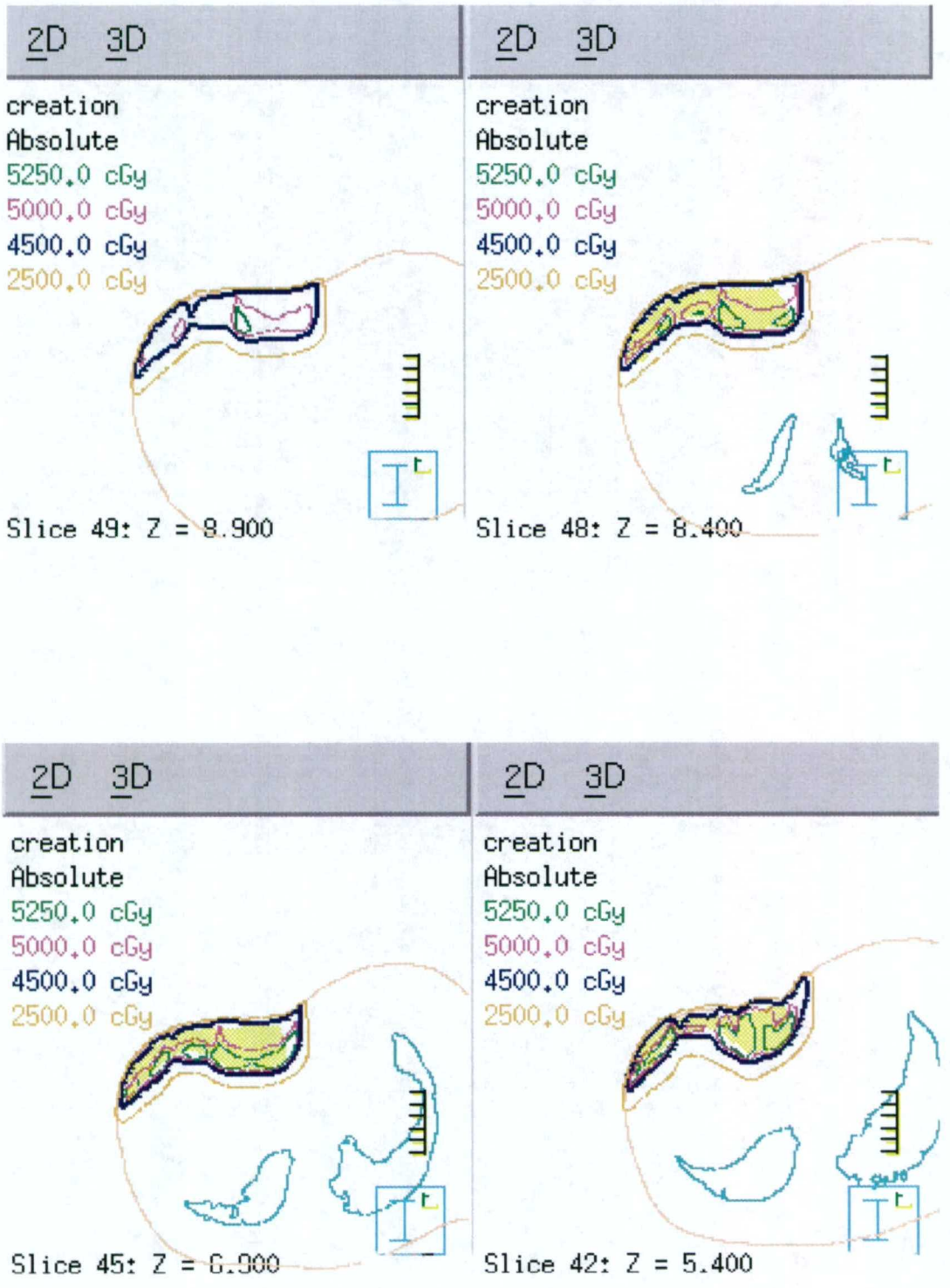

Figure 3.65. Transverse planes of patient 3 showing the dose distribution of the initial treatment plan (creation step).

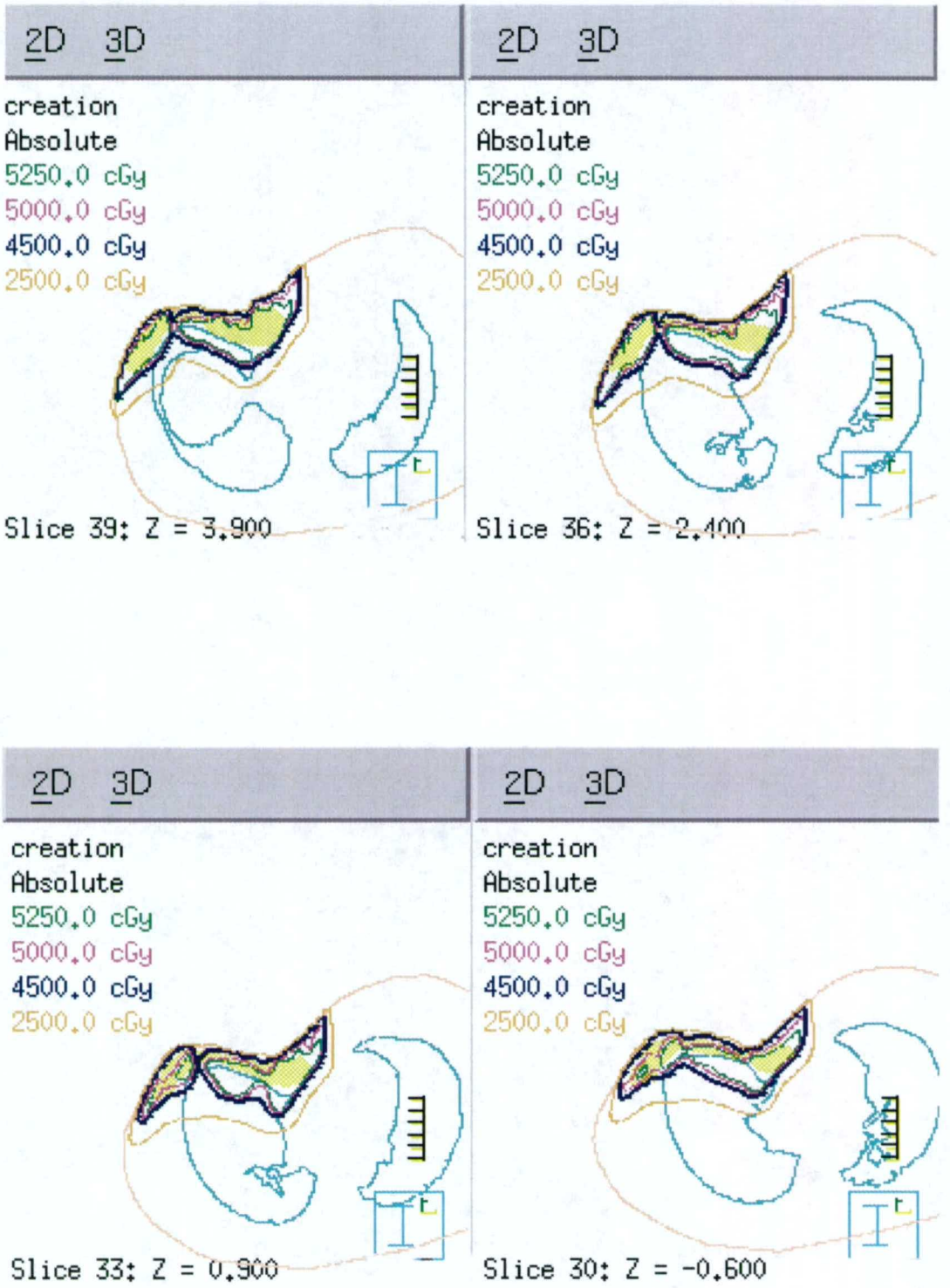

Figure 3.65. Continued.

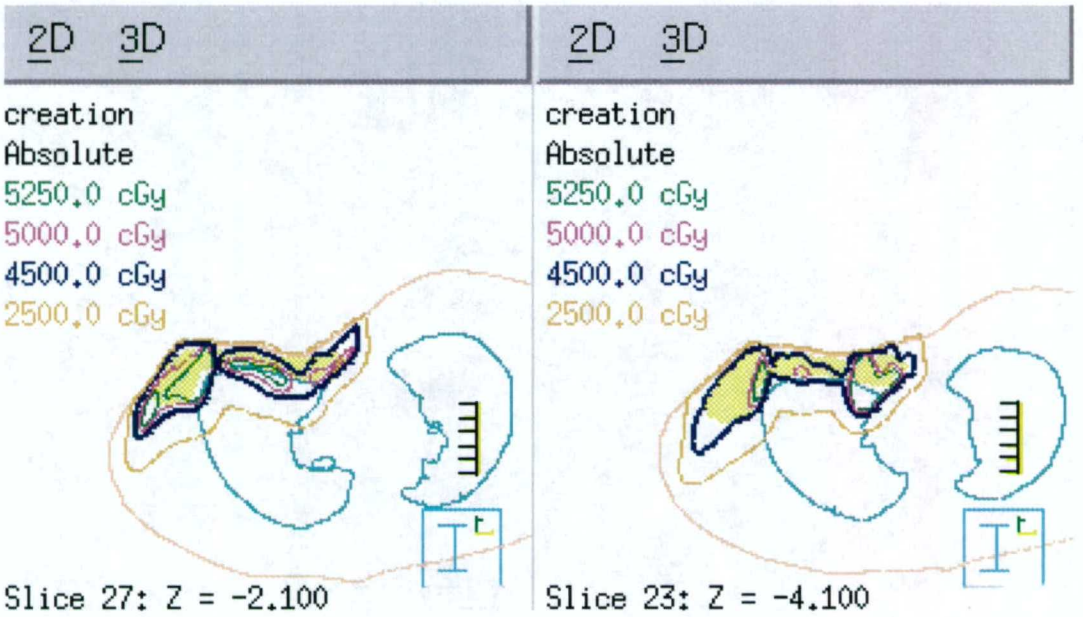

Figure 3.65. Continued.

3.9.3 Patient 3: Optimization

The Pinnacle[3] IMRT module was used to optimize the beam weighting using the standard objectives. The resulting dose distribution is shown in Figure 3.66. The mean dose to the PTV was 4889 ± 354 cGy, and 28% of the right lung received more than 2000 cGy. This plan has lower mean dose to the PTV but better homogeneity, and slightly more lung volume receiving 2000 cGy than the creation plan.

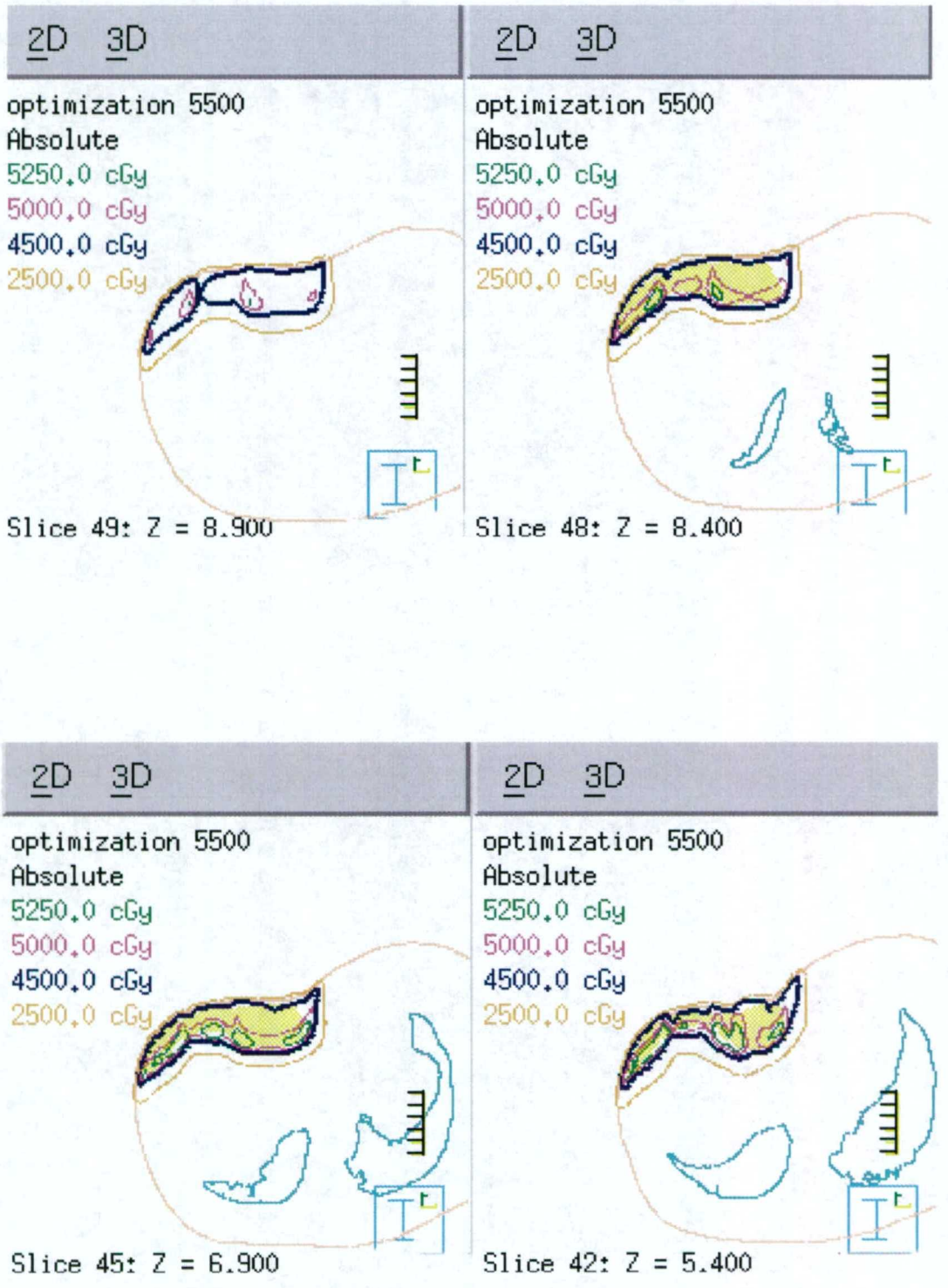

Figure 3.66. Dose distribution for patient 3, creation step plan using beam-weight optimization.

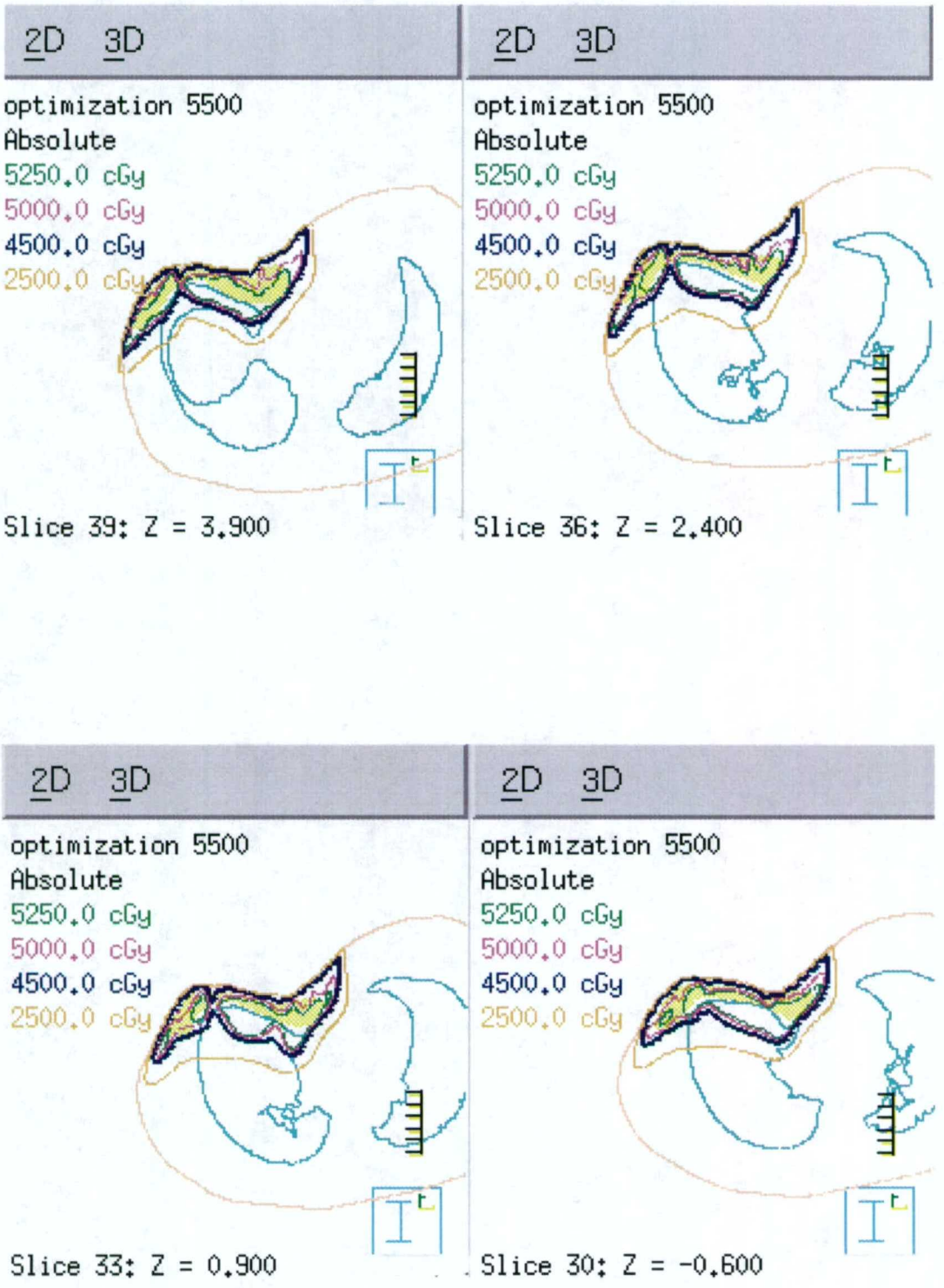

Figure 3.66. Continued.

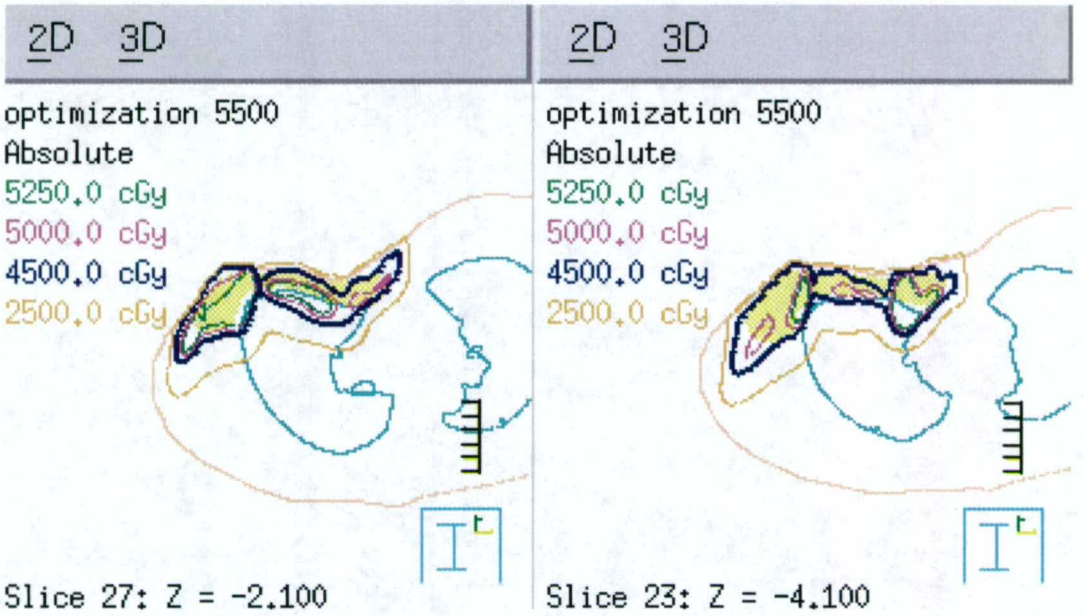

Figure 3.66. Continued.

3.9.4 Patient 3: Modification

The electron fluence decrease technique was used to decrease the MU for the 6 and 9 MeV fields without significantly altering the dose coverage of the anterior surface of the PTV. Figure 3.67 shows the resulting dose distribution after performing these operations. The mean dose to the PTV was 4827 ± 469 cGy, and 26% of the right lung received more than 2000 cGy. The result of this modification was slightly decreased PTV dose homogeneity and slightly improved lung sparing.

A third modified plan was attempted using different beam weighting objectives; the objectives were set to deliver a minimum of 4500 cGy to 90% of the PTV, a maximum of 5500 cGy to 10% of the PTV, and a maximum dose of 2000 cGy to 20% of the lung volume. There was some improvement in the non-target tissue that received more than 20 Gy (22%), however, there was considerable degradation of the 4500 cGy dose coverage and homogeneity of the PTV.

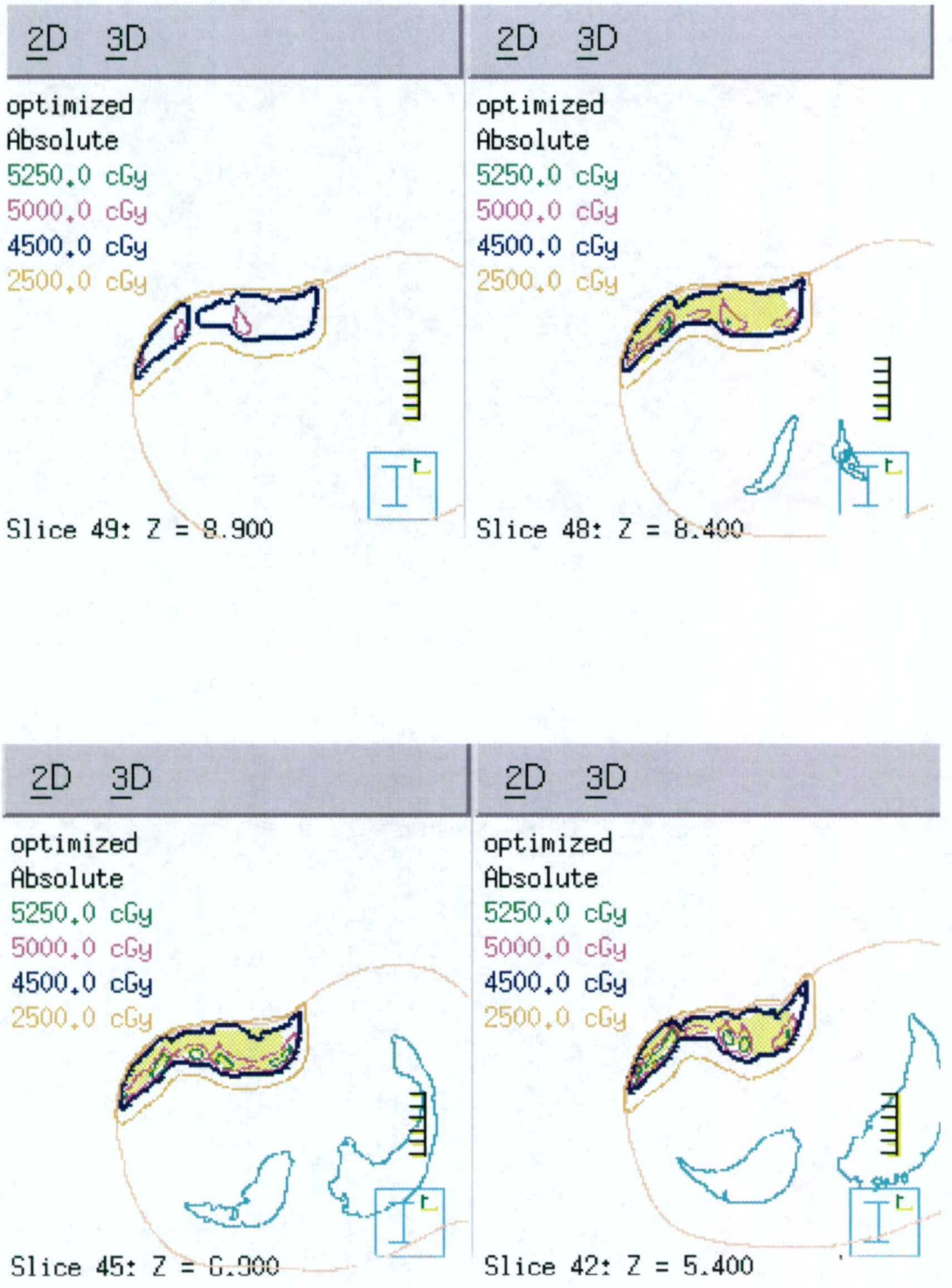

Figure 3.67. Dose distribution for patient 3 after decreasing the fluence (MU) of the 6 and 9 MeV fields to decrease the non-target dose.

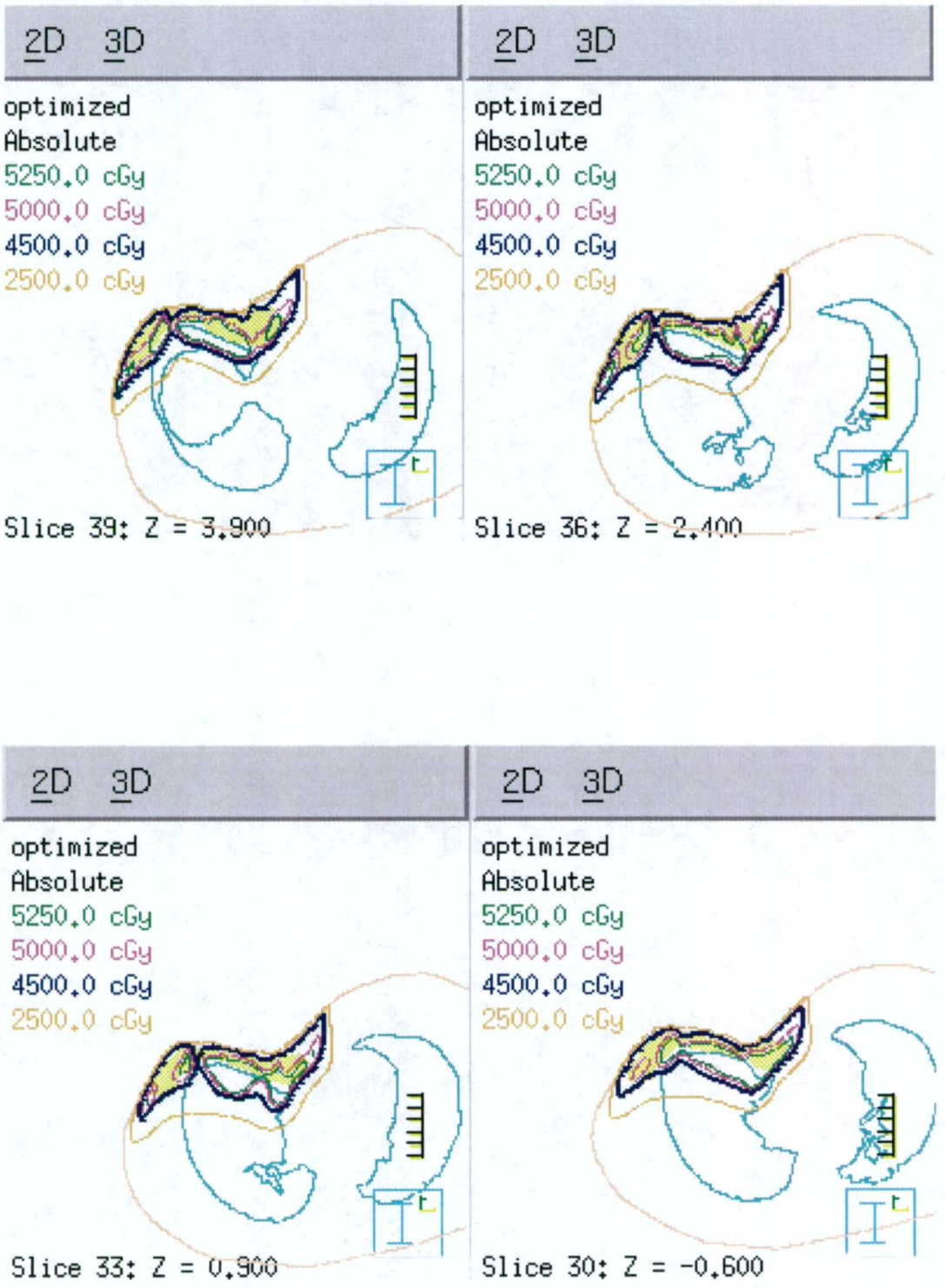

Figure 3.67. Continued.

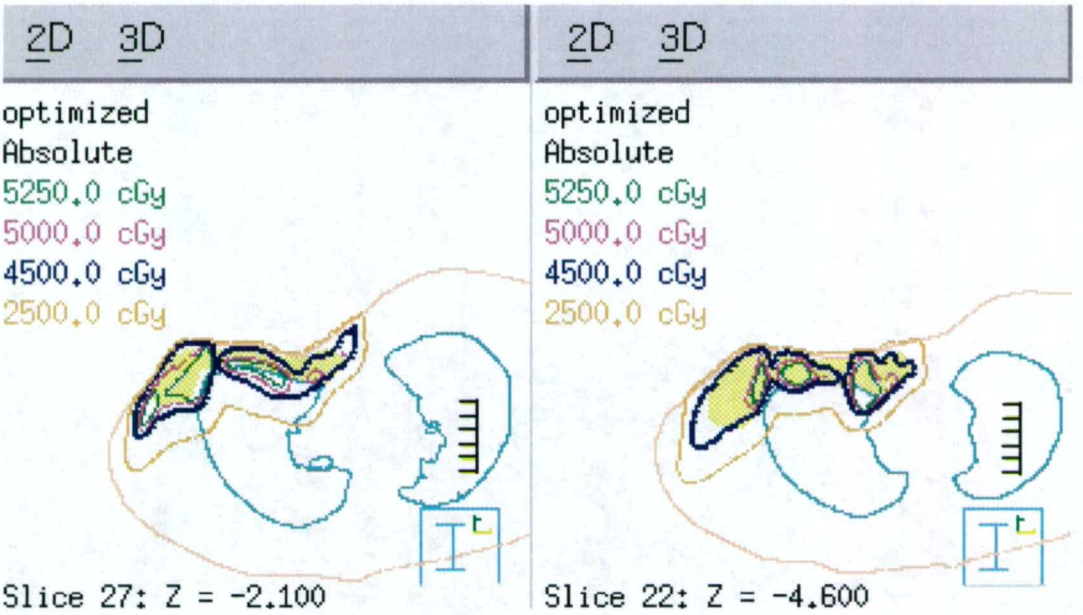

Figure 3.67. Continued.

3.9.5 Patient 3: Summary

Figure 3.68 compares the DVH of the PTV and right lung tissue for these treatment plans. Table 3.9 summarizes the PTV dose homogeneity and the dose to the right lung. The segmented-field ECT algorithm provides good 90% isodose line coverage around the PTV, especially along the distal surface of the target. The optimized creation plan has a higher PTV mean dose, better PTV dose homogeneity, but more lung volume dose than the modified plan. Compared to the bolus plan that was used clinically to treat the patient, the optimized creation plan has better PTV dose homogeneity but the bolus plan spares more lung tissue.

Table 3.9. Dose statistics for patient 3.

	PTV (365 cm^3)			Right Lung (1064 cm^3)	
Treatment Plans	Mean Dose (cGy)	Standard Deviation (cGy)	$D(V_{90}) - D(V_{10})$ (cGy)	Volume > 20 Gy (%)	Mean Dose (cGy)
Creation	5066	437	1057	28	1624
Creation, optimized	4889	354	915	28	1586
Modification, fluence	4827	469	1187	26	1467
Bolus	5163	512	1209	16	824

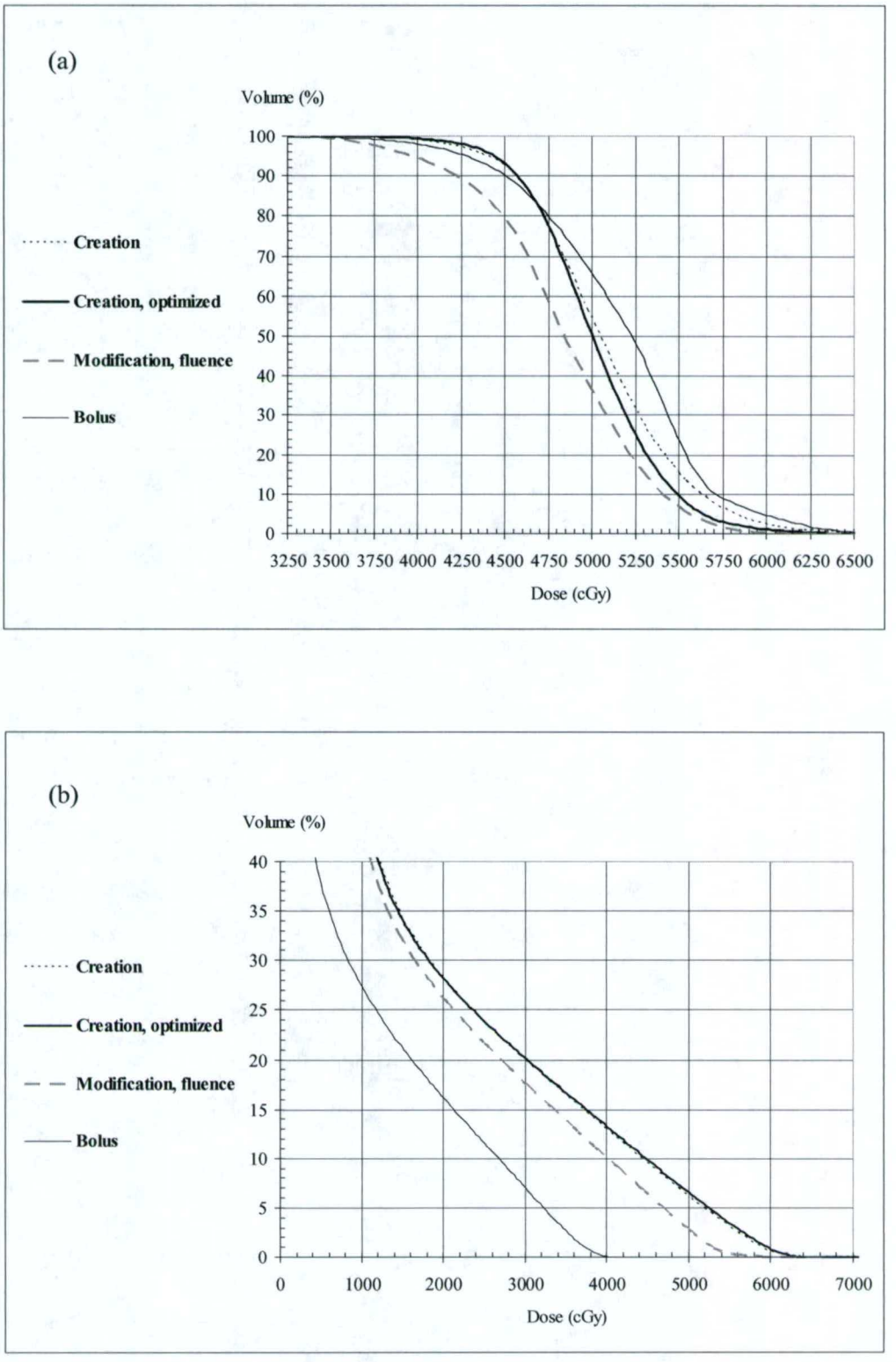

Figure 3.68. Dose volume histogram (DVH) for the PTV (a) and right lung (b) for patient 3.

3.10 Patient 4

3.10.1 Patient 4: Bolus plan

The patient was treated using customized bolus. Figure 3.69 shows the resultant dose distribution; the MU were adjusted to deliver 200 cGy given dose in order to compare the bolus plan to the segmented-field ECT plans. The mean dose to the PTV was 4931 ± 388 cGy, and 14% of the right lung received more than 2000 cGy.

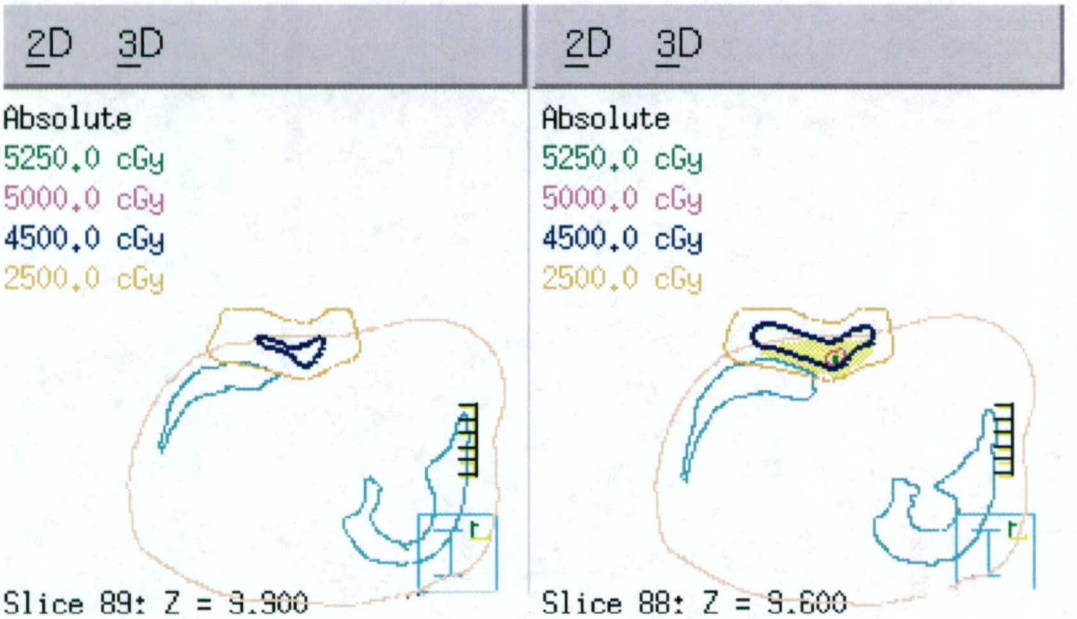

Figure 3.69. Transverse planes of patient 4 showing the dose distribution of the bolus treatment plan.

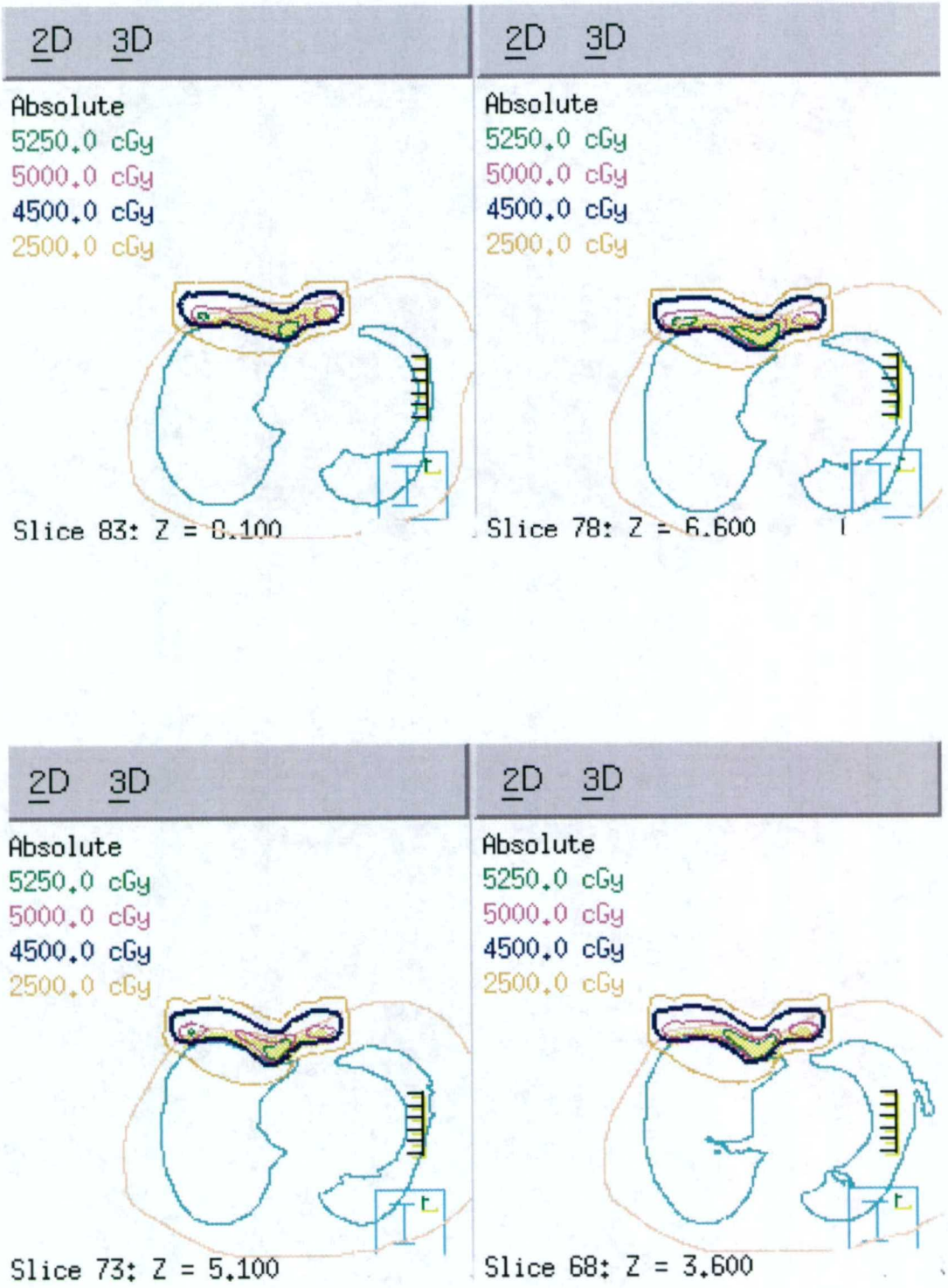

Figure 3.69. Continued.

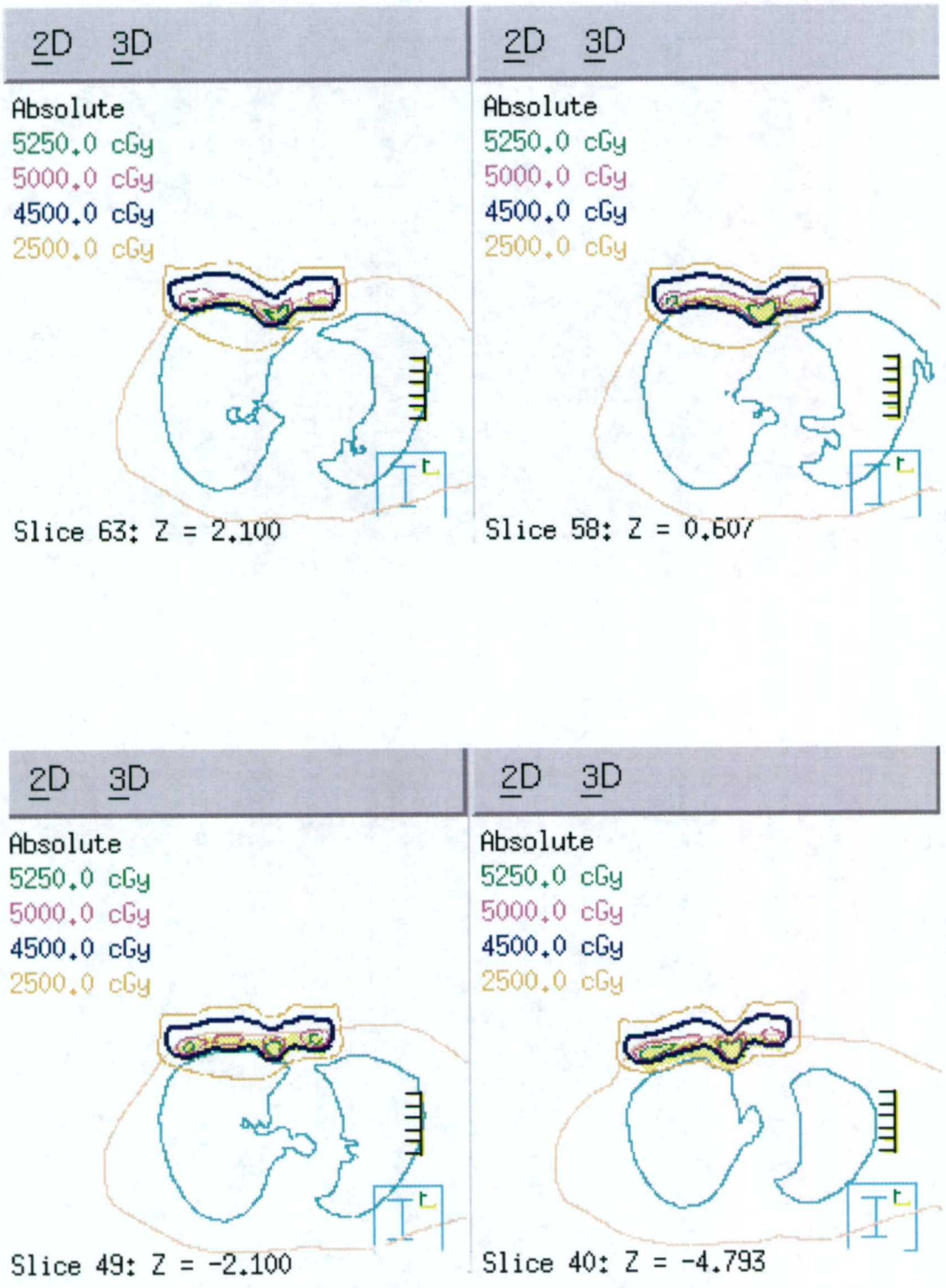

Figure 3.69. Continued.

3.10.2 Patient 4: Creation

The treatment plan consists of nine treatment fields with electron energies ranging from 5 MeV to 12 MeV. Figure 3.70 shows a BEV of the electron fields in relation to the PTV. MU were set to deliver 200 cGy given dose for each field and dose was computed. The resulting dose distribution is shown in Figure 3.71. For a starting point, the 4500 cGy (90%) isodose line has good conformation about the PTV. The mean dose to the PTV was 4739 ± 371 cGy, and 29% of the right lung received more than 2000 cGy.

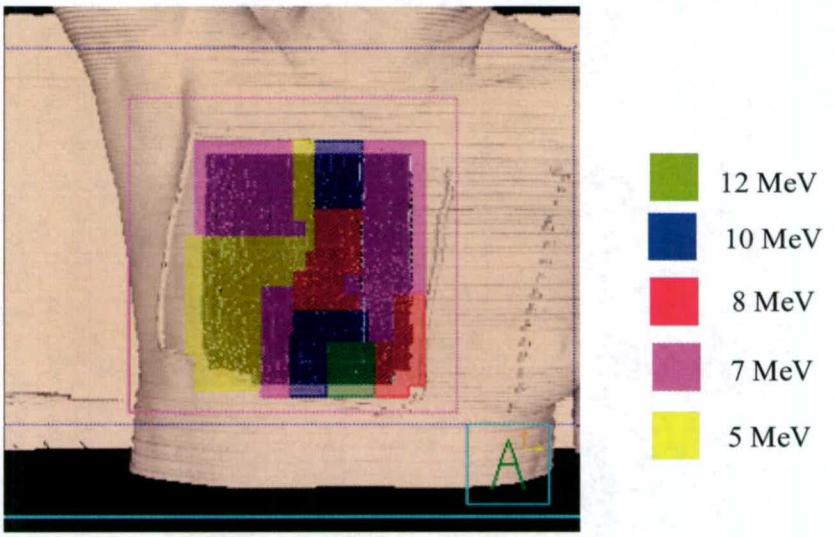

Figure 3.70. A BEV of the treatment fields superimposed on the PTV (dark gray).

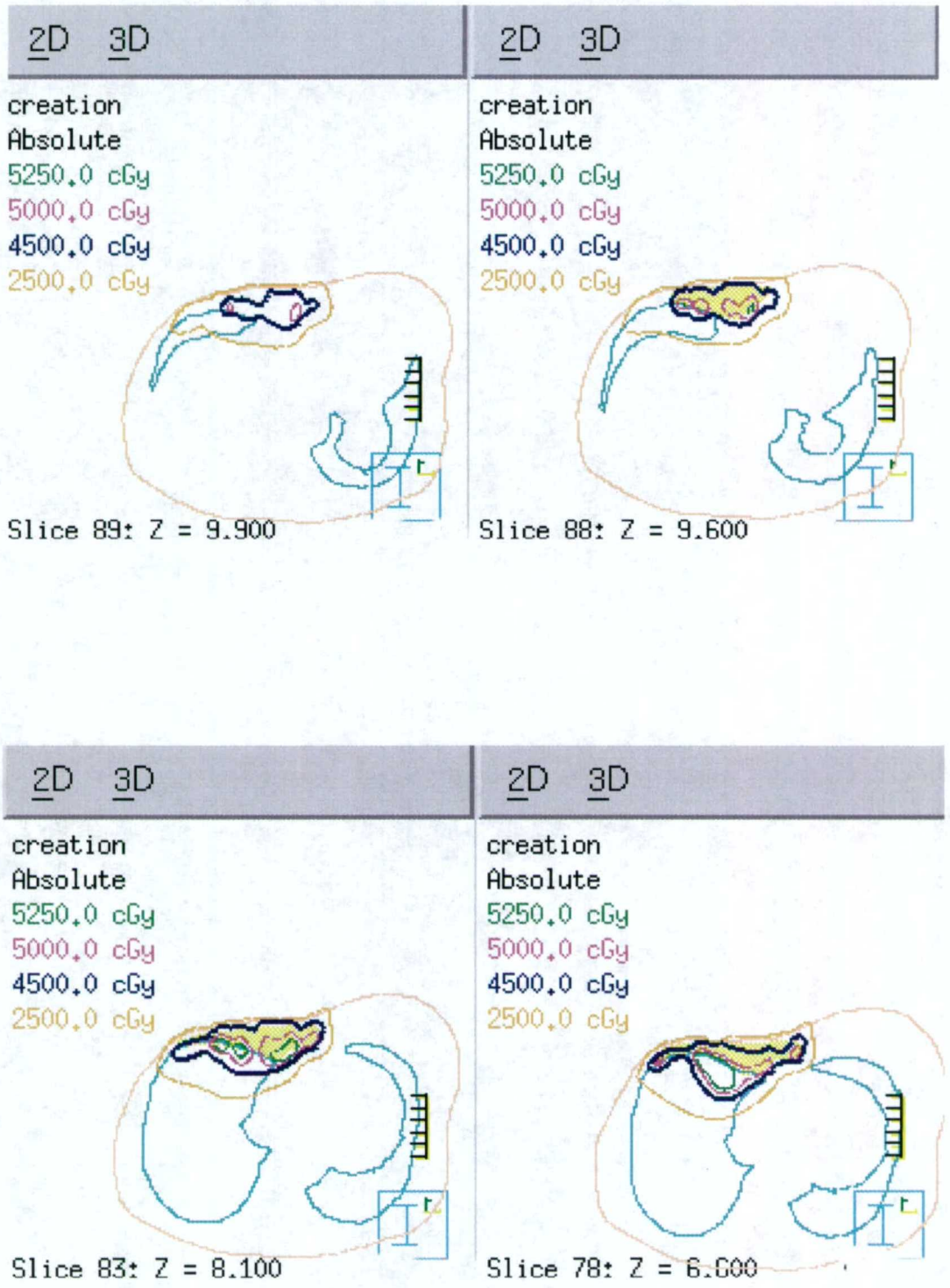

Figure 3.71. Transverse planes of patient 4 showing the dose distribution of the creation plan.

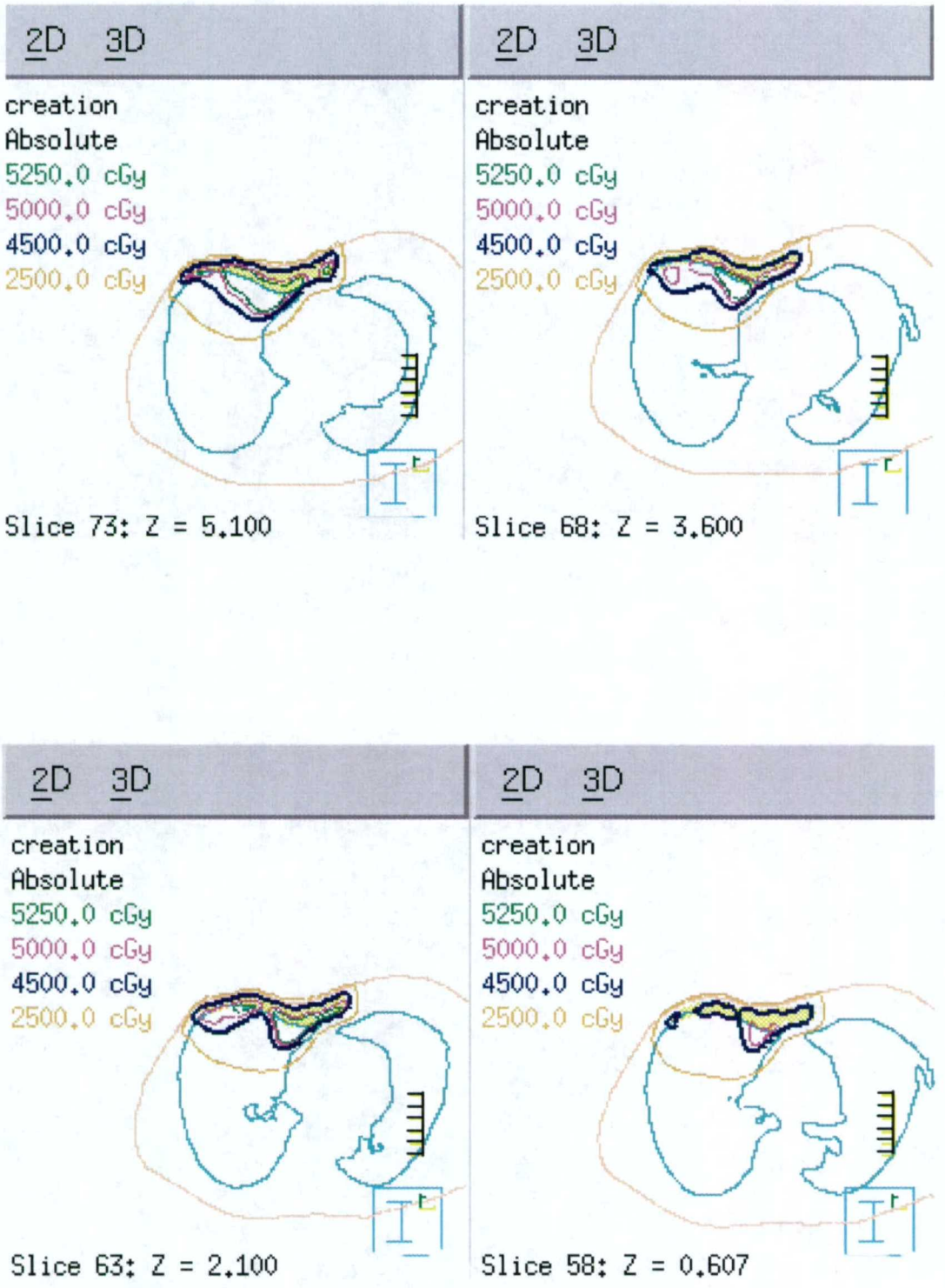

Figure 3.71. Continued.

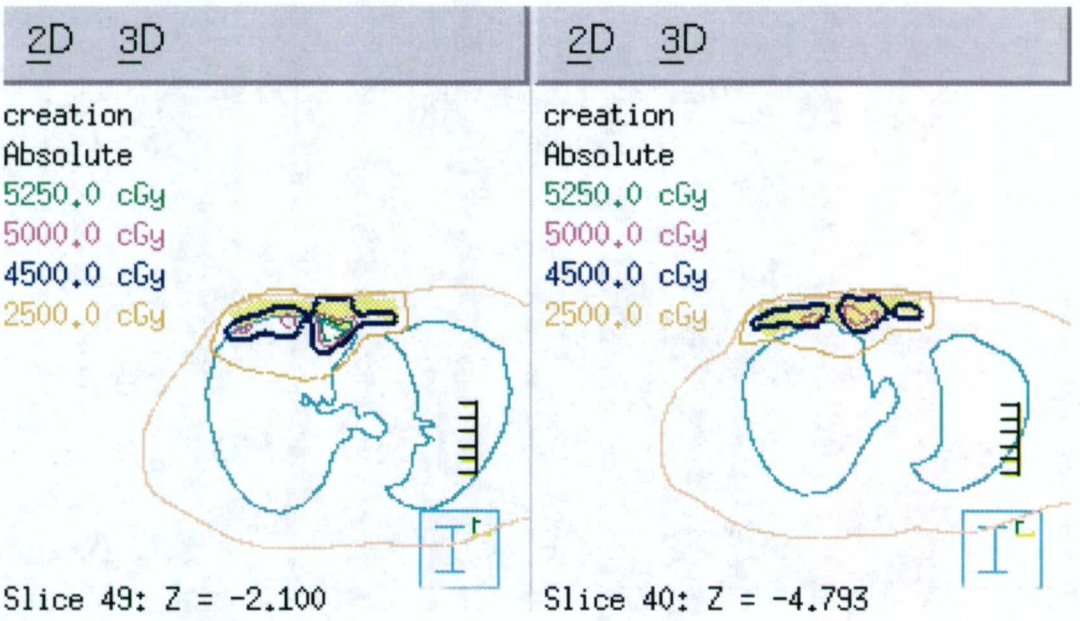

Figure 3.71. Continued.

3.10.3 Patient 4: Optimization

The Pinnacle^3 IMRT module was used to optimize the beam weighting, and the standard objectives were used in an attempt to improve the dose homogeneity. Figure 3.72 shows the resulting dose distribution. The mean dose to the PTV was 4891 ± 347 cGy, and 30% of the right lung received more than 2000 cGy.

Additional attempts to improve the PTV dose coverage and homogeneity, and to reduce the lung dose were made using various beam weight objectives. However, successful decreases in lung volume receiving more than 2000 cGy produced degraded 4500 cGy dose line coverage of the PTV.

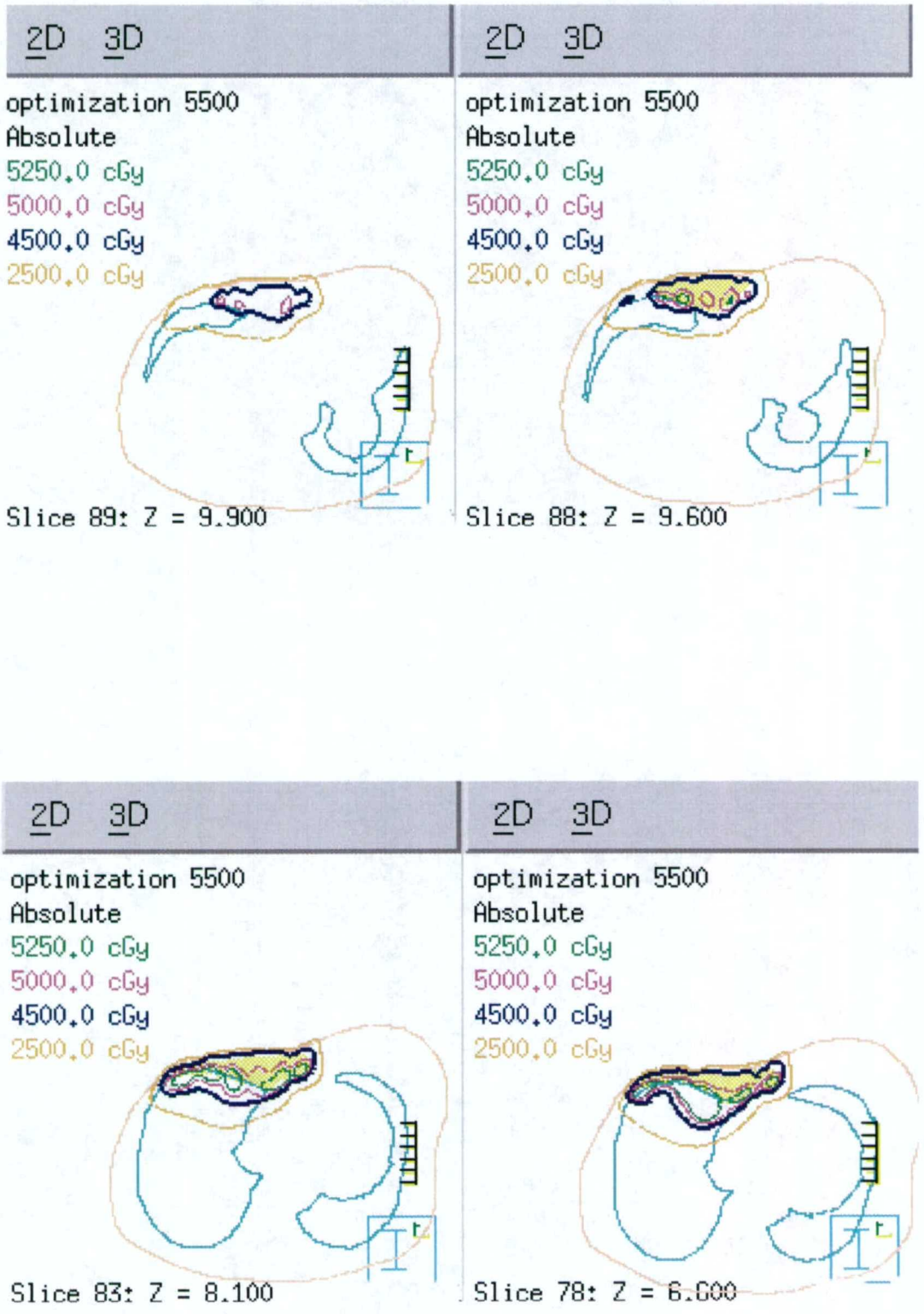

Figure 3.72. Dose distribution for patient 4 after beam-weight optimization.

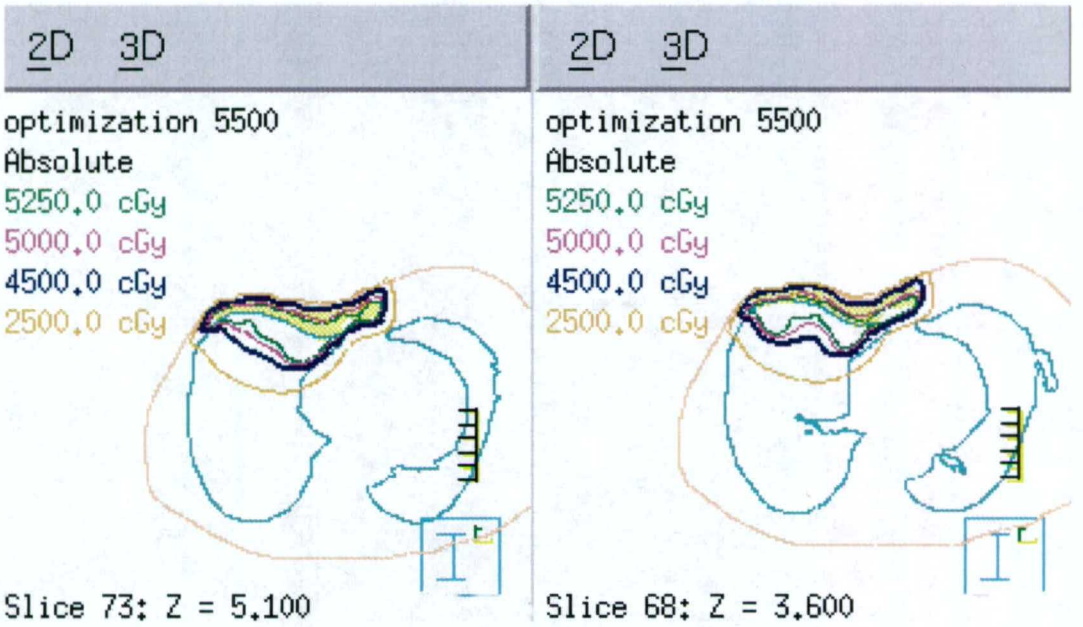

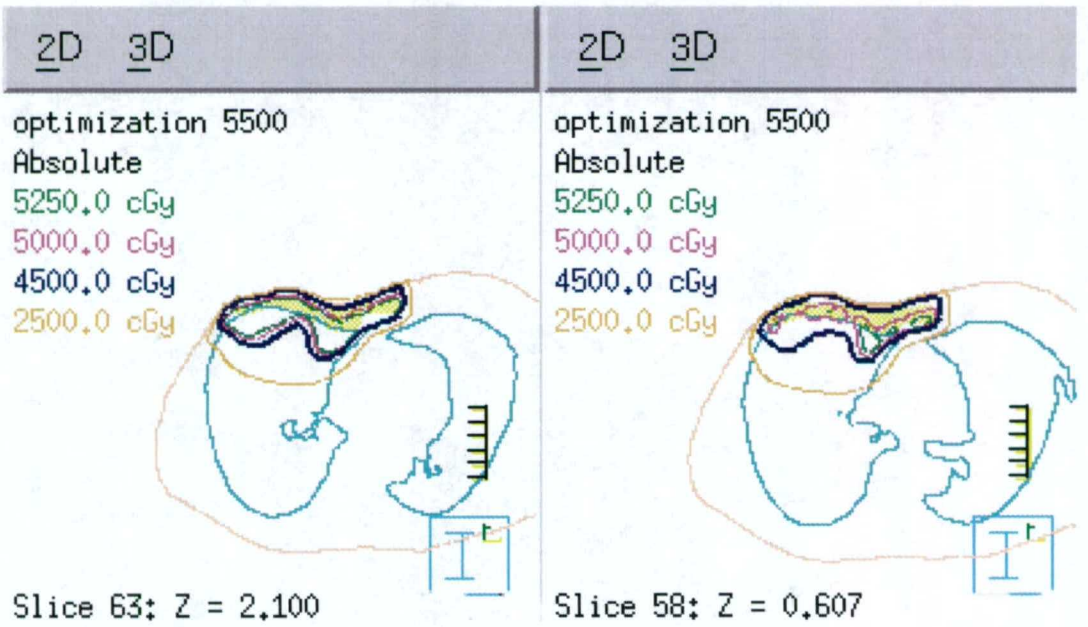

Figure 3.72. Continued.

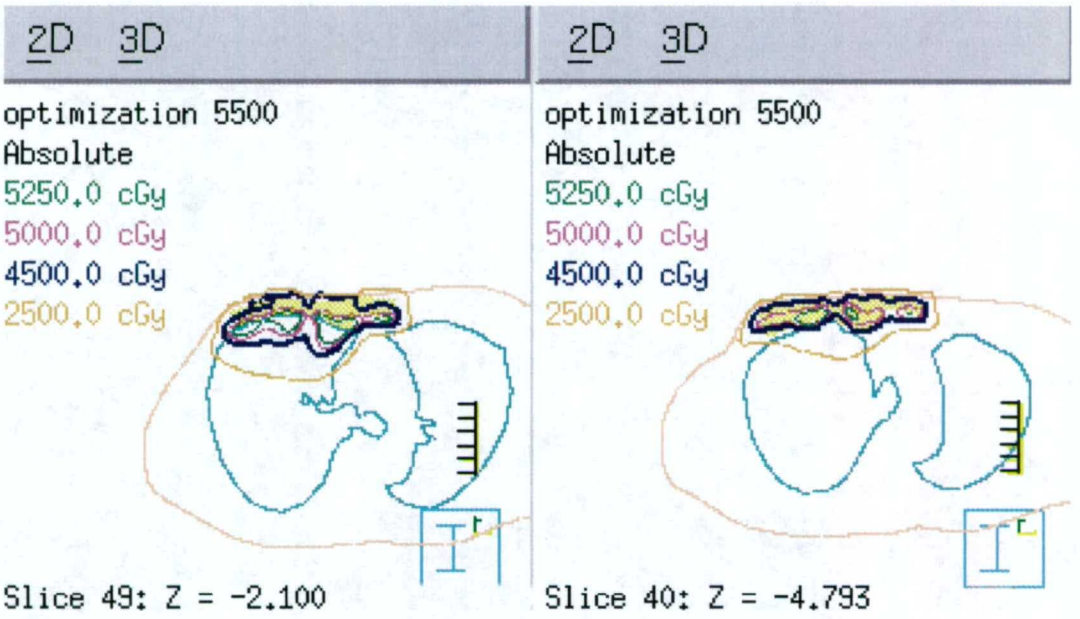

Figure 3.72. Continued.

3.10.4 Patient 4: Modification

The electron energy decrease technique was used to move the 90% isodose closer to the distal surface of the PTV. In particular, the 10-MeV left inferior field energy was changed to 8 MeV, the 10-MeV left superior field energy was changed to 8 MeV, the 8-MeV medial field energy was changed to 7 MeV, the 7-MeV right superior field energy was changed to 5 MeV, and the 7-MeV right inferior field energy was changed to 5 MeV. The standard optimization was used. Figure 3.73 shows the resulting dose distribution after performing these operations. The mean dose to the PTV was 4843 ± 375 cGy, and 23% of the right lung received more than 2000 cGy.

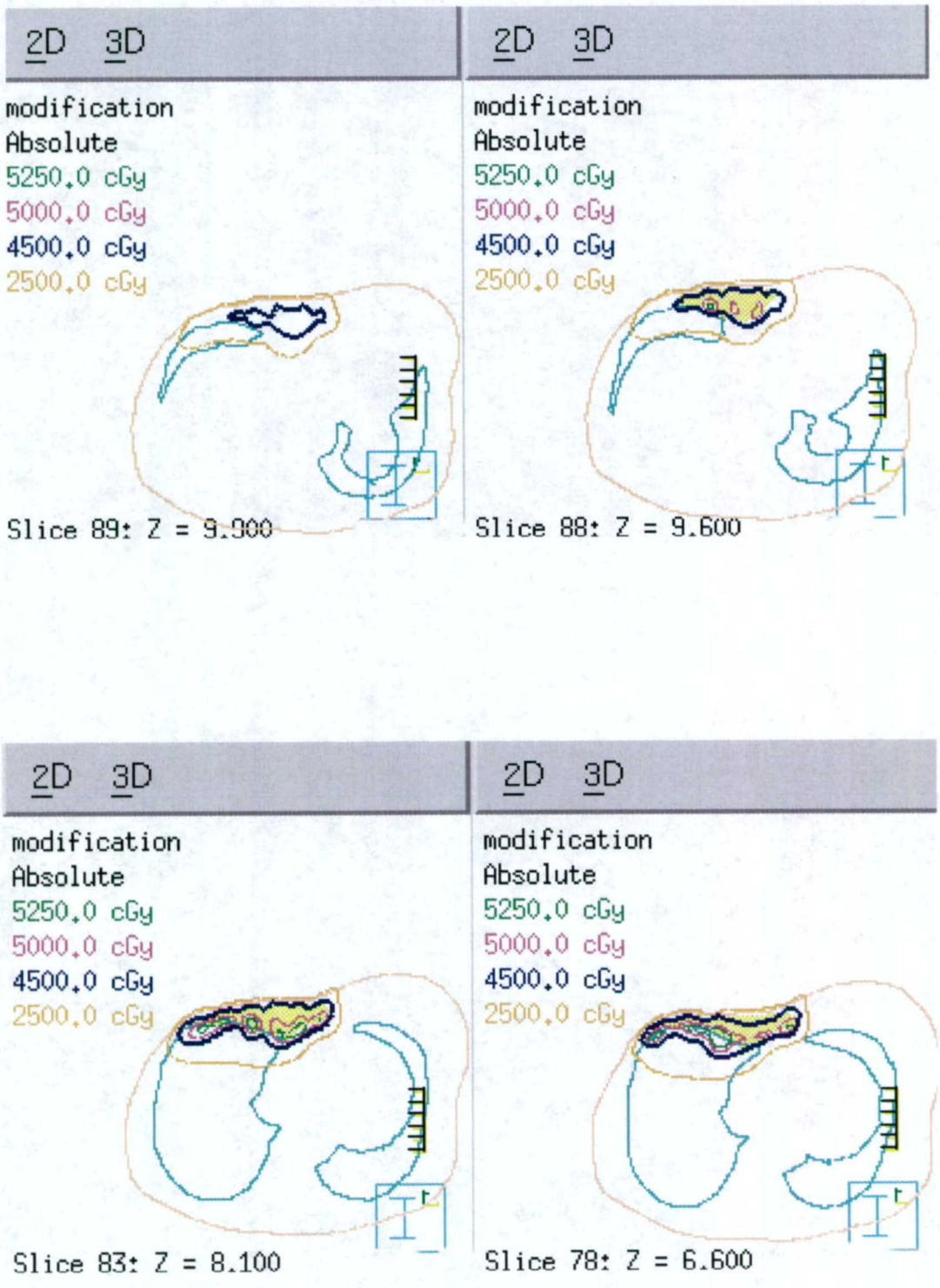

Figure 3.73. Dose distribution for patient 4 after decreasing the energy of several fields.

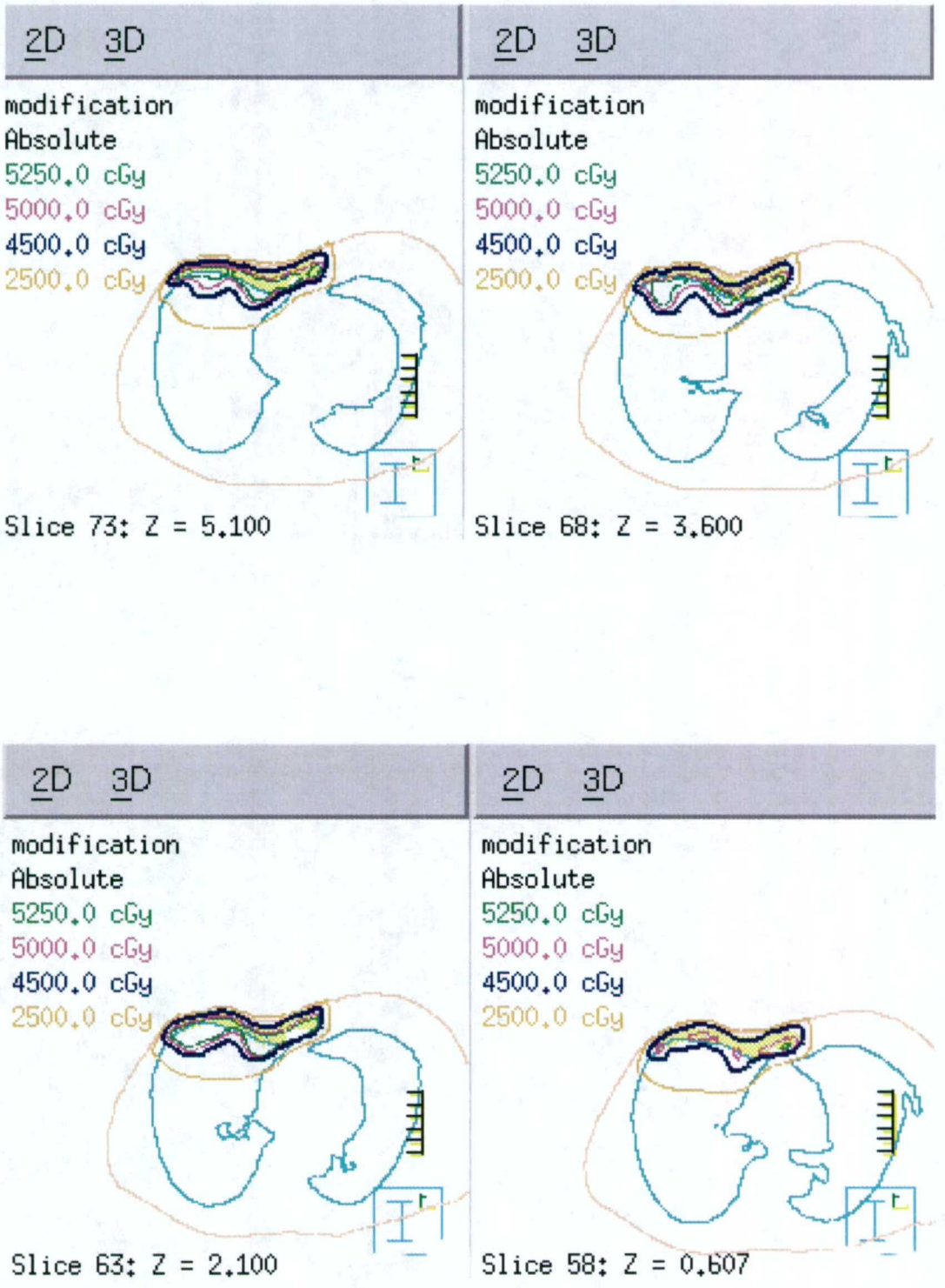

Figure 3.73. Continued.

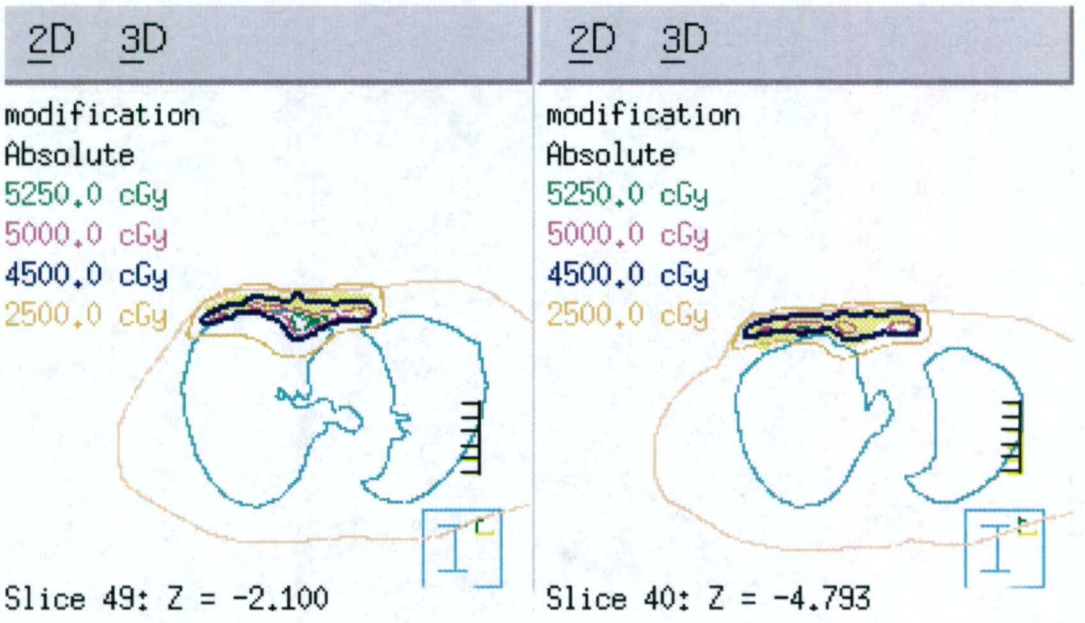

Figure 3.73. Continued.

3.10.5 Patient 4: Summary

Figure 3.74 shows PTV and right lung DVH for the above treatment plans. Table 3.10 summarizes the PTV dose homogeneity and the dose to the right lung. The segmented-field ECT algorithm provides good 90% dose of the PTV. The optimized plan improves the mean PTV dose and target dose homogeneity in comparison to the creation and modification plans; however, the lung dose was higher. Using the electron energy decrease technique, the volume of lung that received more than 2000 cGy was reduced without significantly reducing the 4500 cGy dose line coverage of the PTV and the target dose homogeneity. Compared to the bolus plan that was used clinically to treat the patient, the segmented-field ECT algorithm plans, optimized creation plan in particular, were comparable to the bolus plan for treating the PTV. However, the bolus plan was superior in sparing lung tissue.

Table 3.10. Dose statistics for patient 4.

	PTV (234 cm^3)			Right Lung (1924 cm^3)	
Treatment Plans	Mean Dose (cGy)	Standard Deviation (cGy)	$D(V_{90}) - D(V_{10})$ (cGy)	Volume > 20 Gy (%)	Mean Dose (cGy)
Creation	4739	371	976	29	1479
Creation, optimized	4891	347	928	30	1534
Modification, energy	4843	375	947	23	1170
Bolus	4931	388	888	14	754

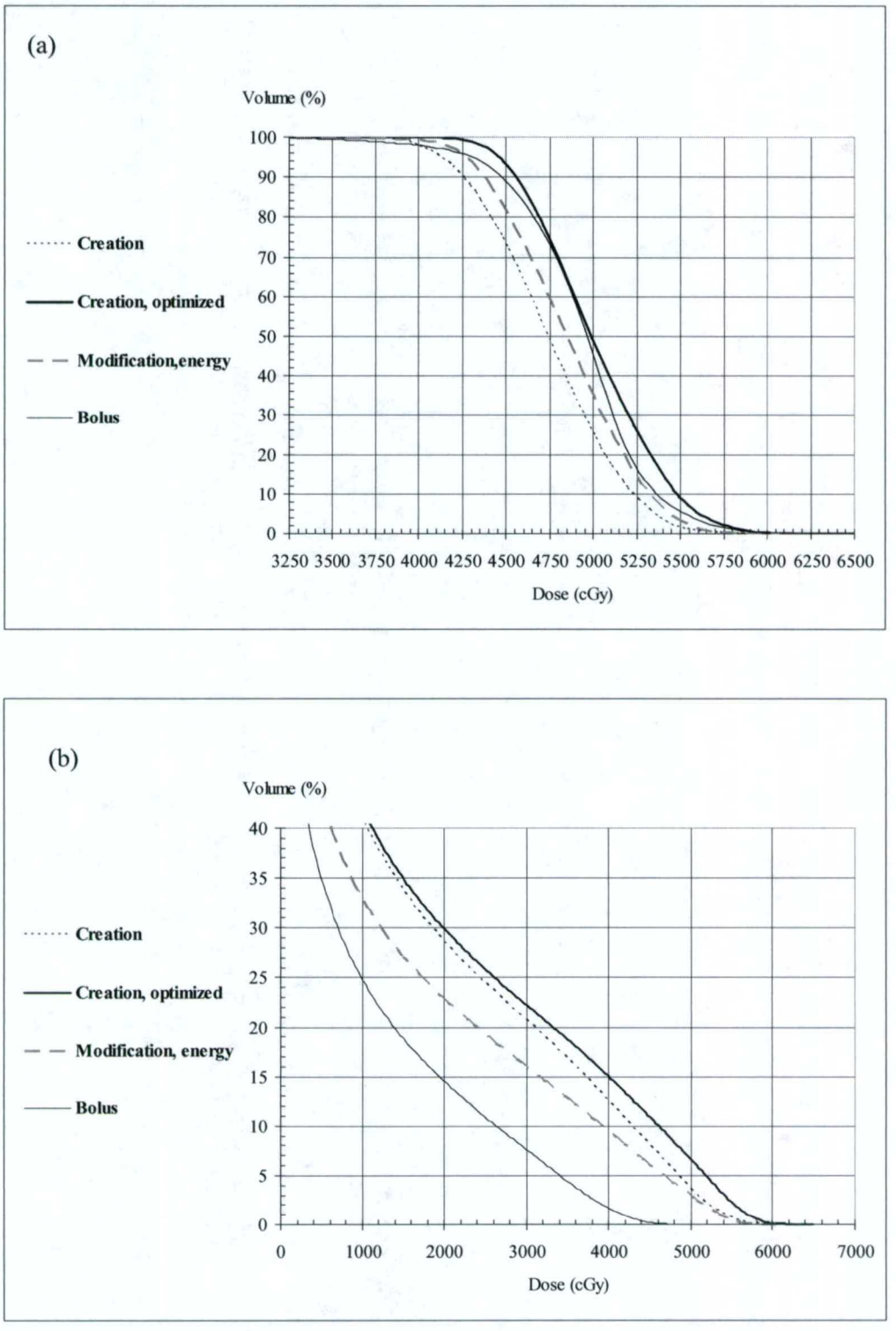

Figure 3.74. Dose volume histogram (DVH) for the PTV (a) and right lung (b) for patient 4.

3.11 Patient 5

3.11.1 Patient 5: Bolus plan

The patient was treated using customized bolus. Figure 3.75 shows the resultant dose distribution; the MU were adjusted to deliver 200 cGy given dose in order to compare the bolus plan to the segmented-field ECT plans. The mean dose to the PTV was 5044 ± 408 cGy, and 37% of the right lung received more than 2000 cGy.

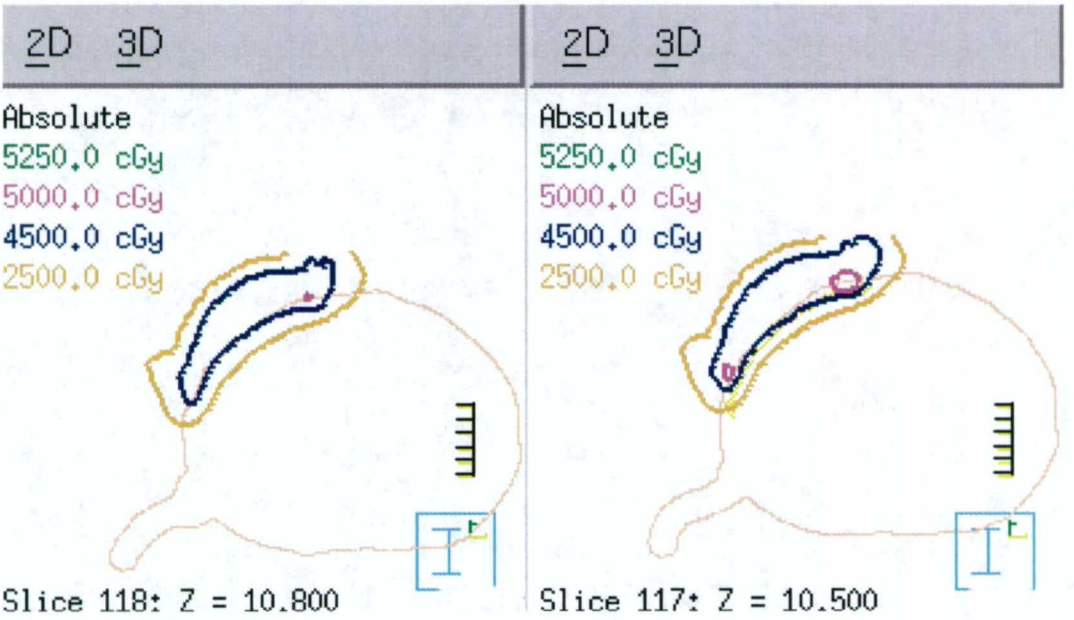

Figure 3.75. Transverse of patient 5 showing the dose distribution of the bolus treatment plan.

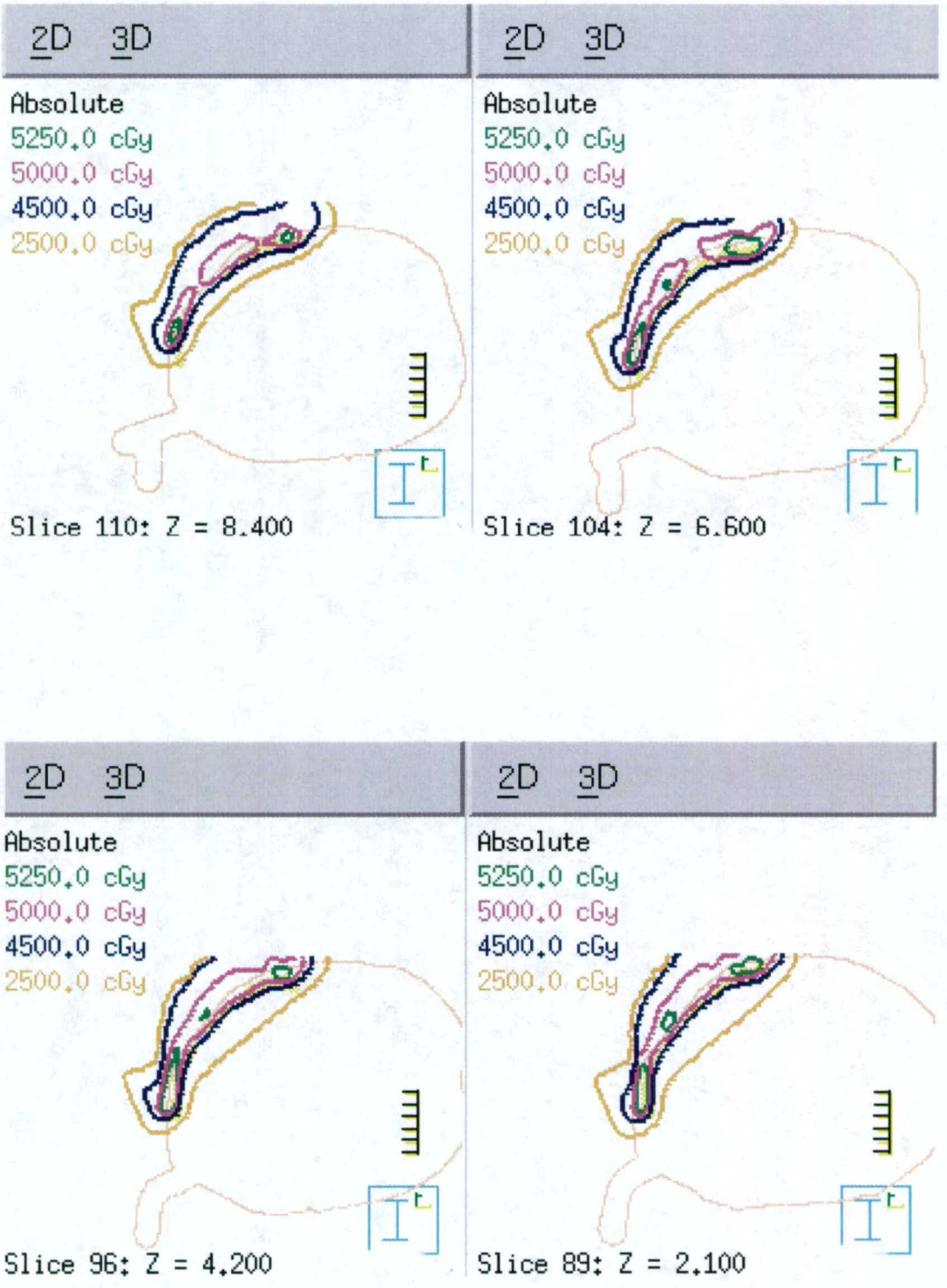

Figure 3.75. Continued.

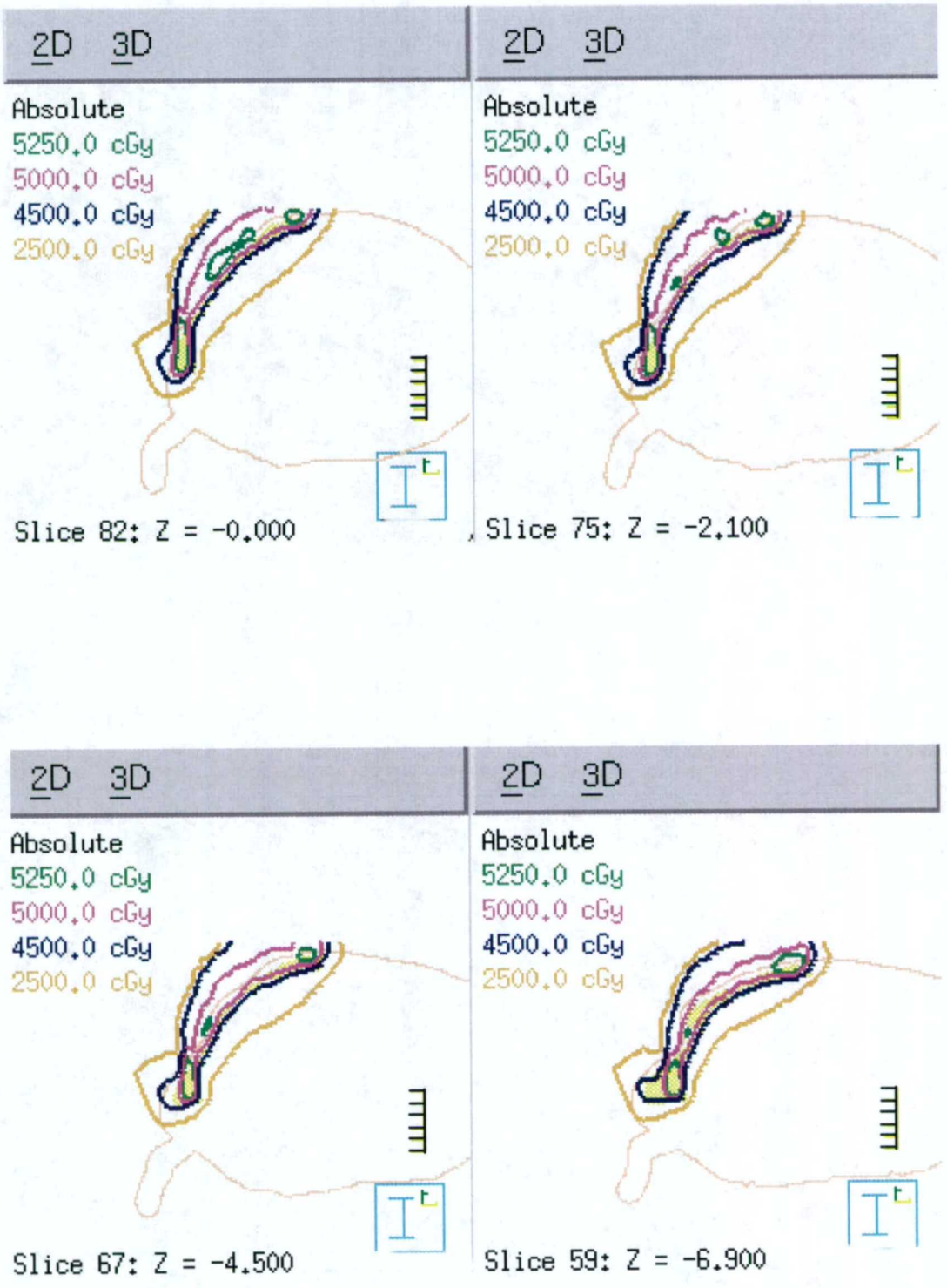

Figure 3.75. Continued.

3.11.2 Patient 5: Creation

The segmented-field ECT algorithm requires that the incident beam use a gantry angle of 0°; to accomplish this, the patient CT images were rotated counter-clockwise 20° placing the distal surface of the PTV approximately perpendicular to the beam's central axis. A treatment plan consisting of seven treatment fields having electron energies ranging from 6 MeV to 16 MeV were set according to the PTV depth. Figure 3.76 shows a BEV of the treatment fields in relation to the PTV. MU were set to deliver 200 cGy given dose for each field and dose was computed. The resulting dose distribution is shown in Figure 3.77. The mean dose to the PTV was 4481 ± 582 cGy, and 36% of the right lung received more than 2000 cGy.

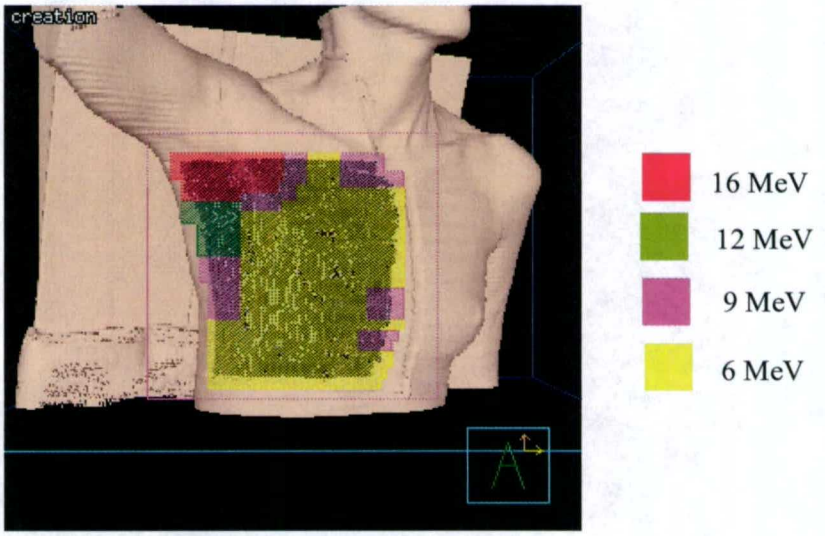

Figure 3.76. A BEV of treatment fields superimposed on the PTV (dark gray).

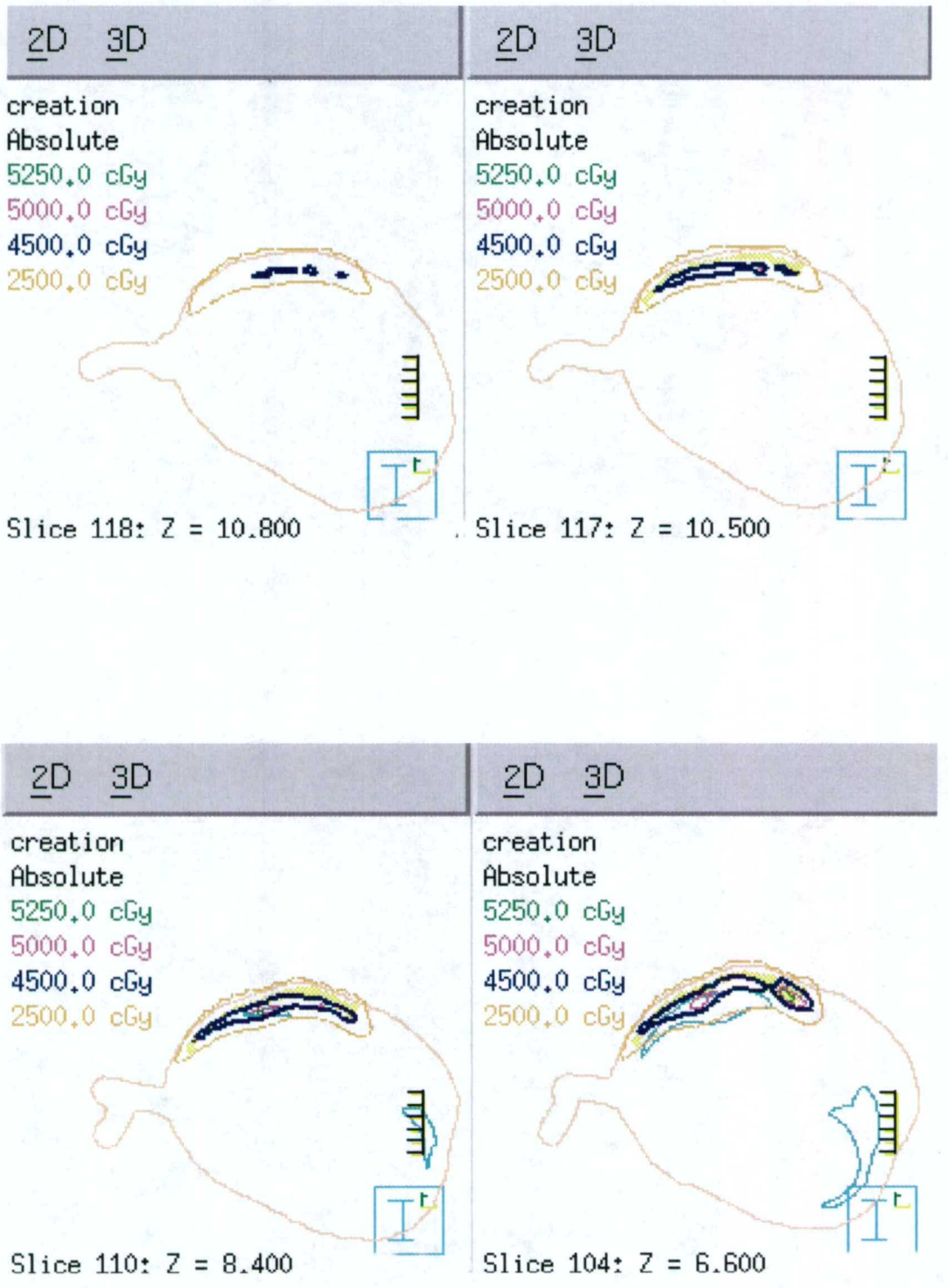

Figure 3.77. Transverse planes of patient 5 showing the dose distribution of the treatment plan using nine electron fields established in the creation step.

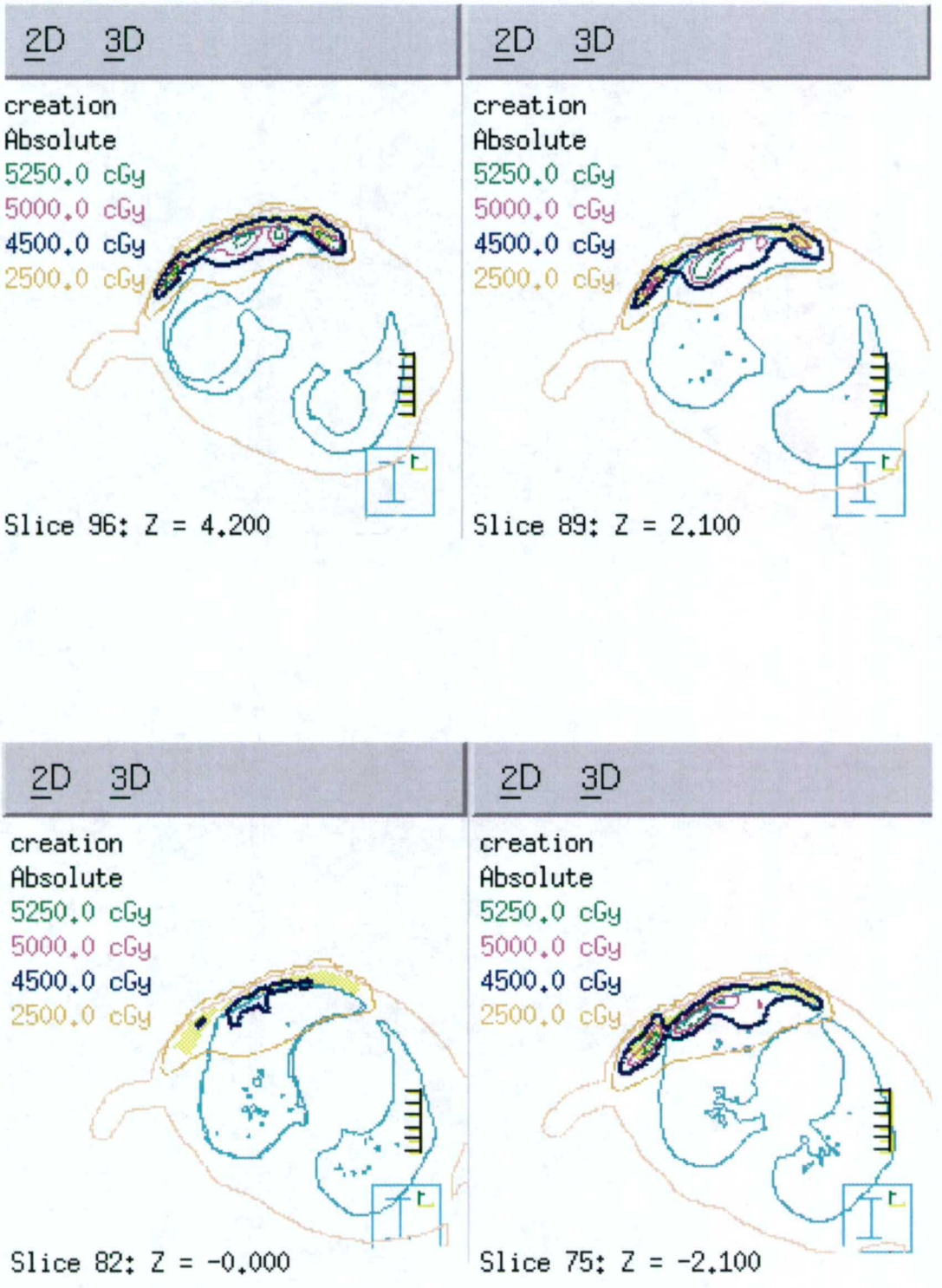

Figure 3.77. Continued.

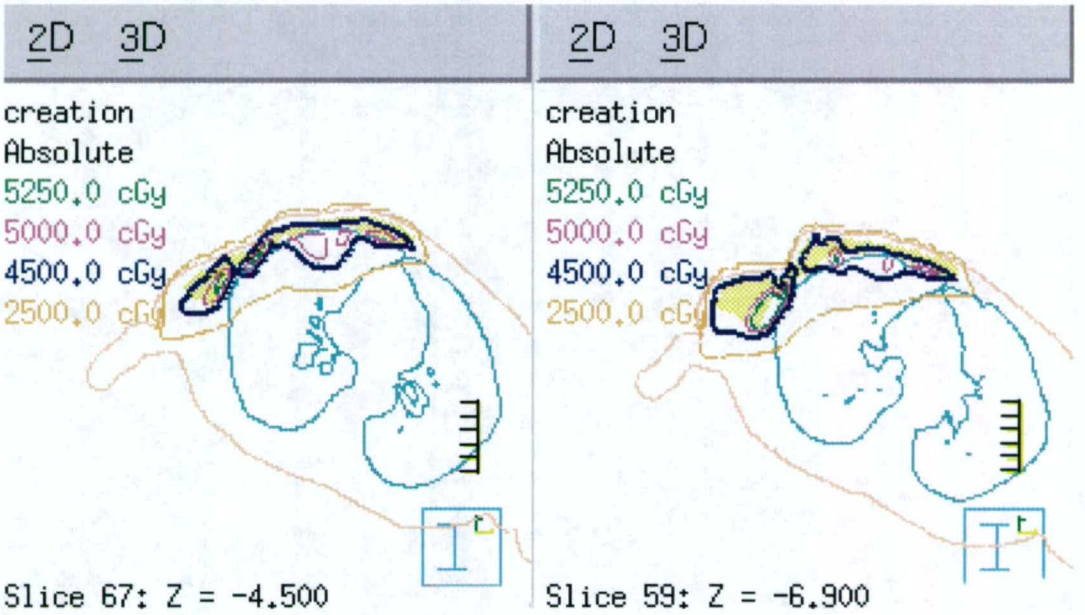

Figure 3.77. Continued.

3.11.3 Patient 5: Optimization

The Pinnacle[3] IMRT module was used to optimize the beam weighting; objectives were set to deliver a minimum of 4500 cGy to 90% of the PTV and a maximum of 5500 cGy to 10% of the PTV. Figure 3.78 shows the dose distribution for the plan. The mean dose to the PTV was 4662 ± 593 cGy, and 38% of the right lung received more than 2000 cGy.

Originally, the standard objectives were used, however, there was considerable lung dose. Reflecting on a similar case (Patient #1, modification plan), the beam weighting objectives were set as described above. The result produced a better plan: less lung irradiated, and better PTV conformality.

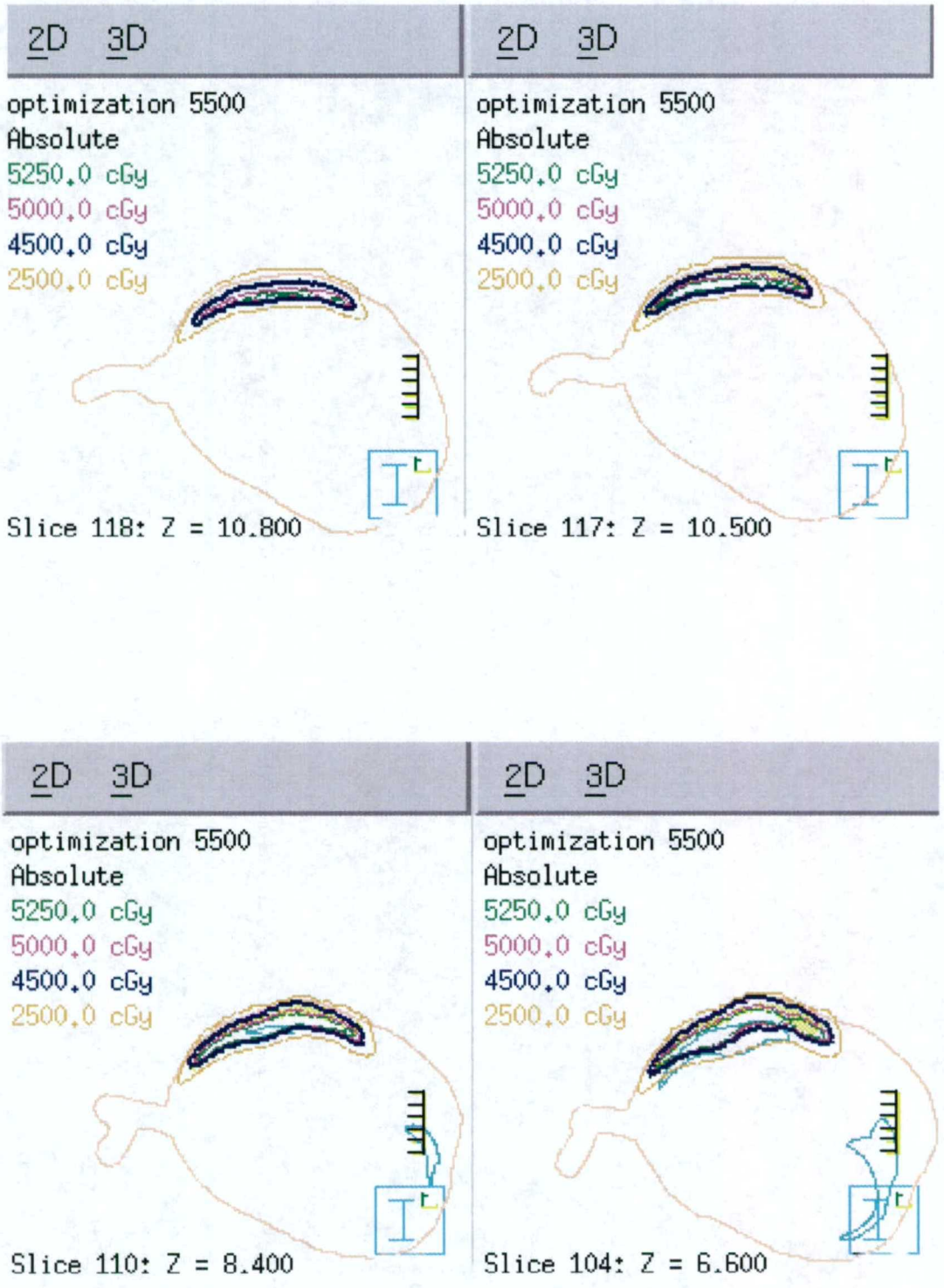

Figure 3.78. Dose distribution for patient 5 after beam-weight optimization. The optimization objectives are described in the text.

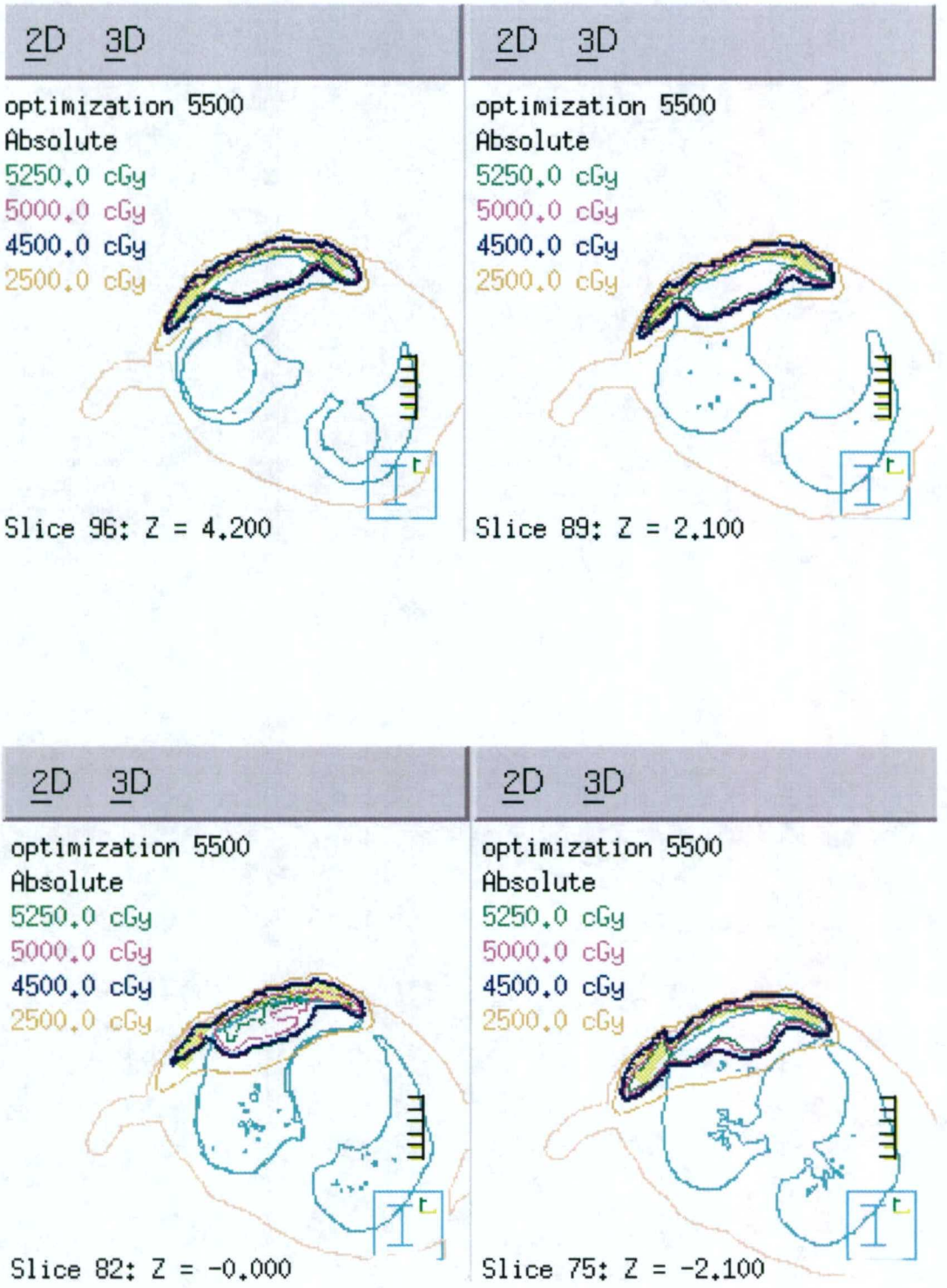

Figure 3.78. Continued.

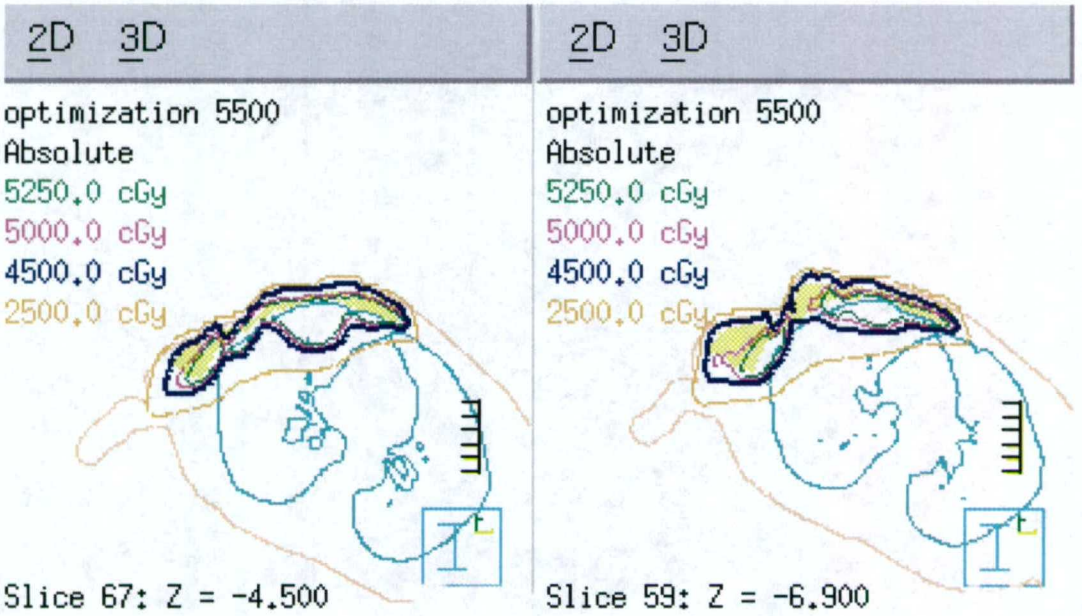

Figure 3.78. Continued.

3.11.4 Patient 5: Summary

Figure 3.79 compares the DVH of the PTV and right lung tissue for these treatment plans, and Table 3.11 summarizes the PTV dose homogeneity and the dose to the right lung. The optimized plan improved the target dose homogeneity and the D_{90-10} in comparison to the creation plan; the plan improved the 90% isodose line coverage of the PTV, especially for the anterior portion of the target. However, the central portion of the treatment plan utilized the lowest available electron energy which results in the 4500 cGy isodose line penetrating into the lung. The optimized creation plan has equivalent treatment results as the bolus plan, except for lung sparing.

Table 3.11. Dose statistics for patient 5.

	PTV (336 cm^3)			Right Lung (1660 cm^3)	
Treatment Plans	Mean Dose (cGy)	Standard Deviation (cGy)	$D(V_{90}) - D(V_{10})$ (cGy)	Volume > 20 Gy (%)	Mean Dose (cGy)
Creation	4481	582	1095	36	1736
Creation, optimized	4622	593	1002	38	1790
Bolus	5044	408	915	37	1221

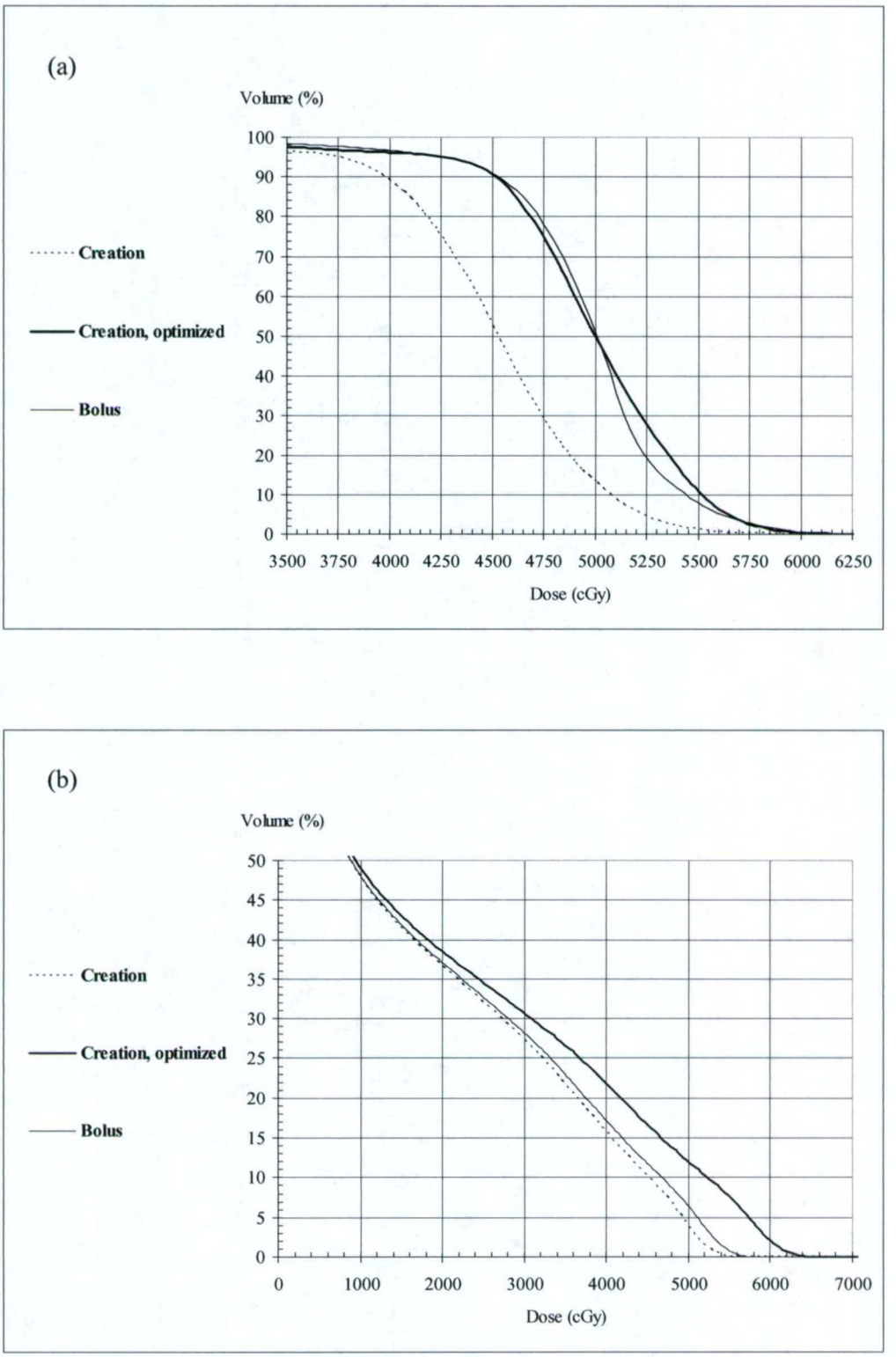

Figure 3.79. Dose volume histogram (DVH) for the PTV (a) and right lung (b) for patient 5.

Chapter 4

Conclusion

4.1 Summary

The purpose of this study was to examine the feasibility of producing conformal electron dose distributions for post-mastectomy radiation therapy without customized electron bolus by using multi-energy, multi-segmented electron fields. Task #1 was to develop a treatment-planning algorithm to generate multi-energy, multi-segmented conformal electron treatment plans. The algorithm was designed to segment an electron field based on target (PTV) depth (i.e., used to form an energy map). Field placement rules were established to place the treatment fields utilizing the energy map. Dose was computed using the modified version of the COPPERPlan TPS implementation of the Hogstrom PBA. The Pinnacle^3 TPS beam-weight optimizer was used to improve the dose distributions in most cases, and the resultant dose distribution was evaluated for conformation about and homogeneity within the PTV in addition to non-target dose sparing. If the plan was acceptable, then the planning process was complete; however, if PTV dose conformation or homogeneity was not favorable, or if the non-target tissue received too much dose, then modifications to the plan were required. Seven modification techniques were devised as a means to further improve the PTV dose conformation and homogeneity, and non-target dose sparing. The modification techniques included field edge expansion (contraction), energy-smoothing, dilation of internal field size, increase (decrease) coverage, region connector, energy increase (decrease), and electron fluence increase (decrease).

Task #2 was to use the algorithm for treatment planning of six simple geometric targets. The first four simple targets had translational symmetry in the superior-inferior direction, the fifth target had eight-fold mirror symmetry, and the latter target did not have any symmetry. The simple targets provided an opportunity to develop and evaluate the algorithm's creation and modification phases.

Task #3 was to utilize the algorithm to create treatment plans for five post-mastectomy clinical cases. These particular cases were previously treated using bolus ECT. After the segmented-field ECT plans were developed, the modification techniques were used to improve the PTV dose conformation and homogeneity, or the dose sparing for the lung tissue. The segmented-field ECT treatment plan for each clinical case was compared to the corresponding bolus ECT plan. **It was hypothesized that compared to customized electron bolus radiotherapy for post-mastectomy irradiation, ECT with multi-energy, multi-segmented treatment fields has equivalent target coverage and equivalent (or better) normal tissue sparing and PTV dose uniformity**.

4.2 Conclusions and future study

The results from this study refuted the hypothesis: (1) Segmented-field ECT was inferior to bolus ECT in providing equivalent target coverage for targets very close to the skin surface, (2) Segmented-field ECT can provide equivalent target coverage for non-shallow PTV (i.e., greater then 0.5 cm from the skin surface), (3) Segmented field ECT can produce equivalent or better dose homogeneity, and (4) Bolus ECT is superior to segmented-field ECT in sparing lung tissue.

4.2.1 Simple target treatment plans

The algorithm was used to create treatment plans for six simple targets, and it performed the creation phase very well. Various modification techniques were used, primarily to create improved treatment plans, but also to evaluate the modification techniques. The seven modification techniques provide a basic corps of operations to help improve a treatment plan. As treatment plans increase in complexity, more modification techniques are utilized per treatment plan.

A future study should entail delivering the treatment plan of the simple targets to a solid water phantom and comparing the measured results to the calculated results. The treatment fields could be formed using a low melting point alloy or an eMLC mounted on a linear accelerator. Monte Carlo

simulations of the treatment delivery could also be performed using the BEAM user code, and the pencil-beam calculated results could be compared to the measured results.

4.2.2 Clinical target treatment plans

The algorithm was used to create treatment plans for five patients that were previously treated with bolus ECT. One assumption of the algorithm is that the PTV is positioned at an angle of 0° with respect to a surface perpendicular to the anterior-posterior direction. The CT data for two of the patients were rotated so that the algorithm could be used. A proper implementation of the segmented-field ECT algorithm should be able to inherently perform this operation. Table 4.1 provides a summary of the patient plan results.

As with the simple targets, the algorithm could create the depth maps quite well. The placement and verification of the electron fields was laborious, but the field position rules were key to reasonable initial treatment plans. The flexibility of the Pinnacle[3] beam-weight optimization was useful to the treatment planning process. The creation step combined with the field placement rules and optimization process allowed the segmented-field ECT algorithm to establish good treatment plans in terms of conformation and reduction of non-target tissue dose.

Table 4.1 A summary of the patient treatment plans. This data compares the segmented-field ECT plan to the bolus ECT plan. Equivalent indicates that the resultant dose is basically equivalent between the two methods.

	Patient #1	Patient #2	Patient #3	Patient #4	Patient #5
PTV rotation	Yes	No	No	No	Yes
Better PTV Coverage	Bolus	Bolus	Bolus	Equivalent	Equivalent
Better PTV Dose Homogeneity	Bolus	Bolus	Segmented Field	Equivalent	Equivalent
Better lung sparing (lung volume < 20 Gy)	Bolus	Equivalent	Bolus	Bolus	Bolus

For three patient cases (#1, #2, and #5), the availability of lower energy electron beams would have helped those treatment plans. The shallow chest wall of these patients resulted in the lowest energy beam penetrating beyond the distal edge of the PTV. Other than those portions of the treatment field, the remaining aspects of the treatment plan appeared good. The use of a 0.5 cm to 1.0 cm thick bolus would also probably have improved the results; however, the COPPERPlan TPS can not currently handle constant thickness bolus. A future study should evaluate use of a constant thickness bolus with segmented field ECT for patients having a shallow PTV.

For patients #3 and #4, the algorithm provided treatment plans providing PTV dose conformality and homogeneity comparable to the bolus plans. However, for almost all cases, the bolus plan was superior in sparing lung tissue. The exception was for patient #2, in which one plan revision provided equivalent results.

4.2.3 Segmented-field ECT algorithm limitations

The algorithm utilizes the treatment planning tools of a commercial TPS to establish the energy map and to place electron fields. It would be possible for a computer programmer to implant this algorithm into a TPS to make planning much easier. Overall the algorithm segments the PTV reasonably well. A proper implementation of the segmented-field ECT algorithm would also perform the depth segmentation automatically, much like the electron bolus design of Low et al. (1992). The main limitation of the PTV segmentation is the available electron beam energies. A finer range of electron beams available on the linear accelerator would enhance the practicality of this algorithm.

A current time constraint in using this algorithm is that the TPS is not robust enough to abut treatment fields. Currently, treatment fields are adjusted via editing a beam data file manually. This process is performed during both the creation phase and any adjustments determined necessary during the modification phase.

In addition, a few minor limitations in the Pinnacle^3 dose calculation were found during this study and are discussed in Appendix C. As a result, the COPPERPlan implementation of the Hogstrom

PBA was used to compute dose. Obviously, these limitations would have to be eliminated from Pinnacle[3] so that segmented-field ECT would be practical.

Appendix A

Post-mastectomy radiation treatment planning

A.1 Overview of general treatment planning techniques

The goal of post-mastectomy radiation therapy is to treat regions at risk for subclinical disease; this includes the chest wall, supraclavicular lymph nodes, axillary lymph nodes, and internal mammary chain (IMC) lymph nodes. The exact extent of the treatment region is determined by the radiation oncologist; however, the following general observations can be made.

The chest wall is usually treated using tangential photon beams. The superior borders of the chest wall fields abut the supraclavicular field. To avoid junctional hot spots, it is helpful if the tangential fields have a non-diverging superior edge. The superior border of the tangential fields and the inferior border of the supraclavicular field are aligned. Careful placement of the boundary between the supraclavicular field and the chest wall fields can substantially reduce the volume of lung included in the treatment fields.

When irradiation of the axilla is desired, most of the axillary dose is delivered through the anterior superclavicular field using photons (Buchholz 2003). A posterior field can be used to supplement the mid-axilla to the desired dose.

An adjacent, matching electron beam field is routinely added to treat the most medial portion of the chest wall and to encompass the lymph nodes of the ipsilateral IMC nodes (Buchholz 2003). Usually, the medial border of the IMC field is 5 to 6 cm wide and extends 1 cm to the contralateral side of the midsternal line, and the lateral border is shaped to precisely match the edge of the tangent fields. A small gantry rotation, about 15°-20°, may also be used to get a better match between the IMC field and the tangent fields.

Alternatively, electrons can be used to treat both the chest wall and IMC nodes (discussed in section 1.1, Statement of problem); this technique improves conformation of the treatment volume to the target volume, but there is a greater risk for geographic miss of microscopic disease or excessive transmission into lung (Buchholz 2003).

A.2 Treatment planning at M. D. Anderson

The steps involved in creating a post-mastectomy radiation treatment plan at M. D. Anderson are rather involved and require the contribution of the entire radiation oncology team: clinicians, medical physicists, dosimetrists, and simulation therapists.

The first step is the simulation process. The main purpose of simulation is to design treatment fields so the target volume may be accurately encompassed without delivering excessive radiation to surrounding normal tissues. Computed tomography (CT) based simulation offers optimal placement of isocenters, optimal placement of treatment fields, and reduced simulation time.

For the simulation, the patient is placed in the supine position on the CT couch and the ipsilateral arm is abducted 90° and externally rotated. The contralateral arm is placed along the torso side, and the head is turned slightly towards the contralateral side. A positioning device (Vac-Lok™, Med-Tec, Orange City, IA) is used to immobilize the patient. In most cases, an incline board (10°-15°) placed under the positioning device is used to elevate and position the patient so that the anterior chest wall is more horizontal, thereby minimizing a cranial-caudal slope of the chest wall relative to the incident radiation beam. The patient's surgical scar and a preliminary isocenter are marked using radiopaque wire.

A scout scan is acquired to ensure the patient is positioned correctly. After reviewing the scout scan, the radiation oncologist selects the superior and inferior borders of the CT-scan volume. The CT-scan region includes the chest wall, supraclavicular, apical, and the IMC lymph nodes. Multiple CT slices are acquired using a slice spacing of 3 mm. The CT images are transferred to a simulation workstation (VoxelQ™, Philips Medical System, Cleveland, OH) which contains software tools used

for placing treatment isocenters and for contouring target volumes or other organs. Three isocenters (tangential, supraclavicular, and IMC) are determined and marked by the radiation oncologist for post-mastecomy radiation treatment plans. Treatment fields are then designed on the CT data set. The planner contours the patient skin surface and the radiation oncologist contours the planning target volume (PTV).

To determine the tangential field isocenter, a CT image slice that is mid-way between the superior and inferior slices is selected. The isocenter is placed within the chest wall at the chest wall and lung interface. For patients with a very thin chest wall, the isocenter is positioned more posteriorly toward the lung to aid in the setup process. The isocenter and accompanying setup points are then marked on the patient's skin.

The superior border of the tangential field collimator edge usually extends 2-3 cm into the supraclavicular field. The tangential field superior border and the supraclavicular field inferior border are usually non-divergent in the same transverse plane. To achieve a geometrically perfect match between the tangential and supraclavicular fields, a rod (Chu 1990) is positioned on the patient's skin at the inferior border of the supraclavicular field. The chains hang freely by gravity on either side of the patient and are checked using the lateral lasers. The collimator is rotated until the posterior field border is parallel to the chest wall. The couch is rotated until the couch angle corresponds to the non-divergent superior border of the medial tangent which is obtained when the image of the chain overlaps with that of the rod (Figure A.1a). The location of the rod and chain also defines the arc of overlap between the tangent and supraclavicular fields introduced by the collimator rotation; this overlap (area above the rod and chain) is then blocked with a customized shielding insert in the tangent fields (Chu 1990). The isocenter of the supraclavicular field is placed about 1/3 to 1/2 the distance medially from the center of the lung within the chest wall along the rod and a half-beam block technique assures that this beam does not diverge into the tangent field (Figure A.1b). The IMC field generally extends 4-5 cm on the patient's ipsilateral side (medial boarder of the tangential field) to 1 cm on the contralateral side (Figure A.1c). The IMC isocenter is placed medially within the IMC field on the patient's skin surface.

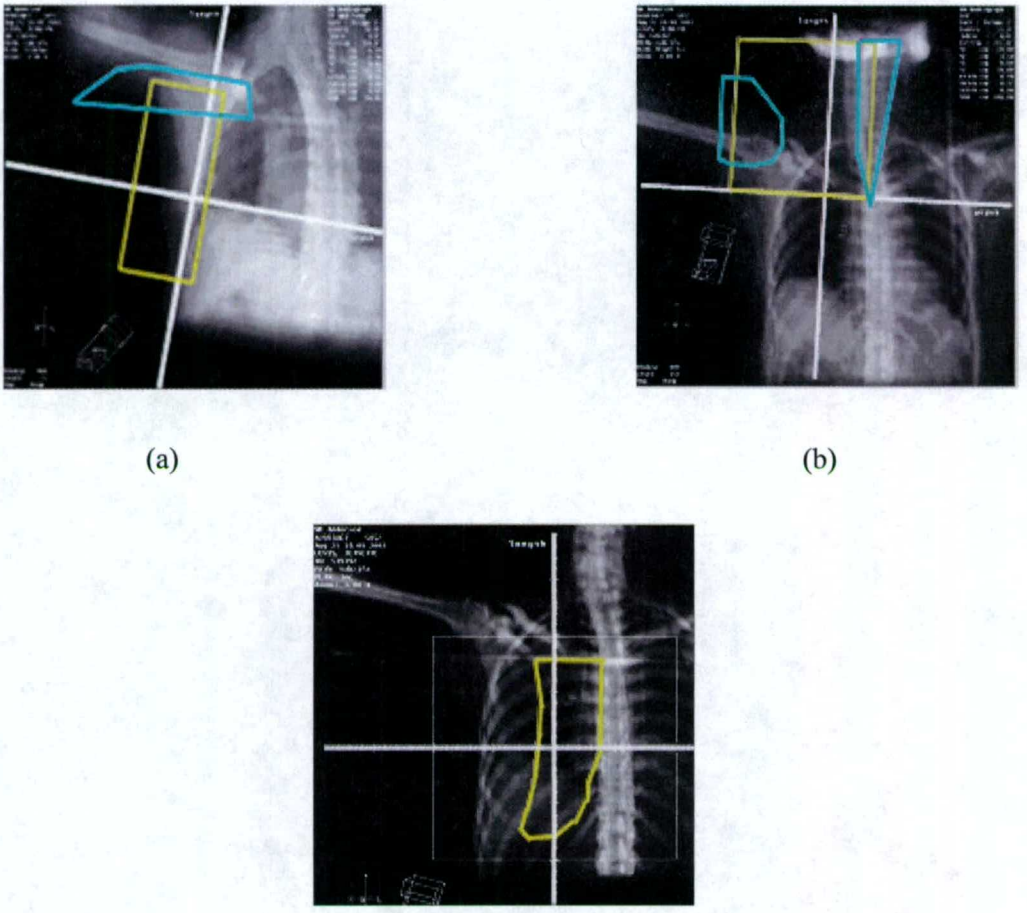

(a) (b)

(c)

Figure A.1 Placement of the treatment fields for postmastectomy irradiation therapy at M. D. Anderson. (a) right medial-tangent field, (b) supraclavicular field, and (c) IMC field. The blue outlined fields indicate blocked regions of the treatment fields (yellow).

The treatment fields are then transferred to the TPS. The planner optimizes the beam energies and weighting and computes dose. Generally, a dose of 50 Gy in 25 fractions is prescribed at an isodose that encompasses the entire target. All electron fields are prescribed to D_{max} and an electron beam energy is chosen using CT planning to assure that 90% of the dose is delivered to the deep portion of the pectoralis major muscle (i.e., an IMC blood vessel that is near the superior lung surface is identified and used to establish the electron beam energy).

Appendix B

Overview of Pinnacle^3 treatment planning system

A commercial treatment planning system (TPS) (Pinnacle^3, Philips Medical Systems, Milpitas, CA) provides tools for developing and evaluating radiation treatment plans. Many features of this commercially available TPS were used to develop a segmented-field electron conformal therapy (ECT) algorithm. This appendix describes some basic aspects of the TPS.

The TPS has two main modules: Physics Utility and Patient Planning (ADAC 1997). Physics Utility is used for entering and modeling physics data that was collected during the accelerator commissioning process. This is performed when the TPS is commissioned and when new machines are put into service. Under normal circumstances, the planner does not have to access this module.

Patient Planning consists of a database and programs for manipulating the treatment planning data within the database. "Institutions" are used to store data for patients belonging to a physical institution. Within an "institution", the planner can add or delete patients, edit patient information, import computed tomography (CT) and magnetic resonance (MR) images, add or delete treatment plans, access existing treatment plans, and archive and restore patient data. In most cases, CT data is used for anatomical input to the TPS because it is geometrically accurate and provides attenuation properties of the various tissues that are useful for heterogeneity corrections (Hogstrom 1983). Each "institution" has one or more treatment units that are shared for all patients within the "institution."

Patient Planning includes tools for displaying the patient data and developing treatment plans. The planner must specify several parameters related to the CT data being used: the window and level settings for viewing patient images, the CT scanner used to obtain the CT data so that the correct CT to density map is used during dose calculation, the patient position during the CT scan, the couch position within the CT image, and the threshold for distinguishing between the patient and the air surrounding the patient.

The TPS allows the planner to display two-dimensional (2D) and three-dimensional (3D) images of patient data and treatment planning data. The 2D and 3D viewing windows are used for viewing patient anatomy, points of interest, regions of interest, beams and dose distributions that are created during the planning process. Beam's eye view (BEV) displays can also be setup. A BEV display allows the planner to view the patient anatomy from the perspective of the radiation source.

The TPS has tools that allow the planner to specify points of interest (POI) and regions of interest (ROI). The POI tool is used to specify the isocenter for each beam, and also points for which the dose to that point is desired. The ROI tool is used to contour anatomical structures of interest. Statistics can be computed for ROIs.

The planner must specify the machine, modality, beam energy, isocenter, couch position, gantry and collimator angles, and collimator jaw positions. All modifiers (e.g. photon blocks, electron cutouts, wedges, compensators, and bolus) must be specified. For this study, electron cutouts will be used extensively in the treatment planning process. Electron cutouts can be set up to automatically block or expose a ROI with or without a margin, or they can be drawn manually by defining a series of points using the blocking tools.

Before computing dose, the dose grid must be set. The dose grid is a 3D grid that specifies where in the patient the planner wants dose to be computed; it also specifies the resolution to use for dose computation. The dose grid should be positioned to cover the target and all critical structures. During the dose computation process, the TPS reads in the CT numbers and determines the densities for each voxel of the patient using the selected CT to density table. The density information in the patient CT images is used to account for tissue inhomogeneities in the electron dose calculations.

In Pinnacle[3], dose is computed as dose (cGy) per monitor unit (MU); MUs are calculated for each beam and displayed as MU/fraction. Dose can be prescribed two ways: 1) dose to a point, or 2) MU for each beam. Beam weights are assigned as 1) percentages of the total prescription or 2) MU. The relative weights for all beams assigned to a prescription will always sum to 100%. Making a change to one beam weight will change the weight for all other beams unless that beam weight is locked. After

dose is computed, the intensity modulated radiotherapy (IMRT) module provides an inverse planning option that can be used to optimize beam weighting in an attempt to improve dose coverage and homogeneity.

Appendix C

Limitations of the treatment planning system dose calculation implementation

C.1 Dose prescription

The Pinnacle^3 TPS supports dose prescription to specified physical points in the patient; however, due to surface irregularities or internal inhomogeneities, the dose prescription point could lie in a region of high dose gradient and consequently not be a suitable prescription point. This method of dose prescription is also inconsistent with AAPM TG-25, which recommends specifying dose at the depth of maximum dose on the central axis in a water phantom for the field size and SSD used to treat the patient. To work around this limitation, individual beams should be weighted using monitor units (MU) calculated as per TG-25 specification from machine data tables rather than from the TPS (Hogstrom, 1983). The TPS allows prescriptions based on MU. At M.D. Anderson, the current clinical practice is to use a MU calculation program to convert electron beam prescriptions from given dose per fraction to MU per fraction, which is then entered into the prescription.

C.2 Field size limitation

The Pinnacle^3 TPS does not compute dose for fields with either dimension of the electron field smaller than the side of square of the smallest square field for which relative output factors are entered (e.g. for the M. D. Anderson TPS, this is 2 x 2 cm^2); this is because the relative output factors for those field sizes were not measured during the accelerator commissioning process.

Depth maps are a topographic representation of the variation of the target region. Usually, the topographic depth map of a PTV can be fairly complex in shape (Figure C.1). Figure C.2 shows five fields outlining the depths of the clinical PTV target in Figure C.1. The Pinnacle^3 TPS auto-blocking

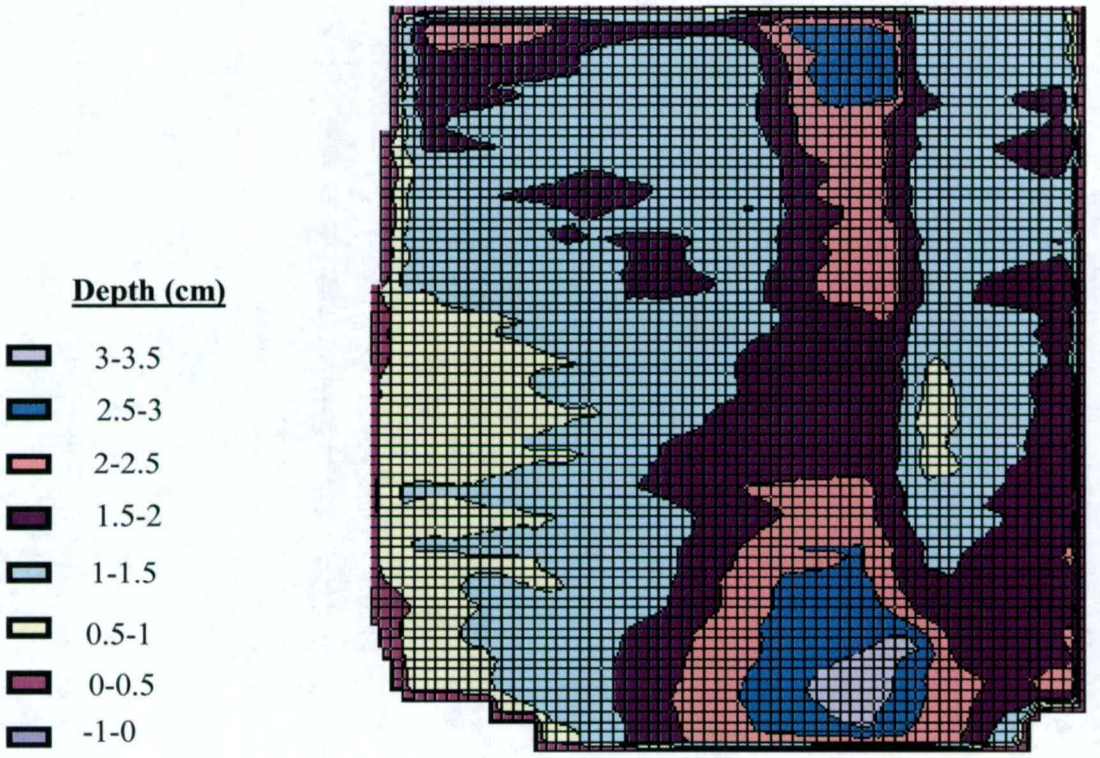

Figure C.1. This picture shows a BEV topographic map of a clinical PTV target (grid scale: 0.25 cm). The indicated PTV topographic regions are 0-0.5 cm, 0.5 -1 cm, 1.5 -2 cm, 2 -2.5 cm, 2.5-3 cm, and 3-3.5 cm from the skin surface.

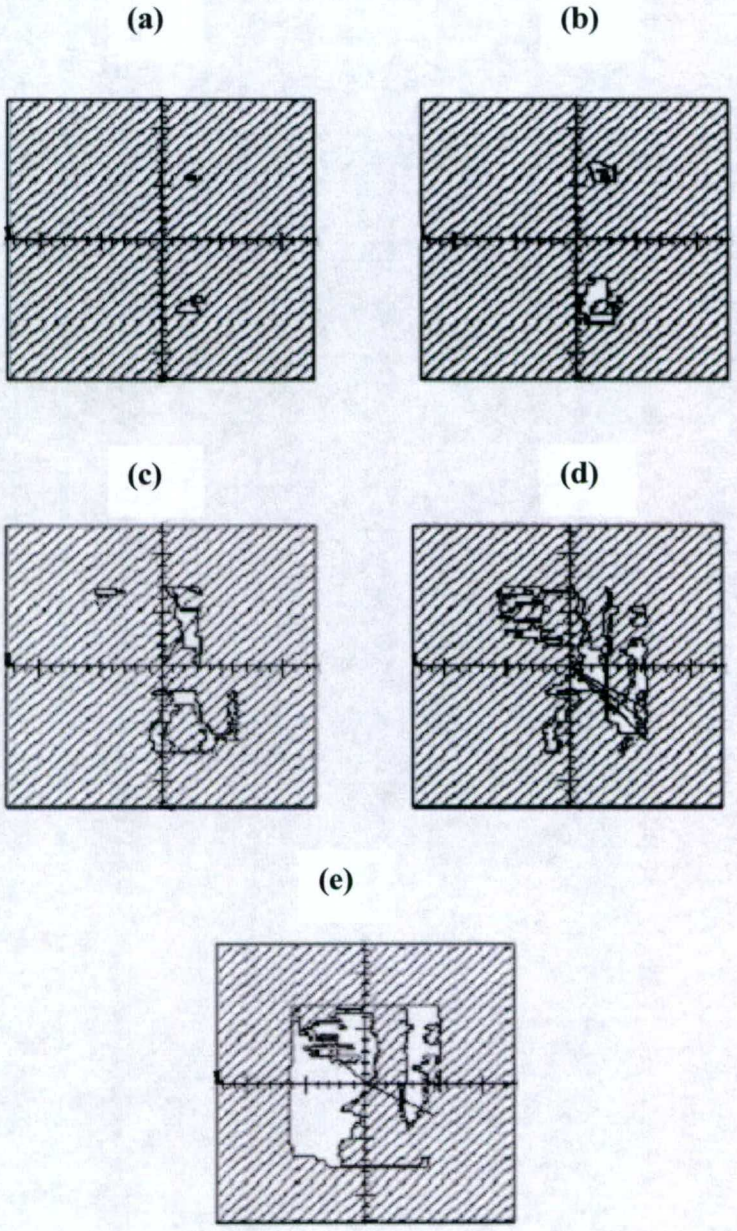

Figure C.2. Treatment fields for same PTV as Figure C.1, indicating specific depths of a clinical PTV (grid scale: 1 cm). The depths are distances (cm) from the skin surface. (a) 2.96-3.72 cm, (b) 2.46-2.96 cm, (c) 1.98-2.46 cm, (d) 1.48-1.98 cm, and (e) 0-1.48 cm. These topographic regions are based on the R_{90} values of the electron beams that are available on a linear accelerator (Primus, Siemens Medical Systems) in our clinic. Pictures (d) and (e) contain a few erroneous lines (projecting radially outward from the origin) due to the graphics display capability.

tools (Appendix B) were used to create the fields for specific PTV depths. The depth maps can contain small, narrow regions that have a lot of structure. The depth of penetration of the electron beam is dependent on many factors including energy and field size. As the field size decreases for a given energy, the R_{90} value decreases (Figure C.3a). This electron beam characteristic could result in the target at a certain depth and location to not be treated completely or at all. One solution is to increase the beam energy to have an R_{90} value that is deeper than current beam energy (Figure C.3b). Another solution is to apply a margin expansion to the field outlining the PTV depth region which "smooths" the jagged edges of the field while increasing small ROIs by a certain margin. The planner can ensure the respective beam energy covers the target depth completely (e.g. a larger field size yields a larger R_{90} value thereby providing deeper electron beam penetration). This method was further investigated. The goal was to apply the same margin expansion value per specific target depth and to use the same or smaller margin value as the beam energy decreases. This process provided complete coverage of the PTV, and reasonable field shapes that were simple in shape and that could be formed using customized electron cutouts or the eMLC. However, this process produced results that left multiple exposed areas or concentric regions at a particular PTV depth that were not easy to treat (Figure C.4) with Pinnacle^3 TPS.

(a)

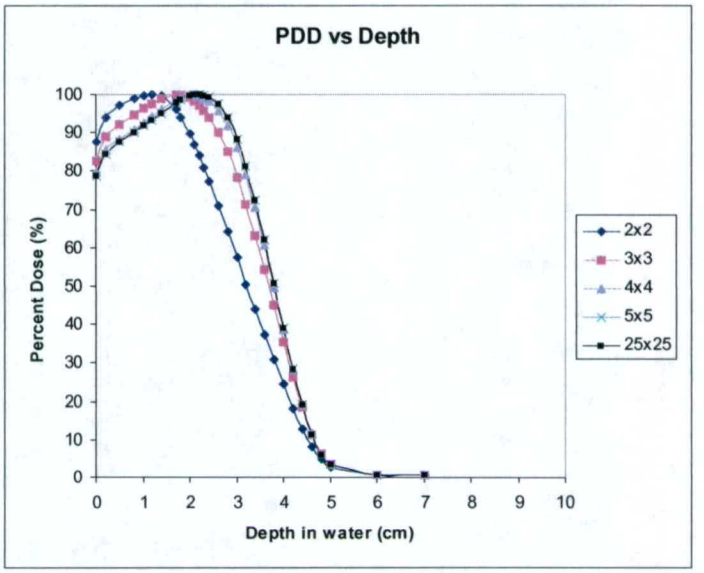

(b)

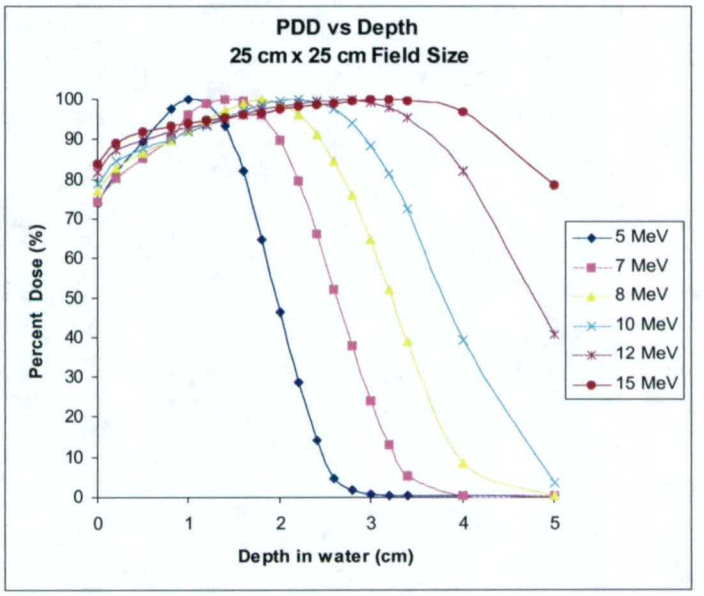

Figure C.3. Percent depth dose (PDD) curve as a function of (a) field size (2x2 cm^2, 3x3 cm^2, 4x4 cm^2, 5x5 cm^2, and 25x25 cm^2) for the 10 MeV beam, (b) as a function of electron beam energy (5, 7, 8, 10, 12, and 15 MeV) for the 25 x 25 cm^2 field size. This data was collected by the medical physics staff at M. D. Anderson during the machine commissioning process for a linear accelerator.

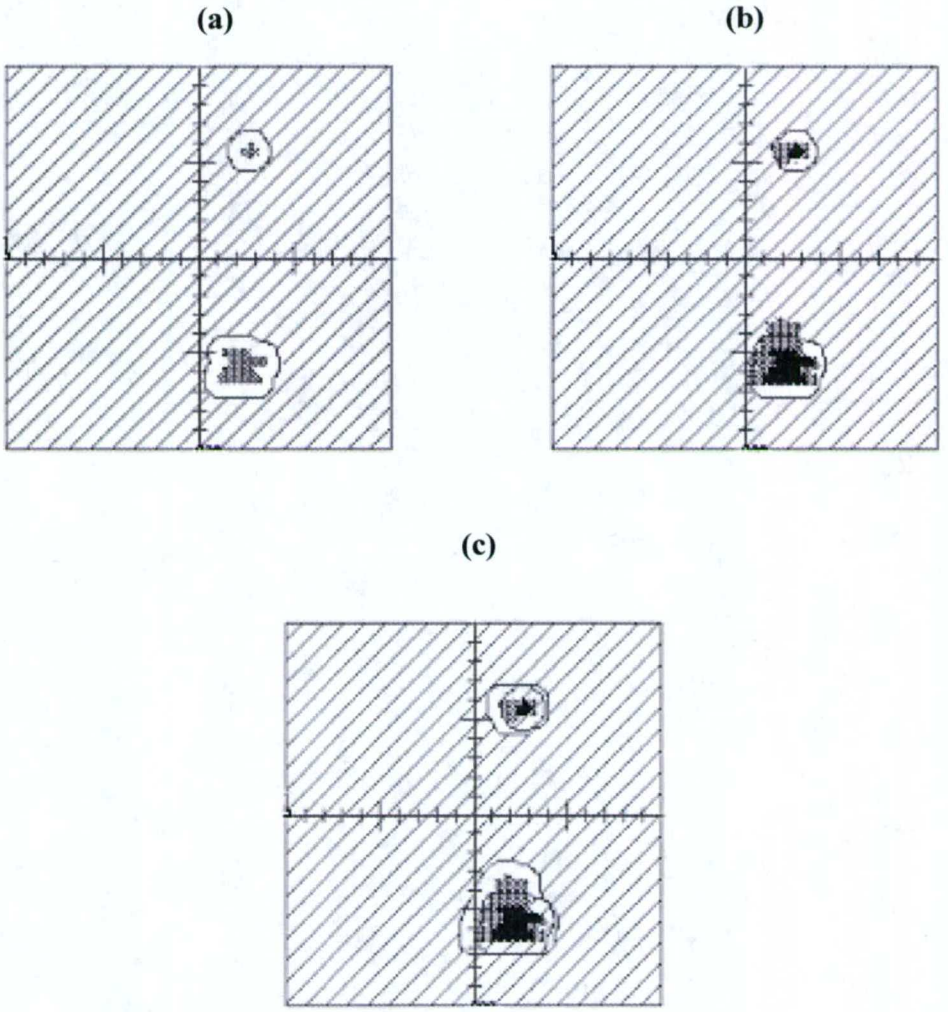

Figure C.4. Field margin expansion method. (a) Treatment fields with 0.75 cm margin encompassing the deepest PTV regions (2.96-3.72 cm depth from skin surface). The margin expansion was used to ensure the field size was at least 2x2 cm^2. (b) PTV depths (2.46-2.96 cm depth from skin surface) in relation to fields with 0.75 cm margin used to treat the deeper target depths. (c) Treatment fields with 0.75 cm margin encompassing the PTV regions (2.46-2.96 cm depth from skin surface). Note that the deeper PTV depth was not included (i.e., the deeper regions were blocked) in the shallower PTV depth. Also note the separated regions of the resulting fields.

C.3 Multiple target regions at the same depth

The Pinnacle^3 TPS electron dose calculation engine computes MU and dose only for a single target region per beam (i.e., compute dose for multiple openings in a cutout). Multiple target regions at the same depth that are separated and/or concentrically confined are not allowed. MU and dose will not be computed for these situations. There are at least two reasonable options to work around this limitation: (1) Divide the multiple target regions of a specific depth map into multiple individual regions while maintaining the rule of one target ROI per beam, (2) Add a "connector" ROI between the separated or concentrically located regions. Using connectors has the potential for reducing the number of fields in the treatment plan.

The "connector" region, which is a narrow (0.5-mm) strip connecting two target regions, is placed by editing the ROI contours within plan.Trial. The plan.Trial file is created by Pinnacle^3, and it describes all of the beam data used in a particular plan (i.e., beam modality, beam energy, field size, electron cutout or photon block coordinates, etc.). In Pinnacle^3, the width of the connector must be at least 0.5 mm, otherwise dose for that field will not be computed. Figure C.5 shows the results of computing dose for this field using both Pinnacle^3 and COPPERPlan with a 0.5 mm and 0.0 mm width connector region. When the connector is collapsed to zero width, the COPPERPlan computed results show no or minimal leakage along the connector.

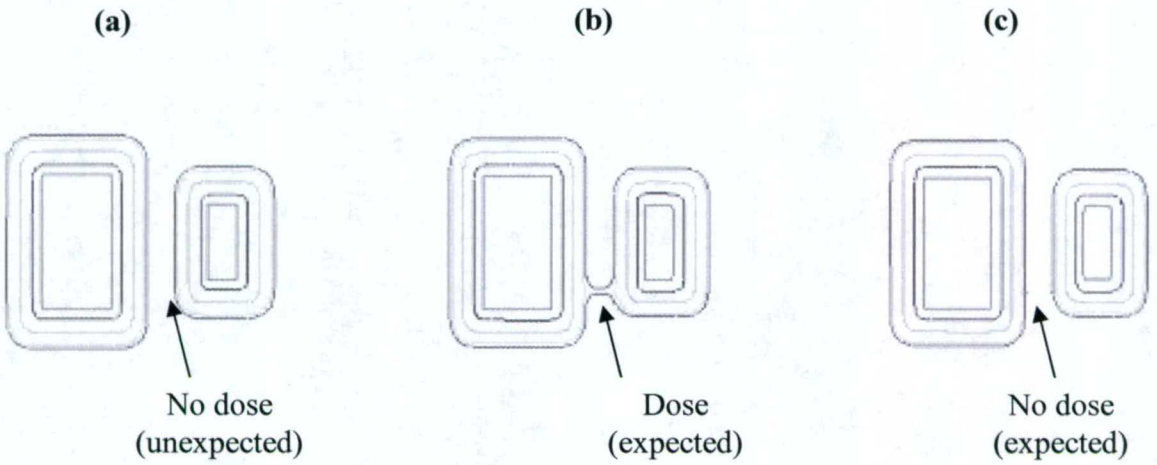

Figure C.5. A comparison of dose distributions computed with Pinnacle[3] and COPPERPlan for a simple target with a connector region. Pinnacle[3] and COPPERPlan are used to compute dose for a simple target with a 0.5 mm connector. The arrows indicate the location of the connector. (a) Pinnacle[3] does not indicate dose along the horizontal connector; whereas (b) COPPERPlan correctly indicates the connector region. (c) As the connector width is collapsed to zero, the COPPERPlan TPS computes dose along the connector as expected.

Pinnacle[3] does not always compute does correctly for fields having a connector width 0.5 mm or greater. Figure C.6 shows two examples of dose being computed incorrectly (Pinnacle[3]) and correctly (COPPERPlan). In both examples, the 50% dose cloud is shown with respect to the field edge. Pinnacle[3] computes dose such that the 50% dose cloud does not meet the field edge (potential cold spots) and extends beyond the field edge (potential hot spots). COPPERPlan computes dose reasonably well for both cases.

Further investigation into the "connector" region method established that the connector strips should be used only between field sizes that are approximately equal in size. Using a connector between two different sized fields would be problematic because of the R_{90} dependency on field size. Also, the connectors should be diagonal rather than horizontal or vertical. The use of non-diagonal connectors can

produce dose artifacts within the dose distribution if the connector happens to be positioned along a dose grid line. A point to note, reducing the number of fields is not the primary rational for using connectors, especially if it leads to fields that cannot be delivered (e.g. eMLC openings that cross a given leaf pair twice). The use of connectors is primarily used because of the limitation on the number of fields that could be used for Pinnacle[3]; not all TPS have a number of fields limitation (e.g. COPPERPlan).

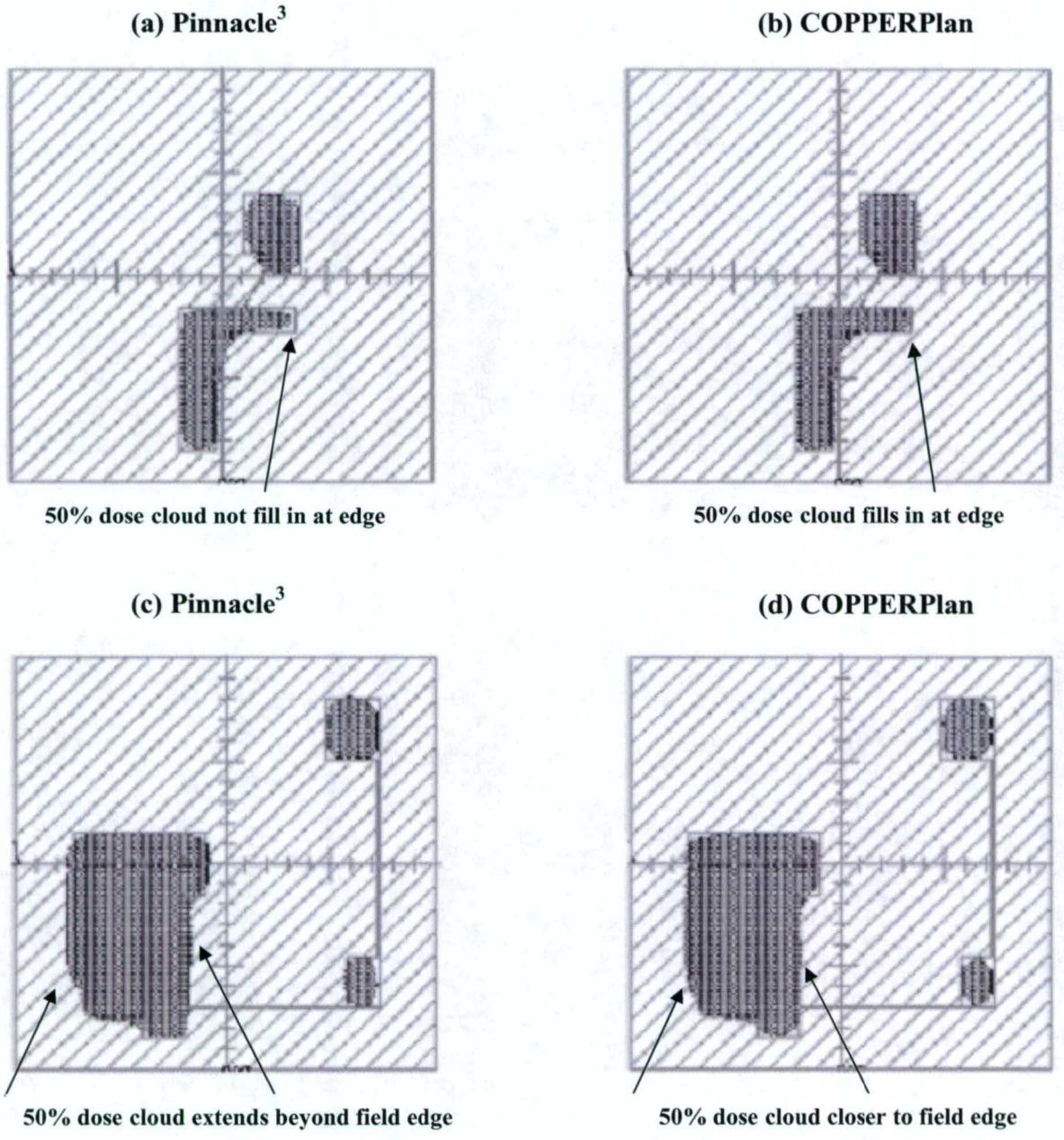

Figure C.6. Evaluation of the "connector" region method using two TPS. The field grid scale is 1 cm and 0.5 mm connector strips were used. Figures (a) and (c) show the 50% dose cloud (gray) computed by Pinnacle[3] for treatment fields having two and three regions, respectively, at the same depth; note that the dose cloud does not properly conform to the field edge. This could cause cold or hot spots at field junctions. However, the COPPERPlan TPS provides improved results, Figures (b) and (d).

C.4 Field Abutment

Segmented-field ECT presents new challenges for ADAC's implementation of PBA for calculating electron dose distributions. One challenge is that segmented-field ECT treatment plans will have multiple junctions and the dose algorithm must be able to compute dose correctly at the junctions. The ADAC TPS does not consistently compute dose at junctions properly.

The dose to a point inside a treatment field is dependent upon direct (radiation passes through the cutout aperture to the point) and indirect (radiation scatters off of the cutout aperture edges to the point) contributions. In general, analytical dose algorithms are commissioned to give an accurate representation of the dose in the unblocked portion of the field and penumbra, since for a single electron field, the in-field bremsstrahlung dose and out-of-field leakage dose are small compared to the given dose. As the complexity of ECT fluence patterns increases, small systematic errors in the dose will be magnified relative to the nominal given dose. It is anticipated that dose computation tools with greater accuracy than the ADAC's implementation of PBA presently on the TPS will be needed to take full advantange of ECT.

In Pinnacle[3] and COPPERPlan, irregular fields are approximated as a collection of strip beams. The strips are approximately 2 mm wide. When junctioning fields, it is important that the strips junction correctly. In Pinnacle[3], the strip locations are determined by the left-most edge of the field (Figure C.7 a). This does not ensure correct junctioning. The COPPERPlan code was modified so that the strips are exactly 2 mm intervals (at the same coordinates) regardless of the shape of the field (Figure C.7b). For these reasons, the modified version of the COPPERPlan implementation of the Hogstrom et al. PBA was used instead for this study.

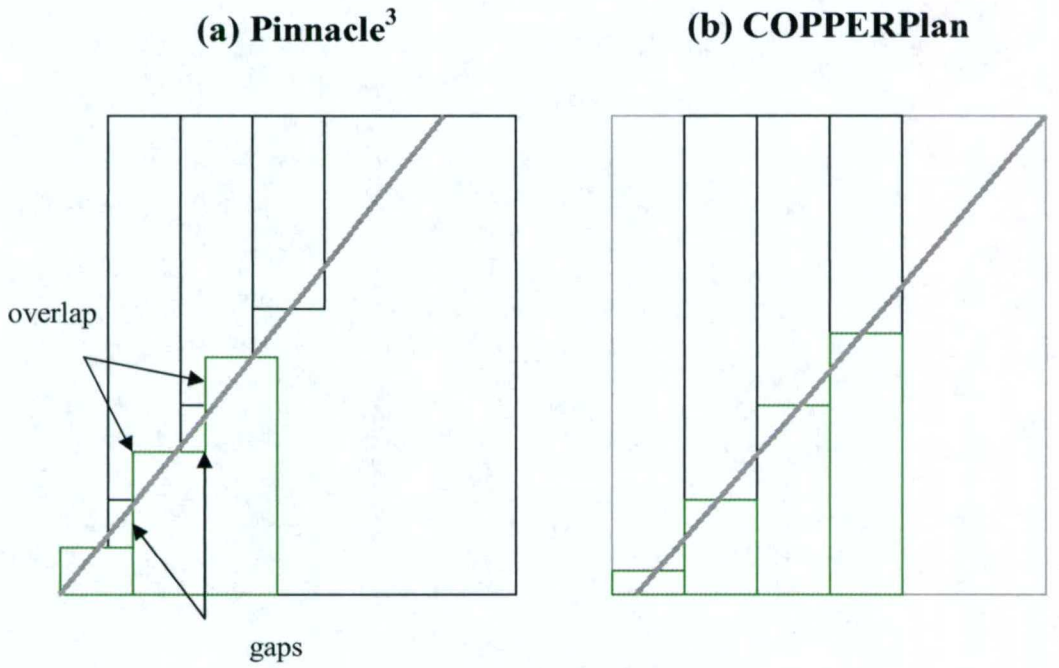

Figure C.7. In Pinnacle[3] and COPPERPlan, irregular fields are approximated as a collection of strip beams. The strips are 2 mm wide. (a) In Pinnacle[3], the strip locations are determined by the left-most edge of the field. This does not ensure correct junction. This picture shows gaping and overlapping that can occur from improper junctioning. (b) In COPPERPlan, the strip beams are placed exactly at 2 mm intervals regardless of the shape of the field.

Bibliography

ADAC Laboratories. 1997 (Version 3.0dU3). Pinnacle[3] User's Guide: external beam and brachytherapy treatment planning.

American Cancer Society. 2005. "http://www.cancer.org/downloads/STT/CancerFacts&Figures2005TM.pdf."

Andrew, J. W., and B. J. McParland. 1987. An automated system for the production of bolus for electron beam treatments. In *Proceedings of the Ninth International Conference on the use of Computers in Radiation Therapy*, edited by I. A. D. Bruinivis, P. H. van der Giessen , H. J. van Kleffens, and F. W. Wittkämper. Scheveningen, The Netherlands. Elsevier Science Publishers, 315-318.

Antolak, J. A., R. A. Boyd, and K. R. Hogstrom. 2002. Evaluation of dosimetric issues related to IMET for a prototype eMLC. *(abstract) Med Phys.* 29(6):1285.

Archambeau, J. O., B. Forell, R. Doria, D. O. Findley, R. Jurisch, and R. Jackson. 1981. Use of variable thickness bolus to control electron beam penetration in chest wall irradiation. *Int. J. Radiat. Oncol. Biol. Phys.* 7(6):835-842.

Beach, J. L., C. W. Coffey, and J. S. Wade. 1981. Individualized chest wall compensating bolus for electron irradiation following mastectomy: an ultrasound approach. *Int. J. Radiat. Oncol. Biol. Phys.* 7(11):1607-11.

Boyd, R. A., J. A. Antolak, and K. R. Hogstrom. 2002. Dosimetric characterization of a prototype eMLC for fixed beam therapy. *(abstract) Med Phys.* 29(6):1285.

Brahme, A. 1987. Design principles and clinical possibilities with a new generation of radiation therapy equipment. A Review. *Acta Oncol* 26(6):403-412.

Buchholz, T. A., E. A. Strom, and M. D. McNeese. 2003. The Breast. *In Radiation Oncology Radation, Technique, Results*. 8th Ed. J. D. Cox and K. K. Ang. St. Louis, Mo: Mosby, 333-385.

Chu, J. C., L. J. Solin, C. C. Hwang, B. F. Fowble, G. E. Hanks, and R. L. Goodman. 1990. A nondivergent three field matching technique for breast irradiation. *Int J Radiat Oncol Biol Phys* 19(4):1037-1040.

Hogstrom, K. R., M. D. Mills, and P. R. Almond. 1981. Electron beam dose calculations. *Phys. Med. Biol.* 26(3):445-59.

Hogstrom, K. R. 1983. Dosimetry of electron heterogeneities. In *Advances in Radiation Therapy Treatment Planning, AAPM Monograph #9*, edited by B. A. Wright. New York, NY: American Institute of Physics, 223-243.

Hogstrom, K. R. 1991. Treatment planning in electron-beam therapy. In *The Role of High Energy Electrons in the Treatment of Cancer*. Frontiers of Radiation Therapy and Oncology, edited by J. M. Vaeth and J. L. Meyer. Farmington, CT: Karger Publishing, 30-52.

Hogstrom, K. R., J. A. Antolak, R. J. Kudchaker, C.-M. Ma, and D. D. Leavitt. 2003. Modulated Electron Therapy. In *Intensity-Modulated Radiation Therapy, The State of the Art*, edited by J. R. Palta, and T. R. Mackie. Madison, WI: Medical Physics Publishing, 749-786.

Hogstrom, K. R., R. A. Boyd, J. A. Antolak, M. M. Svatos, B. A. Faddegon, and J. G. Rosenman. 2004. Dosimetry of a prototype retractable eMLC for fixed-beam electron therapy. *Med. Phys.* 31(3):443-462.

Karlsson, M., H. Nyström, and H. Svensson. 1992. Electron beam characteristics of the 50-MeV racetrack microtron. *Med. Phys.* 19(2):307-315.

Karlsson, M. G., M. Karlsson, and B. Zackrisson. 1998. Intensity modulation with electrons: calculations, measurements and clinical applications. *Phys. Med. Biol.* 43(5):1159-1169.

Khan, F. M., K. P. Doppke, K. R. Hogstrom, G. J. Kutcher, R. Nath, S. C. Prasad, J. A. Purdy, M. Rozenfeld, and B. L. Werner. 1991. Clinical electron-beam dosimetry: Report of AAPM Radiation Therapy Committee Task Group No. 25. *Med. Phys* 18(1):73-109.

Klein, E. E., Z. Li, and D. A. Low. 1996. Feasibility study of multileaf collimated electrons with a scattering foil based accelerator. *Radiother. Oncol.* 41(2):189-96.

Klein, E. E. 1998. Modulated electron beams using multi-segmented multileaf collimation. *Radiother. Oncol.* 48(3):307-311.

Kudchadker, R. J., K. R. Hogstrom, A. S. Garden, M. D. McNeese, R. A. Boyd, and J. A. Antolak. 2002. Electron conformal radiotherapy using bolus and intensity modulation. *Int. J. Radiat. Oncol. Biol. Phys.* 53(4):1023-1037.

Low, D. A., G. Starkschall, S. W. Bujnowski, L. L. Wang, and K. R. Hogstrom. 1992. Electron bolus design for radiotherapy treatment planning: bolus design algorithms. *Med. Phys.* 19(1):115-124.

Ma, C. -M., T. Pawlicki, M. C. Lee, J. S. Li, J. Deng, B. Yi, E. Mok, and A. L. Boyer. 2000. Energy- and intensity-modulated electron beams for radiotherapy. *Phys. Med. Biol.* 45(8):2293-2311.

Perkins, G. H., M. D. McNeese, J. A. Antolak, T. A. Buchholz, E. A. Strom, and K. R. Hogstrom. 2001. A custom three-dimensional electron bolus technique for optimization of postmastectomy irradiation. *Int. J. Radiat. Oncol. Biol. Phys.* 51(4):1142-1151.

Powlis, W. D., A. R. Smith, E. Cheng, J. M. Galvin, F. Villari, P. Bloch, and M. M. Kligerman. 1993. Initiation of multileaf collimation conformal radiation therapy. *Int. J. Radiat. Oncol. Biol. Phys.* 25(2):171-179.

Smith, R. M., J. M. Galvin, M. Needham, and A. Smith. 1989. A computer aided design and fabrication of electron compensation bolus. *Med. Phys.* 16(3):455.

Spirou, S. V., C. S. Chui. 2003. Delivery of Intensity-Modulated Beam Profiles with a Multileaf Collimator. In *A Practical Guide to Intensity-Modulated Radiation Therapy*. Madison, WI: Medical Physics Publishing (2003), 71-80.

Starkschall, G., A. S. Shiu, S. W. Bujnowski, L. L. Wang, D. A. Low, and K. R. Hogstrom. 1991. Effect of dimensionality of heterogeneity corrections on the implementation of a three-dimensional electron pencil-beam algorithm. *Phys. Med. Biol.* 36(2):207-27.

Starkschall, G., J. A. Antolak, and K. R. Hogstrom. 1993. Electron beam bolus for 3-D conformal radiation therapy. In *3-D radiation treatment planning and conformal therapy*, edited by Purdy J. A. and B. Emami. Madison, WI: Medical Physics Publishing. p. 265-282.

Starkschall, G., S. W. Bujnowski, J. A. Antolak. 1994. Tools for 3D Electron Beam Treatment Planning. In *XIth International Conference on the Use of Computers in Radiation Therapy*, edited by A. R. Hounsell, J. M. Wilkinson, and P. C. Williams. Manchester, UK: Christie Hospital NHS Trust, 126-128.

Strom, E. A., and M. D. McNeese. 1999. Postmastectomy Irradiation: Indications and Techniques. In *Breast Cancer*, edited by E. Singletary. New York, NY: Springer, 208-223.

Tapley, N. duV. (ed). 1976. *Clinical Applications of the Electron Beam*. New York, NY: John Wiley & Sons, Inc.

Webb, S. 2001. *Intensity-Modulated Radiation Therapy*. Institute of Physics Publishing, London, 355-421.

Zackrisson, B., and M. Karlsson. 1996. Matching of electron beams for conformal therapy of target volumes at moderate depths. *Radiother. Oncol.* 39(3):261-270.